



Synthesis of functional amphiphilic block copolymers as stabilizer for various nanocarriers and further surface functionalization to change protein interactions

**Dissertation
Zur Erlangung des Grades
„Doktor der Naturwissenschaften“
im Promotionsfach Chemie**

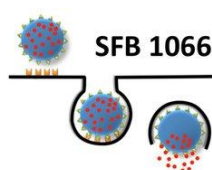
Eingereicht am
Fachbereich Chemie, Pharmazie und Geowissenschaften
der Johannes Gutenberg-Universität in Mainz

von

Sarah Christmann

geb. in Koblenz

Mainz, 2017



Die vorliegende Arbeit wurde im Zeitraum von Juni 2013 bis Dezember 2016 am Max-Planck-Institut für Polymerforschung in Mainz im Arbeitskreis von angefertigt. Ich versichere, die vorliegende Arbeit selbstständig angefertigt zu haben. Alle verwendeten Hilfsmittel und Quellen habe ich eindeutig als solche kenntlich gemacht.

Dekan:

1.Gutachter:

2.Gutachter:

Tag der mündlichen Prüfung: 22.03.2017

Danksagung

Table of contents

Danksagung.....	i
Motivation	1
1. Introduction.....	4
1.1 Functional surfactants in colloid science	4
1.2 Nanocapsule preparation at the interface	44
2. Results and Discussion	52
2.1 Orthogonal protected polyglycerols - surfmers and surfactants for direct and inverse miniemulsions	52
2.2 Amphiphilic ferrocene-containing PEG block copolymers as redox-responsive micellar nanocarriers or surfactants	90
2.3 Stabilization of inverse miniemulsions by silyl-protected homopolymers	106
2.4 Carbohydrate-functionalized HES nanocapsules – changes in protein bindings?.....	121
2.5 Mannose vs Trimannose: Targeting for dendritic cells	140
3. Summary and Outlook	168
4. Zusammenfassung.....	172
5. Literature	176
Appendix	192
a. List of abbreviation	204
b. List of Symbols.....	209
c. Curriculum Vitae.....	210
d. Scientific Contributions	211

Motivation

The first production of soap was mentioned already 2500 years before Christ.^[1] It was obtained from a mixture of olive oil and ash. Since 1775, soaps were used as cleaning agent in daily life and for the first time produced in a synthetic and cheap way.^[2] Today, surfactants are used in textile, cosmetic, pharmacy, food, paint and plastic industry, because they have the opportunity to mix immiscible liquids by decreasing their surface or interfacial tension due to their amphiphilic nature.^[2-4]

Research of surfactants is still present and extended to the use of renewable resources like fats and sugars to reach biocompatible and maybe biodegradable stabilizers.^[3, 5-10] Also surfactants which include additional function, e.g. stimuli responsive groups, have been studied recently. One major aspect is here to recover the surfactant in a simple way, restore it and use it again as stabilizer, resulting in less waste production.^[11, 12]

However, to date, only very few stimuli-responsive and functional surfactants are applied in colloidal science. In this work several surfactants with different properties for the direct and inverse miniemulsion have been prepared. Polymeric surfactants based on polyglycerol block copolymers (chapter 2.1) will be studied in this thesis similar to the commercial, but ill-defined polyglycerol-polyricinoleate (PGPR). Herein, well-defined block copolymers with adjustable length ratios were prepared and allow their use as surfactants in direct or inverse or both miniemulsions. In addition, such copolymers were used as multifunctional surfmers in radical polymerization or polyaddition reactions.

The prior reported redox-responsive ferrocenyl surfactants, most including ionic groups and one redox-responsive unit, exhibited surface active properties.^[13] However, only few of them were studied in any application. Thus, we prepared the first well-defined amphiphilic block copolymers with several ferrocene units in the side chain and established them as non-ionic redox-responsive surfactants for miniemulsions with destabilization 'on-demand' by oxidation of the fc units (chapter 2.2).

In inverse miniemulsions, the synthesized nanocarriers have to be transferred into water. Therefore, an additional water-soluble surfactant is necessary or a stimulus-responsive surfactant to switch the amphiphilicity on demand like the light-sensitive

poly(ethylene glycol)-*b*-poly[(1-pyrenyl methyl)glutamate] surfactant in emulsion polymerization of lactide.^[14] However, most employed oil-soluble surfactants are amphiphilic block copolymers without any switchable group, which resulted in shielding of the nanocarrier surface after transfer into water due to the included hydrophobic block. To decrease such shielding in water, instead switchable amphiphilic block copolymers, poly(acrylic acid) homopolymers with pH sensitive protection groups, were applied as oil-soluble surfactant for polyurea nanocapsules with less shielding after transfer into water by deprotection of the pH-labile protection group (chapter 2.3).

In addition to nanocarrier stabilization research with different types of surfactants, also surface modification studies have to be investigated especially for their use in biomedical applications. The surface of the nanocarriers has first to be functionalized with protein repellent molecules like poly(ethylene glycol) (PEG) or polyphosphoesters to decrease protein adsorption, which led to surface shielding by proteins.^[15-18] Additionally, polyglycerol and polysaccharides are discussed to reduce protein adsorption on surfaces.^[19-21] Because these polymers possess multiple functional groups, they can further be used for additional surface modifications. Thus, the protein repellent properties of our polyglycerol functionalized polystyrene nanoparticles were investigated (chapter 2.1). Besides, different sugar derivatives introduced by copper-free click reaction were studied as protein repellent surface modification on hydroxyethyl starch (HES) nanocapsule surfaces (chapter 2.4) to produce completely carbohydrate and biodegradable non-toxic nanocarriers with stealth properties for biomedical applications. Moreover, the surface of the nanocarriers have to be modified with cell specific linkers like mannose^[22] or folic acid^[23] to control nanocapsule uptake in the body. In addition, trimannose introduced on liposome surfaces was discussed to increase cell uptake into dendritic cells.^[24] Thus, in this work, trimannose and mannose was introduced on the surface of PEGylated HES nanocapsules by copper-free click reaction to compare their cell uptake into dendritic cells (chapter 2.5).

This thesis is divided into three chapters. The first chapter summarizes the different types of existing surfactants in industry and research, whereat the focus is seeded on functional surfactants for colloidal stabilization. In addition, this chapter

integrates the basic foundations of miniemulsion processes to produce nanoparticles or nanocapsules with different shell materials in the field of colloidal chemistry.

All results received in this thesis are presented, explained and discussed in chapter 2. This chapter is divided into 5 sections, which correspond to the different topics processed in this work. At the beginning of each subsection an abstract is given followed by a short motivation and introduction. Then, the results are presented and discussed followed by a conclusion and an outlook. The experimental details are also explained at the end of each subchapter.

In the final chapter 3, the conclusion is given, which summarizes the whole work of this thesis including a short outlook for further studies.

1. Introduction

1.1 Functional surfactants in colloid science¹

What is colloid science and (functional) colloidal stabilization?

Colloid science is the art of forming, controlling, and utilizing hetero-phase materials with a large interfacial area. Emulsions and dispersions are colloidal systems of immense relevance in daily life. For example, a fundamental part of nutritional products, detergents, cosmetics, paints, coatings, and adhesives are based on colloidal systems. Many large-scale heterophase polymerization processes rely on simple but important properties such as low viscosity and effective heat transfer. For medical applications, colloids serve as important carriers for the protection of drugs and enhance their targeted delivery.

Thermodynamically, dispersed systems rely on colloidal stabilization to prevent aggregation and coalescence. Every interface created requires additional energy in proportion to the interfacial tension. In order to overcome this thermodynamic burden, colloidal particles have to be able to repulse one another. This so-called kinetic stabilization can be achieved by physical adsorption of surface active amphiphilic molecules. These molecules can either of low or high molecular weight. Several general terms describe colloidal stabilizers: surfactants, emulsifiers, soaps (especially for fatty acids), and protective agents. The unifying concept and key property of colloidal stabilizers is to provide a significant repulsion between the individual dispersed particles, making the heterophase system kinetically stable, which is typically accomplished via electrostatic or steric stabilization.

Functional colloid stabilization provides additional features in addition to simple repulsion *via* physisorbed molecules. In fact, it is surprising that the majority of artificial hetero-phase systems have overlooked the simple and efficient possibility of spatially resolved chemical modification. The utilization of surface-active functional stabilizers is a fast and flexible method to obtain colloidal particles with strongly

¹ This section is based on the publication 'Functional colloidal stabilization' by Sarah Wald, Ann-Christin Bijlard, Daniel Crespy, Andreas Taden, Frederik R. Wurm and Katharina Landfester published in *Advanced Materials Interfaces* in 2016.[25] A.-C. Bijlard, S. Wald, D. Crespy, A. Taden, F. R. Wurm, K. Landfester, *Adv Mater Interfaces* **2016**, 1600443. The publication is reprinted with permission. Copyright 2016 WILEY-VCH Verlag GmbH & Co. KGaA, Weinheim.

improved interaction properties. This functionalization has proved extremely material- and time-efficient. Due to the self-assembling ability of the stabilizers, the functional groups allow for an exact positioning of chemical and physical interaction sites directly in the surface region of the colloidal particle.

Our main focus of functional colloidal stabilization concentrates on reactive systems, especially hetero-phase polymerization in oil-in-water (o/w) and water-in-oil (w/o) emulsions; water-in-oil emulsion is regarded as an inverse emulsion. We differentiate between various types of surfactants, each representing an amphiphilic molecule consisting of an anchoring moiety providing adsorption or reaction during the dispersed phase and a soluble moiety that is highly compatible or solvated during the continuous phase. The stability of emulsions can be obtained by either low or high molecular weight surfactants. Additionally, we distinguish between surfactants from so-called protective colloids of higher molecular weight without significant self-aggregation properties. Throughout this review, the literature on functional colloidal stabilizers was revised and classified according to molecular weight, preparation technique, chemical structure, and stimuli-responsive behavior. Certain aspects such as inorganic/organic hybrids, or bio-conjugates with sequence-defined structures such as peptides and nucleotides, are not in the scope of the present review and will only be briefly described when relevant.

What are non-functional surfactants?

Low molecular weight surfactants. Figure 1 represents commonly used low molecular weight industrial surfactants for emulsion polymerization. Sodium dodecyl sulfate (SDS) and cetyltrimethylammonium chloride or bromide (CTMA-Cl/Br) are produced on a large scale, mainly for detergents, shampoos, and conditioners.^[26] These compounds are used in emulsion polymerization, but they do not have a specific function besides stabilization and generation of the electrostatic potential of the colloids. Positively charged molecules and colloids, for example, adhere strongly to slightly negatively charged fibers such as polyester yarn or hair. Quarternary ammonium compounds like CTMA-Cl/Br surfactants have antiseptic properties, which are considered beneficial for many commercial applications.^[27-29] Overall, it appears that SDS and CTMA-Cl/Br are often the first choice for colloidal stabilization. This is not necessarily due to better performance, but to the low cost, long-term positive experience, as well as to the well-established, standardized protocols. Other non-

polymer stabilizers, such as alkyldiphenyloxide disulfonates, which carry two ionic charges in close proximity on the molecule, possess a high local charge density and are therefore often superior with respect to colloidal stability to standard sodium dodecylsulfate.^[30, 31]

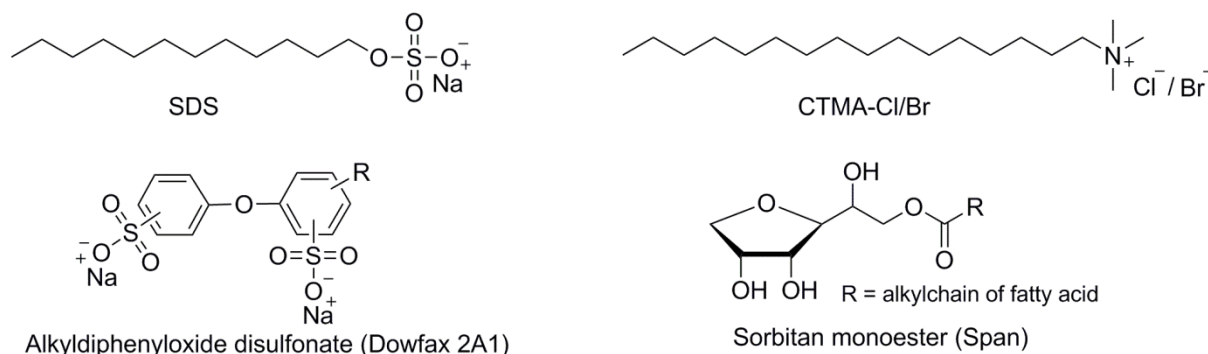


Figure 1. Overview of commonly used low molecular weight surfactants for hetero-phase polymerization.

For inverse emulsions, sorbitan monoesters, e.g. based on laureate or fatty alcohols are conventionally used as food-safe, non-polymeric stabilizers. These compounds, however, can be inferior with respect to their stabilization performance compared to polymeric nonionic stabilizers. Surfactants based on fatty acids can be either non-ionic or ionic and are considered to be *green* or natural surfactants, because they are produced from renewable resources.^[7-10] Furthermore, alkylglycosides or other sugar derivatives can be used to generate surfactants based completely on renewable resources. These surfactants, such as alkyl polyglycosides or glucamides possess an amphiphilic structure with excellent surface activity and solubility and are mainly used for cosmetic, dishwashing or detergent applications.^[32]

Several other, non-polymeric surfactants with additional chemical functionalities will be further classified. In the case of commercial dispersions, reactive non polymer surfactants are occasionally used in order to obtain higher water resistance of the resultant polymer films after film formation. In particular, allyl-functionalized surfactants are used in radical emulsion polymerization. Such reactive surfactants are called surfmers (*surfactant + monomer*) and contain a reactive group such as an allyl group. The surfmers are therefore covalently bound to the colloid during polymerization.^[33, 34] The allyl-group of the amphiphilic monomer does not incline to homo-polymerization. However, its tendency to combine with the polymer at the final

stages of copolymerization (in combination with styrene and/or (meth)acrylates) makes for efficient use and results in similar stabilization characteristics when compared to non-reactive standard surfactants. Mechanistically, the polymerizable surfactants can remain at the interface of a growing latex particle during emulsion polymerization without being buried. Otherwise subsequent particle destabilization would follow and production issues would arise with high amounts of unwanted coagulum formation.^[35] These fairly simple allyl-type surfactants will, however, not be discussed in further detail.

Polymer surfactants. Many polymeric surfactants that are available either commercially or in the scientific literature are synthesized by chain growth polymerizations (selection cf. Figure 2). Polymeric surfactants such as alkylphenol ethoxylates (e.g. Triton®) and poly(ethylene glycol alkylether) (e.g. Brij®, Lutensol®, Genapol®), are industrial PEG-based polymeric surfactants. They possess different hydrophobic groups of linear or branched nature and can vary in their molecular weights. Poly(ethylene glycol)-poly(propylene glycol) copolymers (PEG/PPG) are well-established nonionic surfactants, available in a variety of different block lengths and weight ratios. These PEG-based structures can be adjusted over a wide range of hydrophilic-lipophilic balance (HLB) values, i.e. they can be designed as o/w (oil-in-water, HLB value > 8) or w/o surfactants (water-in-oil, HLB value 3 – 8, according to Griffin), or highly surface-active agents for a variety of purposes, such as wetting, dispersing, pigment grinding, anti-fogging, mold release or anti-friction.^[36] Due to the exothermic anionic ring-opening polymerization and the typically pressurized anionic polymerization, only few suppliers provide such PEG-based surfactants, besides their manifold applications in cosmetics, pharmacy, food and heavy industry. Some of these structures possess a lower critical solution temperature (LCST) and can be considered as temperature-responsive surfactants.^[37] However, during the last decade alkylphenols ethoxylates have been removed from many products and processes, because they are partly broken down in nature to toxic compounds; nonyl phenol and octyl phenol, for example, can accumulate in living tissue and have been shown to mimic estrogen and are strongly suspected of causing endocrine disruption. Their use is either banned or should be at least avoided.^[38-40]

PEG surfactants dominate the field of nonionic polymeric surfactants. With molecular weights of about 25 EO units it can provide efficient steric colloidal

stabilization.^[41] The non-ionic, hydrolysis resistant ether backbone makes the respective colloids very robust against electrolyte contamination and extreme pH values. However, in order to obtain similar particle sizes compared to those that have ionic stabilization, higher stabilizer amounts are required, which influences the film formation properties (increased water uptake, reduced chemical resistance, delamination/adhesive failure, limited anti-corrosion, etc.).

Robust colloidal emulsions and dispersions, based on minimum amounts of surface-active stabilizer, with decreased sensibility against electrolyte contamination and freeze-thaw cycling (frost weathering) can be obtained by combining steric and ionic repulsion. Instead of a mixture of stabilizers, surfactants containing both features in one molecule can be applied, like fatty alcohol ethersulfates as shown in Figure 2. However, already a few EO units (< 10) may act as a “spacer” between the hydrophobic alkyl and the ionic moiety can, in fact, improve the surfactant performance. However, these molecules with rather low molecular weights are not capable of providing high steric stabilization.^[42, 43] In contrast, it seems more plausible that the ionic moiety can be better hydrated by the surrounding water in the inter-phase region of the colloid, thus providing more efficient electrostatic repulsion.

Phosphate esters based on PEG-alkyl ethers follow a similar design (Figure 2) with additional interaction of such stabilized colloids with metals and other inorganic surfaces, increasing performance after film formation. Phosphorous surface-active molecules, especially phosphate and phosphonate structures, are without doubt excellent functional stabilizers with advanced interaction potential way beyond simple repulsion and physical adsorption. Applications range from improved pigment binding (e.g. for durable, glossy coatings) to adhesion and anti-corrosion properties. Given their industrial importance, information on phosphorous water-based dispersions can mainly be found in the patent literature.^[44] Phosphate-containing surfmers were also used for miniemulsion polymerization.^[45] Oligo- or polyamine-based surfactants, such as Lubrizol, are alternatives to the PEG-based materials. The amine groups allow further modification or a pH-dependent profile. Besides block-like structures, so-called protective colloids such as polyvinyl alcohols (PVA) as well as poly(ethylene imine) (PEI) or polyvinylpyrrolidone (PVP) were used to stabilize colloidal systems.^[46, 47] The protective colloids are water-soluble polymers of considerable molecular weight, typically > 10.000 g·mol⁻¹ and do not show the pronounced self-aggregation

behavior that other surfactants do. They possess surface-active properties due to their high polarity and chemical structure. PVA, for example, has a hydrophobic polyvinyl backbone and pendant hydrophilic OH-groups. As PVA is synthesized from saponification of poly(vinyl acetate), a significant number of acetate side groups may remain as well, altering the hydrophilicity. PVP, in contrast, is based again on a hydrophobic backbone, and additionally carries highly polar pyrrolidone-substituents which possess a full interaction and complexation potential. Consequently, most protective colloids serve several purposes and can therefore be considered as functional stabilizers. On a more basic level, they can also serve as rheology modifiers. As a result, molecular weights of $\gg 100.000 \text{ g}\cdot\text{mol}^{-1}$ are frequently applied. A carefully adjusted viscosity is crucial for technical dispersions in order to enable brush application or prevent sedimentation or creaming. Another important feature is their pigment-binding capacity and is of particular relevance when improving mechanical/chemical resistance or optical properties such as color and gloss. The polymeric and polar structure of protective colloids with their functional groups provides significant interaction advantages for this purpose. Furthermore, it should be mentioned that the functional groups can also be utilized for subsequent crosslinking reactions required by many products in the coating and adhesive industry. Finally, protective colloids can assist in film formation and leveling of dispersions upon drying. PEI and PVP, for example, are polymers with high glass temperatures ($T_g \gg 100 \text{ }^\circ\text{C}$) in the dry state, but however are prone to substantial hydroplasticization in contact with moisture.^[48] Consequently, upon water evaporation the respective films eventually undergo a hardening process which can improve the final film properties. The authors of this study reported that polymeric weight stabilizers offer a broad platform for colloid functionalization. Special reactive, protective colloids, for example amphiphilic polymerizable pre-polymers with adjustable LCST behavior introduced by Sawaryn *et al.*,^[49, 50] demonstrated how multiple interactions can be introduced easily in an energy efficient way. When considering their application, novel polymeric stabilizers have the additional advantage that they do not necessarily have to be registered (REACH, TSCA, ...) which saves both time and money.

Natural polymers like polysaccharides or proteins offer tremendous structural variation, which allows them to be used in the stabilization of emulsions. Such natural

surfactants are highly interesting to the food and pharmaceutical sectors. Colloidal stabilizers exclusively based on renewable resources have been recently summarized elsewhere.^[51]

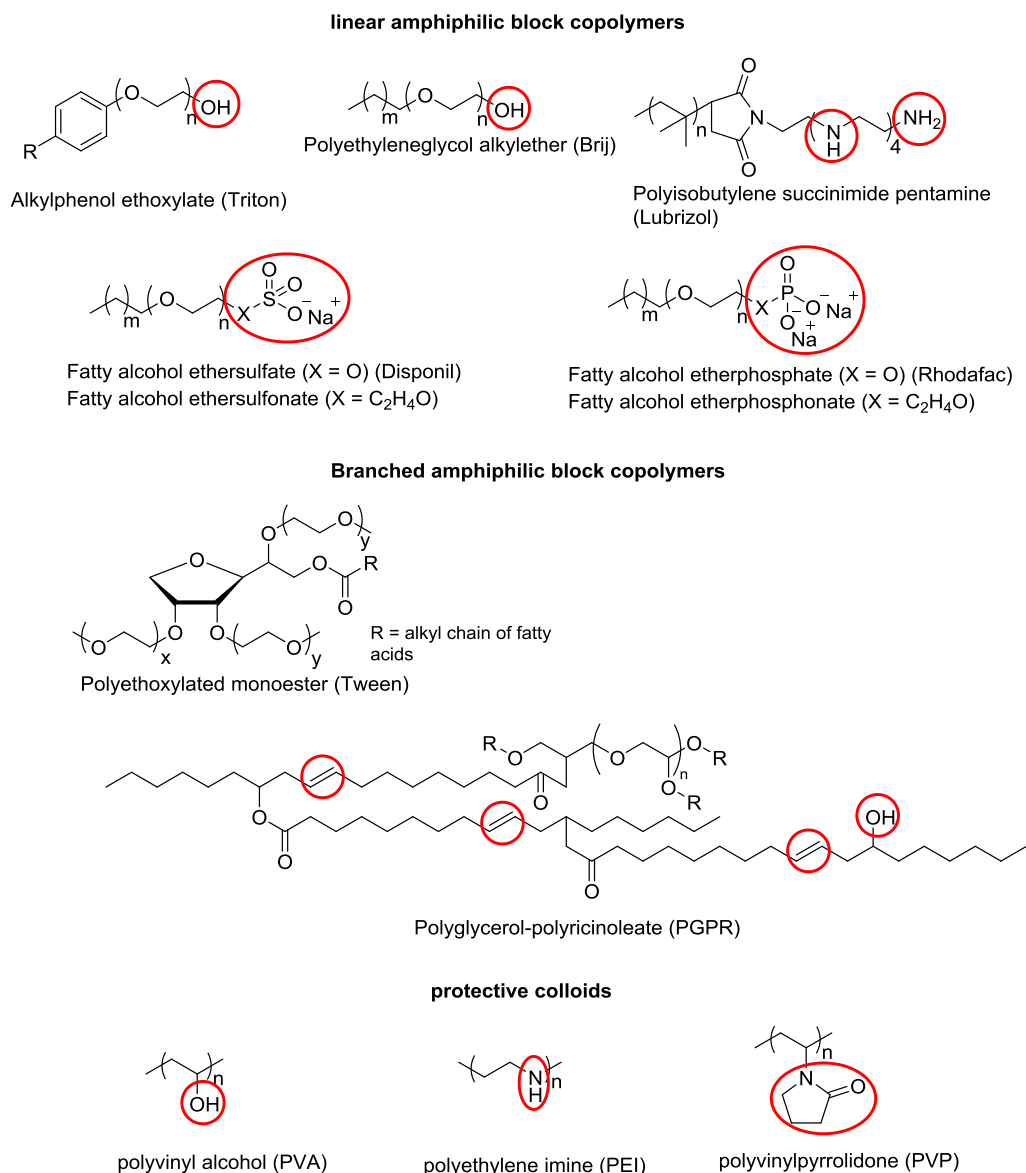


Figure 2. List of amphiphilic surfactants synthesized by chain growth polymerization in industry. The possible functional positions are marked by red circles.

An academically interesting overview of amphiphilic polymers was described by Raffa *et al.*^[52] Most of the polymeric surfactants are based on poly(acrylic acid) (PAA), polymethacrylic acid (PMAA), aromatic sulfonated blocks, polyvinyl pyridine (P2VP, P4VP), PEG macrosurfactants, alkylaminoacrylates or acrylamide with a defined molecular weight and tunable hydrophilic/lipophilic ratio (Figure 3). The

number of compositions and structures of polymeric surfactants now available has increased enormously in comparison to that of low molecular weight surfactants.

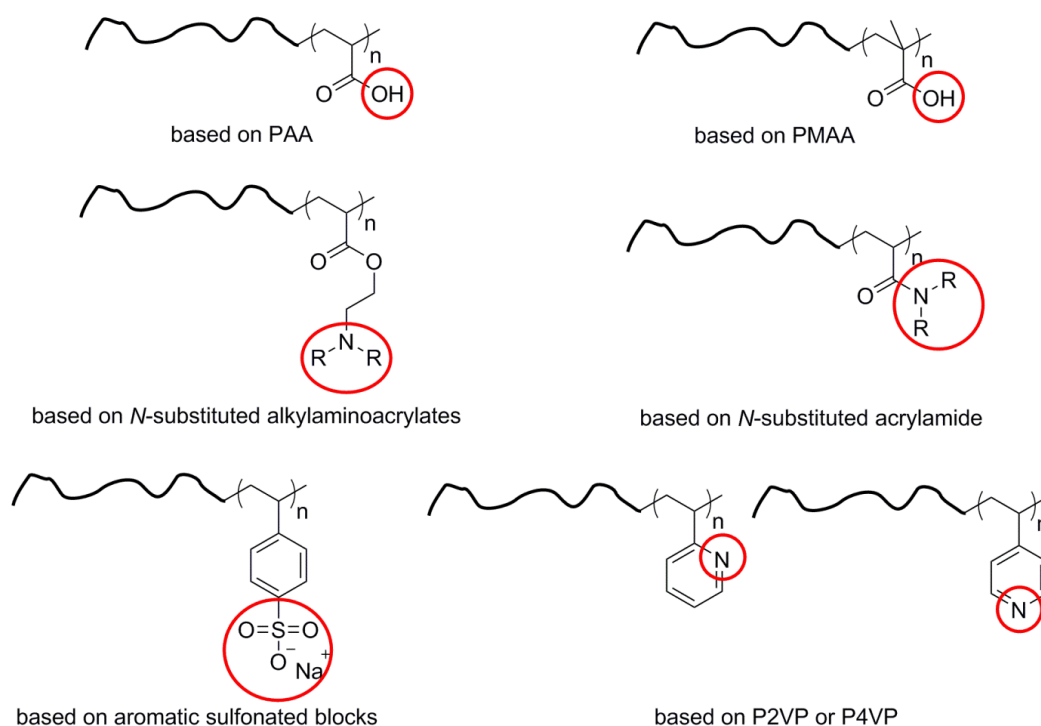


Figure 3. Examples of amphiphilic surfactants synthesized by chain growth oligo- or polymerization. The functional positions are marked with red circles.

An interesting question is whether a narrow polydispersity is advantageous for an efficient stabilization of emulsions. Charleux and colleagues compared the stabilization properties of two groups of copolymers: the first was a group of well-defined monodisperse amphiphilic copolymers synthesized by controlled radical polymerization. The second group consisted of broader distributed copolymers obtained by free-radical polymerization. The result of this comparison demonstrated, that the homogeneous structured copolymer showed higher stabilization for polymer particles in miniemulsion polymerization.^[53] Furthermore, George *et al.* analyzed the effect of molecular weight dispersity of the stabilizing block upon stabilization in emulsion polymerization. The block copolymers poly(styrene)-*b*-poly(acrylic acid) were generated by NMP and used as a stabilizer for emulsion polymerization of styrene.^[54] The authors found that the molecular weight dispersity of the poly(acrylic acid) block influenced the aggregation number of the block copolymer determined by static light scattering ($N_{\text{agg}} = M_{\text{w, aggregate}} / M_{\text{w, copolymer}}$) and the final particle number in

emulsion polymerization, but had no negative effect on the emulsion stability or the size distribution.

Compared to small amphiphilic molecules, synthesized amphiphilic copolymers are more diverse as to their architecture, molecular weight, composition, functionality and interaction, all resulting in better stabilization properties. This in turn expands the potential applications of the common surfactants.^[54] However, although, most of the known amphiphilic polymers include functional groups or possess the ability to introduce functional groups, they are only used as stabilizer for emulsions.

Most of the abovementioned surfactants are prepared by chain growth polymerization strategies. However, several groups also focus on the preparation of polymer surfactants by step-growth polymerization, which will not be part of this thesis. Thus, for detailed introduction into polymeric surfactants polymerized by step-growth polymerization have a look into the published review.^[25]

What are functional surfactants?

Surfactants can be considered functional if they inherit the ability to participate in the polymerization as surfmers (surfactant + monomer), macroinitiators (macromolecular initiator), inisurfs (initiator and surfactant) or transsurfs (transfer agent and surfactant). This adds to the colloidal stability and the compatibility, for example, in film formation. Surfmers are reactive surfactants, containing a reactive group for covalent binding to the colloid. Surfactants which include an initiating site are called macroinitiators, or inisurfs, and are used simultaneously as an initiator and as a stabilizer in emulsions.^[55] If the surfactants include a chain transfer agent, such as xanthate as a reversible addition fragmentation transfer (RAFT) polymerization agent, these surfactants are called transsurfs.^[55] Surfmers and inisurfs lose their function upon polymerization. In contrast, the presence of additional chemical or physical functions in addition to sole stabilization offer synthetic handles for further applications, e.g. in controlled release systems for drug delivery, or catalysis. Functional stabilizers can help reduce the amount of waste in a process compared to conventional surfactants. Additionally, they can be used for fine control over wettability and interfacial tensions in nanotechnology or transport systems. Also waste and environmental remediation costs can be limited by using functional surfactants. Figure 4 summarizes the different functions of surfactants introduced by

pH, temperature or CO₂/N₂, redox, magnetic, or enzyme responsive groups, which will be covered in the following sections.

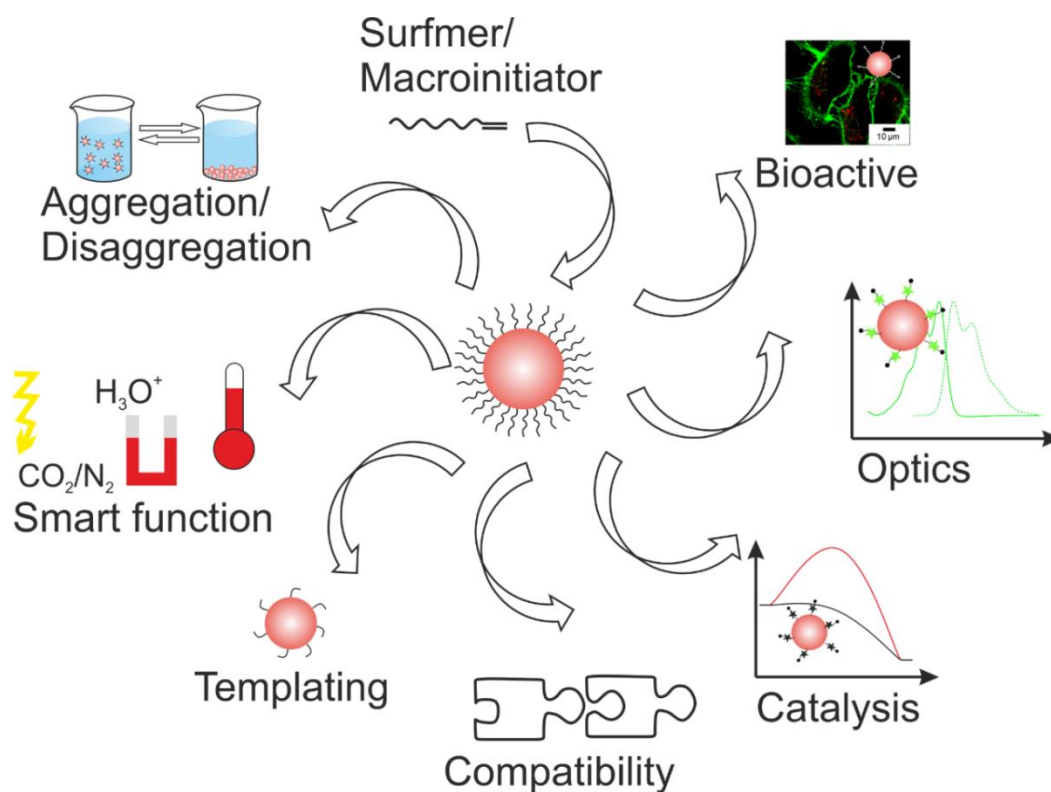


Figure 4. Functional surfactants.

Surfmers/Inisurfs/Transsurfs. Vinyl-based surfmers are typically used in the emulsion polymerization of acrylates.^[35, 56-59] All chemical structure of the described macroinitiators, macromonomers, and macrochain transfer agents are summarized in Table 1. They can lose their functionality upon polymerization into the polymer colloid if the functional groups are entirely converted (this is rarely achieved in the case of macromolecular surfactants) and can therefore be understood as the simplest kind of functional surfactants. Surfmers which participate in or are prepared by step-growth reactions are also listed in Table 1. They demonstrate the versatility of interfacial reactions at hand which provide an increased colloidal stability. Surfmers, or macroinitiators with additional functions are also listed in the subsequent sections.

The use of inisurfs in the miniemulsion polymerization of styrene or (meth)acrylates was shown by Stoffelbach *et al.* The inisurfs were used to generate triblock-copolymers. The atom transfer radical polymerization (ATRP) macroinitiator poly(ethylene glycol)-*b*-poly(styrene)-Br (PEG-*b*-PS-Br, Table 1, entry 1) was reacted with either *n*-butyl methacrylate or a mixture of *n*-butyl methacrylate and styrene to

generate poly(ethylene glycol)-*b*-polystyrene-*b*-poly(*n*-butyl methacrylate) (PEG-*b*-PS-*b*-PBMA) or poly(ethylene glycol)-*b*-polystyrene-*b*-poly(*n*-butyl methacrylate-co-styrene) (PEG-*b*-PS-*b*-P(BMA-co-S)) nanoparticles with diameters below 300 nm.^[60] Furthermore, amphiphilic macro-RAFT agents based on poly(acrylic acid) and polystyrene or poly(butyl acrylate) (Table 1, entry 2) were used as the sole stabilizer of monomer droplets in mini-emulsion polymerization. The amphiphilic molecules were dissolved in the hydrophobic monomer, but were sufficiently insoluble in water, thus avoiding secondary nucleation, due to the absence of polymeric micelles.^[61] In another example a co-oligomer RAFT agent was used based on styrene and aminolyzed maleic anhydride (SMA-RAFT agents, Table 1, entry 3) for a controlled radical miniemulsion polymerization at the droplets interface for the preparation of PS colloids. The defined conditions at the droplet surfaces of the miniemulsion allowed them to adjust the molecular weights, shell thicknesses, surface functionality and inner-wall functionality by semi-continuous polymerization.^[62] Y-shaped macromonomers based on poly[(dimethylamino)ethyl methacrylate] (PDMAEMA) (Table 1, entry 4), synthesized by oxyanion-initiated polymerization using a difunctional potassium alcoholate initiator trimethylol propane allyl ether, were used as pH-responsive surfmers in the miniemulsion polymerization of styrene. The pH-responsivity of the polycationic macromonomer, resulted from the two PDMAEMA arms, was used to perform the reaction at different pH-values. Smaller particles were generated at lower pH values. However, pH-responsive applications of the stabilized nanoparticles were not shown.^[63]

It is also possible to introduce charges onto nanoparticles without the use of low M_w surfactants as shown by Herold *et al.*, who used two acrylamide based dimethylsulfonium methylsulfates as surfmers (Table 1, entry 5) for the preparation of activated ester-functionalized, cationic poly(methyl methacrylate) (PMMA) nanoparticles.^[64] The PMMA nanoparticles could be used in nano-biotechnology for the immobilization of amines from proteins or drugs.

Surfmers are also useful when preparing colloidosomes, or capsules, as the surfmers are able to participate in the formation of the shell at the interface. For example, poly(glycerol monomethacrylate)-*b*-polystyrene (PGMA₅₀-PS, Table 1, entry 6) dispersions prepared by radical polymerization were used as Pickering emulsifier for o/w emulsions with the PGMA as surfactant and as macromonomer. The micro-

emulsions obtained were covalently crosslinked by polyaddition of the OH-groups of the stabilizer with toluene 2,4-diisocyanate-terminated poly(propylene glycol) (PPG-TDI) to prepare colloidosomes with tuneable permeability as demonstrated with dye release experiments for biological applications.^[65] Furthermore, orthogonally-reactive α -azido- ω -2-chloroisobutyrate-poly(oligo(ethylene oxide) monomethyl ether methacrylate)-*b*-poly(*n*-butyl methacrylate) (N₃-POEOMA-*b*-PBMA-Cl, Table 1, entry 7) and mono-reactive poly(ethylene glycol)-*b*-poly(*n*-butyl methacrylate) (PEG-PBMA-Cl) were used as inisurfs for the polymerization of *n*-butyl methacrylate (BMA) and various dimethacrylate crosslinkers to generate functional nanocapsules by ATRP. The azido-functionality of the stabilizer was used to introduce dyes or to create an additional polymer shell.^[66] By using cleavable crosslinkers, with either disulfide or acetal groups, such as (bis(2-methacryloyloxyethyl)disulfide (DSDMA) or di(methacryloyloxy-1-ethoxy)isopropane (DMAEP)), nanocapsules were generated.

Surfmers were also applied for inverse (w/o) miniemulsions. Lubrizol U© (Table 1, entry 8), an amine-containing surfactant, was reacted at the interface with the electrophile TDI to obtain stable polyurea nanocapsules.^[67, 68] Chambon *et al.* used ω -OH groups of commercially available polydimethylsiloxanes ($M_n = 1,000$ and $4,670 \text{ g mol}^{-1}$ (PDMS-OH, Table 1, entry 16) as reactive stabilizers in the polyaddition of ethylene glycol with TDI to prepare core/shell polyurethane-polysiloxane (PUR-PDMS) particles in supercritical CO₂ with a view to a possible application in biomedicine.^[69] The interfacial polyaddition of epoxy surfactants (Table 1, entry 9) and polyamines, in contrast, did not form stable emulsions in water by additional stabilization with SDS or CTMA-Br. Only emulsions which were stable for a few days could be obtained by adding Lutensol AT50.^[70]

Allyl-terminated polyurethane (PUR) surfmers (Table 1, entry 10) were prepared by the polyaddition of TDI with poly(propylene oxide) (PPO) and monoallyl end-capped poly(ethylene glycol) (PEG).^[71] Such surfmers, with allyl endgroup and hydrophobic poly(propylene oxide) chains, but different diisocyanate linkers (such as hexamethylene diisocyanate (HMDI), isophorone diisocyanate (IPDI) and TDI, see Table 1, entry 11) were used for the polymerization with vinylacetate and stable dispersion were obtained.^[72] A similar strategy was used for the encapsulation of a dye into nanocontainers. PUR surfmers (Table 1, entry 12) with terminal vinyl groups were used as crosslinkers in the polymerization of methyl methacrylate (MMA) in the

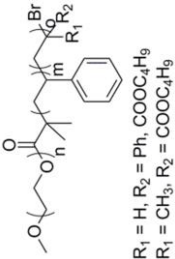
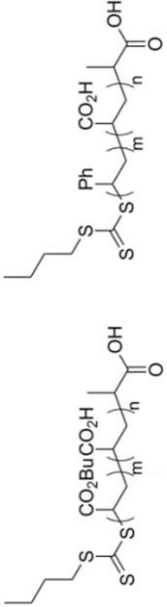
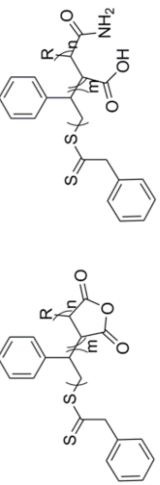
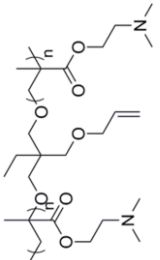
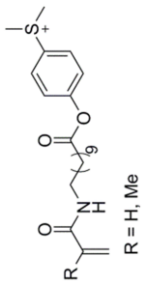
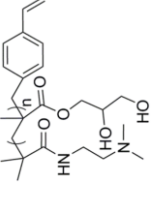
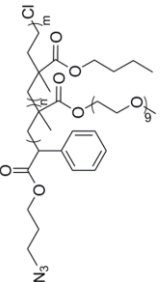
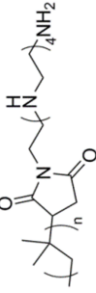
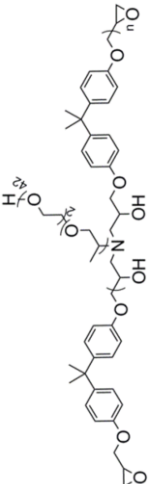
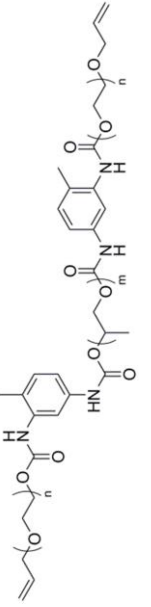
presence of a dye.^[73] Another vinyl-terminated bifunctional PUR surfmer was used for the dispersion polymerization of MMA in ethanol (Table 1, entry 13).^[74] An isocyanate terminated precursor was prepared by the polyaddition of hexamethylene diisocyanate (HMDI) with PEG₂₃ and PEG₁₀₅. This was subsequently endcapped with acrylamide. The authors found a twofold increase in the molecular weight of the PMMA when the PUR surfmer was used instead of conventional poly(*N*-vinylpyrrolidone).

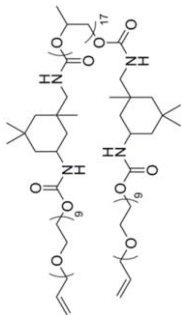
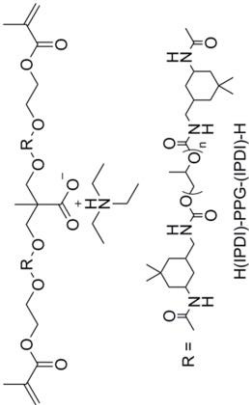
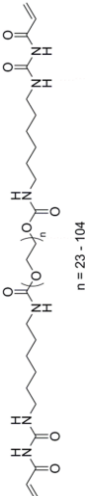
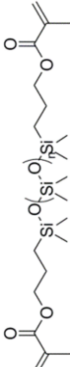
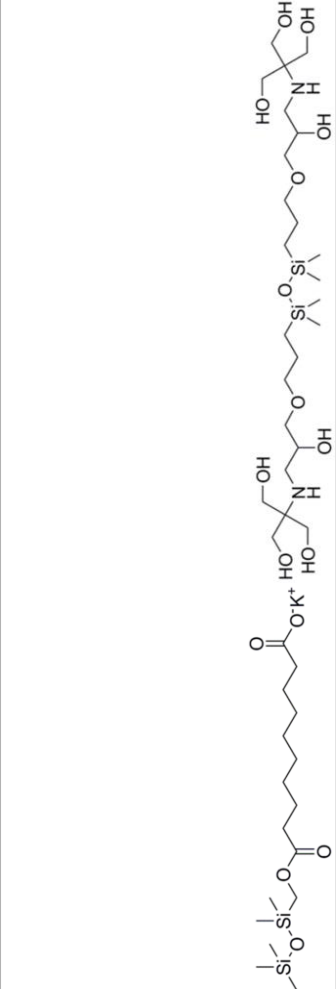
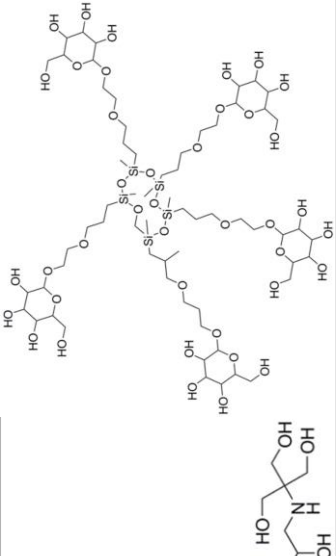
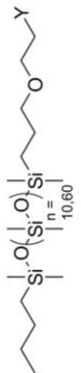
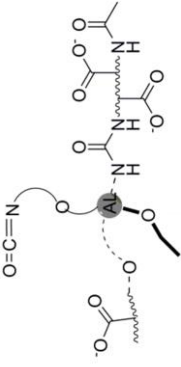
Methacryloxypropyl-terminated poly(dimethylsiloxane)-surfmers (PDMS, Table 1, entry 14) with a molecular weight of 10,000 g·mol⁻¹ were used for the preparation of PMMA microparticles in hexane. Dispersions can be prepared with a solid content up to 26% and are stable in various liquid aliphatics. Furthermore, these dispersions showed well-ordered hexagonal packing at high concentrations, making them useful in photonic crystal templating processes in combination with water-responsive precursors.^[75] In addition, using siloxane based surfactants (Table 1, entry 15), silicon elastomer or polyazomethine, nanoparticles were generated using two crosslinking reactions and one linear polycondensation. The first crosslinking reaction of the PDMS surfmer and tetraethoxysilane (TEOS), as well as the second one via polyhydrosilylation of the dimethyl methylhydrogen siloxane copolymer with divinyltetramethyldisiloxane both led to the formation of silicon elastomer nanoparticles. Polyazomethin nanoparticles were produced by linear polycondensation of bis(formyl-*p*-phenoxyethyl)disiloxane and siloxane dialdehyde (SDA) and *p*-phenylenediamine. The nanoparticles could easily be generated from the reaction mixture in a one-step procedure.^[76]

An approach based on the utilization of renewable resources was demonstrated by the preparation of aqueous acetic acid lignin containing polyurethane (ALPUR) surfmers (Table 1, entry 17). It was done by crosslinking the hydrophobic poly(caprolactone diol) with different concentrations of the multifunctional acetic acid lignin and dimethyl propionic acid as a hydrophilic segment using TDI as the crosslinker.^[77] After the surfmer was generated emulsification was carried out to obtain ALPUR dispersions with different ALPUR particles sizes (diameters: 36 - 260 nm) depending on the concentration of the acetic acid lignin (from 0-10 wt%).

Multifunctional polyglycerol-based surfmers were further introduced in chapter 2.1 with additional functionality.

Table 1. Overview and structure of the macromolecular surfmers, insurfs and transsurfs for the stabilization of colloids.

Entry	Chemical structure	Reference	Entry	Chemical structure	Reference
1	 <p>$R_1 = H, R_2 = Ph, COOC_4H_9$ $R_1 = CH_3, R_2 = COOC_4H_9$</p>	[60]	2		[61]
3		[61]	4		[63]
5	 <p>$R = H, Me$</p>	[64]	6		[65]
7		[66]	8		[67, 68]
9		[70]	10		[71]

11		[72]	12		[73]
13		[74]	14		[75]
15		[76]	15		[76]
16		[69]	17		[77]

Stimuli-responsive surfactants. Stimuli-responsive surfactants allow us to control the properties of a dispersion by the application of an external stimulus, such as change of the pH-value, the temperature, or change of the atmosphere (e.g. argon/ CO₂). In addition to their surface activity, these are the most common stimuli that are found in surfactants.^[12] Our focus centers on the use of stimuli-responsive surfactants in emulsions and dispersions: this concerns mainly aggregation and disaggregation behavior, and additional “smart functions” can be added to functional surfactants. The range of these smart functions include changing the solubility, generating stable systems over a wide temperature range, controlling the release of drugs, catalytic activity, or labeling of particles. The triggers that generate these smart functions are pH, redox, temperature, LCST, CO₂/N₂, light, magnetic and combinations of several triggers.

Surfactants controlling aggregation and disaggregation. In the majority of publications functional surfactants are used in order to transfer the properties (pH, T, CO₂, light, magnetic or redox sensitivity) inherited by the stabilizer to the colloids and are applied for purification and separation steps. A controlled aggregation-disaggregation of polymer dispersions, emulsions and foams can be achieved by changes in pH value or temperature as well as by the addition of CO₂/N₂. Only a few examples made use of magnetic stimuli for a controlled aggregation. The first part of Table 2, which is placed in the appendix, uses the pH value and the second part the redox sensitivity as a trigger for a controlled aggregation of various colloids.

pH-responsive surfactants. The pH value is a straightforward trigger to control surfactant functions and is typically achieved by the incorporation of amines or carboxylic acids in the surfactant structure.

So called gemini surfactants with 2-pyrrolidone based head groups (Table 2, entry 1) and different alkyl chains were used to trigger the surface activity at acidic, neutral and basic conditions.^[78]

Polyvinylamine (PVAm, Table 2, entry 2) was used to prepare pH-responsive PMMA nanoparticles with amino functionality on the surface by surfactant free emulsion polymerization of MMA with *tert*-butyl hydroperoxide (TBHP) as the initiator in aqueous solution. PVAm was included into the nanoparticle shell because the amine groups act as a reductant. They formed radicals during polymerization with the oxidant TBHP, and generated amphiphilic grafted PVAm-g-PMMA and PMMA

polymers by radical polymerization. On account of the presence of amine groups, the nanoparticles had a cationic property with pH response.^[79] Crosslinked poly(*N*-isopropylacrylamide-co-methacrylic acid) (PNIPAm-co-PMAA, Table 2, entry 3) microgels were synthesized either at pH 10 or pH 3 to investigate the comonomer compositions as well as their ability to stabilize octanol/water emulsions. After the synthesis of the microgels under basic conditions the reaction product was divided into three parts: the raw product, the collected supernatant and the purified microgels (both obtained after centrifugation). They were subsequently tested as pH- and thermoresponsive-responsive stabilizers for octanol/water emulsions. Results showed that emulsions stabilized with the raw product are pH and thermo-responsive. If the collected supernatant composed of low molecular weight components were to use as a stabilizer, the generated emulsions would only be responsive to pH because most of the MAA is incorporated in this fraction under basic conditions. The formed PNIPAm-based microgels at pH 10 could not be used for the stabilization of octanol in water because of the low interfacial tension in the system. However, it was used to stabilize heptane-in-water emulsion without pH or thermo-sensitivity. Microgels prepared at pH 3 allowed for the incorporation of PNIPAm and PMAA and could therefore act as stabilizers for different emulsions.^[80]

Darabi *et al.* synthesized macroalkoxyamine inisurfs poly(2-(diethylamino)ethyl methacrylate-co-styrene)-*N-tert*-butyl-*N*-(1-diethylphosphono-2,2-dimethylpropyl)nitroxide (P(DEAEMA-co-S)-SG1, Table 2 entry 4) and poly(2-(dimethylamino)ethyl methacrylate-co-styrene)-*N-tert*-butyl-*N*-(1-diethylphosphono-2,2-dimethylpropyl)nitroxide (P(DMAEMA-co-S)-SG1, Table 2, entry 4) by copolymerization of 2-(diethylamino)ethyl methacrylate or 2-(dimethylamino)ethyl methacrylate and styrene with a neutral azoinitiator 2,2'-azobis[2-(2-imidazoline-2-yl)propane] (VA-061) and the nitroxide *N-tert*-butyl-*N*-(1-diethylphosphono-2,2-dimethylpropyl)nitroxide (SG1) for nitroxide mediated emulsion copolymerization of methyl methacrylate and styrene at pH 6. The resulting pH-responsive polymer particles with diameters between 70 and 90 nm showed excellent colloidal stability and monomodal size distribution. These particles were able to coagulate after neutralization with NaOH. However, redispersion of the nanoparticles was only possible if the dispersions had been dried without prior neutralization.^[81] Cunningham and colleagues synthesized a similar type of macroalkoxyamine inisurf for the same

latex system. A positively charged 2,2'-azobis[2-[2-imidazoline-2-yl]propane] dihydrochloride (VA-044) azoinitiator was used to generate poly(2-(diethylamino)ethyl methacrylate-co-styrene)-*N-tert*butyl-*N*-(1-diethylphosphono-2,2-dimethylpropyl)nitroxide (P(DEAEMA-co-S)-SG1, Table 2, entry 4) macroalkoxyamine as a stabilizer instead of an uncharged azoinitiator (VA-061). It was inserted as an inisurf in the emulsion polymerization of MMA and S to obtain pH-responsive nanoparticles with diameters of 48-65 nm and narrow size distributions. These nanoparticles could also be coagulated after neutralization with NaOH.^[82]

Triblock copolymers based on poly[*N-N*-(dimethylamino) ethyl methacrylate-*b*-poly(ethylene glycol) methyl ether methacrylate-*b*-lauryl methacrylate] (PDMA-*b*-PPMA-*b*-PLMA, Table 2, entry 5) generated by sequential RAFT polymerization were used as surfactants for the preparation of crude oil emulsions. The interfacial activities of the triblock copolymer allow for the addition of these surfactants in concentrations as low as 0.5 mg mL⁻¹. Depending on the pH-responsive amino group (in the DMA segment), the surfactant could be triggered by pH forming micelles with a hydrophobic PLMA core and a cationic PDMA shell with neutral PPMA units under acidic conditions and a PLMA/PDMA core and a PPMA shell under basic conditions. The most efficient stabilizer for crude oil was the triblock copolymer with the composition of PDMA₂₂-*b*-PPMA₂₇-*b*-PLMA₃₆ with balanced hydrophilicity and hydrophobicity.^[83] The amphiphilic macro-RAFT initiator poly(acrylic acid-*block*-styrene) (PAA-*b*-PS, Table 2, entry 6) was used to prepare polymer nanocapsules with a soft poly(*n*-butyl acrylate) core and a hard polystyrene shell (nBA/PS) by RAFT emulsion polymerization. The nanoparticles produced, with diameters between 100 and 130 nm, were used for reversible aggregation by treatment with HCl for the destabilization and NaOH for the redispersion due to the presence of the carboxy group of AA in the RAFT transsurf. From this the authors concluded that the content of nBA needed to be smaller than 60 wt% in order to obtain shell thicknesses above the critical shell thickness of 8 nm, otherwise collapsed sticky particles were obtained.^[84]

Tribet and colleagues described the preparation of modified hydrophobic poly(sodium acrylate)-based polyelectrolytes (Table 2, entry 7) with variable hydrophilic-lipophilic balances and their use in inverse or direct emulsions. By changing the hydrophobic segments of the copolymer from a single-tailed *n*-

dodecylacrylamide to a more hydrophobic twin-tailed di-*n*-dodecylacrylamide, or by increasing the electrolyte concentration and decreasing the pH value, the hydrophilic-lipophilic character of the surfactants was altered. As a result they were able to stabilize the inverse emulsions rather than the direct emulsions. The addition of a photo-active group (azobenzene chromophore) into the polyelectrolyte showed that light could be used as an original trigger for the first time to monitor the emulsion type. The irradiated *cis*-isomer ($\lambda = 365$ nm) of the azobenzene group in the polyelectrolyte was more hydrophilic than the non-irradiated *trans*-isomer and thus leads to the stabilization of direct emulsions. The non-irradiated *trans*-isomer-containing polyelectrolyte, in contrast, stabilized inverse emulsions.^[85] Poly(*N,N*-dimethylaminoethyl methacrylate) (PDMAEMA, Table 2, entry 8) core-crosslinked star polymers synthesized by RAFT-mediated dispersion polymerization of PDMAEMA macro-RAFT agent and the crosslinker 1,6-hexanediol diacrylate (HDDA) were used as stabilizers for oil-in-water emulsions at an oil content below 75 vol%, which was highly viscous but still liquid. At a high oil content (80-89 vol%) the star polymers formed gelled high internal phase emulsions (HIPEs) over a wide pH range. The addition of a base destabilized the HIPEs within two minutes. The core-crosslinked star polymers were used as templates to prepare porous hydrophilic polymers.^[86]

Monomethoxy-capped poly(ethylene glycol) monomethacrylate (PEGMA, Table 2, entry 9) was used as a reactive steric stabilizer to generate poly(2-vinylpyridine) (P2VP) dispersions crosslinked with divinylbenzene (DVB) with low polydispersity (diameters of 380 nm, 640 nm and 820 nm) by aqueous emulsion copolymerization using a cationic azoinitiator (α,α' -azodiisobutyramidine dihydrochloride, AIBA). The generated PEGMA-P2VP dispersions produced similar long-lived foams, achieved either by hand-shaking or by using foam columns. The addition of acid destabilized the foams. This is because the P2VP-segments swell at low pH values resulting in latex-to-microgel transition and desorb from the air-water interface.^[87]

Pickering emulsifiers are frequently used as functional stabilizers to control the destabilization of emulsions. A pH-responsive Pickering emulsifier (Table 2, entry 10) for oil (*n*-dodecane or sunflower oil)-in-water emulsion was synthesized by the emulsion copolymerization using 2-(*tert*-butylamino)ethyl methacrylate (PTBAEMA) as a monomer, DVB as a crosslinker, and PEGMA as a steric-stabilizing

macromonomer. These emulsions were obtained at a basic pH value and were destabilized by lowering the pH value to pH 3, which resulted from the spontaneous desorption from the oil/water interface of the cationic microgel. After four successful emulsification/demulsification cycles, no further demulsification was possible due to the gradual build-up of background salt (KCl).^[88]

Morse *et al.* studied the pH-induced emulsion destabilization by adding either acid (HCl) or CO₂ to various oils (*n*-dodecane, sunflower oil, isononyl isononanoate or isopropyl myristate) in water and stabilized by slightly crosslinked poly(ethylene glycol) methacrylate-poly(2-(diethylamino)ethyl methacrylate) (PEGMA-PDEA, Table 2, entry 11) latex particles as a Pickering emulsifier. The destabilization was caused by a protonation of the tertiary amine, which led from a latex to a microgel transition. Adding CO₂ for destabilization resulted in the protonation of the tertiary amine group. This is due to the fact that H₂CO₃ is formed during the process in aqueous dispersions. Redispersion was achieved by adding KOH to the system, which was successfully demonstrated during 6 cycles.^[89]

Temperature- and pH-responsive micelles of poly(styrene-*alt*-maleic acid)-*graft*-poly(*N*-isopropyl acrylamide) (PSMA-*g*-PNIPAm, Table 2, entry 12) were used as emulsifiers for o/w emulsions in different micelle states by changing the pH value and temperature. Micelle states included shrunken, moderately swollen, extremely swollen, and inverted states.^[90] As the moderately swollen micelles combine the benefits (i.e., interfacial tension reduction operated by moderate penetration through the oil/water interface) of polymeric surfactants and solid particulate emulsifiers, the moderately swollen micelles showed the best stabilization behavior without coalescence. Such grafted self-assembled micelles could act as a model polymeric particulate emulsifier in order to study the surface activity of polymeric surfactants and to explain the emulsification mechanism of stimuli-responsive emulsifiers.

Armes and colleagues synthesized polystyrene/poly(2-(dimethylamino)ethyl methacrylate-*stat*-ethylene glycol dimethacrylate) (PS/P(DMA-*stat*-EGDMA), Table 2, entry 13) core-shell latex particles as a pH-responsive Pickering emulsifier for oil-in-water emulsions. At a value of pH 8, stable emulsions were formed, which could be destabilized under acidic conditions on account of the protonation of the amino groups.^[91]

Poly(4-styrenesulfonic acid-co-maleic acid) sodium salt (PSSMA, Table 2, entry 14) was applied as a calcium (Ca^{2+})-responsive Pickering emulsifier. Nano-aggregates of PSSMA were formed at high calcium concentrations with average diameters of 10-40 nm, which stabilized oil-in-water droplets with diameters between 150-400 nm. After dilution with water, which decreased the Ca^{2+} concentration, individual PSSMA chains were formed which led to an immediate de-emulsification. Diluting the emulsion with CaCl_2 solution delayed destabilization, which demonstrated the response of the emulsion to the calcium concentration. According to the authors, such a system may find application in oil recovery, food science, or environmental protection, due to its simplicity, potential biocompatibility, and broad applicability.^[92]

Benzoxazines were functionalized using the Mannich reaction with phenolphthalein, 3-aminopropyltriethoxysilane, and paraformaldehyde (Table 2, entry 15) and used after hydrolysis and condensation of the polysiloxane group to form polysiloxane microspheres including phenolphthalein groups. These microspheres were used as color-changing, pH-responsive Pickering emulsifiers for stabilization of toluene in water. The emulsion was doubly pH-responsive, as one emulsification/de-emulsification process appeared at pH 9 and another one at pH 12. In addition, the microspheres at both pH-values changed color from pink to deep red while increasing the pH value from 9 to 12, due to the presence of the pH-responsive phenolphthalein indicator. As a result, these Pickering emulsifiers have potential applications when preparing color changing smart coatings, or in oil recovery.^[93]

Stable and biodegradable poly(lactic-co-glycolic acid) (PLGA, Table 2, entry 16) microcapsules were generated by a combination of a 'Pickering-type' emulsion and the solvent volatilization method used in tissue engineering or orthopedic and reconstructive surgery.^[94] Iron oxide nanoparticles were used as an emulsifier and removed with aqueous HCl after the formation of the PLGA microcapsules. The combination of a Pickering-type emulsion with solvent evaporation is a versatile technique to generate a variety of magnetic and biocompatible microcapsules using a broad range of polymers (vinyl and nonvinyl) with the potential to encapsulate functional compounds. Wei *et al.* coated PLGA microcapsules with pH-responsive chitosan nanoparticles (Table 2, entry 17) applying a combination of 'Pickering-type' emulsion and solvent evaporation. Both non cross-linked chitosan coated

microcapsules and crosslinked (with glutardialdehyde) chitosan coated PLGA microcapsules were produced. The cross-linked microcapsules were stable under acidic conditions, while in the case of the non-crosslinked chitosan coated PLGA microcapsules, chitosan dissolved under acidic conditions.^[95]

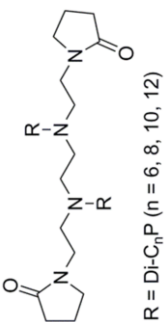
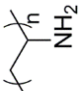
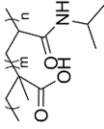
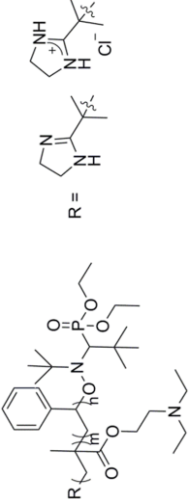
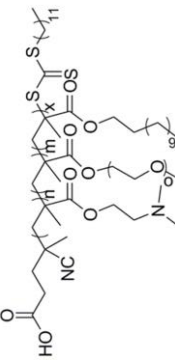
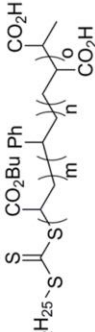
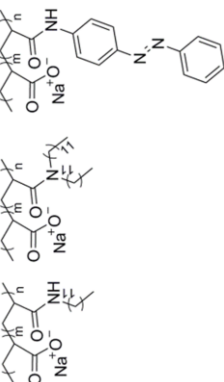
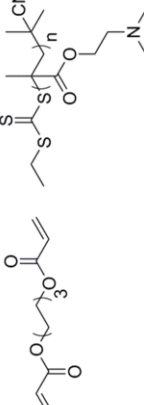
Poly(7-(4-vinylbenzoyloxy)-4-methylcoumarin-co-acrylic acid) (PVMAA containing 12 mol% of the hydrophobic VM monomer, Table 2, entry 18) self-assembled in dimethyl formamide (DMF)/H₂O mixtures to photo-crosslinkable and pH-responsive micelles, which stabilized toluene-in-water emulsions. Photo-crosslinking of the micelles resulted in their shrinking and lower emulsifying efficiency. Photo-crosslinking (0% and 95%) of the micelles in combination with a pH value change were also studied. The non-crosslinked micelles generate more stable emulsions by increasing the pH value to 8. The 95% crosslinked micelles showed lower emulsifying efficiencies with increasing pH values due to their more rigid structure.^[96]

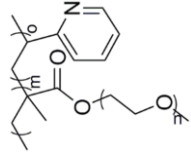
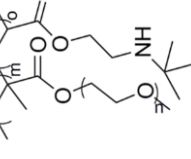
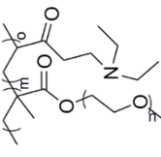
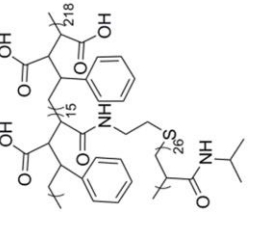
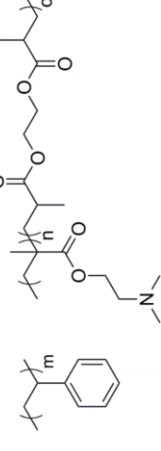
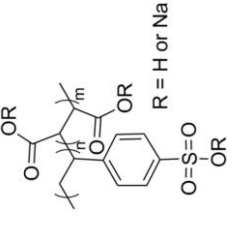
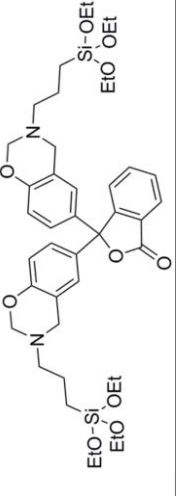

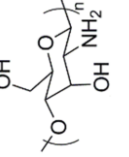
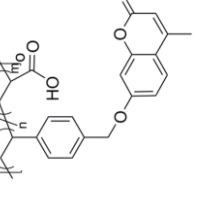
Redox-responsive surfactants. Surfactants with a good affinity to a surface are necessary to overcome high-energy surfaces of nanocrystals and to prevent aggregation. Furthermore, an optimal surfactant should include, for example, a redox-responsive trigger, which allows for varying size distribution and nanocrystal uptake. To this end, Leroux and coworkers synthesized a library of 10 redox-responsive surfactants by post-polymerization of two block copolymers (methoxy polyethylene glycol-*b*-[α -propagyl- δ -valerolactone] (mPEG-*b*-[P δ VL]) or (methoxy polyethylene glycol-*b*-[α -propagyl- δ -valerolactone-co- ϵ -caprolactone] (mPEG-*b*-[P δ VL-co- ϵ CL], Table 2, entry 19) with ethyl-, butyl-, octyl-, benzyl or cholesteryl-thiols. The thiol-yne reaction was chosen for post-polymerization to introduce redox responsive thiol groups into the surfactant. The stabilizing potential of the synthesized polymers was tested for paclitaxel nanocrystals and the influence of oxidation on size and dissolution after treatment with reactive oxygen species. These synthesized stabilizers provide general tools for preparing triggered-cleavable stabilized nanoparticles for imaging and coatings for nanocrystals.^[97]

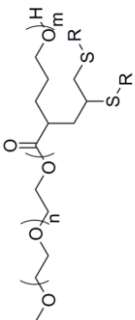
A redox-responsive surfactant including ferrocene units was used in chapter 2.2 to stabilize polystyrene nanoparticles. By oxidation, the generated ferrocinium groups got water-soluble, resulted in a complete water-soluble block copolymer and led to destabilization on-demand.

In addition to pH- and redox-responsive groups, also thermoresponsive, light-responsive, CO₂/N₂ sensitive or magnetic responsive groups were introduced into several surfactants for controlled aggregation and deaggregation in colloid science. Detailed information of these surfactants were summarized by Bijlard *et al.*^[25]

Table 2. Overview and structure of the functional surfactants used for aggregation/disaggregation of described dispersions/emulsions.

Entry	Chemical structure	Reference	Entry	Chemical structure	Reference
	pH responsive				
1	 <p>R = Di-C_nP (n = 6, 8, 10, 12)</p>	[78]	2		[79]
3		[80]	4	 <p>R =</p>	[81, 82]
5		[83]	6		[84]
7		[85]	8		[86]

9	[87]	10	[88]
			
11	[89]	12	[90]
			
13	[91]	14	[92]
			
15	[93]	16	[94]
			
17	[95]	18	[96]
			

	redox-responsive					
19	<div><p>R = alkyl chains</p></div>	[97]				

Smart surfactants. “Smart surfactants” is used throughout this chapter to describe all functions in addition to a sole aggregation/disaggregation of colloids. The order of the following sections follows the last paragraph, but highlighting additional features of the surfactants’ function. The chemical structures of these smart surfactants are listed in Table 3, 4 and 5 in the appendix.

pH-responsive surfactants. Changes in pH value are an attractive stimulus for surfactants including pH responsive groups to change emulsion and dispersion properties. The majority of studies reported in this part either makes use of (meth)acrylic acid or dialkylamino ethyl methacrylates as pH-responsive functional units in polymeric surfactants. Upon protonation, the solubility or swelling of the polymer is changed. Yin *et al.* synthesized sterically stabilized protonated poly(2-vinylpyridine) (P2VPH⁺) microgels which collapsed after the addition of negatively charged sodium dodecylbenzenesulfonate surfactants (SDBS). The stabilizer was, in fact, internalized into the cationic microgel by electrostatic interaction and formed electrostatic P2VPH⁺/SDBS complexes. These complexes were loaded with fluorescent dyes, which were then released after the addition of an anionic polyelectrolyte poly(sodium 4-styrenesulfonate). Such microgels could be applied in the field of controlled release.^[98]

Poly(ethylene glycol)-*b*-poly(*N*-vinylimidazole) (PEG-*b*-PVIIm, Table 3, entry 2) block copolymers were synthesized by RAFT polymerization of *N*-vinylimidazole with a PEG-based xanthate chain transfer agent. The copolymer, which contains a relatively high molecular weight fragment of PVIIm (over 4500 g·mol⁻¹) compared to the copolymers with PVIIm fragment below 4500 g·mol⁻¹, showed a relatively sharp phase transition behavior at pH ranges of 7-8.5. This type of block copolymer was used as pH-responsive stabilizer after cleavage of the xanthate group to stabilize superparamagnetic iron oxide nanoparticles in aqueous media with diameters of 5 - 30 nm. The particles were stabilized with PEG-*b*-PVIIm by dipole-dipole interactions of the deprotonated imidazole ring and the surface of the iron oxide NP. Under acidic conditions, the imidazole groups were protonated, thus achieving stabilization of the iron oxide nanoparticles by ionic-dipole interactions of the protonated PVIIm and the iron surface as well as steric stabilization by the PEG block with variation of their size dependent on the pH in solution; under acidic conditions the nanoparticles looked optically larger than the one under basic conditions.^[99] Furthermore, triblock

copolymers of PEG, *N*-vinylimidazole (pH-responsive segment), and 3-(methacrylamido)phenylboronic acid (glucose-responsive segment) prepared by RAFT polymerization (Table 3, entry 3) were studied as pH- and glucose-responsive stabilizers for iron oxide nanoparticles. To obtain a read out the glucose-responsive behavior of 3-(methacrylamido)phenylboronic acid, Alizarin Red S was added. This dye emits fluorescence by complexation with boronic acid.^[100]

Amalvy *et al.* investigated a series of well-defined di- or triblock copolymers of 2-(diethylamino)ethyl methacrylate (DMA) and MMA (Table 3, entry 4) as pH-responsive steric stabilizers for emulsion and dispersion polymerizations of styrene.^[101] The triblock copolymers PDMA-*b*-PMMA-*b*-PDMA were most efficient stabilizers in emulsion polymerization, whereas the triblock copolymer consisting of PMMA-*b*-PDMA-*b*-PMMA possessed a reduced ability to stabilize. Both triblock copolymers showed low stabilization in emulsion polymerization under acidic conditions. The PDMA-*b*-PMMA diblock copolymers as surfactants resulted in efficient stabilization of polystyrene dispersions. Colloidal stability was strongly influenced by the amount of DMA, whereby more stable latices were generated at low pH values because of the protonation of tertiary amine groups. In addition, a styrene-functionalized PDMA surfmer was synthesized, which generated latex particles of 180 - 750 nm dependent on the surfmer concentration. The synthesized pH-responsive stabilizers could also be used for oil-in-water emulsions.^[101]

A new class of responsive polymeric surfactants which have proved to be highly stable and functional oil-in-water emulsifiers was reported by Cooper and colleagues.^[102] Amphiphilic branched surfactants based on methacrylic acid (MAA) and poly(ethylene glycol) methacrylate (PEG₂₂MA, Table 3, entry 5) were used as stabilizers on account of their reversible hydrogen-bonding interactions between the hydrogen of acrylic acid and the oxygen of PEG. These specific interactions can be triggered by the change of the pH value. Given basic conditions, steric and electrostatic stabilization occurs, whereas multiple hydrogen bonds are formed under acidic conditions (Figure 5). Depending on the pH value, spheroids, macro-Janus spheroids or fibers were generated with these amphiphilic branched polymers.

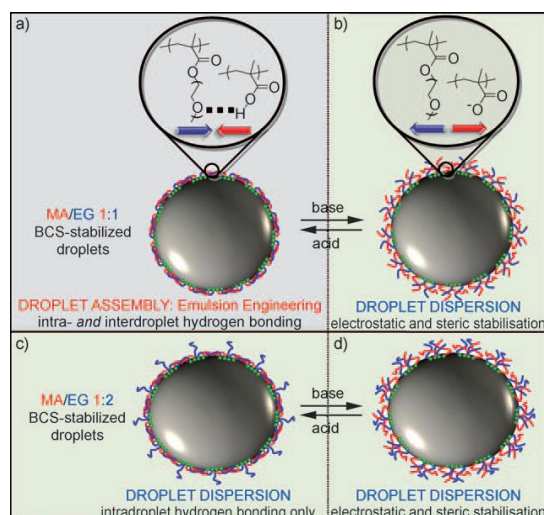


Figure 5. Droplet stabilization with branched PDMA-*b*-PPEGMA with different compositions under acidic and basic conditions. Reproduced with permission from Ref.^[102] Copyright 2009 John Wiley & Sons Inc.

Carbohydrate derivatives are also known as pH-responsive stabilizers. Chitosan (Table 3, entry 6) was mixed with two biocompatible co-stabilizers, Gluadin (flexible peptide) and Jeffamine (a polyamine). Functional biopolymer surfaces were produced on hollow capsules of chitosan-epoxy hybrid polymers or polystyrene nanoparticles. After the addition of a diepoxide (epikote E828) and a diamine to the chitosan co-stabilizer solution, biopolymer hybrid nanocapsules were obtained using the mini-emulsion technique. The co-stabilizer was grafted/cross-linked to the chitosan. The nanocapsules that formed could find applications in drug delivery, due to their biocompatibility and degradability.^[103] An amphiphilic triblock copolymer poly(acrylic acid-co-acrylamidophenylboronic acid)-*block*-poly(2-acryloxyethyl galactose)-*block*-poly(acrylic acid-co-acrylamidophenylboronic acid) (((PAA-co-PAAPBA)-*b*)₂PAEG, Table 3, entry 7) was synthesized by ATRP and self-assembled into pH and glucose-responsive nanoparticles. Under acidic conditions the nanoparticles aggregated and precipitated. At pH values of 5, 7, and 9, the self-assembled copolymers were stable because of their negative charge. By increasing the pH value to 11, the formed nanoparticles then increased in size from 230 nm to 307 nm. The glucose-responsive behavior was dependent on the pH value and was stronger at pH 9 than 7.4. For *in vitro* studies, insulin was encapsulated into the self-assembled nanoparticles and released by changing the pH value and glucose concentrations.^[104] Furthermore, pH responsive surfmers were used to form particles. Styrene-functionalized PDMA

(Table 3, entry 8) was employed as a surfmer in the emulsion polymerization of poly(2-vinylpyridine) (P2VP) and DVB as a crosslinker to obtain pH responsive polymer dispersions. At pH values < 4 the dispersions were transformed into swollen cationic hydrogels and into flocculated particles at pH = 8.5 with neutral PDMA chains in the surfactant structure. These colloids were also used as Pickering emulsifiers to stabilize water-in-undecanol emulsions.^[105]

Deen *et al.* reported on a cationic surfmer based on piperazine (*N,N'*-dimethyl-*N*-acryloyloxyundecyl piperazinium bromide, Table 3, entry 9) were applied as a pH-responsive stabilizer and co-monomer in micro-emulsions, whereas the stabilization was achieved by the protonation of the tertiary nitrogen in the piperazine moiety. The first micro-emulsion system included MMA and HEMA as monomers, and the second acrylonitrile crosslinked with ethyleneglycol dimethacrylates. Most of the bi-continuous systems gelled within 10 min resulting in a transparent solid polymer. The micro-emulsions including acrylonitrile resulted in open-cell type micropores in the range of 33 nm in the dry state, whereas the micro-emulsions of MMA and HEMA did not contain any micropores. All microgels that formed, especially in the acidic range, were highly responsive to pH changes and swell.^[106] Cationic piperazine based surfmers of the type *N*-acryloyl-*N'*-methyl-*N*-alkyl piperazinium bromide (decyl, dodecyl, tetradecyl or hexadecyl, Table 3, entry 10) were used by the group to induce swelling of hydrogels after a change in the pH value. Hydrogels formed upon polymerization of the surfmer in a bicontinuous microemulsion of MMA and HEMA. The hydrogels showed a high degree of swelling in acidic media.^[107]

Nakamura's group studied poly[2-(diethylamino) ethylmethacrylate] (PDEA, Table 3, entry 11) as a pH-responsive inisurf for the preparation of hairy PS NPs. The nanoparticles with diameters between 90 and 460 nm that they created were dispersed at acidic pH value and flocculated in basic conditions.^[108, 109] Under basic conditions, these particles were used as foam stabilizers (stability > 1 month).^[108] Furthermore, their pH responsiveness was used as a gas-responsive stabilizer for liquid marbles which immediately disintegrated in the presence of HCl gas.^[109] Additionally, when using PDMA instead of PDEA as a pH- and temperature-responsive inisurf, foam stabilization/destabilization was achieved by temperature changes above and below the LCST of PDMA (33 °C) as shown in Figure 6.^[110]

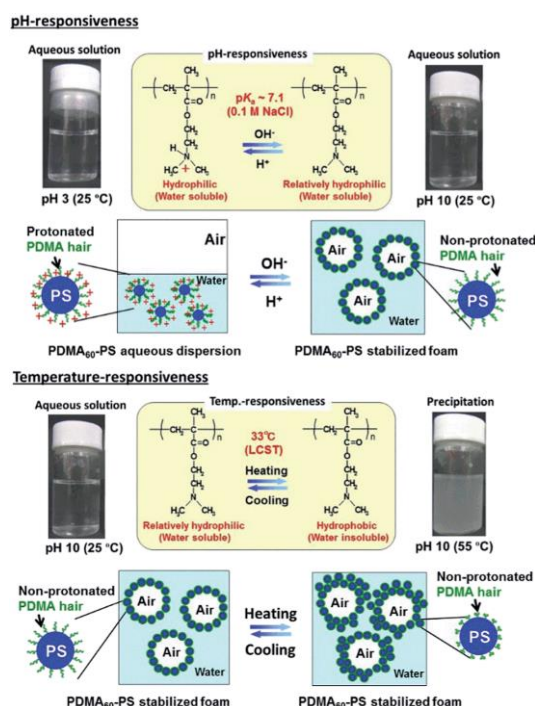
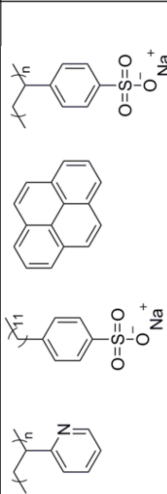
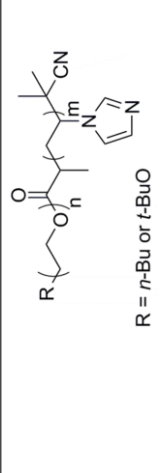
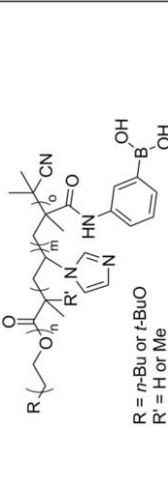
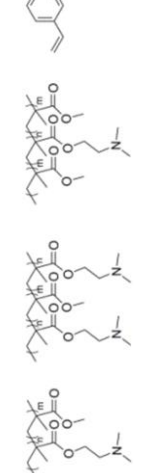
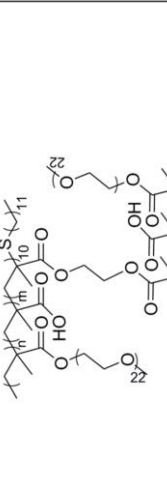
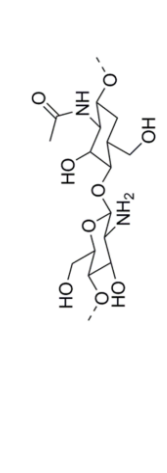
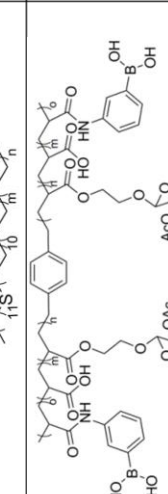
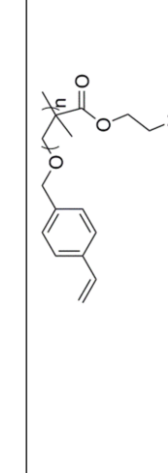

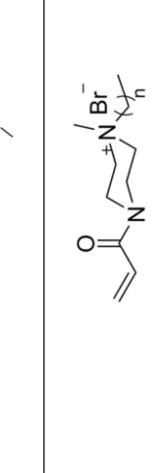


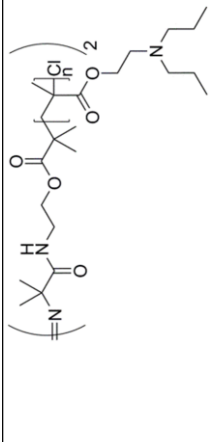
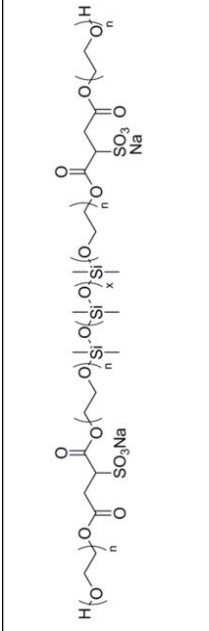
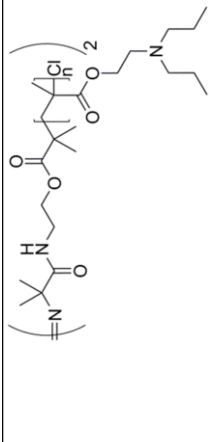
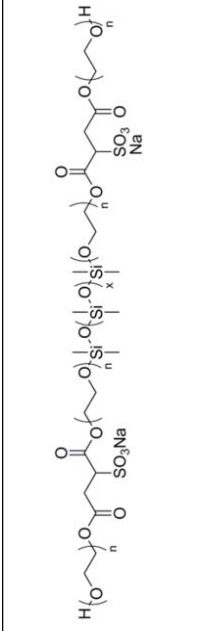
Figure 6. Hairy PDMS/PS nanoparticles as a pH- and temperature-responsive foam stabilizer. Reproduced from Ref^[110] with permission from The Royal Society of Chemistry.

Chen and colleagues synthesized a water soluble pH-responsive silicon surfactant with a cleavable ester-group in the backbone (Table 3, entry 12), but did not use it as a colloidal stabilizer. In acidic media, the surfactant was cleaved into a water-insoluble silanol and two water soluble molecules. The degradation of the surfactant was also demonstrated by photolysis in the presence of TiO_2 .^[111] Acid labile nonionic surfactants were prepared by a thiol-acrylate Michael addition of a hydrophobic thiol to a hydrophilic acrylate (Table 3, entry 13). The micellar assembly of the surfactant was studied, as well as the cleavage of the β -thiopropionate ester bond by dye release experiments under acidic conditions.^[112] The β -thiopropionate linker was also used to form acid-labile crosslinked nanocapsules using maleoyl-functionalized chitosan as a surfactant and precursor for the shell material (Table 3, entry 14). The nanocapsules with encapsulated doxorubicin that were generated showed a controlled release of doxorubicin in acidic tumor tissue by cleaving with the β -thiopropionate group.^[113]

In addition, a poly(acrylic acid) homopolymer with pH-sensitive triisopropylsilyl protection groups in the side chain was used as pH-sensitive surfactants in chapter 2.3 to generate stable polyurea nanocapsules by the inverse miniemulsion process.

Table 3. Overview and structure of the functional surfactants triggered by pH.

Entry	Chemical structure	Reference	Entry	Chemical structure	Reference
1		[98]	2	 R = <i>n</i> -Bu or <i>t</i> -BuO	[99]
3	 R = <i>n</i> -Bu or <i>t</i> -BuO R' = H or Me	[100]	4		[101]
5		[102]	6		[103]
7		[104]	8		[105]
9		[106]	10		[107]

11		[108-110]		12		[111]
13		[112]		14		[113]

Redox-responsive surfactants. Redox-active groups, for example, anthraquinone, disulfide or ferrocene units (Figure 7) have been used in surfactants and allow their cleavage or changes in the hydrophilicity. Liu and Abbott reviewed the spatial and temporal control of surfactants using redox- or light-responsive surfactants, focusing on ferrocene as a redox-active compound.^[114] Surfactants controlled by redox reactions can be applied in templating materials, catalysis or drug delivery. Ferrocene, in particular, is an interesting building block for redox-responsive surfactants, due to its stability, reversibility in redox-chemistry and a versatile chemistry at the periphery. For example, amphiphilic block copolymers either with ferrocene side chains or in the polymer backbone are both potential candidates for emulsion stabilization.^[115-117]

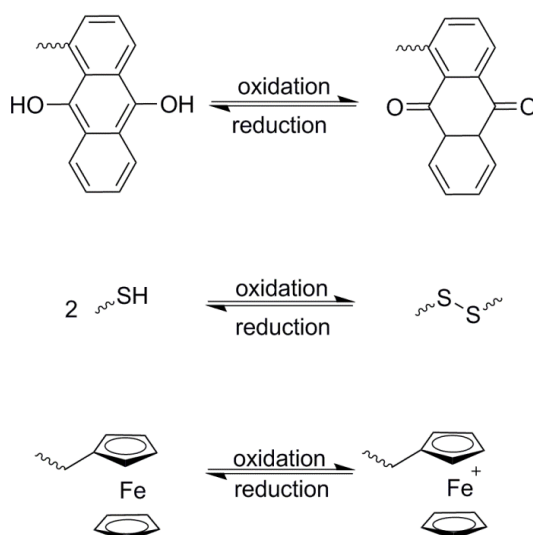


Figure 7. Redox triggers which can be incorporated into surfactants.

Two anthraquinone-based nonionic surfactants (Table 4, entry 1) were synthesized by Susan *et al.* and tested for their interfacial behavior at the air/water interface. The increase in the hydrophobic chain length of α -anthraquinonyloxyhexyl- ω -hydroxy-*oligo*(ethylene oxide) (ACPEG) in comparison to α -anthraquinonyl- ω -hydroxy-*oligo*(ethylene oxide) (APEG) raised the hydrophobic interaction and resulted in enhanced aggregation as well as significant variation in interfacial and micellization properties. After oxidation, the diffusion of both surfactants through the solution was studied. Results showed lower diffusion of ACPEG in comparison to APEG, because the relative molar mass of the ACPEG aggregates was higher than that of the APEG aggregates.^[118]

A redox-responsive anilinium-based surfmer (Table 4, entry 2) was used for the emulsion polymerization of styrene to generate a PS core, which afterwards acted as a seed for the oxidative polymerization of a polyaniline shell.^[119]

Disulfide bonds are a well-known redox-trigger in polymer chemistry and are often used in monomers, crosslinkers, etc., in order to be cleaved under mild, often biological relevant, conditions. The introduction of disulfide bonds into the hydrophobic segment of amphiphilic copolymers, which self-assembled in water, was an effective trigger to release payloads after reductive cleavage of the S-S-bonds (Table 4, entry 3).^[120] Copolymers were prepared from 1-vinyl-2-pyrrolidone (VP) and polymerizable 2-benzothiazolyl-2'-methacryloyloxyethyl disulfide (MBTMA) by free-radical polymerization with different molar ratios VP/MBTMA from 70:1 to 4:1. In water, the poly(VP-co-MBTMA) copolymers self-assembled into NPs of 230-430 nm. Reductive cleavage of the disulfide bonds led to the release of MBT which functions as a corrosion inhibitor. It was possible to encapsulate and release hydrophobic payloads such as Nile Red (Figure 8).

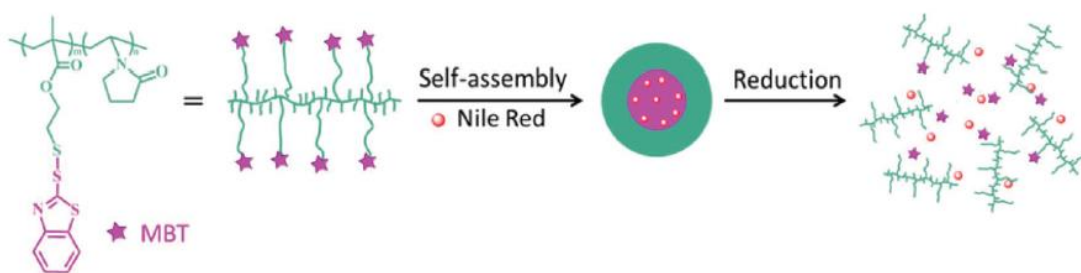


Figure 8. Self-assembly of poly(VP-co-MBTMA) copolymers to nanoparticles with incorporation of Nile Red. After reductive cleavage of the functional amphiphilic copolymer Nile Red was released. Adapted from Ref^[120] with permission from The Royal Society of Chemistry.

Table 4. Overview and structure of the functional red/ox- surfactants.

Entry	Chemical structure	Reference	Entry	Chemical structure	Reference
1		[118]	2		[119]
3		[120]			

Bioactive surfactants. Polysaccharides are polyfunctional and typically low-cost biopolymers that are frequently used as stabilizers or surfactants.^[121-123] Such stabilizers are mostly biocompatible or bioactive and may be useful in drug delivery systems.^[124] In addition, polymeric surfactants including polyglycerol could further be used as bioactive surfactants as introduced in chapter 2.1. For example, the pH-responsive crosslinked maleoyl-functionalized chitosan nanocarriers mentioned above did not show any cytotoxicity (Table 3, entry 15).^[113] Laroui *et al.* prepared hyaluronic acid (HA) and chondroitin sulfate (CS) functionalized NPs (700 nm) by double emulsion/solvent evaporation for controlled drug delivery to cartilage cells (Table 5, entry 1).^[125] The CD44 receptor present on the cartilage cells was addressed by HA and CS and particles are taken up. Amphiphilic HA ($M_n = 366,000 \text{ g mol}^{-1}$) was prepared by the attachment of aliphatic C_6 or C_{12} alkyl chains to the polysaccharide backbone by esterification. Dellachiere's group found that when HA was present at the particle's surface an increased cellular uptake was observed compared to that of the reference particles coated with poly(vinylalcohol).

The surfactant Kollipor[®]ELP is a commercially available PEG-castor oil derivative with free hydroxyl groups. These OH groups were used as anchor groups in the preparation of o/w nano-emulsions to form NPs of 25-55 nm (Table 5, entry 2).^[126] Polyurethane (PEG 400) and polyurea NPs (L-lysine) were obtained by reacting with isophorone diisocyanate (IPDI), which is suitable for endovascular applications as demonstrated by hemolysis and cell viability assays on erythrocytes and human umbilical vein endothelial (HUVEC) cells.

In addition to polysaccharides, amino acids are often incorporated into surfactants. An example is the case of gemini lysine-based surfactants, which were investigated on cervical cancer (HeLa) cells (Table 5, entry 3).^[127] These double-(alkyl) chained anionic amphiphiles only differ in their alkyl chain length from C_6 , C_8 and C_{10} . Dellachiere's team found an increase in toxicity with increasing alkyl chain length. However, all surfactants showed a lower toxicity compared to the conventional commercial surfactant CTMA-Br. As an additional function, these surfactants form mixed micelles with ethyl (hydroxyethyl) cellulose (EHEC). This resulted not only in enhanced biocompatibility, but also to the formation of thermo-responsive gels. These functions could be used for processes which require *in situ* gelation.

Cationic polylysine surfactants were studied by Pérez *et al.* with respect to their phospholipid bilayer-perturbing properties (Table 5, entry 4).^[128-130] The surfactants were synthesized consisting of a cationic polar head and an alkyl chain of either C₁₄ (N^ε-myristoyl lysine methyl ester) or C₁₆ (N^ε-palmitoyl lysine methyl ester) attached on the ε-amino group of the lysine. For N^α-myristoyl lysine methyl ester the hydrophobic tail was attached at the α-position. They found that the pH-responsive surfactants significantly disturb biomembranes at acidic pH-values.

A library of multifunctional siRNA carriers was synthesized with polymerizable peptide surfactants. These structures showed pH-responsive amphiphilicity (Table 5, entry 5) and were used for the preparation of siRNA loaded NPs.^[131] Their general composition included in addition to two lipophilic tails, two cysteine linkers and a pH-responsive amino head-group. Pérez and team discovered that depending on the pH-value, these surfactants displayed either cell membrane disruption properties or hemolytic activity with red blood cells of rats at pH values between 6.5 and 5.4. At pH 7.4 the hemolysis was found to be low. In addition, the polymerizable surfactant could form nanoparticles (160-200 nm) with siRNA by charge complexation due to the influence of the amino headgroup, condensation and auto-oxidative polymerization of dithiols with low cytotoxicity.

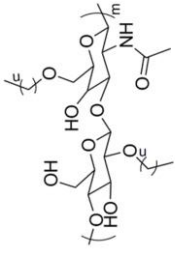
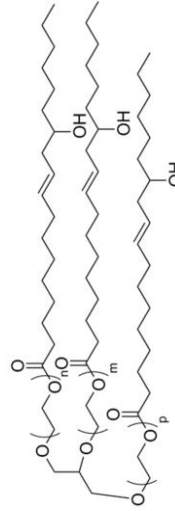
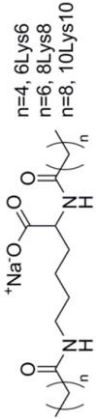
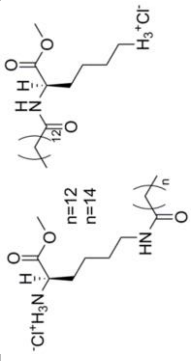
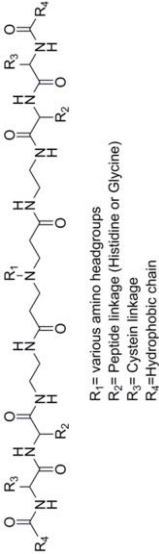
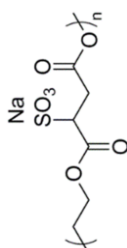
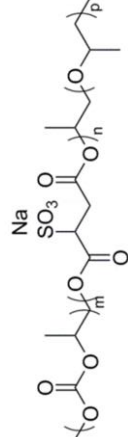
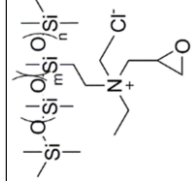
Bicak and coworkers prepared sulfonated (with sodium hydrogen sulfite) unsaturated polyesters as biodegradable polymer surfactants (Table 5, entry 6 and 7). They were synthesized from ethylene glycol with cyclic (phthalic-, maleic or succinic) anhydrides with a boric acid-pyridine mixture as a catalyst for the polycondensation (Table 5, entry 6).^[132] Liu *et al.* utilized the terpolymerization of CO₂, propylene epoxide and maleic anhydride with zinc adipate as a catalyst to prepare a series of biodegradable terpolymers (Table 5, entry 7).^[133] If these surfactants lose their surface active properties upon degradation, they could, in principle, be used for drug delivery, compatibilization or also in demulsification processes. However, Meng's group has not yet investigated these possibilities.

Cationic and epoxide-functionalized polysiloxanes exhibited antimicrobial behavior (Table 5, entry 8). They were prepared by ring-opening polymerization of octamethylcyclotetrasiloxane and hydrolysis of *N,N*-diethyl-aminopropyl-methyldimethoxysilane and subsequent epoxidation (with epichlorohydrine) and quarternization. All surfactants showed high antibacterial activity against *B. subtilis*,

S. aureux and *E. coli* with minimum bacterial concentration values of $< 1.5\text{-}2.8 \cdot 10^{-5}$ mol L⁻¹.^[134]

Smart surfactants with temperature-responsive, pH- and T-responsive or light-responsive groups as well as surfactants with catalytic, optical or templating effects were not summarized here, because they were not part of this work. However, the different kinds and applications of these smart surfactants are reviewed by Bijlard *et al.*^[25]

Table 5. Overview and structure of the functional bioactive surfactants.

Entry	Chemical structure	Reference	Entry	Chemical structure	Reference
1	 n = 6-12	[125]	2		[126]
3	 n=4, 6Lys6 n=6, 8Lys8 n=8, 10Lys10	[127]	4	 n=12 n=14	[130]
5	 R ₁ = various amino headgroups R ₂ = Peptide linkage (Histidine or Glycine) R ₃ = Cystein linkage R ₄ =Hydrophobic chain	[131]	6	 Na SO ₃ O	[132]
7	 Na SO ₃ O	[133]	8	 Na SO ₃ O	[134]

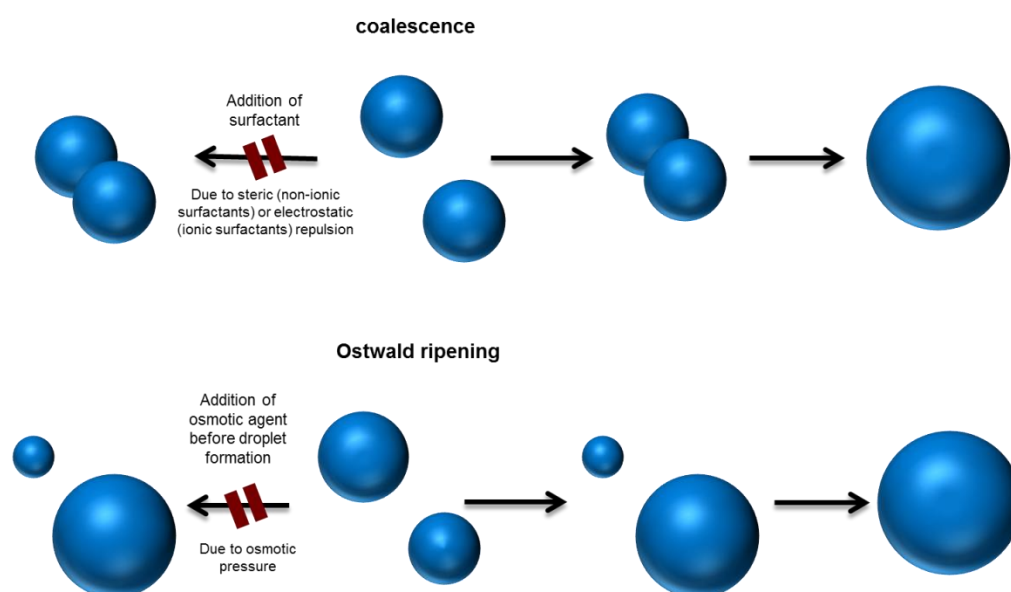
1.2 Nanocapsule preparation at the interface

Nanocapsules are composed of a liquid (hydrophilic or hydrophobic), solid or gaseous core and a polymeric shell. Depending on the liquid core, hydrophilic as well as hydrophobic payloads can be encapsulated. Through the preparation and their applications, the contents are protected against oxygen, light and degradation.^[15] Their various applications range from drug delivery,^[135-139] magnetic resonance imaging (MRI)^[140, 141] to anti-fouling,^[142] self-healing^[143-146] and anti-corrosion.^[142, 147] Nanocapsules are generated by crosslinking polymeric micelles,^[148] crosslinking lipid or polymeric vesicles,^[15, 149] layer-by-layer self-assembly,^[150-154] (nano)precipitation,^[153, 155, 156] double emulsion,^[153] spontaneous emulsification/solvent diffusion,^[153, 156] solvent evaporation^[157-159] and miniemulsion polymerization.^[160] The miniemulsion polymerization is used in this work because it can produce numerous nanocapsules in a single step^[161] with high encapsulation efficiency.^[160, 162-165] Dependent on the employed monomers/polymers and chemical reactions, different types of nanocapsules with hydrophilic (water-in-oil systems) or hydrophobic (oil-in-water systems) core can be produced with controlled size and used for further surface functionalization.^[138, 166, 167] Independent of the utilized polymerization techniques (radical, ionic or polyaddition/polycondensation) in direct (oil-in-water) or inverse (water-in-oil) miniemulsions, various nanoreactor morphologies including hollow nanocapsules, nanoparticles, or layered nanostructures can be obtained.^[168, 169] Nanocapsules are often formed by interfacial polymerizations of hydrophilic and hydrophobic monomers, which are dissolved in the two different phases (dispersed and continuous phase) and polymerize at the droplet interface. During the polymerization, phase separation of the synthesized polymer occurs, because the polymer is immiscible in the different phases, which led to adsorption at the liquid-liquid interface followed from different interfacial tensions between the polymer, the encapsulated liquid (oil or water) and the dispersed phase.

Generally, in a miniemulsion process, two immiscible liquids are mixed and treated with high shear stress using rotor stator systems (Ultra Turrax), sonifiers (ultrasonication tip) or high-pressure homogenizers (microfluidizer)^[166] to create stable nanodroplets as oil-in-water or water-in-oil emulsions. In addition, the Ouzo effect as a spontaneous emulsification is an alternative to ultrasonic and high-shear

devices to produce nanoparticles or nanocapsules.^[170] The droplets formed in miniemulsions have diameters between 50 to 500 nm with narrow size distribution because high shear stress is used to produce the droplets and monomer diffusion between the droplets is less compared to macro- and microemulsions.^[171] The size of the generated droplets depends on the amount of monomer in the dispersed phase, ultrasonication time and the amount and type of surfactant. A surfactant has to be added into the miniemulsion polymerization mixture to prevent coalescence and aggregation of the generated droplets and later on the formed nanocapsules (Scheme 1).^[160, 172, 173] To obtain smaller particles more surfactant per interfacial area is required to reach a steady state after emulsification. In comparison to microemulsions, the surface of the droplets in a miniemulsion is not densely covered with surfactant, thus the concentration of surfactant in the continuous phase has to be below the critical micelle concentration (CMC) of the system.^[174] Due to partial droplet coverage, the interfacial tension in miniemulsions is significantly higher than zero and causes therefore also a Laplace pressure higher than zero.^[175, 176] The surface of the nanocarrier can be covered with anionic, cationic (electrostatic stabilization) or non-ionic (steric stabilization) surfactants, sometimes including stimuli responsive groups as shown in chapter 1.1.^[177] For direct miniemulsions, water-soluble surfactants have to be used with a HLB larger than 9. In inverse miniemulsions, the surfactants have to be soluble in the organic solvent. These types of surfactants have HLB values between 4-8, as defined by Griffin.^[36, 178] In addition, the nanodroplets have to be stabilized against monomer diffusion from small to large droplets during polymerization – referred to as Ostwald ripening (Scheme 1). To reduce the monomer diffusion, an osmotic agent, also called a costabilizer, has to be added into the dispersed phase before mixing, which is less soluble in the continuous phase as the monomer or the cargo. This creates an osmotic pressure inside each droplet, which has to be equal to each other. The efficiency of the osmotic agent depends on the chemical nature of the used compound.^[176] In hydrophobic droplets, chemicals like hexadecane,^[179] cetylalcohol,^[180, 181] mercaptanes^[182] or alkyl methacrylates^[183] as well as a triglyceride mixture containing caprylic and caproic acid from coconut oil (Neobee M5)^[184] can be added as osmotic agents. If the droplets are hydrophilic (in the case of w/o miniemulsions), sodium chloride or other salts are dissolved inside the dispersed phase to reduce Ostwald ripening. Certainly,

the osmotic pressure may lead to swelling of the nanocapsule shell. To sustain the release profile, the nanocapsule shell should be crosslinked.^[185] In conclusion, miniemulsions are kinetically stabilized and not thermodynamically stabilized like microemulsions. A 1:1 copy of the mini-droplet while polymerization can be achieved after several days to nanoparticles or nanocapsules when the osmotic and the Laplace pressure are counterbalanced. This can be analyzed by a combination of small-angle neutron scattering (SANS), surface tension and conductivity measurements.^[186] If inverse miniemulsions are used to produce the nanocapsules, the capsules typically have to be transferred into water before their use.



Scheme 1. General explanation of coalescence and Ostwald ripening and how it is prevented in miniemulsions.

In contrast to radical polymerization and polyaddition/polycondensation, ionic polymerizations (anionic or cationic) are limited to be conducted in heterophase, because they are very sensitive to water or other impurities. Alkyl cyanoacrylates were polymerized by anionic miniemulsion polymerization because they are highly reactive due to the combination of two electron withdrawing groups (ester and nitrile bond) and the initiation by a nucleophilic group, such as water. Thus, poly(*n*-butyl cyanoacrylate) nanocarriers with encapsulated DNA were synthesized by anionic inverse miniemulsion polymerization at the water-oil interface (Scheme 2b).^[187]

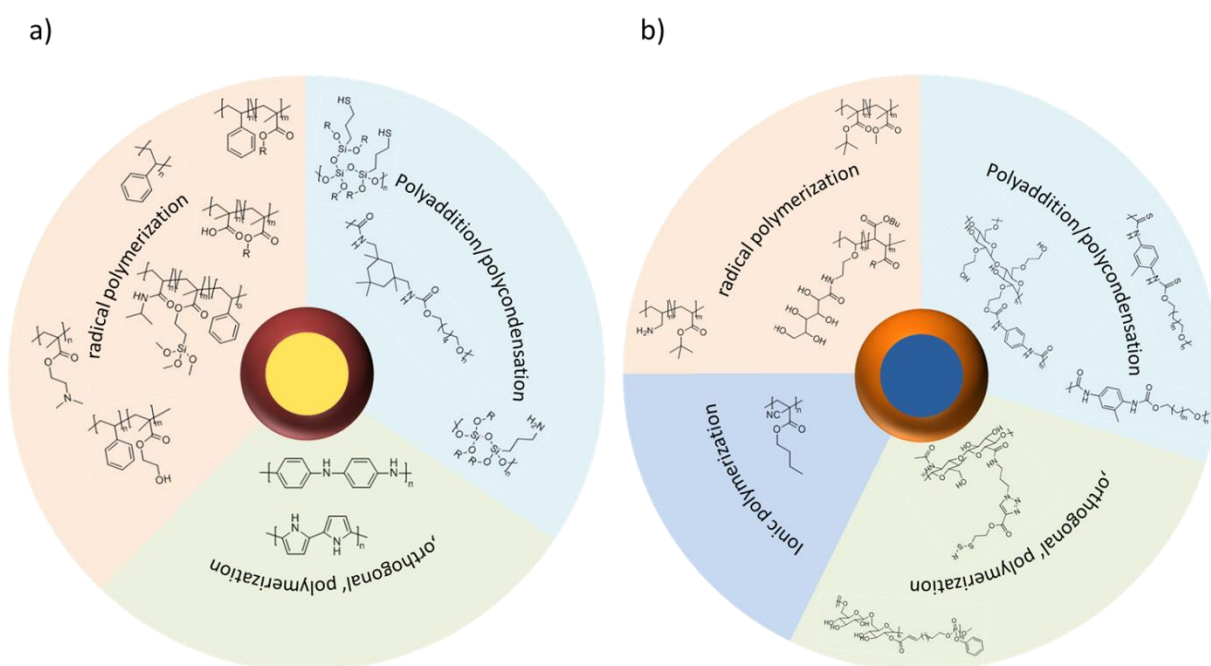
Radical polymerization and polyaddition/polycondensation are well known to generate nanocapsules with a hydrophobic or hydrophilic core and various polymeric

shells with different triggered release functionalities to release the encapsulated payload. Oxygen and light sensitive dyes for triplet triplet annihilation upconversion systems,^[188] or biocompatible oils like Neobee M5^[184] or miglyol^[189] were encapsulated in polystyrene nanocapsules generated by interfacial free radical polymerization. The formation of polystyrene nanoparticles by free-radical polymerization using different block copolymers as stabilizers are shown in chapter 2.1 and 2.2. Instead of styrene also other monomers can be used to synthesize polymer shells by free-radical polymerization (Scheme 2a). Thus, nanocapsules based on poly(methyl methacrylate),^[190] polydivinylbenzene, poly (γ -methacryloyloxy propyl trimethoxysilane) and poly(N-isopropyl acrylamide)^[191] or poly(isohexylcyanoacrylate)^[189] were generated. In addition, the copolymerization of two monomers, which were alternatedly incorporated into the copolymer, was shown at the interface for the first time by Scot et al.^[192] using dibutyl maleate and divinyl-terminated PEG. Radical polymerization was also used as orthogonal reaction to encapsulate self-healing agents into nanocapsules with various functional groups. Here, the polymeric shell was based on copolymers of styrene and different hydrophobic (meth)acrylates including functional groups like sulfonate, amine, carboxylic acid or PEG.^[143] In addition, the polymer shell can also be obtained by controlled radical polymerization techniques like RAFT^[193] or ATRP^[194] to generate crosslinked poly(dimethylaminoethyl methacrylate) or poly(styrene-*b*-hydroxyethyl methacrylate) nanocapsules. A combination of radical polymerization and polycondensation reaction was employed to produce organic-inorganic silica nanocapsules.^[195] Indeed, also nanocapsules with a hydrophilic core were obtained by free-radical polymerization using the inverse miniemulsion (Scheme 2b). The nanocapsule shell was based on poly(*tert*-butyl acrylate)-*co*-poly(allylamine)^[196] or poly(dibutyl maleate-*co*-polygluconamide).^[197] Using RAFT polymerization, P(MMA/*t*BMA) crosslinked pH sensitive nanocapsules were generated.^[198] In chapter 2.1 we also used inverse free-radical miniemulsion polymerization to obtain poly(hydroxyethyl methacrylate) and poly(acrylamide) nanoparticles^[199] using a *tert*-butyl protected polyglycerol block copolymer as surfactant.

Nanocapsules and nanoparticles based on polyurea, polyamide, polyurethane, and poly(ether urethane) are synthesized by interfacial polyaddition or polycondensation (Scheme 2).^[166, 174, 200-202] In addition, different kinds of silica

nanocapsules (Scheme 2a) can be generated by polycondensation reactions to encapsulate antifouling agents,^[142] contrast agents by multi-step reaction,^[203, 204] or self-healing agents.^[145] Other payloads, which are encapsulated by polycondensation reactions, range from water-insoluble herbicides, pesticides, flame retardants, perfumes or colorants^[205] to water-soluble fluorescence dyes and therapeutics.^[206] Using isophorondiisocyanate (IPDI) in combination with different kinds of diols or triols, polyurea/urethane nanocapsules were produced with hexane, heptane, hydrocarbon, aldehyde or ester cores (Scheme 2a).^[207, 208] Ibuprofen loaded nanocapsules with Miglyol 812, a triglyceride oil, core were used for drug delivery applications.^[209] If toluene-2,4-diisocyanate was used as crosslinker, nanocapsules with a hydrophilic core (water or formamide) were primarily synthesized.^[163] Depending on the monomer used, polyurea, polyurethane or polythiourea nanocapsule shells can be formed including pH, T, UV light or enzyme sensitive groups (Scheme 2b).^[210-212] The formation of polyurea nanocapsules are described in chapter 2.1 using polyglycerol based block copolymers as surfmer and in chapter 2.3 with a pH sensitive homopolymer as surfactant. In addition, biocompatible nanocapsules were composed by polyaddition with TDI. Thus, nanocapsules were based on albumin proteins,^[213] (potato) starch,^[214] hydroxy ethyl starch (Scheme 2b),^[17] heparin,^[215] or lignin.^[212] HES nanocapsules were obtained in chapter 2.1, to study the functional surfmer properties of synthesized polyglycerol-block copolymers. The highly reactive electrophilic isocyanate group did not only react with the hydroxyl, amine or thiol groups of the monomers, but also with additional nucleophilic groups of the payloads. As a result, the payloads were incorporated into the shell. To decrease the quantity of incorporated cargo into the shell, other polymeric reactions have to be studied. Thus, thiol-disulfide exchange or UV induced thiol-ene reactions could create nanocapsules based on DNA^[216] or polylactide^[217, 218] to encapsulate different payloads. In addition, thiol-maleimide or thiol-disulfide click reactions at the water-oil interface were used to obtain nanocapsules for drug delivery with cleavable disulfide bonds.^[219] Certainly, biomolecules like proteins or siRNA could also include thiol groups. Encapsulation without shell incorporation of these payloads could be observed by biorthogonal reactions like 1,3-dipolar azide-alkyne cycloaddition (Scheme 2b) (with and without using copper as catalyst^[220]) at the water-oil interface. The nanocapsules synthesized by 1,3-dipolar azide-alkyne cycloaddition were based

on modified sucrose with an oily core,^[221] hyaluronic acid^[222] for drug delivery systems or water-soluble difunctionalized azides (2,2-bis(azidomethylene)-9,1,3-propanediol). Conversely, the hydroxyl groups can be used for further functionalization.^[223] Another biorthogonal reaction is the olefin cross metathesis polymerization, which has the potential to form pH sensitive dextran-organophosphate nanocapsules (Scheme 2b) under mild conditions for biomedical applications.^[224] For encapsulation of anticorrosion agents, aniline^[225] and pyrrol^[147] were polymerized by oxidative polymerization to form redox- and pH- sensitive nanocapsules with an oily core (Scheme 2a).



Scheme 2. Summary of various synthesized polymeric nanocapsule shells using different polymerization techniques in direct (a) or inverse (b) miniemulsions.

Instead of miniemulsion polymerization, the solvent evaporation method in miniemulsion can also be used to prepare nanoparticles and nanocapsules. The production of nanocapsules by solvent evaporation instead of polymerization in miniemulsion is preferred if the purification of the dispersion is difficult or maintained in destabilization, because the polymers are synthesized before their use in emulsion polymerization. Thus, the polymer shell is not contaminated with unreacted monomer or initiator and does not incorporate payloads into the shell. In addition, the preparation of the nanocapsules could occur with fast handling in a simple and versatile way. However, nanoparticles or -capsules prepared by solvent evaporation

typically have a broader size distribution compared to other methods, lower solid contents and residual of used surfactant, which could be partially included into the shell. However, the solid content can be increased by concentrating *at reduced pressure* or by centrifugation and redispersion. Most of the surfactant can be removed by dialysis after the synthesis.^[157] In comparison to miniemulsion polymerization, in the solvent evaporation method, nanocapsule shells based on PS, PMA, PMMA, PLLA and various block copolymers were utilized to encapsulate TTA-UC^[226] or hydrophobic self-healing agents.^[144] Furthermore, polymers like poly(vinylferrocene), poly(vinyl acetate), poly(phenylene oxide) or poly(vinylcinnamate) were prepared as shell materials.^[144] Biodegradable poly(caprolactone) was used to encapsulate sunscreen (Parsol MCX, octyl methoxycinnamate) for new skin drug delivery systems.^[158] Nanocapsules with redox-responsive shells were also established. Thus, using ferrocene based polymers, the encapsulated payload could be released by redox-trigger,^[227] whereas the encapsulated payload changed the hydrophilicity to release into the hydrophilic surrounding.^[228] In addition, double^[229] and triple^[230] stimuli responsive nanocapsules with pH and T or pH, T and redox-trigger were studied using diblock copolymers poly(vinylferrocene-*b*-2-vinylpyrrolidone) (PVFc-*b*-P2VP), PS-*b*-PDMAEMA or PVFc-*b*-PMMA and PDMAEMA-*b*-PMMA as well as the triblock copolymer poly(vinylferrocene-*b*-poly(methyl methacrylate)-*b*-poly(*N,N*-dimethylaminoethyl methacrylate)) (PVFc-*b*-PMMA-*b*-PDMAEMA) as shell material. The hydrophobic payloads were selectively released by two (pH and T) or three different triggers (pH, T and redox). Although, most nanocapsules prepared by solvent evaporation exhibit a hydrophobic core, generating a hydrophilic core is possible by using nylon 6 as a polymer shell.^[159]

For biomedical applications, the release of the payload, the interaction of the polymer shell with the surrounding and cell specific addressing are equally important. Thus, functional groups at the nanocapsule surfaces like hydroxyl or amine groups are needed for further surface functionalization. Generation of functional polymers was realized by (co)polymerizing one monomer with a functional group or several monomers with different functional groups. In addition, functional polymers are obtained by modifying the presented polymer in the dispersed phase. Numerous functional groups were modified with biomolecules for biosensing or specific

targeting.^[138] HES nanocapsules have been functionalized after the nanocapsules formation with PEG using different chemical reactions to study the amount of surface PEGylation and the protein interactions after incubation in human plasma.^[17] Protein interactions with different sugar functionalized HES nanocapsule surfaces are also part of this work and studied in chapter 2.4 for further biomedical applications. Furthermore, mannose derivatives^[22, 231] or folic acid^[23] were prior placed at the surface of HES nanocapsules to study cell specific uptake by active cell targeting. HES nanocapsules functionalized with mannose and trimannose on the surface were synthesized in chapter 2.5 to compare their cell specific uptake into dendritic cells.

2. Results and Discussion

2.1 Orthogonal protected polyglycerols - surfmers and surfactants for direct and inverse miniemulsions²

Orthogonal protected poly(glycerol)-based block copolymers, using ethoxyethyl glycidyl ether (EEGE) as monomer to produce a hydrophilic block and allyl glycidyl ether (AGE) or *tert*-butyl glycidyl ether (*t*BuGE) as monomer to obtain a hydrophobic block, were synthesized by anionic ring-opening polymerization with defined block length ratios as determined by ¹H-NMR spectroscopy and narrow molecular weight distribution as analyzed by size exclusion chromatography (SEC). After complete cleavage of the acetal groups at each polymer, the block copolymers reached an amphiphilic structure with surface active properties. Thus, dependent on their solubility, they were tested as completely polyglycerol-based surfactants (P*t*BuGE-*b*-PG) or multifunctional surfmers (PG-*b*-PAGE) with additional functionality in direct and / or inverse miniemulsions. All water-soluble block copolymers were used to prepare stable polystyrene (PS) nanoparticles as a model system by direct free-radical miniemulsion polymerization, in which the allyl-protected PG surfmers were incorporated during the synthesis analyzed by proton diffusion NMR spectroscopy. Using the oil-soluble block copolymers (PG-*b*-PAGE), stable PU nanocapsules were prepared by polyaddition reactions, in which the hydroxyl groups were integrated into the polymer shell. If the water- and oil-soluble *tert*-butyl protected block copolymer with equal block length ratio was used, stable polystyrene nanoparticles were synthesized in direct miniemulsions or poly(hydroxyethyl methacrylate) (PHEMA) or poly(acrylamide) (PAA) nanoparticles were produced in inverse miniemulsion by free-radical polymerizations. Because polyglycerol (PG) is known to reduce protein adsorption on different surfaces similar to PEG, stability tests of PG stabilized polystyrene nanoparticles were examined in citrate plasma. In all cases, aggregated nanoparticles were determined besides single stable nanoparticles. In addition, the existing hydroxyl or allyl groups on the surface, resulted from incorporation of the PG surfmer into the nanocarrier, were further employed to modify the nanocapsule

² The work in this chapter is based on the manuscript 'Polyglycerol surfmers and surfactants for direct and inverse miniemulsion' by Sarah Wald, Frederik R. Wurm and Katharina Landfester.

surface for example by thiol-ene reactions. In addition, the water-soluble *tert*-butyl protected block copolymer was tested as surfactant for the transfer of produced polyurethane nanocapsules into water with similar results as common used SDS.

Motivation

The applications of surfactants range from paints, coatings, laundry, food and personal care to pharmaceutical industry.^[4] Surfactants are used in a huge variety of applications due to their ability to modify the interfacial properties by surface or interfacial tension change and to self-assemble into micelles or other nanostructures.^[4] The most common and commercially available surfactants exhibit low toxicity and are applied either in direct or inverse emulsion, but not in both emulsion types at the same time. Thus, depending on the application, different types of ionic or non-ionic surfactants have to be used.^[4] In colloid science, surfactants are utilized to generate for example nanocarriers (nanoparticles or nanocapsules with core-shell structure) for several applications.^[15, 135, 136, 138, 147, 232] The nanocarriers can be produced by various methods. The miniemulsion approach is a robust method, because the nanocarriers are synthesized in a single step by free-radical polymerization,^[196, 197, 199] polyaddition/polycondensation^[17, 163, 210] or bioorthogonal reactions^[220, 222-224] with high encapsulation efficiency and well-defined structure resulted from high droplet stability.^[160-163] However, the droplet stability is determined by the used surfactant, which decreases the interfacial tension of the liquids and further protects the produced nanocarriers against coalescence and aggregation.^[172, 176, 233] Thus, the right type of surfactant has to be used to produce stable well-defined nanocarriers. Dependent on the miniemulsion technique, water-soluble or oil-soluble ionic or non-ionic surfactants have to be added, in which the stabilization mechanism of the ionic surfactant is based on electrostatic repulsion and the non-ionic one is based on steric repulsion. Therefore, the surfactants are classified by the hydrophilic-lipophilic balance values which were established by Griffin into water miscible and immiscible surfactants.^[36, 178] Thus, nanocarriers synthesized in direct miniemulsion are stabilized with water-soluble surfactants, which have a HLB value larger than 8, including ionic surfactants like SDS,^[234, 235] CTMA-Cl/Br^[236] or non-ionic surfactant as LutensolAT50.^[234, 235] If nanocarriers are prepared by the inverse miniemulsion, first oil-soluble surfactants have to be employed, normally with a HLB

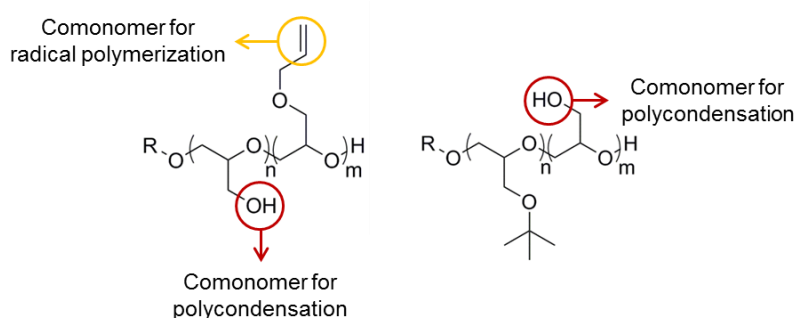
value between 4 and 8.^[36, 178] For most applications, the obtained nanocarriers have to be transferred into water. Therefore, a second water-soluble surfactant has to be inserted to stabilize the nanocarriers in water by the use of an additional surfactant, often SDS.^[17, 163, 224] Hence, the inverse miniemulsion is one example, where different types of surfactants have to be added to produce one material. A drawback of the currently used oil-soluble surfactants is their presence on the surface after transfer into water. Thus, in water the oil-soluble surfactants would shield the nanocapsule surface, which influences surface modification and further applications, especially in complex fluids, such as blood.^[163] In addition, most of these surfactants are only used as stabilizers without additional function. For such cases, surfactants, which could switch their amphiphilicity on requirement or would be incorporated like surfmers (surfactant and monomer),^[165, 236, 237] led to less shielding of the nanocarrier surface and decreased waste production. Therefore, non-toxic biocompatible surfactants were employed including pH-, T-, light- or redox-sensitive groups to have the opportunity to change their solubility on demand as summarized in chapter 1.1 to reduce waste production and make surface functionalization simple by less shielding. However, most of these surfactants led to flocculation or aggregation of the stabilized material, whereat only a low amount had additional functions. Müllen et al.^[14] generated a photo-cleavable PEG-based surfactant, which stabilized poly(L-lactide) (PLLA) nanoparticle in oil and during the transfer step in water due to the cleavage of the light sensitive protection group. After deprotection the polymer got water soluble and kept the nanoparticles stable in water. Certainly, the cleaved protection groups are toxic, thus this surfactant is not suitable for biomedical applications.

Most commonly used non-ionic amphiphilic block copolymers as surfactant independent of the miniemulsion type were based on PEG as hydrophilic block and different hydrophobic blocks with various PEG:alkyl ratios.^[163, 238, 239] However, alternatives to PEG are currently under debate, because PEG also has some drawbacks, such as reported immunogenicity,^[240, 241] and only includes one functional group at the chain end to attach further groups. A promising biocompatible alternative is PG,^[242] which can be produced with a linear^[243-246] or hyperbranched^[247-249] structure dependent on the used monomer and polymerization technique with defined block length ratios. PG is an alternative to PEG, because it has a similar structure including hydroxyl groups in every monomer unit for further

functionalization. In addition, polyglycerols are more stable against oxygen^[243] than PEG with similar protein repellent properties.^[250, 251] Thus in prior studies, they were used as linear multifunctional polyethers in biomedical and pharmaceutical applications.^[245] One example of a commercially available PG surfactant is polyglycerol-polyriccinoleate (PGPR), which is an oil-soluble stabilizer for inverse (mini)emulsions.^[212, 214] The formation of water-soluble PG-based surfactants was achieved by replacing PEG in Pluronic (PEG-PPO-PEG) surfactants.^[252-254] The PG-based Pluronic derivatives (PG-PPO-PG) were synthesized by anionic ring-opening polymerization of EEGE using poly(propylene oxide) (PPO) as macroinitiator followed by deprotection of the acetyl groups in acidic media with variation of the PPO (2000 and 4000 g mol⁻¹) and PG (10 to 84 wt%) block length ratios.^[252-254] Critical micelle concentration of the different block copolymers depend on the introduced PG block length, in which the CMC values decreased by increasing temperature.^[252, 253] However, the aggregation number of the formed micelles and the sizes of the generated particles were larger compared to the commercially available Pluronics.^[255, 256] Furthermore, surfmers based on polyglycerols were studied by Dworak et al.,^[246] who synthesized a PG-based surfmer by anionic ring-opening polymerization of EEGE terminated with *p*-chloromethyl styrene. After cleavage of the acetal groups under mild acidic conditions, PS microspheres were produced with bimodal size distribution and diameters of 216 and 900 nm.^[20] The generated microspheres with protein-repellent character were used in medical diagnostics after postfunctionalization with proteins (antigens or antibodies).^[21, 257, 258] In addition, linear and hyperbranched oligoglycerol macromonomers were tested as surfmer in free-radical emulsion polymerization of styrene to generate polystyrene particles with sizes of 100 to 600 nm, in which branched surfmers produced more effective monodisperse particles at lower concentrations.^[259] However, only less amount of functional PG-based surfactants or surfmers, including one reactive group to introduce the surfmer into the particles, exist for the miniemulsion approach.

Herein, two different orthogonal protection strategies were used to synthesize linear completely polyglycerol-based block copolymers with defined block length ratios to tune their hydrophilic-lipophilic balance. The block copolymers were synthesized by the anionic ring-opening polymerization in bulk using EEGE in combination with AGE or *t*BuGE as the hydrophobic segments. After acidic hydrolysis

of the acetal groups, the polymers reached an amphiphilic structure with surface and interfacial active behavior. Depending on the block ratios they were either water- or oil-soluble and could be applied as surfactants or surfmers for direct, inverse or both miniemulsions. The water-soluble allyl-functionalized PG block copolymers were used as surfmers in the radical miniemulsion polymerization of styrene (Scheme 3). Insertion was studied by proton diffusion NMR spectroscopy. The surfmer was further tested to stabilize the synthesized nanoparticles in citrated human blood plasma due to the protein repellent character of PG. The oil-soluble allyl-functionalized block copolymers were used as surfmer to produce polyurethane nanocapsules by polyaddition reactions of 1,4-butanediol or HES with TDI. Because the isocyanate groups react with all existing hydroxyl groups, also the polyglycerol block copolymer could be incorporated into the nanocarriers (Scheme 3). In addition, the allyl-protection groups on the polyurethane nanocarrier surface were used for further surface functionalization by thiol-ene addition in water. For this purpose, the nanocarriers were transferred into water including water soluble-surfactants like SDS, Lutensol or a water-soluble *tert*-butyl protected polyglycerol block copolymers. The *tert*-butyl protected polyglycerol block copolymers could also be used as surfmer in polyaddition miniemulsions (Scheme 3). However, in this chapter they were only used as surfactant to generate polystyrene nanoparticles in direct miniemulsions for comparison with the allyl-protected surfmer and in inverse miniemulsions to produce stable PHEMA and PAA nanoparticles by free-radical polymerization.



Scheme 3. Allyl-protected polyglycerol block copolymers as surfmers in free-radical miniemulsion polymerization or in polyaddition/polycondensation miniemulsion. The *tert*-butyl protected polyglycerol block copolymers were used as surfactants in free-radical miniemulsion polymerization. Due to the hydroxyl side chain the *tert*-butyl protected block copolymers could also be used as surfmers in polyaddition miniemulsions. R = (CH₂)₃-Ph.

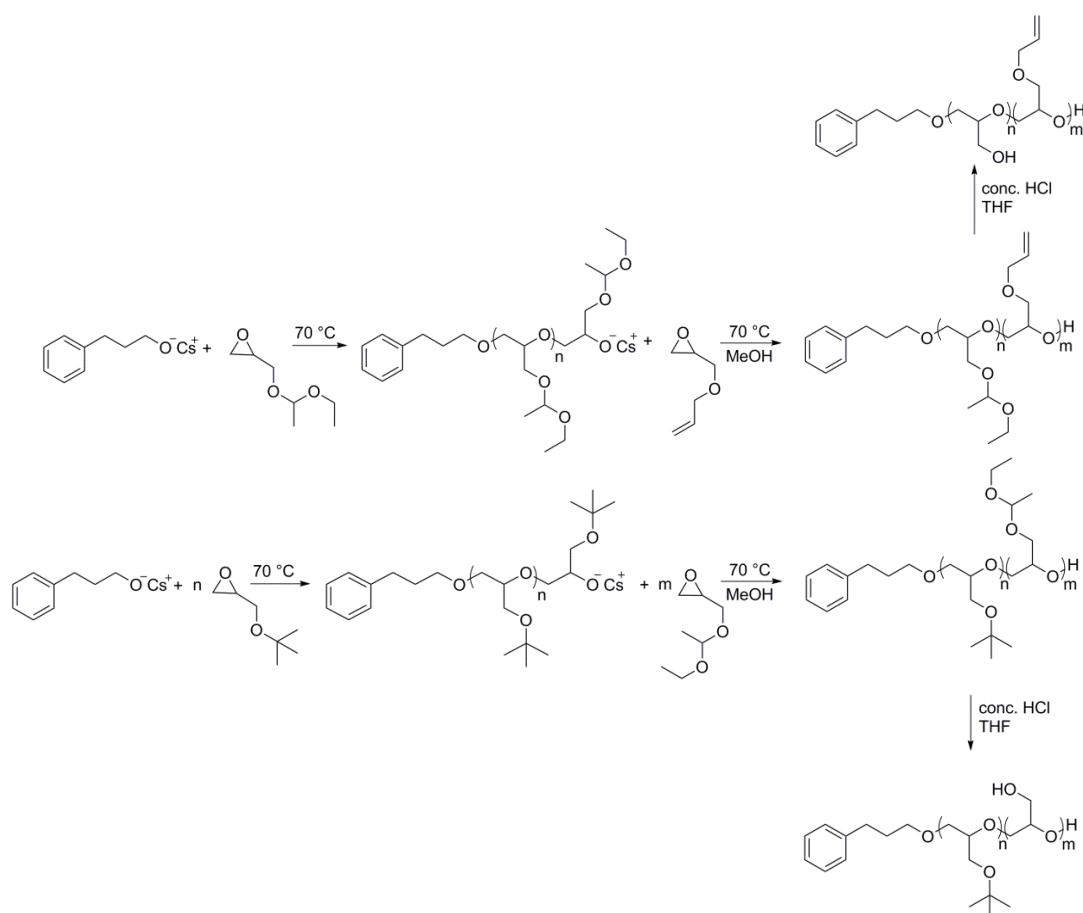
Results and Discussion

Synthesis of amphiphilic polyglycerol block copolymers

PG block copolymers with defined block length ratios were obtained by sequential anionic ring-opening polymerization with cesium alkoxides^[260, 261] as initiators. To obtain linear block copolymers including one hydroxyl block, monomers with different protection groups, which can be removed separate from each other without influencing all other protection groups, have to be used. A common linear PG copolymer with selective cleavage was produced using the monomers *t*BuGE (commercially available) and EEGE, which was synthesized as reported by Fitton *et al.*^[262] This monomer configuration was used in several publications to produce random^[263] or block^[264] copolyglycerols, because the acetal group can be cleaved under mild acidic conditions, whereat the removal of the *tert*-butyl groups is achieved at strong acidic conditions. After cleavage of the protection groups, the hydroxyl groups could further be used for post-functionalization of the side chain to change the polymer properties or to introduce other functional groups.^[264] In addition to the EEGE and the *t*BuGE, Erberich *et al.*^[263] used AGE as monomer to reach homopolymers or orthogonal protected random copolymers of EEGE, *t*BuGE and AGE. The AGE was used as the third monomer, because it is stable under acidic conditions and could be removed using Pd/C, in which the ethoxyethyl and *tert*-butyl groups keep stable. AGE was also incorporated into the PG, because the generated polymer could be post-modified using thiol-ene reactions. Thus, further functionalities like hydroxyl, amine or carboxyl groups as well as peptides were introduced in prior studies into the allyl protected PGs.^[265]

As shown in Scheme 4, herein two different orthogonal protected block copolymers with various block length ratios, controlled degree of polymerization and narrow molecular weight distribution (PEEGE₃₆-*b*-PAGE₁₄ (**P1-2**), PEEGE₁₇-*b*-PAGE₁₇ (**P2-2**), PEEGE₁₃-*b*-PAGE₂₈ (**P3-2**), P*t*BuGE₁₅-*b*-PEEGE₃₅ (**P4-2**) and P*t*BuGE₃₁-*b*-PEEGE₂₈ (**P5-2**), Table 6) were synthesized by anionic ring-opening polymerization. In general, the polymerization was initiated using the cesium salt of 3-phenylpropanol at 70 °C in bulk followed by sequential monomer addition, in which AGE was added as second monomer due to lower reactivity compared to EEGE and *t*BuGE to reach a narrow size distribution.^[263] The acetal protection groups were

removed in all block copolymers with concentrated HCl in THF to obtain the amphiphilic structure and different solubility due to different block length ratios.



Scheme 4. Synthesis of orthogonal protected PG using allyl glycidyl ether or *tert*-butyl glycidyl ethers in combination with ethoxyethyl glycidyl ether by anionic polymerization. Deprotection of the acetal block lead to amphiphilic block copolyglycerols.

Polymer characterization

The block ratios as well as the molecular weights of all polymers were analyzed by ^1H -NMR comparing the integrals of the initiator with defined integrals of both repeating units, as shown in Figure 9 and summarized in Table 6. PEEGE₁₃-*b*-PAGE₂₈ was used as example (Figure 9): the integral of the aromatic initiator at 7.21 ppm were compared with the integral at 5.84 ppm of one CH allyl group and the CH₂ group at 3.93 ppm, in order to calculate the number of repeating units of the AGE monomer. The repeating units of EEGE were determined by comparison of the acetal proton's resonance at 4.64 ppm to the benzene groups and the allyl groups. Thus,

PEEGE-*b*-PAGE with three different block length ratios of PEEGE₃₆-*b*-PAGE₁₄ (**P1-2**), PEEGE₁₇-*b*-PAGE₁₇ (**P2-2**) and PEEGE₁₃-*b*-PAGE₂₈ (**P3-2**) were synthesized (Table 6). The block length ratios of the P*t*BuGE-*b*-PEEGE, using P*t*BuGE₃₁-*b*-PEEGE₂₈ as example, were also determined by the ¹H-NMR with the same method. However, the CH groups of the benzene ring did not serve as reference, because these polymers were dissolved in deuterated chloroform instead of DMSO. Thus, there was an overlap of the solvent peaks with the benzene protons. The block length ratio of these block copolymers was analyzed using the CH₂ groups of the initiator derived from the propyl group at 2.67 and 1.86 ppm. In addition, the CH and CH₃ protons of *t*BuGE around 1.36 and 1.01 ppm overlap with the CH₃ groups of the ethoxyethyl groups, which made analysis of the *tert*-butyl repeating unit difficult in the block copolymer spectrum. Because the *t*BuGE was polymerized first, the repeating unit of this block was analyzed in the ¹H-NMR spectrum of the first block assuming full conversion. The repeating units of EEEGE were evaluated as before using the CH group at 4.64 ppm. Thus, block copolymer with two different block length ratios of P*t*BuGE₁₅-*b*-PEEGE₃₅ (**P4-2**) and P*t*BuGE₃₁-*b*-PEEGE₂₈ (**P5-2**) were synthesized (Table 6). To use the generated block copolymers as surfactant, the acetal groups were removed by acidic hydrolysis. Complete deprotection is proven by ¹H-NMR (Figure 9) as the resonances for the acetal protection group disappear (CH group at 4.6 ppm and CH₃ groups at ca. 1.25 ppm).

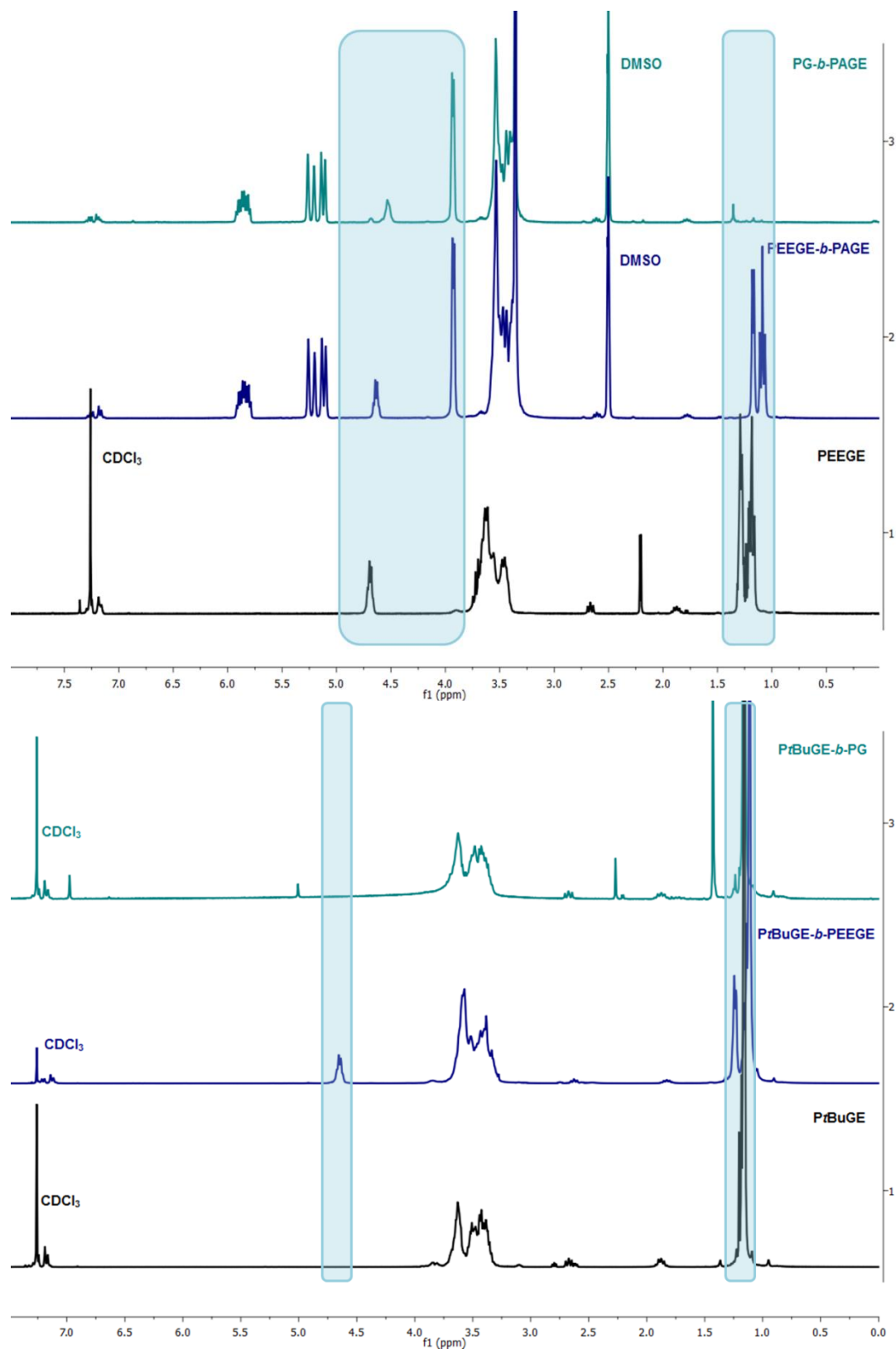


Figure 9. ^1H -NMR spectra (300 MHz, DMSO- d_6 or CDCl_3 , 293 K or 25 °C) of first block (black), protected block copolymers (blue) and deprotected block copolymers (cyan blue) of **P3** (PGE₁₃-*b*-PAGE₂₈, top) and **P5** (P*t*BuGE₃₁-*b*-PGE₂₈, bottom).

Molecular weight distribution was determined by size exclusion chromatography using dimethylformamide as solvent. All polymers prepared by this method exhibited monomodal molecular weight distributions and low polydispersities ($PDI = M_w/M_n$) below 1.2 (Figure 10 and Table 6). The molecular weights obtained from SEC were underestimated compared to molecular weights from $^1\text{H-NMR}$ spectroscopy (Table 6), due to the conventional calibration and comparison to PEG standards. The multiple protection groups and hydroxyl groups in PG polymers led to hydrophobicity changes, therefore, have an impact on the hydrodynamic volume and the elution volume and consequently, occurred in determination of lower molecular weights.

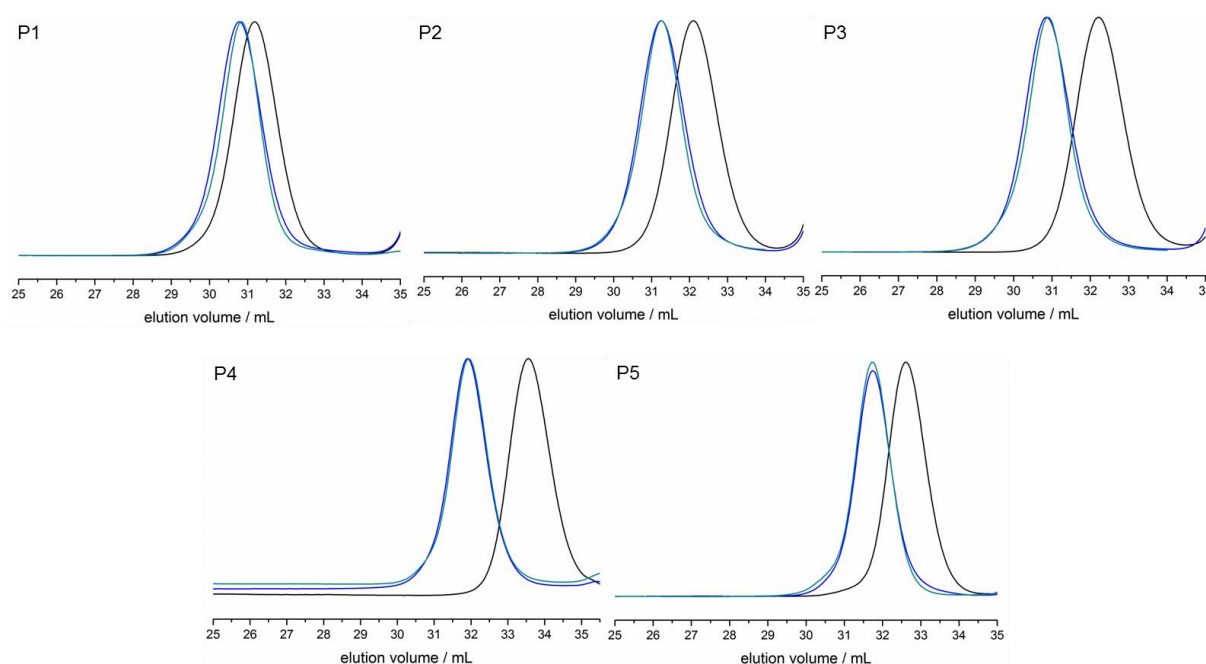


Figure 10. SEC elugrams (DMF, 60 °C or 333 K, RI detection, 1 mL min⁻¹) of first block (black curve), protected block copolymers (blue curve) and deprotected block copolymers (cyan blue curve) of **P1**, **P2**, **P3**, **P4** and **P5**, all SEC traces were normalized.

The thermal behavior of all deprotected block copolymers was studied by differential scanning calorimetry (Figure 11). In contrast to highly crystalline PEG with a melting point of ca. 63 °C,^[37] linear polyglycerols are amorphous materials, because of distribution of dense polyether chain order due to the additional hydroxyl groups in every monomer unit. The glass transition temperatures (T_g) of linear polyglycerols are in the range of -8 °C to -27 °C.^[266-268] In addition, the herein prepared block copolyglycerols are amorphous and viscous materials. Phase

separation in bulk was proven by the existence of two glass points in the allyl-functionalized block copolymers with the T_{g1} of $-70\text{ }^{\circ}\text{C}$ for PAGE and the T_{g2} between $-48\text{ }^{\circ}\text{C}$ and $-34\text{ }^{\circ}\text{C}$ for the PG block (Figure 11). The *tert*-butyl protected block copolymer exhibited only one T_g between $-29\text{ }^{\circ}\text{C}$ and $-14\text{ }^{\circ}\text{C}$ (Figure 11), probably in those samples the difference between the two T_g 's is too close and cannot be resolved in the DSC measurement.

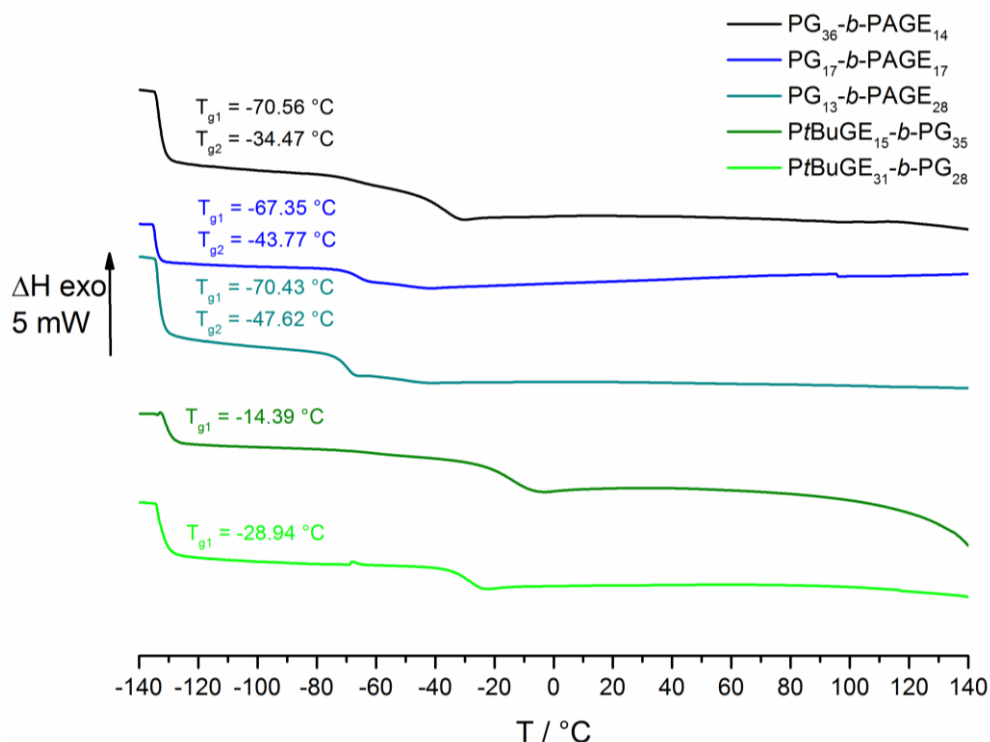


Figure 11. Differential scanning calorimetry (DSC) results of the generated block copolymer after deprotection of the acetal groups.

Surface active properties

To identify the potential of the PG-block copolymers as surfactant or surfmer, their solubilities were tested in water, cyclohexane and toluene. In addition, the HLB of all block copolymers were calculated by the method of Griffin (Table 6).^[36, 178] The deprotected block copolymers **P2**, **P3** and **P5** had HLB values between 4 and 8 and were soluble in toluene. Furthermore, **P5** was also soluble in cyclohexane. Thus, these amphiphilic block copolymers should be used as stabilizer in inverse miniemulsions using toluene or cyclohexane as solvents in the continuous phase. **P1** and **P4** with HLB values of 11 and 12 were soluble in water and suitable as

surfactants for direct miniemulsions. In addition, **P5** was soluble in water. Hence, this block copolymer was tested as surfactant for direct and inverse miniemulsions.

The surface-active properties of the block copolymers were studied by determination of the critical micelle concentration. The CMC of the water-soluble block copolyglycerols **P1** and **P4** was investigated utilizing the ring tensiometer at 22 °C. The allyl protected block copolymer **P1** decreased the surface tension of water from 72 mN m⁻¹ to 34 mN m⁻¹. The critical micelle concentration was reached at a concentration of ~0.16 mg mL⁻¹ (Figure 12). The CMC of **P4** was analyzed at a concentration of 0.07 mg mL⁻¹ with a decrease of the surface tension of around 42 mN m⁻¹, from 72 mN m⁻¹ to 30 mN m⁻¹ (Figure 12). Comparing the CMC of **P1** and **P4** with other non-ionic water soluble amphiphilic PEG based block copolymers like Lutensol AT50 (C₁₆₋₁₈-alkyl-*block*-PEG₅₀) with a hydrophilic block length (EO) of 50 and a CMC of 0.03 mg mL⁻¹,^[269] the CMC of **P4** is in a similar range, whereat the CMC of **P1** is one order of magnitude larger, indicating a lower interfacial activity. However, both block copolymers showed surface active behavior and were tested as stabilizer to generate stable polystyrene nanoparticles.

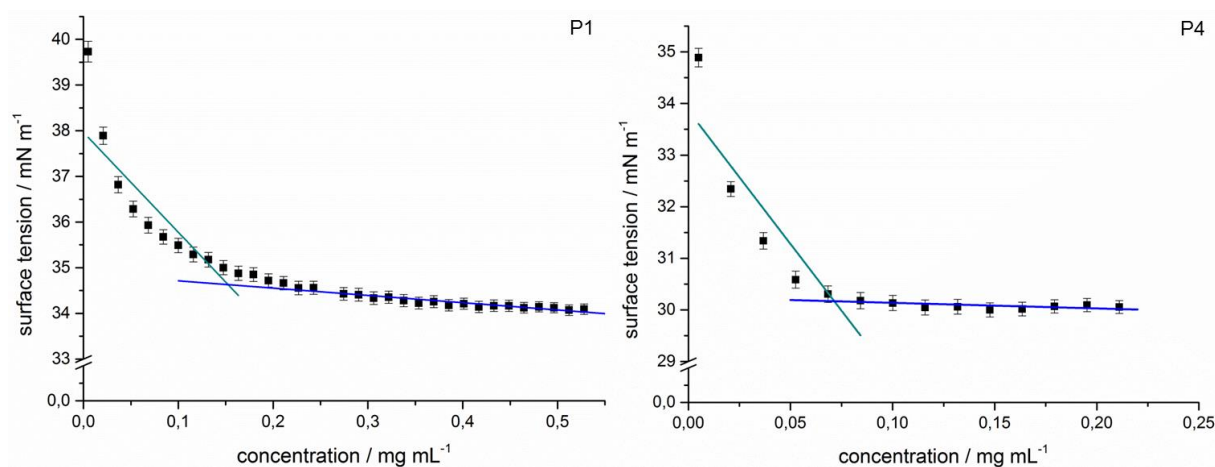
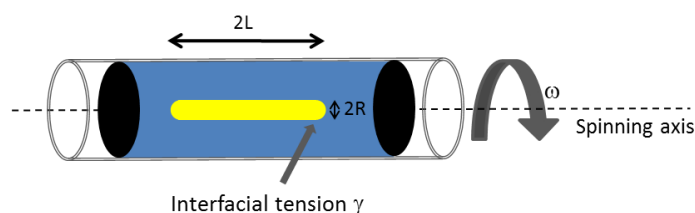


Figure 12. Determination of the critical micelle concentration (CMC) using ring tensiometer measurements at 22 °C of deprotected **P1** (0.16 ± 0.03 mg mL⁻¹) and **P4** (0.07 ± 0.01 mg mL⁻¹) in pure water.

The surface active properties of the two oil-soluble PG-*b*-PAGE block copolymers with two different block length ratios (**P2** and **P3**) were studied with the spinning drop method. Furthermore, in the spinning drop method interfacial tensions less than 10⁻² mN m⁻¹ can be measured. The CMC of the block copolymers were compared with the commonly used P(E-co-B)₃₃-*b*-PEG₅₈ surfactant in inverse miniemulsions, which was

determined by the same method. The spinning drop analysis was first proposed by Bernard Vonnegut in 1942 to identify the interfacial or surface tension of a rotating droplet.^[270] During the method a small droplet of an immiscible liquid (herein toluene including different surfactant concentrations) was mixed with a liquid (here water). Due to horizontal rotation of the mixture as shown in Scheme 4, the drop forms a cylindrical shape at the equilibrium state in the center of the tube because of centrifugal force.



Scheme 4. Spinning drop method.

The surface or interfacial tension is calculated using Eq.1, which was suggested by Vonnegut considering the following conditions. If the centrifugal force is balanced by the surface tension forces, the elongation of the drop stops at circular cylindrical form (length of drop > radius) with hemispherical ends and negligible effect of gravity at increased speed of rotation. At this point it is possible to write an equation for the total energy of the droplet and solve it for the equilibrium state with the minimum energy to

$$\gamma = \frac{\Delta\rho\omega^2}{4} R^3 \quad (1)$$

where γ is the interfacial tension, $\Delta\rho$ the density difference between the phases, ω the angular speed and R the radius of the cylindrical drop. Differently to the ring tensiometer analysis, where one stock solution was added dropwise into the solvent, several solutions with different block copolymer concentrations had to be measured separate from each other.

According to this method, an interfacial tension of 33.3 mN m^{-1} of a water-toluene mixture without the addition of any surfactant was determined at 22°C (in literature, $\gamma = 36.1 \text{ mN m}^{-1}$ at 20°C).^[271] The interfacial tensions of **P2** and **P3** toluene solutions against water in dependence on different block copolymer concentrations were summarized in Figure 13. As expected, the interfacial tension of all solutions decreased by increasing polymer concentration until the CMC was reached. The

CMC of **P2** in toluene was detected to be 0.05 mg mL^{-1} by decreasing the interfacial tension down to 5 mN m^{-1} . The CMC of **P3** in a toluene-water emulsion was similar to of **P2** of ca. 0.05 mg mL^{-1} and decreased the interfacial tension to 5 mN m^{-1} . However, the values for the CMC could not be determined very accurately, because the interfacial tension slightly decreased during the whole analyzed concentration range. In comparison, the CMC of $\text{P(E-co-B)}_{33}\text{-}b\text{-PEG}_{58}$ was also detected as 0.05 mg mL^{-1} with a decrease of the interfacial tension to 4 mN m^{-1} . This indicates a similar performance of the PG-block copolymers.

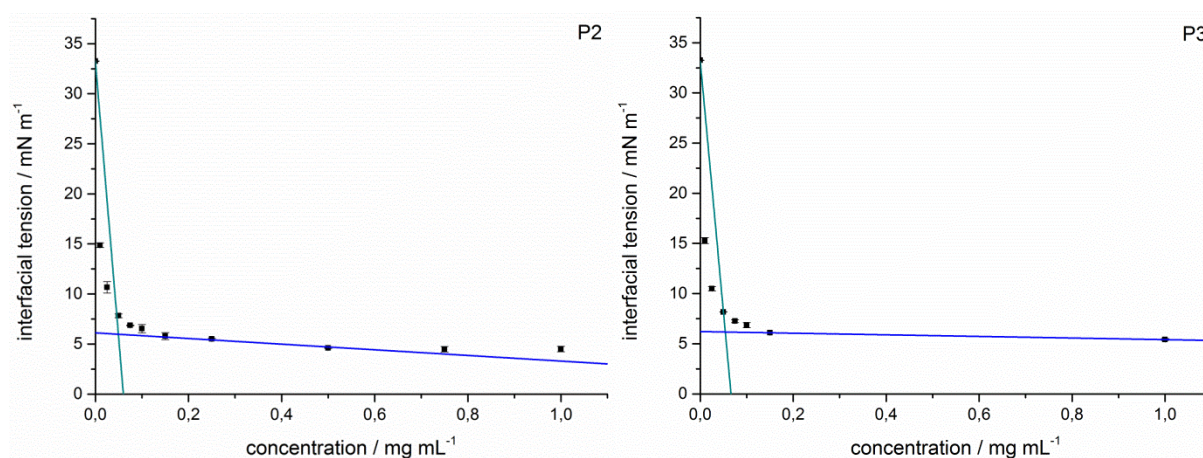


Figure 13. Critical micelle concentration determination of deprotected **P2** ($\text{PG}_{17}\text{-}b\text{-PAGE}_{17}$, $0.05 \pm 0.02 \text{ mg mL}^{-1}$) and **P3** ($\text{PG}_{13}\text{-}b\text{-PAGE}_{28}$, $0.05 \pm 0.02 \text{ mg mL}^{-1}$) by the spinning drop method using different concentrations of the polymer in toluene (between 0 mg mL^{-1} and 1 mg mL^{-1}) at the toluene water interface at 22°C .

$\text{P}t\text{BuGE}_{31}\text{-}b\text{-PG}_{28}$ (**P5**) was soluble in water and cyclohexane. Thus, the surface active properties of the polymer were also tested at the water-air surface, by diluting 1 mg mL^{-1} of the polymer in water. The surface tension decreased from 72.53 mN m^{-1} (pure water, in literature $\gamma = 72.75 \text{ mN m}^{-1}$ at 20°C)^[272] to 34.65 mN m^{-1} at 22°C . Furthermore, the CMC of **P5** in water was measured by isothermal titration calorimetry and seemed to be below 0.1 mmol L^{-1} ($< 0.63 \text{ mg mL}^{-1}$). However, the CMC could not be clearly detected, because no significant heat flow was measured below 0.1 mmol L^{-1} . Thus, the concentration range relevant for the cmc seemed to be too low for determination with ITC (isothermal titration calorimetry).

Table 6. Summary of generated orthogonal protected and selectively deprotected polyglycerol block copolymers.

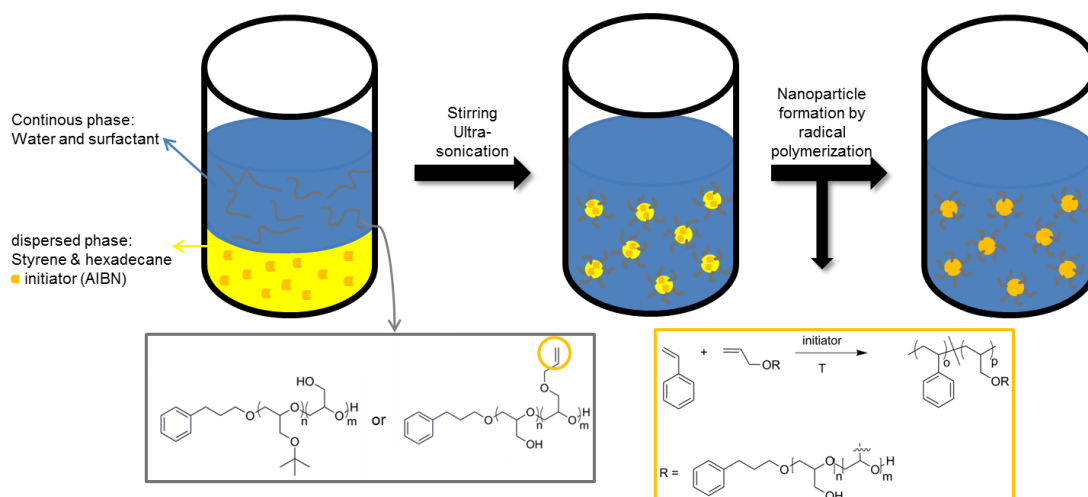
	DP _n	Monomer /mmol	M _n ^{NMR} /g mol ⁻¹	M _n ^{SEC} /g mol ⁻¹	\bar{D}^a	Tg ¹ / °C	Tg ² / °C	HLB ^b	CMC/ mg mL ⁻¹
P1-1	PEEGE ₃₆	25	5400	2200	1.13				
P1-2	PEEGE ₃₆ - <i>b</i> -PAGE ₁₄	8.5	7000	2700	1.13				
P1	PG ₃₆ - <i>b</i> -PAGE ₁₄	-	4400	2800	1.10	-70.56	-34.47	12	0.16 ± 0.03 ^b
P2-1	PEEGE ₁₇	12.5	2600	1300	1.17				
P2-2	PEEGE ₁₇ - <i>b</i> -PAGE ₁₇	12.5	4600	2100	1.15				
P2	PG ₁₇ - <i>b</i> -PAGE ₁₇	-	3400	2200	1.12	-67.35	-43.77	7	0.05 ± 0.02 ^c
P3-1	PEEGE ₁₃	10	2000	1200	1.17				
P3-2	PEEGE ₁₃ - <i>b</i> -PAGE ₂₈	20	5300	2600	1.14				
P3	PG ₁₃ - <i>b</i> -PAGE ₂₈	-	4300	2600	1.11	-70.43	-47.62	5	0.05 ± 0.02 ^c
P4-1	PtBuGE ₁₅	8.5	2100	800	1.17				
P4-2	PtBuGE ₁₅ - <i>b</i> -PEEGE ₃₅	24.5	7200	2300	1.12				
P4	PtBuGE ₁₅ - <i>b</i> -PG ₃₅	-	4700	2300	1.10	-28.94	-	11	0.07 ± 0.01 ^b
P5-1	PtBuGE ₃₁	12.5	4100	1400	1.11				
P5-2	PtBuGE ₃₁ - <i>b</i> -PEEGE ₂₈	12.5	8100	2400	1.09				
P5	PtBuGE ₃₁ - <i>b</i> -PG ₂₈	-	6300	2500	1.09	-14.39	-	7	< 0.63 ^d

a) $\bar{D} = M_w/M_n$, b) calculated by the method of Griffin,^[36, 178] c) CMC in water at 22 °C, d) in toluene at 22 °C, e) in water at 25 °C.

Surfactant / Surfmer for polystyrene nanoparticles in direct miniemulsion

The water-soluble PG₃₆-*b*-PAGE₁₄ was studied as surfmer due to incorporation of the allyl-protection groups during polymerization and compared with the non-polymerizable surfactant PtBuGE₁₅-*b*-PG₃₅ in direct free-radical miniemulsion polymerization of styrene. Polystyrene nanoparticles were produced as a model system, because they can be generated in a single step with monodisperse size distribution and defined particle size.

In a direct miniemulsion, the surfactant is dissolved in water (continuous phase) and mixed with a defined amount of a styrene, initiator and hexadecane as osmotic stabilizer (Scheme 5). After ultrasonication, styrene nanodroplets partially covered with surfactant were generated and polymerized by free-radical polymerization of styrene at 70 °C.



Scheme 5. Scheme to produce polystyrene nanoparticles by free-radical miniemulsion polymerization in water using **P4** (*Pt*BuGE₁₅-*b*-PGE₃₅) as surfactant or **P1** (PG₃₆-*b*-PAGE₁₄) as surfactant and comonomer.

P1 (surfmer) and **P4** (surfactant) were used to produce stable nanoparticles. After optimization by changing the surfactant, surfactant concentration and the temperature, the conditions and results of obtained stable polystyrene nanoparticles were summarized in Table 7.

Table 7. Summary of conditions to produce polystyrene nanoparticles and obtained mean diameters using **P4** (P*t*BuGE₁₅-*b*-PG₃₅) as surfactant or **P1** (PG₃₆-*b*-PAGE₁₄) as surfmer in direct miniemulsions.

Entry	Type of surfactant	$c_{\text{surfactant}}/\text{mg mL}^{-1}$	wt% surfactant to styrene	T/°C	d^{DLS}/nm
ME1	P4	1.19	4.67	70	230
ME2	P1	1.00	3.92	70	510/4000
ME3	P1	1.04	4.08	100	230

Stable polystyrene nanoparticles were generated using a surfactant concentration of 1.19 mg mL⁻¹ of **P4** at 70 °C. The synthesized nanoparticles had mean diameters of 230 nm determined by dynamic light scattering (DLS) and confirmed by scanning

electron microscopy with narrow size distribution (Figure 14, **ME1**). If the surfmer **P1** was used at 70 °C with a concentration of 1 mg mL⁻¹, nanoparticles with mean diameters of 510 nm were analyzed by DLS besides aggregated nanoparticles. In SEM diameters between 220 and 580 nm were detected (Figure 14, **ME2**). It seemed that the nanoparticles partially aggregate during polymerization. In addition, the surface of the generated nanoparticles was covered with small bullets, which could be a result of phase separation of adsorbed PG block copolymers on the nanoparticle surface or incorporated PG block copolymers in the polystyrene chains. An increase of the used surfmer concentration also led to aggregated nanoparticles. An increase of the temperature to 100 °C (**ME3**) with a surfmer concentration of 1 mg mL⁻¹ led to stable single polystyrene nanoparticles with mean diameters of 230 nm in DLS and diameters between 140 to 300 nm in SEM (**ME3**, Figure 14). Thus, increasing the temperature from 70 °C to 100 °C resulted in smaller nanoparticles without any aggregation. Indeed, the nanoparticles generated at 100 °C using the surfmer **P1** exhibited bigger size distribution than the ones generated with the surfactant **P4** at 70 °C. The polydisperse size distribution could be a consequence of decreased amphiphilicity of the surfmer during nanoparticles synthesis, which could maintain in less nanoparticle stability and led in nanoparticles coalescence.

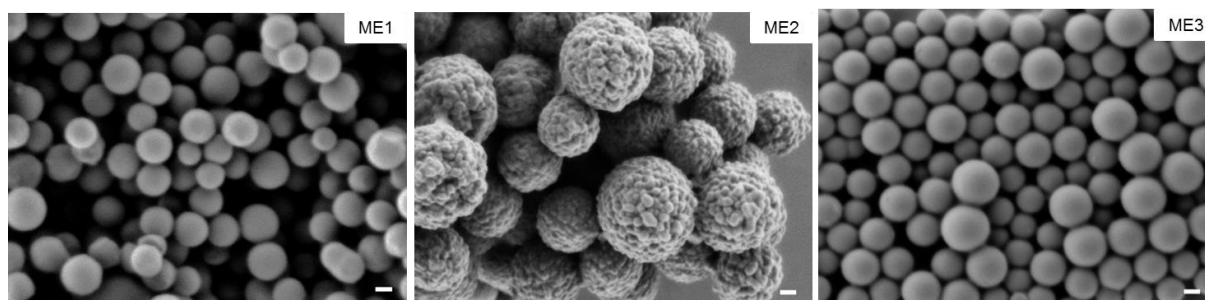


Figure 14. Scanning electron microscopy images (SEM, scale bar 100 nm) of generated polystyrene nanoparticles using **P4** as surfactant (**ME1**) or **P1** as surfmer (**ME2** and **ME3**).

In addition, mixtures of **P1** and **P4** were tested as stabilizers at 70 °C to generate stable polystyrene nanoparticles, in which **P1** should be incorporated into the nanoparticle. If a 1:1 mixture of **P1** (0.5 mg mL⁻¹) and **P4** (0.5 mg mL⁻¹) was used, nanoparticles with a mean diameter of 330 nm besides aggregates were determined by DLS. In SEM polydisperse nanoparticle were detected with diameters between 100 nm to 600 nm in aggregated nanoparticles (**ME4**, Figure 15). Because **P4** alone

showed good stabilization behavior at 70 °C, a higher amount of **P4** in combination with **P1** was tested to decrease the nanoparticle size and avoid aggregation. A mixture of 1:3 of **P1** (0.25 mg mL^{-1}) and **P4** (0.76 mg mL^{-1}) was studied to stabilize polystyrene nanoparticles (**ME5**). In DLS mean diameters of 186 nm were investigated, but also low percentage of diameters between 600 to 865 nm were detected. In SEM, nanoparticles with polydisperse size distribution were analyzed including sizes of 100 nm up to 800 nm (Figure 15). Thus, a higher amount of **P4** in combination with **P1** generated stable single nanoparticles without aggregation compared to a 1:1 mixture. However, the size distribution of the obtained nanoparticles was still broad and has to be optimized in the future.

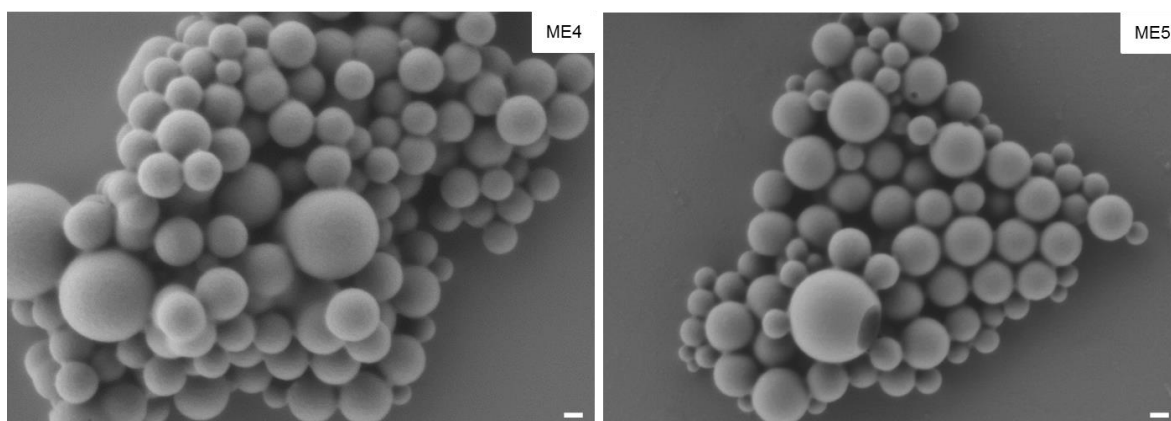


Figure 15. SEM (scale bar 100 nm) results of polystyrene nanoparticles stabilized with mixtures of **P1** and **P4** (**ME4** stabilized with 1:1 mixture and **ME5** stabilized with a 1:3 mixture).

Furthermore, different mixtures of the surfmer **P1** with the commercially available sodium dodecyl sulfate was tried as stabilizer to generate stable monodisperse polystyrene nanoparticles (Table 8), in which the nanoparticles shall be stable after complete removal of SDS. SDS was chosen, because it is a well-known commercially available ionic surfactant for direct miniemulsion, which formed monomodal polystyrene nanoparticles with defined nanoparticle sizes around 100 nm in diameter.^[234]

Table 8. Summary of optimized conditions to prepare polystyrene nanoparticles stabilized with different mixtures of **P1** as surfmer and the commercially available ionic surfactant SDS in direct miniemulsion.

Entry	$c_{P1}/\text{mg mL}^{-1}$	$c_{SDS}/\text{mg mL}^{-1}$	wt% surfactant to styrene	d^{DLS}/nm
ME6	1.11	3.04	16.27	80/260
ME7	1.03	1.02	8.05	100/210
ME8	1.26	0.50	6.91	160
ME9	1.27	0.99	8.87	140

A 1:3 wt% mixture of **P1** and SDS was used at 70 °C to generate stable polystyrene nanoparticles in water. In DLS polystyrene nanoparticles with mean diameters of 80 nm and 260 nm were detected. In SEM a polydisperse size distribution was detected including the identified diameters from DLS (Figure 16, **ME6**). Decreasing the amount of SDS and surfactant to styrene ratio, to reach a 1:1 mixture (1 mg mL⁻¹ of each surfactant) also maintained in polystyrene nanoparticles with mean diameters of 100 nm and 210 nm analyzed by DLS and polydisperse size distribution detected by SEM (Figure 16, **ME7**) similar to the results of **ME6**. Increasing the amount of **P1** to 1.26 mg mL⁻¹ (**ME8**, 2.5:1 mixture) by decreasing the amount of SDS to 0.5 mg mL⁻¹ led to more monomodal size distribution compared to **ME6** and **ME7** with mean nanoparticle diameters of 160 nm in DLS (Figure 16, **ME8**). The synthesized nanoparticles in **ME9** stabilized with a 1.3:1 mixture of **P1** to SDS had mean diameters of 140 nm detected by DLS. Thus, the nanoparticle sizes decreased with increasing surfactant to styrene ratio, as expected. In SEM still polydisperse size distribution was detected (Figure 16, **ME9**). In summary, a higher amount of **P1** compared to SDS in the surfactant mixture maintained in polystyrene nanoparticles with mean diameters between 140 nm to 160 nm.

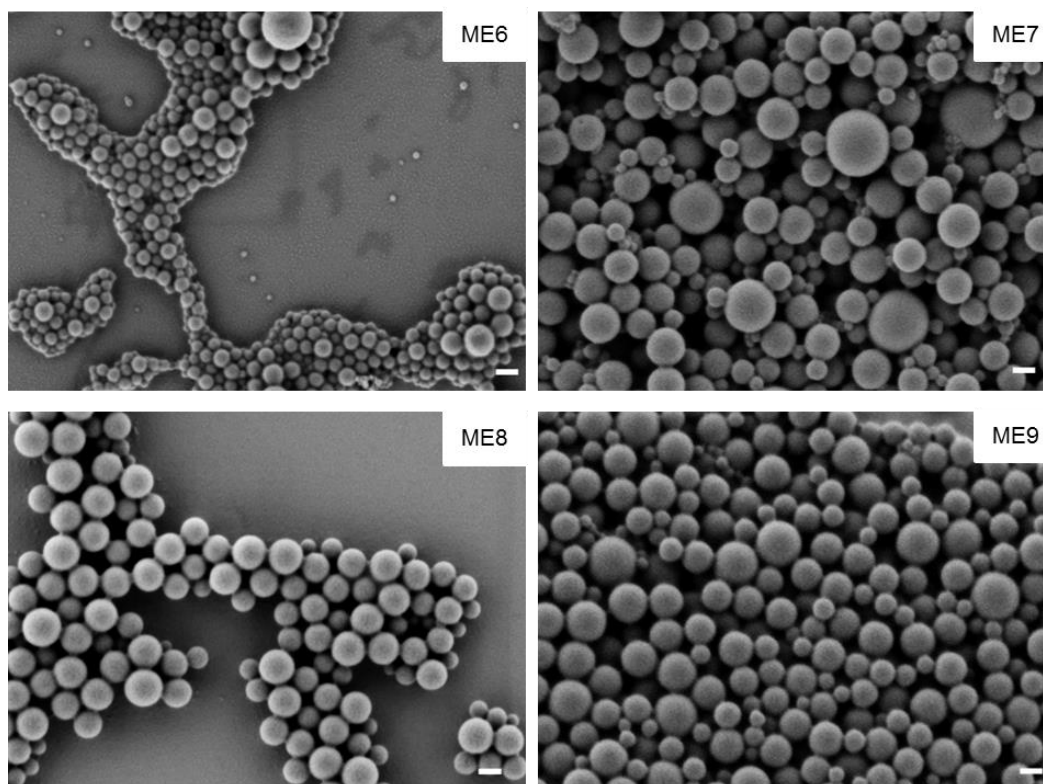


Figure 16. SEM images of the generated polystyrene nanoparticles using **P1** to SDS ratios of 1:3 (**ME6**), 1:1 (**ME7**), 2.5:1 (**ME8**), 1.3:1 (**ME9**), scale bar 100 nm.

Incorporation of the amphiphilic block copolymer **P1** into the polystyrene chain was analyzed by ^1H -Diffusion-Ordered NMR spectroscopy (DOSY). In Figure 17, the ^1H -DOSY-NMR spectrum of **ME8** is shown as representative for all other generated stable polystyrene nanoparticles, measured in deuterated THF. The x-axis shows the conventional ^1H -NMR spectrum of the whole mixture. The y-axis illustrates the diffusion coefficient. From the 2D plot it is clear that the chemical shift of polystyrene between 7.22-6.35 ppm and 2.07-1.32 ppm and the chemical shift of the **P1** backbone at 3.72-3.53 ppm appear at the same diffusion coefficient and the allyl peaks between 6 and 5 ppm disappeared. Thus, the allyl groups of the protected PG block copolymer were incorporated into the polystyrene nanoparticles and proofed the thesis, that **P1** could be used as surfmer in miniemulsion polymerization also in combination with non-ionic or anionic surfactants.

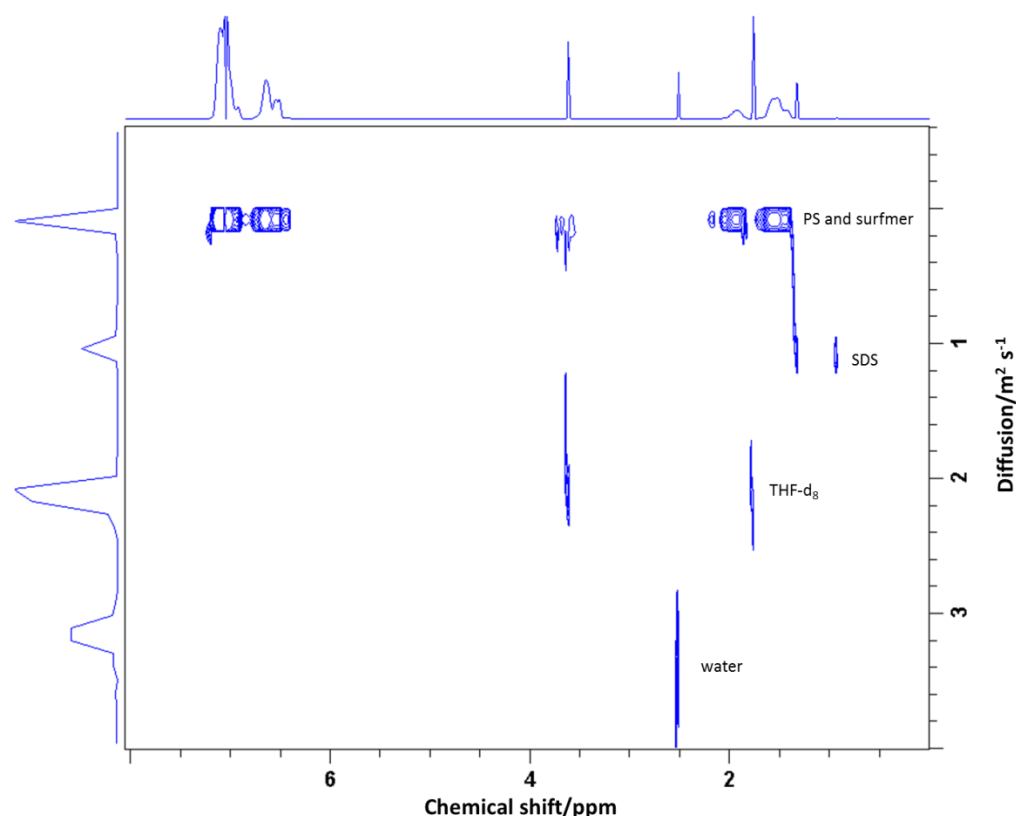


Figure 17. ^1H -DOSY-NMR spectrum of **ME8** dissolved in THF-d_8 (700 MHz, 298K) to determine incorporation of the surfmer into the polystyrene nanoparticle.

Because PG has similar properties in protein mixtures as PEG like decreasing protein adsorption, the stability of the herein produced PS nanoparticles with the covalent incorporated surfmer and adsorbed surfactant in blood plasma was studied by DLS.^[235] The nanoparticles (**ME6**, **ME8** and **ME9**) were incubated with human plasma after removal of any excess of SDS by dialysis. Afterwards, DLS of the nanoparticles in the protein mixtures was used to identify the stability of the PG-functionalized nanoparticles in protein mixtures and compared to the PS nanoparticles stabilized with **P4** (**ME1**), which adsorbed at the nanoparticle surface. The results of DLS analysis of all incubated dispersions were summarized in Figure 18. The stability in blood plasma of nanoparticles only stabilized with **P1** or mixtures of **P1** and **P4** could not be tested, because the sizes of the synthesized nanoparticles were too large or size distribution was too broad to give a clear statement of nanoparticle stability in a protein mixture. **ME1** in plasma led to macroscopic aggregated nanoparticles analyzed from the ascertained data points as shown in Figure 18, whereat the nanoparticle size in buffer solution and in water was between

230 and 270 nm detected by DLS. In **ME6** also macroscopic aggregates were detected from the determined data points. Indeed, the amount of aggregated nanoparticles was less compared to the one in **ME1**, which could be explained by covalent binding of the PG into the nanoparticles instead of adsorption of the surfactant at the nanoparticle surface. The higher amount of aggregates in **ME1** compared to **ME6** could be a reason of an exchange of adsorbed surfactant with present proteins. Increasing the amount of polyglycerol on the nanoparticle surface in **ME8** and **ME9** resulted in less aggregated nanoparticles compared to **ME1** besides single stabilized nanoparticles. Thus, the surfmer has the potential to stabilize polystyrene nanoparticles in protein mixtures better than the adsorbed PG surfactant with smaller nanoparticle aggregates using a higher amount of surfmer. Stabilization of these nanoparticles is possible using PG as surface functionalization, because of known decreased protein adsorption properties of polyglycerol.^[235] However, further stability tests in protein mixtures as well as cell uptake studies have to be done in the future. Furthermore, the protein amount and composition on the nanoparticle surface shall be analyzed in further tests.

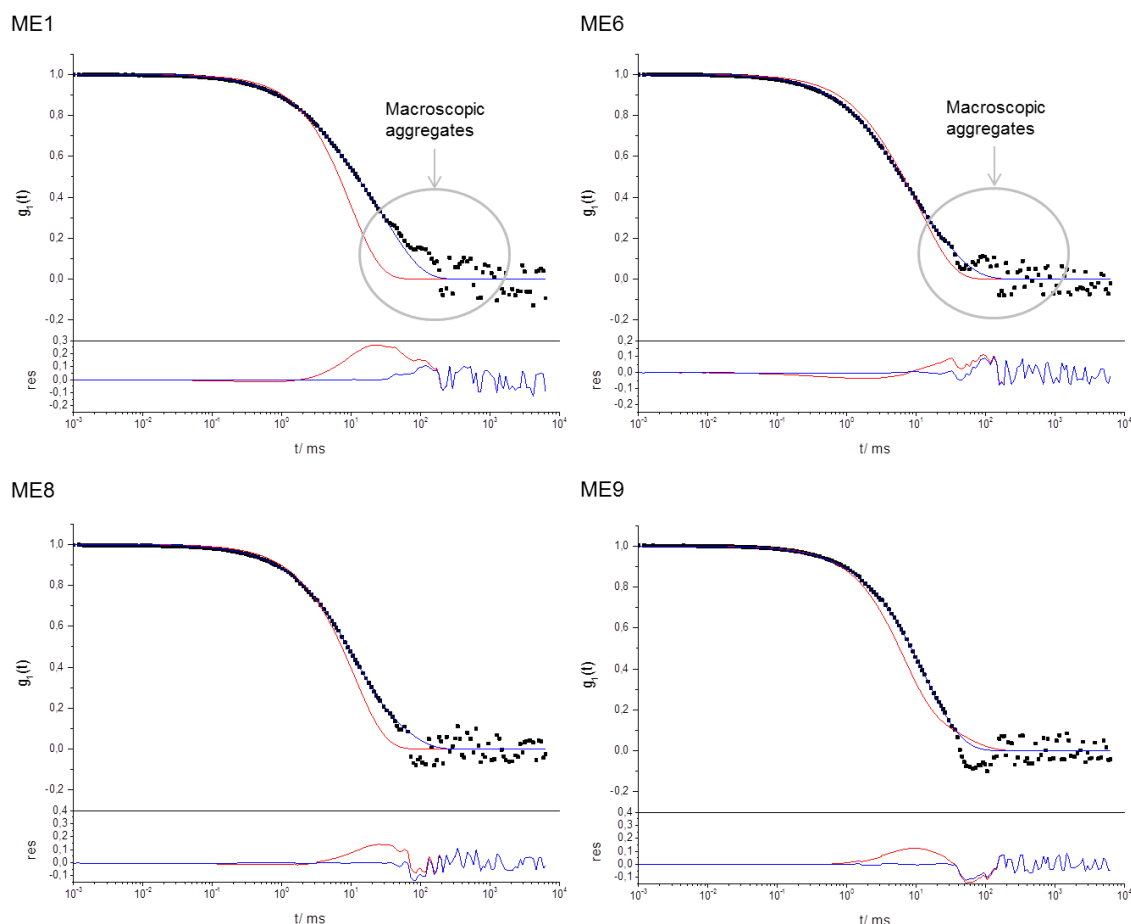
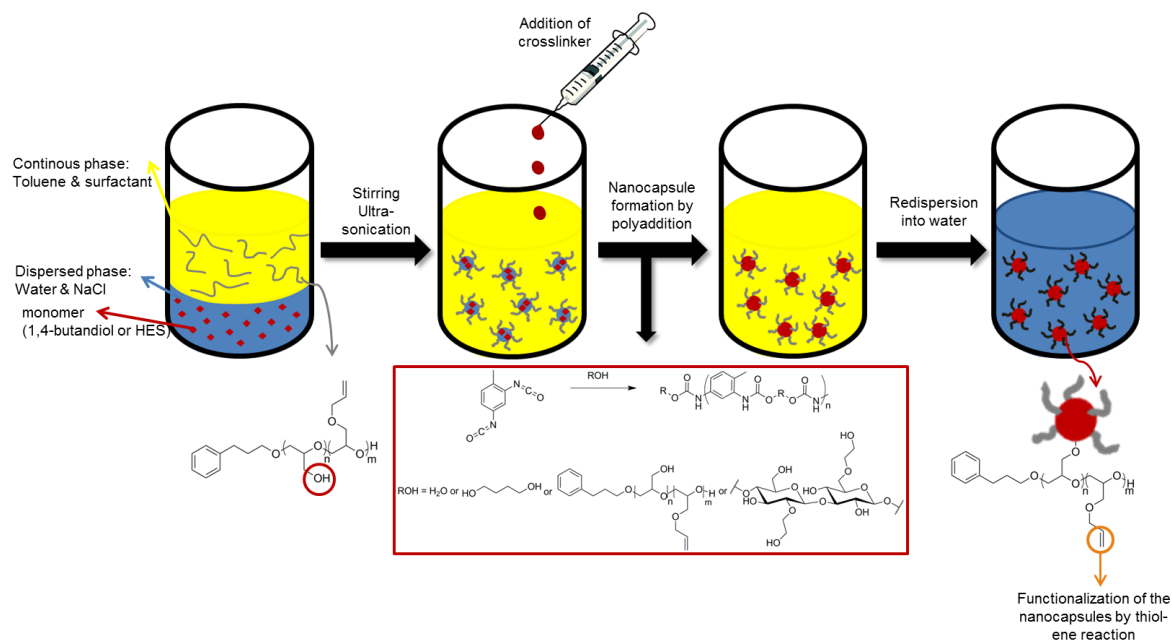


Figure 18. Autocorrelation functions (ACFs) of different particles (**ME1** stabilized by **P4** and **ME6**, **ME8** and **ME9** stabilized with **P1** and SDS) in citrate plasma at $\Theta = 30^\circ$ including data points (\bullet), forced fit (red) as the sum of the individual components and fit with additional aggregate function (blue) with the corresponding residuals resulting from the difference between data and the two fits.

Surfmer for polyurethane/urea nanocapsules in inverse miniemulsions

The two oil-soluble PG block copolymers (**P2** and **P3**) were used as functional surfmers in the inverse miniemulsion. For the formation of the inverse miniemulsion, the surfactant was diluted in the continuous phase toluene, and mixed with the dispersed phase including the monomer (1,4-butanediol or hydroxyethyl starch), an osmotic agent (sodium chloride) and water, as shown in Scheme 6. After ultrasonication, stable water nanodroplets were formed. The dropwise addition of the crosslinker (TDI) allowed reaction of the hydroxyl groups with the isocyanate groups at the droplet-interface to generate polyurea/urethane shells with an aqueous core. Here, the available hydroxyl groups of the block copolymers were in competition to

the hydroxyl groups of the monomer, which should result in an incorporation of the surfactant into the polymer shell. Furthermore, the surface of the produced nanocapsules was tried to modify by thiol-ene reactions with the existed allyl groups on the surface from the surfactant.



Scheme 6. General procedure of inverse miniemulsion to produce crosslinked polyurethane/polyurea nanocapsules stabilized with $\text{PG}_n\text{-}b\text{-PAGE}_m$ surfmers. After transfer into water the surfmer can be used to modify the nanocapsule surface by thiol-ene reactions.

The formation of polyurethane nanocapsules including the block copolymer was studied using 1,4-butandiol as a common difunctional monomer with different concentrations of **P2** and **P3** (2.17 mg mL^{-1} to 3.47 mg mL^{-1}) and different monomer to TDI ratios. Employing **P3** as surfactant resulted in aggregated nanocapsules independent of the used concentration or monomer to TDI ratio analyzed by DLS and SEM. After optimization by changing the surfactant concentration and the monomer to TDI ratios, best results were achieved with a **P2** concentration of 3.47 mg mL^{-1} and a 1:3 ratio of 1,4-butandiol to TDI (**ME10**). SEM proves the formation of nanocapsules with sizes between 120 and 500 nm (Figure 19). However, it seemed that the nanocapsules aggregated during polymerization, because in DLS only diameters around 750 nm were detected with broad size distribution and in SEM the nanocapsules seemed to be connected with each other. Aggregation of the formed nanocapsule during polymerization could happen due to the incorporation of the

hydroxy groups of the surfactant, which could lead to less stabilization behavior of the surfactant.

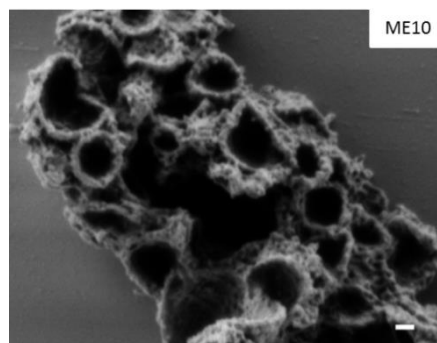


Figure 19. SEM image (scale bar 100 nm) of polyurethane nanocapsules generated by interfacial polyaddition reactions of 1,4-butandiol and TDI using **P2 (ME10)** as a surfmer in toluene.

Because the formation of single stable nanocapsules with 1,4-butandiol was not possible, hydroxyethyl starch (HES) was used as a polyfunctional alternative. The higher amount of hydroxyl groups in the sugar monomer should lead to a higher reactivity with TDI and better crosslinking of the nanocapsule shell also with better nanocapsule stability during polymerization compared to 1,4-butandiol. However, also with this monomer, the surfmer could act as comonomer. For the HES reactions, again different concentrations of **P2** and **P3** were tried and different HES to TDI ratios. In contrast to 1,4-butandiol, stable HES nanocapsules were only generated using **P3** as surfmer. The nanocapsules stabilized with **P2** were not stable and aggregated independent of the used concentration and monomer to TDI ratio. If **P3** was used as surfmer, the nanocapsule sizes decreased with increasing surfactant concentration, as expected. Using 4.8 mg mL^{-1} of **P3** the generated nanocapsules had mean diameters of 380 nm analyzed by DLS and SEM (**ME11**, Figure 20). Increasing the surfmer concentrations to 5.6 mg mL^{-1} smaller nanocapsules with mean diameters of 300 nm were detected by DLS (**ME12**, Figure 20). In SEM the mean diameter of the nanocapsules is even lower at around 200 nm. The differences can be due to nanocapsule swelling in cyclohexane during DLS measurements or due to drying effect during SEM measurements, which could result in nanocapsule shrinking.

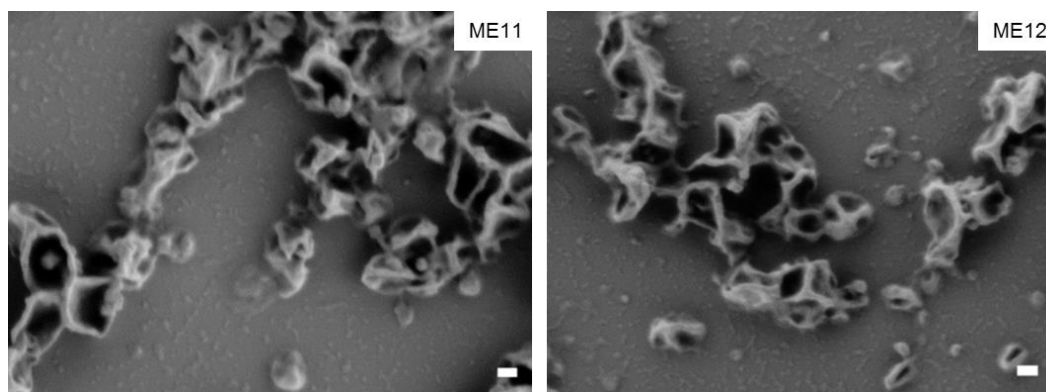


Figure 20. SEM images of the generated HES crosslinked nanocapsules stabilized by **P3** (**ME11** and **ME12**).

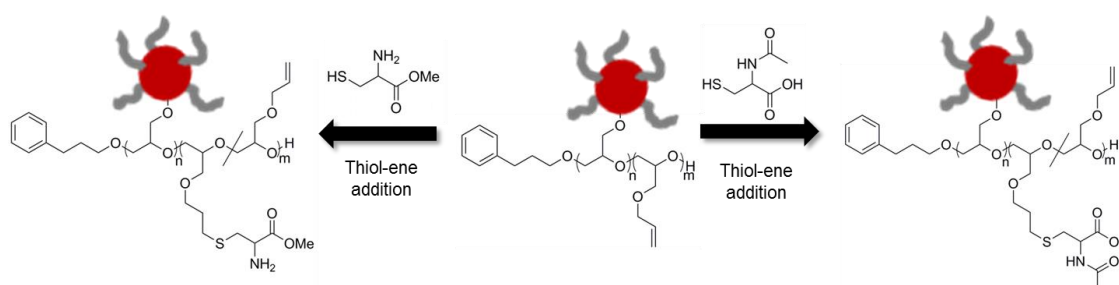
For further applications, the produced nanocapsules have to be transferred into water. Therefore, a second water-soluble surfactant is needed to keep the nanocapsules stable. Thus, the water-soluble **P4** and for comparison also the non-ionic commercially available LutensolAT50 was used as stabilizer during the transfer of the nanocapsules into water. If non-ionic surfactants were used to stabilize the nanocapsules of **ME11** during the transfer into water, stable dispersions were obtained, in which the nanocapsules have diameters between 130 nm and 400 nm or 200 and 600 nm in DLS (Table 9). However, the transfer into 0.1 wt% SDS solution led to diameters of 270 nm sizes besides macroscopic aggregates detected by DLS (Table 9). The transfer of **ME12** into 0.1 wt% SDS and 0.1 wt% LutensolAT50 solutions stable nanocapsules with diameters between 100 and 550 nm were investigated in DLS, in which the diameters of 550 nm maybe aggregated nanocapsules (Table 9). No aggregated nanocapsules were obtained by the transfer of **ME12** into 0.1 wt% **P4**. The mean diameter of the transferred HES nanocapsules was 200 nm (Table 9). To conclude, transfer of the synthesized HES nanocapsules into different aqueous surfactant solutions was possible and generated stable dispersions. **P4** with same chemical nature as the used oil-soluble surfactant showed similar stabilization properties after transfer into water as commercially available surfactants (SDS or LutensolAT50).

Table 9. Summary of determined mean diameters of HES nanocapsules in toluene (**P3**) and after transfer into 0.1 wt% aqueous surfactant solutions (SDS, LutensolAT50 and **P4**).

Surfactant			surfactant		
		d^{DLS}/nm			d^{DLS}/nm
ME11	P3	380	ME12	P3	300
ME11	P4	130/400	ME12	P4	201
ME11	LutensolAT50	200/600	ME12	LutensolAT50	130/540
		270 /			
ME11	SDS	macroscopic aggregates	ME12	SDS	110/440

Thiol-ene addition at the nanocapsule surface

Due to the present allyl groups at the nanocapsule surface after incorporation of the oil-soluble PG-*b*-PAGE block copolymers into the polymer shell, the surface could be further modified for example by thiol-ene reactions. Thiol-ene addition at allyl-protected poly(ethylene glycol)-*co*-polyglycerol (PEG-*co*-PAGE) copolymers was reported by Obermeier et al.^[265] with different thiol compounds to introduce multiple bioconjugates at the polymer side chain. Herein, thiol-ene addition using L-cysteine methyl ester hydrochloride or *N*-acetyl-L-cysteine was studied as model system by changing the surface charge on the nanocapsule surface after transfer into water, as shown in Scheme 7.



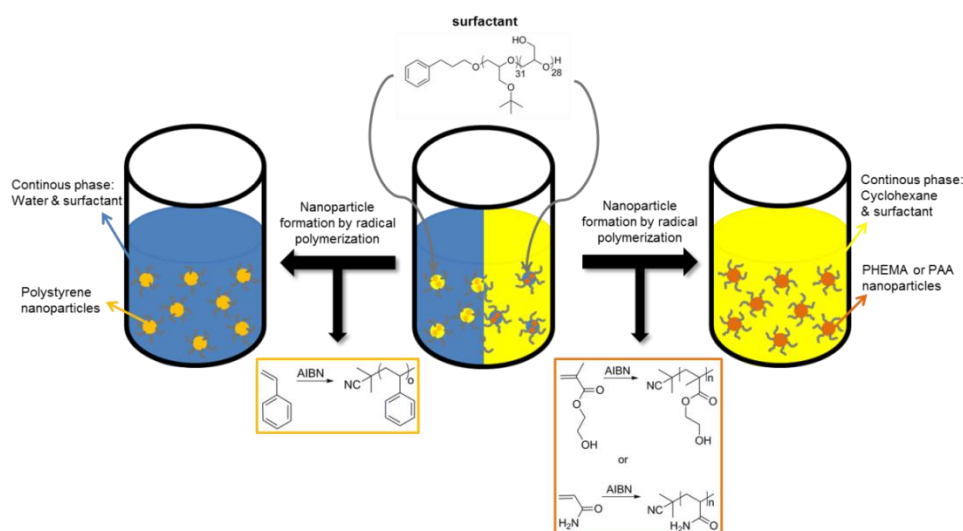
Scheme 7. Thiol-ene reaction on nanocapsule surface after transfer into water with L-cysteine methyl ester hydrochloride or *N*-acetyl-L-cysteine was studied to change the charge of the nanocapsule surface.

To reach high conversion, a thiol to allyl ratio of 20:1 was applied, similar to the conditions of PEG-*co*-PAGE copolymer functionalization. Successful thiol-ene addition at the nanocapsule surface was determined by zeta potential measurement as method of choice, because the amount of introduced surfactants and further

introduction of thiol-groups was at the detection limit of NMR or IR determination. Due to changes in the zeta potential of 10 mV from -11.85 ± 1.65 mV to -22.2 ± 0.40 mV after thiol-ene addition using *N*-acetyl-L-cysteine resulted from the introduced carboxyl group, effective functionalization could be supposed. Adsorption of the thiol-compound on the nanocapsule surface was excluded, because before zeta potential analysis the dispersion was centrifuged two times to remove free cysteine derivative. In addition, during thiol-ene addition optimization no changes of the zeta potential were observed. Thiol-ene addition using L-cysteine methyl ester did not change the surface charge. The zeta potential before and after functionalization was the same of -11.85 ± 1.65 mV. However, the conditions have to be optimized in the future by using fluorescent thiol-compounds or antibodies including thiol-groups.

One PG surfactant for inverse and direct miniemulsions

Since *PtBuG*₃₁-*b*-*PG*₂₈ dissolves both in water and oil, this block copolymer was used as a surfactant for both direct and inverse miniemulsion polymerization (Scheme 8). In both miniemulsions, the nanoparticles were produced by free-radical polymerization using AIBN as initiator. In direct miniemulsions polystyrene nanoparticles were produced, while for the inverse miniemulsions, poly(hydroxyethyl methacrylate) or poly(acrylic acid) nanoparticles were formed using **P5** as stabilizer.



Scheme 8. **P5** as one surfactant for direct miniemulsions to generate PS nanoparticles and for inverse miniemulsions to stabilize poly(acrylamide) (PAA) or poly(hydroxyethyl methacrylate) (PHEMA) nanoparticles.

The formation of stable polystyrene nanoparticles was possible using 1 mg mL^{-1} of **P5**, AIBN as initiator and a polymerization temperature of 75°C in direct miniemulsion, in which the surfactant was dissolved in the continuous water phase. In DLS, the generated polystyrene nanoparticles had mean diameters of 190 nm and 730 nm (Figure 21b). In SEM, polydisperse size distribution is observed with diameters between 300 nm and $1 \mu\text{m}$.

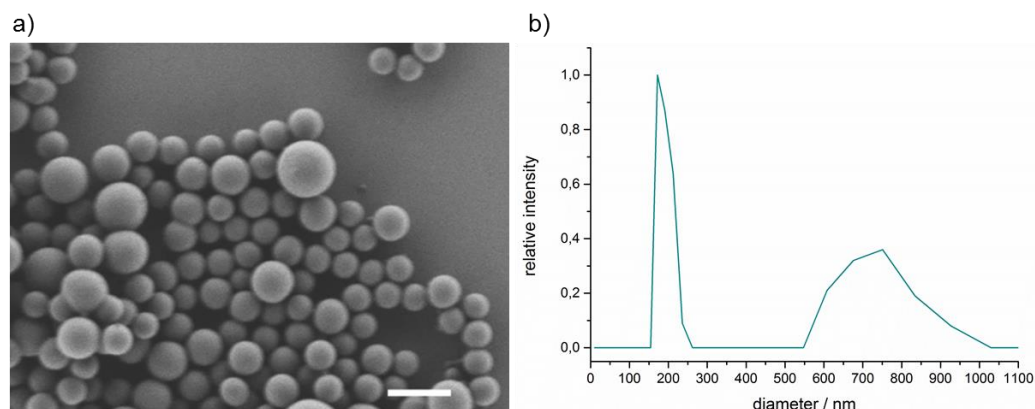


Figure 21. SEM (a, scale bar $1 \mu\text{m}$) and DLS (b) results of generated polystyrene nanoparticles (**ME13**) stabilized with **P5**.

Furthermore, this amphiphilic *tert*-butyl protected PG block copolymer was tested as stabilizer for PHEMA or PAA nanoparticles produced by inverse free-radical miniemulsion polymerization. To obtain PHEMA or PAA nanoparticles, the surfactant was diluted in cyclohexane (continuous phase) and mixed with the monomer solution including sodium chloride as osmotic pressure agent. After treatment with ultrasonication, small monomer droplets were dispersed in the continuous phase. The dispersion was heated to 65°C and the initiator (AIBN) was added to obtain stable polymer nanoparticles. With the surfactant concentration of 7 mg mL^{-1} and 2.6 wt% of AIBN, stable PHEMA nanoparticles were produced with polydisperse size distribution and mean diameters of 80 and 190 nm determined by DLS and SEM (**ME14**, Figure 22). Stable PAA nanoparticles were generated using 7 mg mL^{-1} of **P5** and 1.4 wt% AIBN, with a rather polydisperse size distribution and diameters between 30 nm, which could be micelles of the surfactant, and 110 nm as analyzed by DLS and SEM (**ME15**, Figure 22).

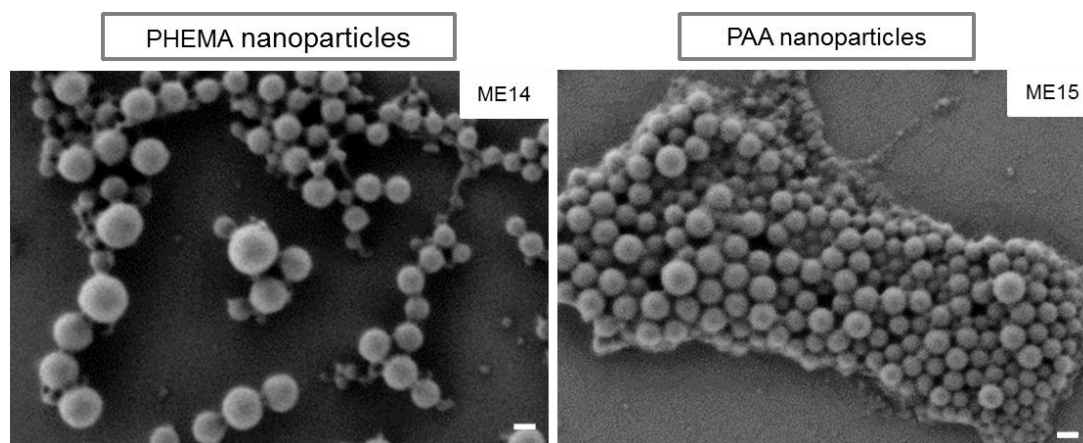


Figure 22. SEM (scale bar 100 nm) results of the PHEMA (**ME14**) and PAA (**ME15**) nanoparticles stabilized with **P5** in cyclohexane.

Conclusion and Outlook

Two different types of orthogonal protected polyglycerol copolymers PEEGE-*b*-PAGE and P*t*BuGE-*b*-PEEGE were synthesized by sequential anionic ring-opening polymerization with defined block length ratios and narrow molecular weight distributions using EGE and AGE or *t*BuGE as monomers. For their use as functional surfactant, all acetal groups were cleaved under acidic conditions to reach an amphiphilic structure with surface active characteristics. The water-soluble PG₃₆-*b*-PAGE₁₄ and the P*t*BuGE₁₅-*b*-PG₃₅ were used to stabilize polystyrene nanoparticles in direct miniemulsions by free-radical polymerization, in which the allyl-protected block copolymer was incorporated into the polystyrene chains. With **P4** stable polystyrene nanoparticles were produced with mean diameters of 230 nm. Because, only polydisperse nanoparticles with diameters between 140 and 300 nm were determined using the surfmer, combinations of both block copolymers or of **P1** and SDS were tested to produce nanoparticles with narrow size distributions and diameters around 100 nm including the surfmer. Polystyrene nanoparticles with mean diameters around 150 nm were generated using a combination of 1.2:1 of **P1** and SDS. In addition, the stability of the obtained nanoparticles was studied after incubation into citrate plasma. In all studied dispersions, aggregated nanoparticles were detected besides single stable polystyrene nanoparticles, in which a higher amount of surfmer led to smaller and less aggregated nanoparticles. In the future, more studies shall be done to generate stable nanoparticles only stabilized by the

surfmer. In addition, the surface shall be functionalized with cell specific linkers or fluorescence dyes using the hydroxyl groups from the surfmer. Moreover, the stability in citrate plasma has to be optimized and cell experiment as well as protein adsorption on the surface has to be analyzed for biomedical applications. The oil-soluble allyl-protected block copolymers were used as surfmer for inverse miniemulsions, in which the polymer shell was generated by polyaddition reaction to incorporate the surfmer due to the contained hydroxyl groups. We were able to show that stable HES nanocapsules with an aqueous core were produced and successfully transferred into water using the water-soluble $PtBuGE_{15}-b-PG_{35}$ or commercially available LutensolAT50 or SDS. In water the nanocapsules surface was functionalized by thiol-ene reaction of a cysteine derivative with the allyl protection groups from the surfmer. In next steps, other thiol derivatives shall be introduced on the surface like fluorescence dyes or cell specific linkers to replace prior surface modification reactions. In addition, protein adsorption and stability tests have to be done in the future. The water and cyclohexane-soluble $PtBuGE_{31}-b-PG_{28}$ (**P5**) was used as surfactant for direct as well as inverse miniemulsion free-radical polymerization. It was possible to prepare either polystyrene nanoparticles in a direct miniemulsion polymerization or PHEMA and PAA nanoparticles with the same surfactant in the inverse miniemulsion polymerization.

Experimental Part

Materials

Cesium hydroxide monohydrate ($CsOH \cdot H_2O$, Sigma-Aldrich, $\geq 99.5\%$), benzene (Sigma-Aldrich, anhydrous, 99.8%), methanol (Sigma-Aldrich, anhydrous 99.8%), hydrochloric acid (HCl, Sigma-Aldrich, ACS reagent, 37%), 2,3-epoxypropanol (Sigma-Aldrich, 96%), ethyl vinyl ether (Sigma-Aldrich, 98.0%), magnesium sulfate ($MgSO_4$, Fluka, anhydrous, reagent grade, $\geq 99.5\%$), *p*-toluenesulfonic acid (*p*-TsOH, Sigma-Aldrich, ACS reagent, $\geq 98.5\%$), 1,4-butanediol (Sigma-Aldrich, *ReagentPlus*, 99%), hydroxyethyl starch solution (HES 200k, 0.5 degree of substitution, Fresenius Kabi), toluene-2,4-diisocyanate (TDI, Sigma-Aldrich, 95%), sodium chloride (NaCl, Fisher Scientific, $\geq 99\%$), Lutensol AT50 (BASF), sodium dodecylsulfate (SDS, Fluka, ACS reagent, $\geq 99\%$), L-cysteinemethyl ester hydrochloride (Sigma-Aldrich, 98%), *N*-

acetyl-L-cysteine (Sigma-Aldrich, analytical grade, $\geq 99\%$ (TLC)), VA-044 (Stockhausen), 2-hydroxyethyl methacrylate (HEMA, Sigma-Aldrich, $\geq 99\%$), acrylamide (AA, Sigma-Aldrich, 98%), hexadecane (Sigma-Aldrich, *ReagentPlus*, 99%), tetrahydrofuran (THF, Fisher Scientific, analytical grade), cyclohexane (Fisher Scientific, analytical grade), toluene (Fisher Scientific, analytical grade), chloroform-*d* (CDCl_3 -*d*, Acros Organics, 99.8 atom% D), dimethyl sulfoxide-*d*₆ ($\text{DMSO-}d_6$, Carl Roth, 99.8 atom% D) and tetrahydrofurane-*d*₈ (Deutero GmbH, ≥ 99.5 atom% D) were used as received. Ethoxyethyl protected glycidyl ether was synthesized according to the published procedure by Fitton et al.^[262] Allyl glycidyl ether (AGE, Sigma-Aldrich, 99%), *tert*-butyl glycidyl ether (*t*BuGE, Sigma-Aldrich, $>99\%$) and the synthesized EEGE were stored over CaH_2 and distilled *in vacuo* over molecular sieve before use to remove traces of water. Styrene (Sigma-Aldrich, *ReagentPlus*, $\geq 99\%$) was purified before use by passing through neutral Al_2O_3 . 2,2'-Azobis(2-methylpropionitrile) (AIBN, Acros Organics, 98%) was recrystallized in methanol before used.

Methods

A Bruker Avance 300 spectrometer was used to detect ^1H -NMR spectra at a Larmor Frequency of 300.23 MHz. 15 mg of the generated polymer was dissolved in 0.6 mL deuterated solvent CDCl_3 -*d* or $\text{DMSO-}d_6$. If CDCl_3 was used as solvent the spectra were calibrated according to the chemical shift of 7.26 ppm. If the polymer was dissolved in $\text{DMSO-}d_6$, the spectra were calibrated according to the chemical shift of 2.50 ppm. Proton diffusion-ordered NMR spectroscopy was measured to detect the incorporation of the surfmer into the nanoparticle at a Bruker Avance III spectrometer with a Larmor Frequency of 700 MHz. Before dissolving the polymer mixture in deuterated THF-*d*₈, 150 μL nanoparticle dispersion was freeze dried to obtain the solid polymer. The proton NMR spectra in the 2D-NMR were calibrated according to the chemical shift at 3.58 ppm. Size exclusion chromatography (SEC) was used to detect the molecular weight dispersity (\mathcal{D}) and molecular weight in DMF using an Agilent PSS SECcurity. The concentration of the generated polymer in DMF was 5 mg min^{-1} . Before injection of the sample with a 1260 ALS sample injector into the SEC equipment, the solution was filtered through a 0.45 μm teflon filter. The sample was pumped through the three GRAM columns (PSS) with a flow rate of 1 mL min^{-1} . The GRAM columns (PSS) with dimensions of 300 x 80 mm have a particle

size of 10 μm and pore sizes of 100, 1000 and 10000 \AA . For detection a UV (270 nm) 1260 VWD detector and a 1260 RID RI detector were utilized. The molecular weights were calculated by comparing with a polyethylene oxide standard provided by the Polymer Standards Service GmbH. Differential scanning calorimetry (DSC) measurements were performed at a Mettler Toledo DSC 823 calorimeter. Between temperature ranges of $-150\text{ }^{\circ}\text{C}$ to $150\text{ }^{\circ}\text{C}$ three scanning cycles of heating and cooling were performed using a heating rate of $10\text{ }^{\circ}\text{C min}^{-1}$ under nitrogen atmosphere. The critical micelle concentration was determined with the ring tensiometer DCAT 21 from DataPhysics. An aqueous polymer solution of 1.55 mg mL^{-1} was added in $5\text{ }\mu\text{L}$ steps into water. After each addition, the mixture was stirred for 2 min and afterwards the surface tension was measured by pushing and pulling the ring into the aqueous solution. Interfacial tension of water and toluene or water and toluene surfactant solution of different concentrations was measured at the spinning drop tensiometer SVT 20N from DataPhysics. A glass capillary was filled with water ($\sim 1.2\text{ g}$) and a small droplet of toluene or surfactant mixture ($\sim 0.012\text{ g}$). Then the capillary was placed horizontally and equilibrated at $20\text{ }^{\circ}\text{C}$ for 10 min under rotation at 8000 rpm to obtain one cylindrical droplet at the axis of rotation. The interfacial tension based on the theory of Vonnegut was measured over 10 min.^[270] The surface tensions at the water-air interface or at the aqueous surfactant solution to air interface were measured with a ring tensiometer DCAT 21 from DataPhysics. The obtained value of water and air ($\gamma = 72.53\text{ mN m}^{-1}$ at $22\text{ }^{\circ}\text{C}$) was comparable to the value reported in the literature ($\gamma = 72.75\text{ mN m}^{-1}$ at $20\text{ }^{\circ}\text{C}$).^[272] The critical micelle concentration (CMC) in water was measured by isothermal titration calorimetry using a MicroCal VP-ITC (GE Healthcare, Piscataway, USA). Therefore, a stock solution of $\text{P}t\text{BuGE}_{31}\text{-}b\text{-PG}_{28}$ with concentrations between 0.2 g L^{-1} to 1.5 g L^{-1} above the critical micelle concentration was added drop-wise ($2\text{ }\mu\text{L}$ in 25 steps) into an ITC chamber at $25\text{ }^{\circ}\text{C}$. During the measurement, the heat flow was recorded, whereas dilution of the surfactant solution exhibited an exothermic heat flow. At the beginning the exothermic heat flow increases with the concentration of the surfactant. After micelles were formed the peak intensity decreases due to dilution of the micelle solution. At the inflection point, micelles were formed, thus the critical micelle concentration was reached. Dynamic light scattering (DLS) was used to determine the hydrodynamic diameter of the generated nanoparticles in water at a Nicomp 380 Submicron particle

Sizer (PSS-Nicomp) at a fixed scattering angle of 90°. 10 µL of the emulsion was diluted in 1 mL toluene or cyclohexane or 3 mL distilled water. DLS measurements after incubation with 100% citrate plasma were performed on a commercially available instrument from ALV GmbH (Langen, Germany). The DLS instrument is equipped with a goniometer and an ALV-5000 multiple tau full-digital correlator including 320 channels. As light source a helium-neon laser from JDS Uniphase (Milpitas, USA) was used with an operating intensity of 25 mW and a wavelength of $\lambda = 632.8$ nm. All analyzed protein-nanoparticle mixtures were filled into dust-free quartz cuvettes from Hellma (Müllheim, Germany) with an inner diameter of 18 mm, which were cleaned before using distilled acetone. Before the nanoparticles were incubated into citrate plasma, the plasma was filtered through a Millex-GS filter (Merck Millipore, Darmstadt, Germany) with a pore size of 0.2 µm into the cuvette. The sample was prepared by adding 1 µL of the nanoparticle dispersion (solid content 1 wt%) into 1 mL filtered citrate plasma. After incubation at 37 °C for 30 min DLS analysis followed at the same temperature. The nanoparticle formation were detected by scanning electron microscopy (SEM) using a Zeiss 1530 LEO Gemini microscope. 10 µL of the nanoparticle dispersion was diluted in 3 mL distilled water, toluene or cyclohexane, drop-cast onto silica wafers, and dried under ambient conditions. Afterwards the silica wafers were placed under the microscope and each sample was analyzed at a working distance of ~3 mm and an accelerating voltage of 0.2 kV. The zeta potential analysis of the nanocapsule was performed at a Zeta Nanosizer (Malvern Instruments, U.K.) at 20 °C. 10 µL of the sample (1 wt% solid content) was diluted in 1 mL 0.001 M KCl solution, added into a cuvette and placed in the zeta sizer to measure the zeta potential.

Synthesis

Polymer synthesis

P(EEGE-*b*-AGE). 3-Phenylpropanol (68.1 mg, 0.5 mmol) was added to a mixture of benzene (5 mL) and caesium hydroxide (83.4 mg, 0.5 mmol) under Schlenk conditions. After 30 min stirring at 60 °C, benzene was removed at 90 °C by distillation *in vacuo* over 3 h. Ethoxyethyl glycidyl ether (monomer 1) was added to the initiator at room temperature and stirred over night at 70 °C. Before the addition of the allyl protected glycidyl ether, a sample for NMR and SEC analysis was taken

from the viscous mixture to ensure full conversion. The allyl protected glycidyl ether (monomer 2) was added at room temperature to the mixture and heated again to 70 °C under stirring for 16 h under argon. To the viscous mixture dry methanol (0.5 mL) was added and the added excess was removed after stirring for 1 h by distillation *in vacuo* to obtain the yellow viscous oil and used without further purification for the next step. For added amount of monomer and further analytical data, see Table 1 (**P1-P3**). Yield: 97.6% to 99.6 %.

Poly(ethoxyethyl glycerol). ^1H NMR (300 MHz, CDCl_3 -*d*): $\delta(\text{ppm}) = 7.22 - 7.12$ (m, 5H, Ar H), 4.69 (q, $J = 5.0$ Hz, 1H, -O-CH-O-), 3.83 – 3.36 (m, 5H, polymer backbone, -CH-CH₂-O-), 2.72 – 2.61 (m, 3H, -CH₂-CHH-CH₂-O-), 1.94 – 1.82 (m, 3H, -CH₂-CHH-CH₂-O-), 1.38 – 1.04 (m, 6H, 2 -CH₃).

Poly(ethoxyethyl glycerol-*b*- allyl glycerol). ^1H NMR (300 MHz, DMSO-*d*₆): $\delta(\text{ppm}) = 7.30 - 7.12$ (m, 5H, Ar H), 5.84 (dq, $J = 16.9, 5.1$ Hz, 1H, CH₂-CH-CH₂-O-), 5.32 – 5.05 (m, 2H, CH₂-CH-CH₂-O-), 4.64 (q, $J = 5.2$ Hz, 1H, -O-CH-O-), 4.01 – 3.85 (m, 2H, CH₂-CH-CH₂-O-), 3.74 – 3.17 (m, 5H, polymer backbone, -CH-CH₂-O-), 2.61 (t, $J = 7.7$ Hz, 3H, -CH₂-CHH-CH₂-O-), 1.85 – 1.70 (m, 3H, -CH₂-CHH-CH₂-O-), 1.28 – 1.00 (m, 6H, 2 -CH₃).

P(*t*BuGE-*b*-EEGE). Under Schlenk conditions 3-phenylpropanol (68.1 mg, 0.5 mmol) was added to a mixture of benzene (5 mL) and caesium hydroxide (83.4 mg, 0.5 mmol). After stirring at 60 °C for 30 min, benzene was removed by distillation *in vacuo* at 90 °C for 3 h. The mixture was cooled down to room temperature, then the *tert*-butyl protected glycidyl ether (monomer 1) was added and stirred over night at 70 °C. Before the addition of the ethoxyethyl protected glycidyl ether, a sample was taken for NMR and SEC analysis at room temperature under argon. The ethoxyethyl glycidyl ether (monomer 2) was added at room temperature to the yellow viscous mixture and stirred at 70 °C for 20 h under argon atmosphere. Dry methanol (0.5 mL) was added to the viscous mixture, stirred for 1 h and afterwards unreacted methanol was removed by distillation *in vacuo* to give the yellow viscous oil and used without further purification for the next step. For added amount of monomer and further analytical data, see Table 1 (**P4** and **P5**). Yield: 72 % to 80 %.

Poly(*tert*-butyl glycerol). ^1H NMR (300 MHz, CDCl_3 -*d*): $\delta(\text{ppm}) = 7.18$ (d, $J = 7.1$ Hz, 5H, Ar H), 3.92 – 3.21 (m, 5H, polymer backbone, CH-CH₂-O-), 2.80 (dd, $J = 5.1$,

4.1 Hz, 3H, $-\text{CH}_2\text{-CHH-CH}_2\text{-O-}$), 1.99 – 1.77 (m, 3H, $-\text{CH}_2\text{-CHH-CH}_2\text{-O-}$), 1.40 – 0.79 (m, 9H, 3^*-CH_3).

Poly(*tert*-butyl glycerol-co-ethoxyethyl glycerol). ^1H NMR (300 MHz, $\text{CDCl}_3\text{-}d$): $\delta(\text{ppm}) = 7.17$ (dd, $J = 22.8, 7.1$ Hz, 5H, Ar H), 4.65 (q, $J = 5.4$ Hz, 1H, $-\text{O-CH-O-}$), 3.79 – 3.24 (m, 5H, polymer backbone, $\text{CH-CH}_2\text{-O-}$), 2.61 (q, $J = 8.0$ Hz, 3H, $-\text{CH}_2\text{-CHH-CH}_2\text{-O-}$), 1.90 – 1.75 (m, 3H, $-\text{CH}_2\text{-CHH-CH}_2\text{-O-}$), 1.54 – 0.68 (m, 15H, 5^*-CH_3).

Hydrolysis of the ethoxyethyl protection group

Synthesis of P(*t*BuGE-*b*-PG) or P(PG-*b*-AGE). The block copolymer was dissolved in THF (120 mL per gram polymer) and treated with concentrated HCl (0.4 mL per EEGE repeating unit by 1 g polymer) for 1 h under stirring at room temperature. The solution was neutralized with aqueous KOH solution (30 wt%) and filtered afterwards to remove occurred KCl. After drying over anhydrous magnesium sulfate, the solvent was removed by distillation *in vacuo* to obtain the product as yellow viscous oil. For amounts of reagents and further analytical results, see Table 1.

Poly(*tert*-butyl glycerol-*b*-glycerol). ^1H NMR (300 MHz, $\text{CDCl}_3\text{-}d$): $\delta(\text{ppm}) = 7.25 - 7.14$ (m, 5H, Ar H), 3.78 – 3.27 (m, 5H, polymer backbone, $\text{CH-CH}_2\text{-O-}$), 2.74 – 2.62 (m, 3H, $-\text{CH}_2\text{-CHH-CH}_2\text{-O-}$), 1.95 – 1.81 (m, 3H, $-\text{CH}_2\text{-CHH-CH}_2\text{-O-}$), 1.16 (t, $J = 1.8$ Hz, 9H, 3^*-CH_3).

Poly(glycerol-*b*-allyl glycerol). ^1H NMR (300 MHz, $\text{DMSO-}d_6$): $\delta(\text{ppm}) = 7.32 - 7.12$ (m, 5H, Ar H), 5.86 (ddt, $J = 16.3, 10.4, 5.2$ Hz, 1H, $\text{CH}_2\text{-CH-CH}_2\text{-O-}$), 5.31 – 5.07 (m, 2H, $\text{CH}_2\text{-CH-CH}_2\text{-O-}$), 4.52 (d, $J = 6.4$ Hz, 1H, OH), 4.03 – 3.85 (m, 2H, $\text{CH}_2\text{-CH-CH}_2\text{-O-}$), 3.63 – 3.22 (m, 5H, polymer backbone, $\text{CH-CH}_2\text{-O-}$), 2.68 – 2.55 (m, 3H, $-\text{CH}_2\text{-CHH-CH}_2\text{-O-}$), 1.78 (p, $J = 6.6$ Hz, 3H, $-\text{CH}_2\text{-CHH-CH}_2\text{-O-}$).

General procedure of direct miniemulsion to generate polystyrene nanoparticles using one block copolymer

56 μL styrene, 3.2 μL hexadecane and 0.5 mg AIBN was mixed and added into 2 mL of water containing $\text{PG}_{36}\text{-}b\text{-PAGE}_{14}$, $\text{P}t\text{BuGE}_{15}\text{-}b\text{-PG}_{35}$ (for amount see Table 2) or $\text{P}t\text{BuGE}_{31}\text{-}b\text{-PG}_{28}$ (1 mg mL^{-1}). After pre-emulsification for 1 h at 1000 rpm, the dispersion was treated by inverse ultrasonication at 70 % amplitude for 2 min and stirred in heat (temperature see Table 2) for 24 h. The solid content was analyzed by freeze-dry 150 μL of the dispersion. Results are listed in Table 2.

General procedure of direct miniemulsion to generate polystyrene nanoparticles using a block copolymer mixture

A mixture of PG₃₆-*b*-PAGE₁₄ and P*t*BuGE₁₅-*b*-PG₃₅ (1:1 or 1:3) was dissolved in 2 mL water. A solution of 56 μ L styrene, 3.2 μ L hexadecane and 0.5 mg AIBN was added and the dispersion was pre-emulsified by stirring at 1000 rpm for 1 h. After treatment by inverse ultrasonication at 70 % amplitude for 2 min, the dispersion was stirred at 70 °C for 24 h. The solid content was analyzed by freeze-dry 150 μ L of the dispersion. Results see Figure 15.

General procedure of direct miniemulsion to generate polystyrene nanoparticles using a surfactant mixture of PG-*b*-PAGE and SDS

A mixture of PG₃₆-*b*-PAGE₁₄ and SDS (amount see Table 3) was dissolved in 2 mL water. A solution of 56 μ L styrene, 3.2 μ L hexadecane and 0.5 mg AIBN was added and the dispersion was pre-emulsified by stirring at 1000 rpm for 1 h. After treatment by inverse ultrasonication at 70 % amplitude for 2 min, the dispersion was stirred at 70 °C for 24 h. The solid content was analyzed by freeze-dry 150 μ L of the dispersion. Results are listed in Table 3.

General procedure of inverse miniemulsion to generate polyurethane nanocapsules

1,4-butanediol (40.7 mg) was dissolved in PBS buffer (375 μ L) and added to a toluene polyglycerol-surfactant solution (3.75 g including 3.47 mg mL⁻¹ of **P2**) under stirring at room temperature. After pre-emulsification for 1 h, the dispersion was treated with ultrasonication under ice-cooling using a ½ inch tip for 3 min in a pulse-pause regime of 30 s and 10 s at a Branson W450-D sonifier. TDI (118.6 mg) dissolved in toluene polyglycerol-surfactant solution (1.25 g) was added drop-wise to the emulsion and stirred for 24 h at room temperature. The morphology and nanocapsule sizes were analyzed by SEM and DLS.

General procedure of inverse miniemulsion to generate biodegradable polyurethane nanocapsules

NaCl (10 mg) was dissolved in a hydroxyethyl starch solution (360 mg) and added to a toluene polyglycerol-surfactant solution (3.75 g including 4.8 or 5.6 mg mL⁻¹ of **P3**) under stirring at room temperature. After pre-emulsification for 1 h, the dispersion was treated with ultrasonication under ice-cooling using a ½ inch tip for 3 min in a

pulse-pause regime of 30 s and 10 s at a Branson W450-D sonifier. TDI (27 mg) dissolved in toluene polyglycerol-surfactant solution (1.25 g) was added drop-wise to the emulsion and stirred for 24 h at room temperature. The morphology and nanocapsule sizes were analyzed by SEM and DLS. The nanocapsule dispersion was washed two times by centrifugation at 4000 rpm for 20 min at 22 °C in 2 mL Eppendorf tubes to remove unreacted monomer. The washed miniemulsion (1 g) was transferred into 0.1 wt% aqueous surfactant solution (5 mL, SDS, LutensolAT50 or **P4**) and stirred for 24 h without cap. The size and morphology was again analyzed by DLS and SEM. The solid content was analyzed by freeze-dry of 150 µL of the nanocapsule dispersion.

Thiol-ene coupling reaction

A cysteine derivative (20 equiv per PG-*b*-PAGE, L-cysteinemethyl ester hydrochloride or *N*-acetyl-L-cysteine) and the water soluble initiator VA-044 (0.75 equiv per PG-*b*-PAGE) was added to the transferred nanocapsule dispersion (1 mL) under argon atmosphere and stirred at 55 °C overnight. The nanocapsule dispersion was washed two times by centrifugation at 5000 rpm for 30 min at 22 °C in 2 mL Eppendorf tubes to remove unreacted cysteine derivative and initiator. Successful thiol-ene addition was analyzed by zeta potential measurement.

General procedure of inverse miniemulsion to generate polyacrylamide or poly(2-hydroxyethyl methacrylate) nanoparticles

PtBuGE₃₁-*b*-PG₂₈ (45 mg) was dissolved in cyclohexane (3.75 g). The monomer (375 mg) was mixed with water (15 µL) and NaCl (7.5 mg) and added to the surfactant solution. After pre-emulsification for 1 h, the dispersion was treated with ultrasonication at a ¼ inch tip for 3 min in a pulse-pause regime of 30 s and 10 s at a Branson W450-D sonifier. AIBN (10.3 mg or 5.1 mg) was dissolved in cyclohexane (1.25 g), added to the dispersion at 65 °C and stirred at 65 °C for 24 h. The sizes and morphology was analyzed by DLS and SEM.

2.2 Amphiphilic ferrocene-containing PEG block copolymers as redox-responsive micellar nanocarriers or surfactants³

Besides polyfunctional polyglycidols as surfactant or surfmer to produce polystyrene nanoparticles in direct miniemulsion with further properties, also other non-ionic surfactants with additional chemical or physical handles triggered by an external stimulus are promising in colloidal chemistry. The redox stimulus is an attractive feature, however, to date only few non-ionic redox-responsive surfactants have been reported. Herein, the first nonionic and non-cytotoxic ferrocene-containing block copolymers are prepared, carrying a hydrophilic PEG chain and multiple ferrocenes in the hydrophobic segment. These amphiphiles were studied as redox-sensitive surfactants that destabilize particles as obtained in miniemulsion polymerization. Due to the nonionic nature of such PEG-based copolymers, they can stabilize nanoparticles also after the addition of ions, while particles stabilized with ionic surfactants would be destabilized by the addition of salt. The redox-active surfactants are prepared by the anionic ring-opening polymerization (AROP) of ferrocenyl glycidyl ether (fcGE) with PEG monomethyl ether as the macroinitiator. The resulting block copolymers with molecular weights (M_n) between 3600 to 8600 g mol⁻¹ and narrow molecular weight distributions ($M_w/M_n = 1.04-1.10$) were investigated via ¹H and DOSY-NMR spectroscopy, SEC, and MALDI-ToF mass spectrometry. Furthermore, the block copolymers were used as building blocks for redox-responsive micelles and as redox-responsive surfactants in the radical

³ This section is based on the manuscript 'Amphiphilic ferrocene-containing PEG block copolymer as micellar nanocarriers and smart surfactants' by Sarah Wald, Arda Alkan, Benoit Louage, Bruno G. De Geest, Katharina Landfester and Frederik R. Wurm, published in 2016 in *Langmuir* and is reprinted with permission from Langmuir. Copyright 2016 American Chemical Society.[273] A. Alkan, S. Wald, B. Louage, B. G. De Geest, K. Landfester, F. R. Wurm, *Langmuir* **2016**. I developed the nanoparticle synthesis and their redox-responsive stability test and conducted the characterization concerning DLS, SEM, ITC and ICP; the block copolymers were synthesized and characterized by Alkan Arda and the formation, characterization and cell-uptake of the redox-responsive micelles including a fluorescence dye as well as cytotoxicity tests of the block copolymers was done by the group of Bruno G. De Geest at the University of Ghent in Belgium, which are also acknowledged after each corresponding contribution.

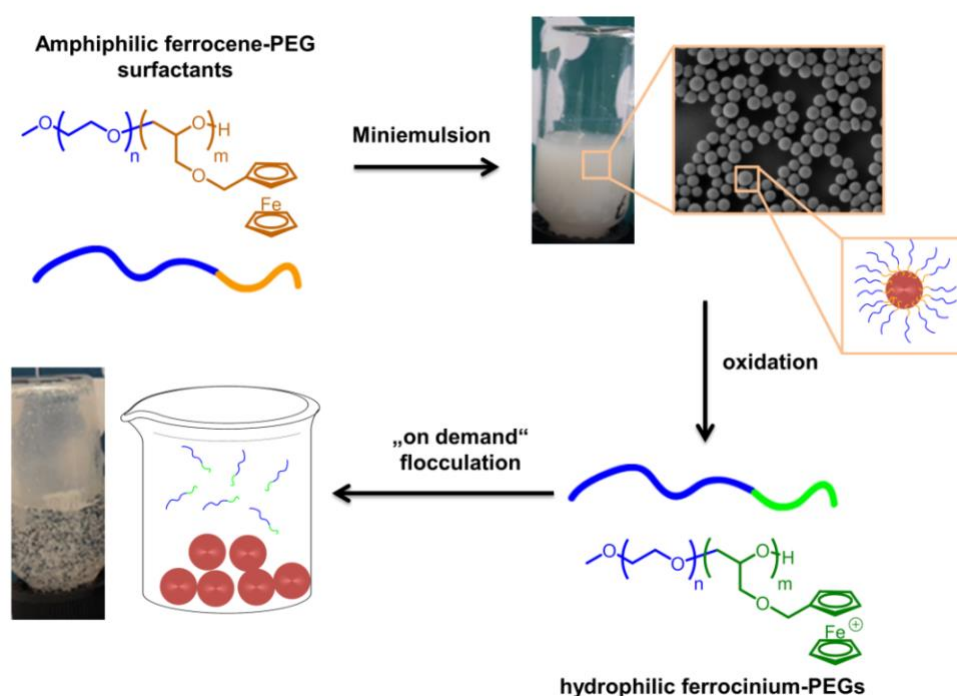
polymerization in miniemulsion to stabilize model polystyrene nanoparticles. Oxidation to the ferrocenium species converted the amphiphilic block copolymers into double hydrophilic macromolecules, which led to the destabilization of the nanoparticles. This destabilization of nanoparticle dispersions may be useful for the formation of coatings and the recovery of surfactants.

Motivation

Surfactants are commonly used as stabilizing or cleaning agents in industrial applications, because of their ability to modify the interfacial properties by changing the surface or interfacial tension and to self-assemble into micelles or other nanostructures.^[274] Stimuli-responsive surfactants (responding to pH, T, light or redox changes) are of special interest, because of their potential applications in separation methods,^[275] foam formation,^[276] and their ability to reduce surfactant waste and usage or process costs.^[12] Ferrocene, viologens and *N*-alkylated nicotin acids are typical redox-active building blocks in surfactants.^[277] While *N*-alkylated nicotinic acid derivatives do not show reversible redox behavior in water, ferrocene and viologen surfactants exhibit a reversible redox-behavior with drastic solubility changes. The most studied redox-active surfactants are based on ferrocene-derivatives carrying ionic groups; fc is attractive because it is chemically stable over a wide range of solution conditions.^[278] These low molecular weight surfactants carry a single redox-active site and several modifications, e.g. in the number and length^[13] of alkyl chains,^{[278-282],[283-287]} non-ionic,^[287-292] cationic^[278, 280-286, 293-296] or anionic^[279, 287, 297] (head) groups have been reported. Polymeric ferrocene surfactants with more than a single fc-unit have not been studied, in spite of various elegant routes to ferrocene-containing (block) (co)polymers, which could have been used as surfactants.^[298-300] Amphiphilic fc-containing block copolymers are mainly based on organometallic poly(vinyl ferrocene) (PVfc) or poly(ferrocenyl silane) (PFS) and a water-soluble block, e.g. poly(ethylene glycol)^[301, 302] or poly(*N*-isopropylacrylamide).^[116] PFS-block copolymers assemble in cylindrical micelles if the PFS segment is crystalline, allowing to generate stable micellar structures with variable morphology.^[303, 304] Several years ago, we introduced ferrocene into the epoxide chemistry: the first water-soluble random copolymers of EO and ferrocenyl glycidyl ether (fcGE) have been prepared^[305] and later extended to polyvalent^[306] or hyperbranched polyethers

by the copolymerization of fcGE with glycidol (G).^[307] However, despite the omnipresence of PEG-based surfactants in industry and academia, the combination of the redox-responsive fc units with PEG-containing surfactants have not been reported. In addition, due to the hydrophobicity of fc itself, this allows for the first time to generate nonionic surfactants with several fc's in the hydrophobic segment, which lose their stabilization upon oxidation and are released into the continuous phase.

The current work describes the first block copolymers based on ethylene oxide and fcGE, prepared by anionic polymerization. These biocompatible block copolymers have been used as micellar carriers to encapsulate a hydrophobic dye, which was incorporated into SKOV-3 human ovarian cells. In addition, the generated block copolymers were tested as redox-responsive surfactants to prepare nanoparticles via free radical polymerization using a miniemulsion polymerization approach^[168] (Scheme 9). We investigated the influence of the nanoparticle sizes by using block copolymers with different EO: fcGE ratio and by changing the surfactant concentration. The nanoparticle dispersions were stable over at least several months and allowed an 'on-demand' destabilization by pH- or redox-trigger leading to flocculation or film formation.

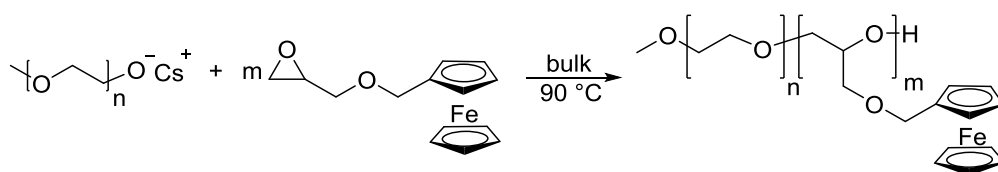


Scheme 9. “Destabilization on demand”: mPEG-*b*-PfcGE block copolymers as redox-active surfactants for nanocarriers.

Results and Discussion

Block copolymer synthesis and characterization

The anionic ring-opening polymerization of fcGE was achieved by the cesium alkoxide of mPEG (with $n = 25, 44$, or 124 in Scheme 10 respectively) acting as a macroinitiator. The latter was generated by the reaction of mPEG with cesium hydroxide^[308] and then used to initiate the polymerization of fcGE in bulk leading to mPEG-*b*-PfcGE block copolymers (Scheme 10).



Scheme 10. Synthetic protocol for PEG-*b*-PfcGE block copolymers (polymerization executed by Arda Alkan).

Only short PfcGE blocks (ca. 10 repeating units) have been targeted to ensure water-solubility of the block copolymer with the formation of spherical micelles. Molecular weights were calculated from ^1H NMR spectra by comparing the integrals of the resonances for the initial mPEG and the resonances of the PfcGE block. Starting from mPEG5000 (with a detected M_n of $5,500 \text{ g mol}^{-1}$ in GPC) as the macroinitiator, molecular weights from $7,400$ to $8,500 \text{ g mol}^{-1}$ were achieved by varying the molar fraction of fcGE from 5.7 to 8.2% (**P1-P4**). The molecular weight dispersities, determined by size exclusion chromatography (Figure 23), ($D=M_w/M_n$) range from 1.05 to 1.10 indicating a controlled polymerization (Table 10).

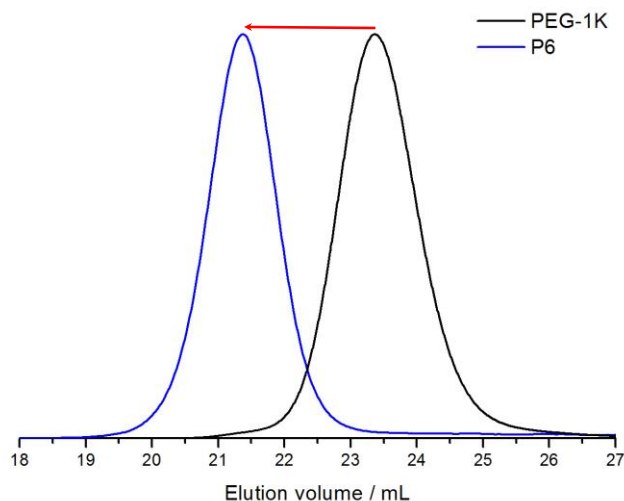


Figure 23. SEC traces of the macroinitiator PEG (1,000 g mol⁻¹) and **P6** (DMF, 323 K, RI detection, 1 mL min⁻¹).

Molecular weights determined via SEC are underestimated compared to molecular weights from ¹H-NMR spectroscopy, as previously reported for other fc-containing polymers. In addition, mPEG₄₄ and mPEG₂₄ was used as a macroinitiator to generate block copolymers with higher fcGE fractions. Therefore, mPEG2000 led to a block copolymer with 11.7 mol% fcGE, a molecular weight of 3600 g mol⁻¹ and a dispersity of 1.08 (**P5**). With mPEG1000 a block copolymer with 27.2 mol% of fcGE was prepared (**P6**).

Table 10. Characterization data for PEG-*b*-PfcGE block copolymers.

code	Formula	fcGE/mol%	M_n^a	M_n^b	\bar{D}^b	CMC/ mmol L ⁻¹
P1	mP(EG) ₁₂₄ - <i>block</i> -P(fcGE) _{7.5}	5.7	7400	5100	1.05	n.d. ^c
P2	mP(EG) ₁₂₄ - <i>block</i> -P(fcGE) ₁₀	7.3	7900	5900	1.10	0.053
P3	mP(EG) ₁₂₄ - <i>block</i> -P(fcGE) _{11.1}	8.2	8500	5700	1.06	n.d. ^c
P4	mP(EG) ₁₂₄ - <i>block</i> -P(fcGE) _{10.4}	7.7	8300	5700	1.07	n.d. ^c
P5	mP(EG) ₄₅ - <i>block</i> -P(fcGE) ₆	11.7	3600	2600	1.08	n.d. ^c
P6	mP(EG) ₂₄ - <i>block</i> -P(fcGE) _{9.1}	27.2	3600	1900	1.05	0.034
a) M_n and molar ratio of fcGE (mol%) determined from ¹ H-NMR; b) M_n determined via SEC in DMF vs PEG standards, $\bar{D}=M_w/M_n$; c) not determined.						

The block copolymer **P3** is further analyzed via ¹H-DOSY-NMR spectroscopy. Figure 24 displays the spectrum: the x-axis shows the conventional ¹H NMR spectrum, and the y-axis gives the diffusion coefficient. From the 2D plot it is clear that the resonances of ferrocene (4.36- 4.00 ppm) and the PEG backbone (3.56-

3.41 ppm) of the 1D ^1H NMR spectrum appear at the same diffusion coefficient proving the formation of a block copolymer.

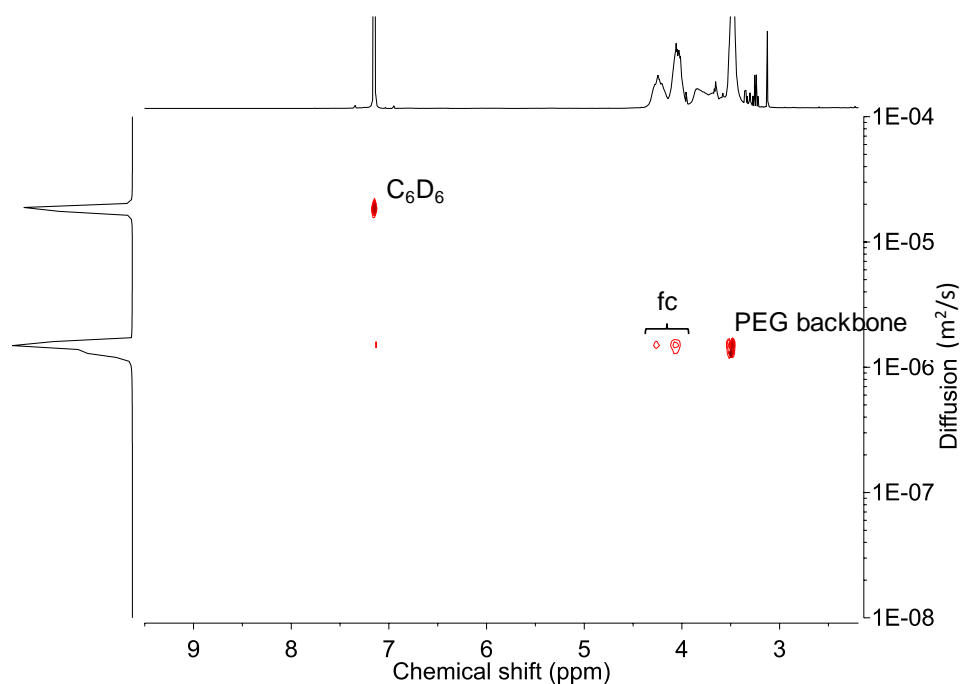


Figure 24. ^1H DOSY NMR spectrum of **P3** (benzene- d_6 , 400 MHz, 298K).

To further confirm the incorporation of fcGE into the block copolymer structure, matrix-assisted laser desorption/ionization time-of-flight mass spectrometry (MALDI-ToF MS) was performed. Figure 25 shows the MALDI-ToF mass spectrum of **P2**. The repeating units of EO and fcGE are clearly recognizable (all distributions are marked with different colors). Each detected signal corresponds to the mass of a linear combination of both monomers in the copolymer. It is important to note that different combinations can have very similar masses and therefore the respective peaks overlap in the spectrum.

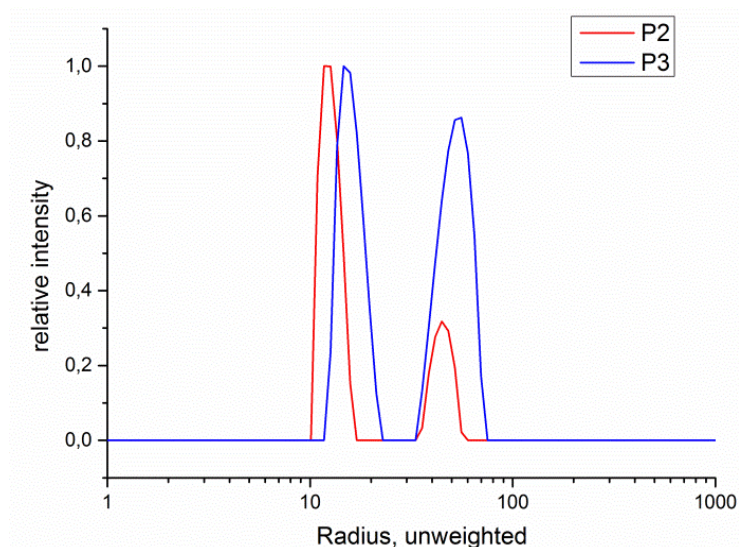


Figure 26. Dynamic light scattering analysis of the micelle formation of polymer **P3** (1 mg mL⁻¹) and **P2** (5 mg mL⁻¹) in aqueous medium at 90°.

Redox-responsive micellar nanocarriers

Both micelle formulations were tested for their cytotoxicity on SKOV-3 human ovarian cells. An MTT assay performed 48 h post incubation of the cells with a concentration range of micelles ranging from 0.01 to 1 mg·mL⁻¹ did not show any cytotoxic effect of both polymers **P2** and **P3** (Figure 27A), which indicates a promising biocompatibility profile for these materials either as micellar carrier or as surfactant. In contrast, the random copolymers of EO and fcGE exhibited a strong cytotoxic effect, probably due to the absence of the micellar structure, which shields the fc-units from intracellular oxidation and thus prevents them from being cytotoxic.^[305] Encouraged by these findings we investigated the potential of these polymers to solubilize a hydrophobic model drug and to assess whether they can enhance the uptake of this model drug by *in vitro* cultured cells. For this purpose, rhodamine octadecyl ester (Rho-C18) was dissolved in ethanol and encapsulated into the micelles via solvent displacement. Non-encapsulated Rho-C18 was removed via filtration. Cell association of Rho-C18 with SKOV-3 cells was measured by flow cytometry and showed a dose-dependent association of the dye with the cells (Figure 27B). Confocal microscopy (Figure 27C) indicated that the dye was located inside the cells, proving that micelles from both types of polymers are capable to enhance intracellular delivery of a hydrophobic compound. These findings highlight the potential of these polymers as non-toxic carriers for hydrophobic drugs.

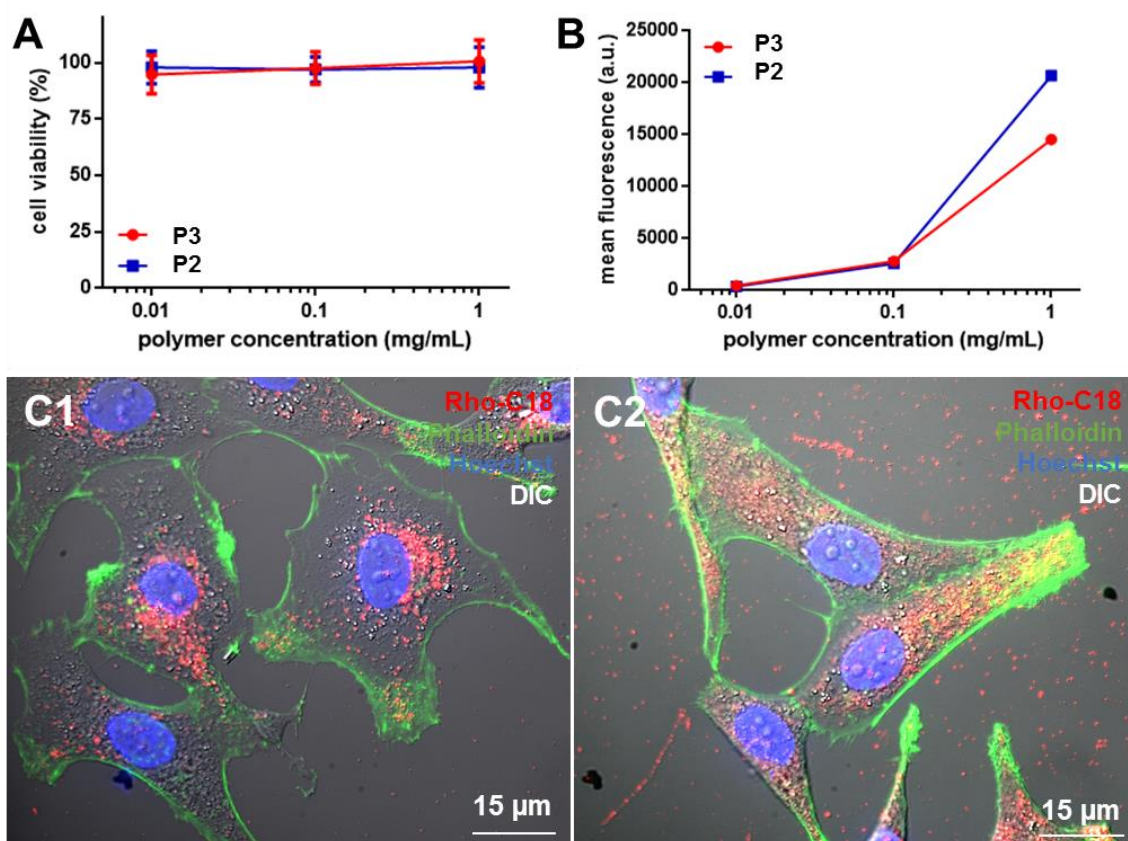


Figure 27. (A) Cell viability assessment of polymer **P2** and **P3** on SKOV-3 human ovarian cells. MTT assay was performed over 48 h ($n = 6$). (B) Cell association measured by flow cytometry of SKOV-3 cells incubated with Rho-C18 loaded micelles. (C) Corresponding confocal microscopy images. Cell membrane was stained green with phalloidin and cell nuclei stained blue with Hoechst. The images are an overlay of a maximum intensity projection of a Z-stack and one DIC channel (experiments conducted by Benoit Louage).

Nonionic and redox-sensitive surfactants for stabilization and destabilization of polystyrene nanoparticles

The block copolymers were studied as redox-active surfactants for oil-in-water miniemulsions. Free radical miniemulsion polymerization of styrene was performed to produce a model nanocarrier. In all miniemulsion polymerizations, an osmotic pressure agent (hexadecane) and AIBN as the initiator for the radical polymerization were dispersed together with styrene in water using different concentrations of the surfactants **P2**, **P3** and **P6**. As reference, PS nanoparticles stabilized with LutensolAT50 were also prepared. Stabilization of the miniemulsion with **P6** (at concentrations between 0.26-1.5 mg mL⁻¹) led to PS nanoparticles with broad size

distributions. Changing to the more hydrophilic block copolymers **P2** and **P3**, monomodal size distributions were obtained with a concentration dependent size: at a concentration of 0.43 mg mL^{-1} of **P2**, nanoparticles with mean diameters of ca 400 nm (Table 11, entry A, Figure 28A) were obtained. Increasing the surfactant concentration to 1 mg mL^{-1} , polystyrene nanoparticles with diameters of about 200 nm for **P2** (entry B in Table 11, Figure 28B) and 245 nm (entry D Table 11) for **P3** were obtained. Increasing the concentration of **P2** to 1.5 mg mL^{-1} (entry C Table 11, Figure 28C) resulted in a further decrease of the nanoparticle diameter to 180 nm and also lead to more monodisperse nanoparticles with a polydispersity of 0.03. Under the same conditions LutensolAT50 (1 mg mL^{-1} , entry E Table 11) produced nanoparticles with ca. 190 nm diameter indicating a similar performance of the fc-PEG-surfactants.

Table 11. Results of generated PS-nanoparticles by miniemulsion polymerization.

#	surfactant	$c_{\text{surfactant}} / \text{mg mL}^{-1}$	d/nm^a	PDI^a
A	P2	0.43	402	0.14
B	P2	1.02	216	0.05
C	P2	1.50	178	0.03
D	P3	1.04	245	0.09
E	Lut.AT50	1.03	193	0.3

a) determined by dynamic light scattering (DLS) analysis.

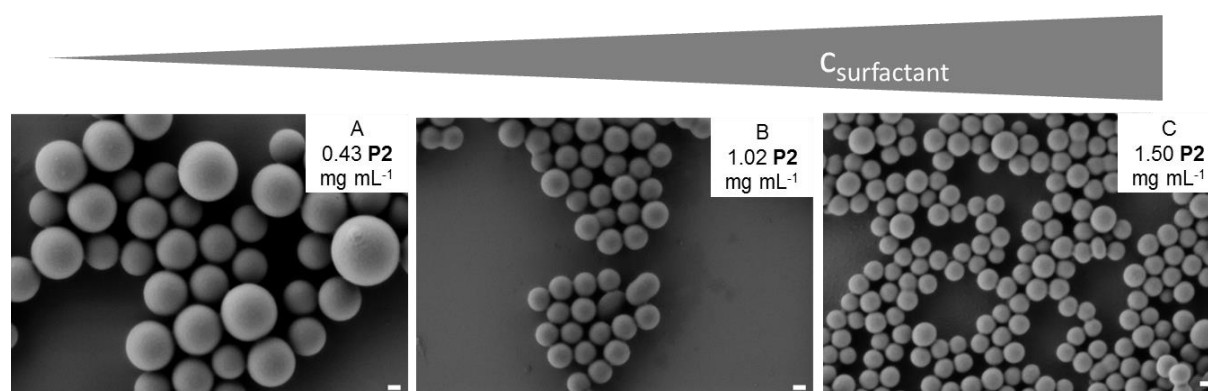


Figure 28. SEM images of PS nanoparticles generated by the miniemulsion with the amphiphilic copolymer **P2** as surfactant at different concentrations (A: 0.43 mg mL^{-1} ; B: 1.02 mg mL^{-1} ; C: 1.50 mg mL^{-1}), scale bar: 100 nm.

Redox- and pH-triggered destabilization of the nanocarrier dispersions was investigated by addition of acid or an oxidant (different concentrations of H_2O_2 ,

AgSO_3CF_3 or KMnO_4). After the oxidation of the iron(II) in fc to the ferrocinium species, a double hydrophilic block copolymer is produced,^[228] resulting in the destabilization of the dispersion and the precipitation of the nanoparticles (Figure 29). Miniemulsions stabilized with the nonionic, redox-responsive surfactants **P2** and **P3** were stable at neutral pH and/or in the presence of salt ions (NaCl, 1M) for at least several months. After acidification to pH=3 (HCl) after three days (or at pH=5 after 5 days) the dispersion destabilized due to the oxidation of fc under the acidic conditions. The rather slow response might be attributed to the proximity of the hydrophobic ferrocene groups on the nanoparticle surface, thus shielded by the PEG block from the water phase including the acid or oxidation agent. When the pH was further decreased to pH=1, the nanoparticles precipitated in several hours. Also the addition of oxidants led to spontaneous precipitation of the nanocarriers due to the redox response of fc. In contrast, the miniemulsions stabilized with LutensolAT50 remained stable under all these conditions.

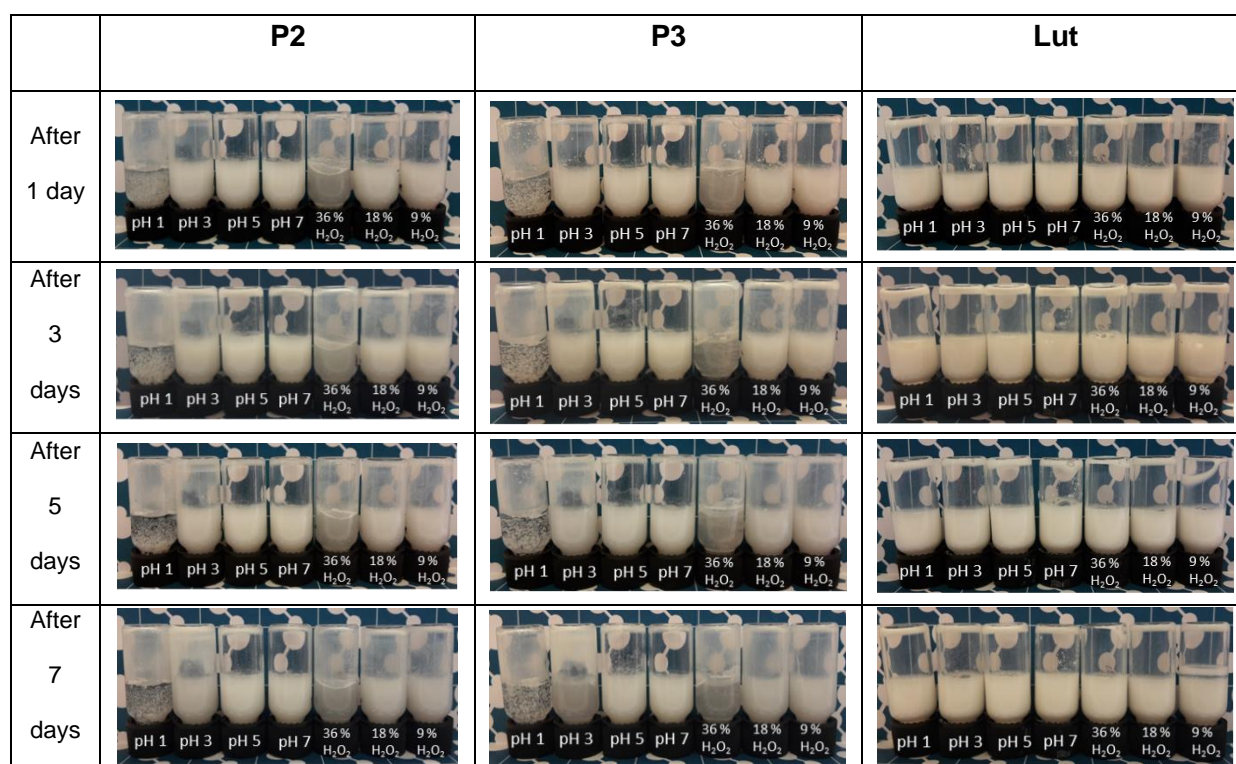


Figure 29. Destabilization of PS nanoparticles stabilized with **P2** and **P3** as well as LutensolAT50 at pH = 1, 3, 5, 7 or 37 %, 18 % or 8 % H_2O_2 detected over 1 week.

The oxidation of ferrocene to the cationic ferrocenium is reversible and allows a fast change of the hydrophilicity of fc-containing materials, which was used in micellar structures and on the surface.^[115, 309] The nanocarriers stabilized with the PfcGE-*b*-PEG surfactants were oxidized and the iron content was studied by inductive coupled plasma (ICP) measurements (Figure 30). After treatment with HCl or H₂O₂, the surfactants become hydrophilic and a majority is dissolved from the surface of the nanoparticles and detected in solution. At pH=7 the detected iron concentration at the PS nanoparticles surface at pH=7 remained higher compared to the supernatant. Still, part of the surfactant could be removed from the surface after washing with water. The redox-triggered destabilization renders the surfactants attractive for film formation “on demand” from aqueous dispersion and allows recovering of the surfactant.

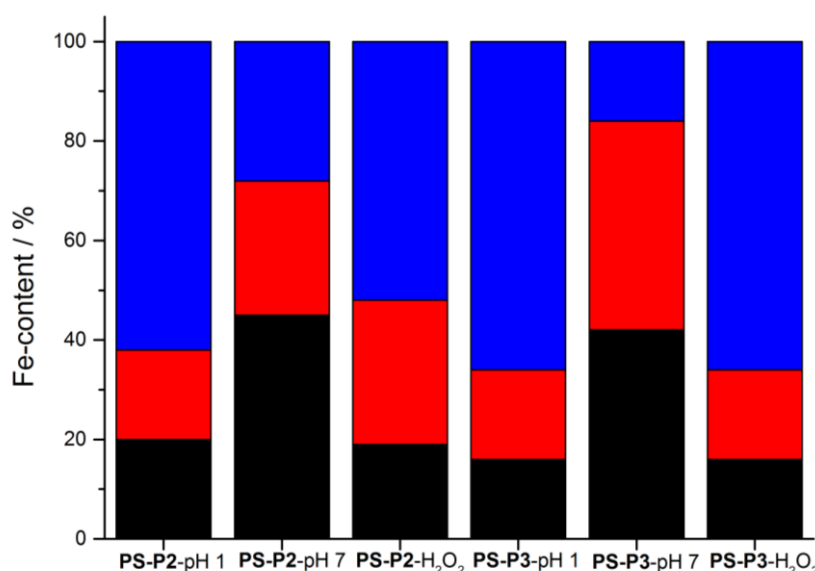


Figure 30. Iron detection (measured by ICP) in the supernatant (blue), the washed water (red) and at the PS nanoparticle surface (black) of dispersions stabilized with **P2** or **P3** at pH 7, after treating with HCl (pH=1), and 36% H₂O₂.

Conclusions

The first redox-responsive and nonionic fc-PEG-based surfactants have been prepared. They were used to generate micellar carriers and as stabilizers in the miniemulsion polymerization. The amphiphilic block copolymers contain several fc-units in their hydrophobic segments, which were prepared by the anionic polymerization of fcGE, a ferrocene-containing epoxide. The block copolymers with

different PEG:PfcGE ratios exhibit low CMCs in water ($< 0.1 \text{ mmol L}^{-1}$), which are in the same range as other polymeric nonionic surfactants. The block copolymers including 7.3 mol% and 8.2 mol% fcGE did not show any cytotoxic effect at concentration ranging from 0.01 to 1 mg mL^{-1} . These two block copolymers were employed as redox-responsive micelles carrying a hydrophobic dye, which were absorbed by SKOV-3 human ovarian cells. In addition, the redox-responsive nanoparticle dispersions were prepared by miniemulsion polymerization. The dispersions were stable against salt addition, but destabilized after the addition of oxidants or strong acid due to the formation of hydrophilic ferrocinium ions that cannot stabilize the nanoparticles. ICP measurements proved that the surfactant is mainly found in the supernatant after the oxidation (detection of the Fe-content), allowing a redox-sensitive destabilization of emulsions “on demand” and the potential recovery of the surfactant from the supernatant by reduction. We foresee that this new type of amphiphilic ferrocene block copolymers will find application as “smart” redox-responsive surfactants.

Experimental Section

Materials

Cesium hydroxide monohydrate ($\text{CsOH} \cdot \text{H}_2\text{O}$, $\geq 99.5\%$), benzene (anhydrous, 99.8%) hydrochloric acid (HCl, ACS reagent, 37%), potassium permanganate (KMnO_4 , ACS reagent, $\geq 99.0\%$), hydrogen peroxide solution (H_2O_2 , meets analytical specification of Ph. Nord, 34.5-36.5%), silver trifluoromethanesulfonate (AgSO_3CF_3 , $\geq 99.0\%$) and polystyrene (PS, $M_n = 35 \text{ kDa}$) were purchased from Sigma Aldrich, chloroform (CHCl_3) from VWR Chemicals, Lutensol AT50 ($\text{C}_{16/18}\text{-EO}_{50}$) from BASF and used as received. Chloroform-*d* and benzene-*d*₆ were purchased from Deutero GmbH. fcGE was synthesized according to the published procedures.^[305] fcGE and poly(ethylene glycol) methylether (mPEG, Sigma-Aldrich) were dried by azeotropic distillation of benzene to remove traces of water. Styrene (Sigma-Aldrich, *ReagentPlus*, $\geq 99\%$) was purified before use by passing through neutral Al_2O_3 . 2,2'-Azobis(2-methylpropionitrile) (azo-isobutyronitrile, AIBN, Acros Organics, 98%) was recrystallized in methanol before used.

Methods

^1H -NMR spectra (300, 400 MHz) and ^{13}C -NMR spectra (75.5 MHz) were recorded using a Bruker AC300 and a Bruker AMX400. All spectra were referenced internally to residual proton signals of the deuterated solvent. For SEC measurements in DMF (containing $0.25\text{ g}\cdot\text{L}^{-1}$ of lithium bromide as an additive) an Agilent 1100 Series was used as an integrated instrument, including a PSS HEMA column ($106/105/104\text{ g}\cdot\text{mol}^{-1}$), a UV detector (275 nm), and a RI detector at a flow rate of 1 mL min^{-1} at $50\text{ }^\circ\text{C}$. Calibration was carried out using PEG standards provided by Polymer Standards Service. Matrix-assisted laser desorption/ionization time-of-flight (MALDI-ToF) measurements were performed using a Shimadzu Axima CFR MALDI-ToF mass spectrometer, employing dithranol (1,8-dihydroxy-9(10*H*)-anthracenone) as a matrix. Scanning electron microscopy (SEM) of the formed nanoparticles was operated at a Zeiss 1530 LEO Gemini microscope with an accelerating voltage of 0.2 kV and a working distance of $\sim 3\text{ mm}$. Therefore, the nanoparticles were diluted in water, dropped onto a silica wafer and dried under ambient conditions.

Dynamic light scattering was used to detect the hydrodynamic diameter of the nanoparticles by a Nicomp 380 Submicron particle Sizer (PSS-Nicomp) at a fixed scattering angle of 90 ° . $10\text{ }\mu\text{L}$ of the emulsion was diluted in $1000\text{ }\mu\text{L}$ distilled water. Critical micelle concentration was measured by isothermal titration calorimetry using a MicroCal VP-ITC (GE Healthcare, Piscataway, USA). Therefore, a stock solution of each polymer with concentrations above the critical micelle concentration ($\text{cmc's} < 0.1\text{ mmol L}^{-1}$, polymers were used with **P2** or **P3** 1 mmol L^{-1} (8 g L^{-1}), **P6** 0.6 mmol L^{-1} (2 g L^{-1})) was added drop-wise ($2\text{ }\mu\text{L}$ in 25 steps) into an ITC chamber at $25\text{ }^\circ\text{C}$. During the measurement, the heat flow was detected, whereas an exothermic heat flow contributes from dilution of the surfactant solution, which first increases with the concentration of the surfactant and decreases after micelles were formed because of dilution of the micelle solution. At the inflection point, micelles were formed, thus the critical micelle concentration was reached. Inductively coupled plasma optical emission spectroscopy (ICP-OES) was used to determine the iron concentration in solution and at nanoparticle surface. ICP-OES measurements were performed at an ACTIVA M spectrometer (Horiba Jobin Yvon, Bernsheim, Germany) equipped with a cyclone chamber and a Meinhardt-type nebulizer. The system is controlled by a ACTIVAnalyst 5.4 software. As conditions were employed: 1250 W

forward plasma power, 12 L min⁻¹ Ar flow and 15 rpm pump flow. The emission line of argon at 404.442 nm was used as reference line. For concentration determination four different iron standard concentrations, two different elemental emission lines were detected before using 5 s integration time. The software provided a dynamic underground correction for baseline corrections. For iron quantification the emission lines at 238.863 nm, 259.940 nm and 261.187 nm were chosen. For total iron loading measurement 0.1 mL of the solution or dispersion was diluted in 10 mL water.

Synthesis

General procedure for the polymerization of fcGE: (mPEG-*b*-PfcGE). The initiator, 800.0 mg (0.1600 mmol) mPEG, and 24.2 mg (0.1441 mmol, 0.9 eq.) of cesium hydroxide monohydrate were placed in a 100 mL Schlenk flask and suspended in 10 mL of benzene. The mixture was stirred at 60 °C under an argon atmosphere for 1 h and evacuated at 40 °C (10⁻² mbar) for 12 h to remove benzene and the water formed (as an azeotrope with benzene) to generate the corresponding cesium alkoxide. The flask was filled with argon and cooled to room temperature, and then fcGE (824.4 mg (3.03 mmol) was added. The reaction mixture was heated up to 100 °C and stirred for 24 h before the living chain ends were terminated with methanol and the block copolymer was precipitated in cold diethyl ether to remove any unreacted fcGE. The block copolymer was obtained as a yellow to orange solid. Yields: 70-85%. ¹H NMR (C₆D₆, 400 MHz, 298 K): δ(ppm) = 4.40-4.15 (br, 4H, -O-CH₂-Cp(2, 5)), 4.15-3.92 (br, 7H, -O-CH₂-Cp(3, 4)-Fe-Cp), 3.60-3.38 (br, PEG-backbone), 3.13 (s, 3H, H₃C-O-).

General procedure for polymerization of styrene by free radical oil-in-water miniemulsion. PEG-*b*-PfcGE or Lutensol AT50 was dissolved in 2 mL water. After a solution of 56 µL styrene, 3.2 µL hexadecane and 0.5 mg AIBN was added, the dispersion was stirred for 1 h at 1000 rpm. The dispersion was treated by inverse ultrasonication at 70% amplitude for 2 min to produce a stable miniemulsion and the polymerization was allowed to proceed for 24 h at 72 °C.

General procedure for destabilization of polystyrene nanoparticles. 0.1 mL emulsion were added to 0.75 mL HCl solution with different pH values (pH = 1, 3, 5, 7) or oxidant solutions (36%, 18% or 8% H₂O₂, 4 mg·mL⁻¹ KMnO₄, 8 mg·mL⁻¹ AgSO₃CF₃). At the latest after 3 days the emulsions destabilized and the

nanoparticles aggregated. As comparison also 0.1 mL polystyrene emulsion stabilized with Lutensol AT50 was added to 0.75 mL HCl solutions with different pH values or hydrogen peroxide solution.

Preparation of miniemulsions for ICP-OES measurements: 0.1 mL emulsion was added to 0.75 mL HCl solution at pH 1 or 36% H₂O₂. After 3 days the emulsions destabilized. After centrifugation at 6000 rpm for 15 min, the supernatant was removed and diluted in 9.25 mL water for ICP-OES measurements. The nanoparticles were redispersed in 0.75 mL water and centrifuged again at 6000 rpm for 15 min. Subsequently, the water was removed and also diluted in 9.25 mL water for ICP-OES measurements. The nanoparticles were redispersed in 10 mL water to detected remained iron on the nanoparticle surface by ICP-OES measurements.

2.3 Stabilization of inverse miniemulsions by silyl-protected homopolymers⁴

Besides direct miniemulsions, also inverse miniemulsions are used to generate different kinds of nanocarriers with encapsulated hydrophilic payloads like oligonucleotides or peptides, as mentioned in chapter 1.2. In contrast to direct miniemulsions, the surfactant variety is less and even worse for surfactants with additional functionality like the introduced polyglycidol block copolymers in chapter 2.1 for further surface functionalization. In addition, most of the stabilizers in inverse miniemulsions are block copolymers that are difficult to synthesize and/or that cannot be easily removed after transfer from a hydrophobic continuous phase to an aqueous continuous phase. We describe here a new strategy for the synthesis of a pH-sensitive surfactant for inverse miniemulsions by radical addition-fragmentation chain transfer (RAFT) polymerization, which consists in a homopolymer with triisopropylsilyl protecting groups. The protecting groups ensure the efficient stabilization of the inverse miniemulsions. Nanocapsules can be formed and the protecting group can be subsequently cleaved for the re-dispersion of nanocapsules in an aqueous medium with a minimal amount of additional surfactant.

Motivation

Nanocapsules, core-shell nanoparticles with a liquid core, have found successful applications in controlled and targeted delivery of therapeutics^[135-137] or as contrast agents.^[140] Nanocapsules can be generated by different techniques such as the layer-by-layer self-assembly,^[150-152] the (nano)precipitation method,^[155] solvent evaporation^[157-159] or miniemulsion polymerization.^[160] The miniemulsion polymerization process is suitable for the synthesis of well-defined nanocapsules because of the high stability of the miniemulsion droplets generated. With this method, nanocapsules with a liquid core can be prepared in a single step^[161] with high encapsulation efficiency.^[160, 162-165] Their properties can be controlled by the

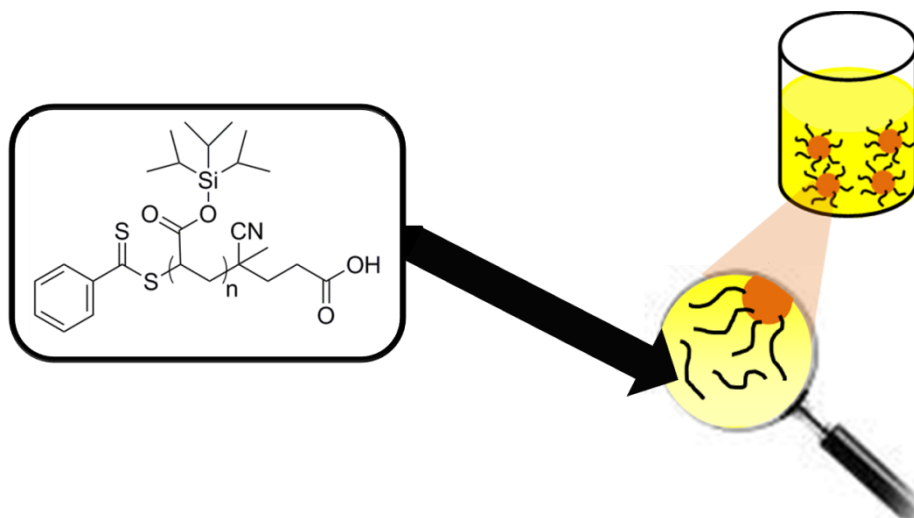
⁴ This section is based on the publication "Stabilization of Inverse Miniemulsions by Silyl-Protected Homopolymers" by Sarah Wald, Frederik R. Wurm, Katharina Landfester and Daniel Crespy published in 2016 in *Polymers*, volume 8 on page 303 (1-10).^[310] S. Wald, F. Wurm, K. Landfester, D. Crespy, *Polymers* **2016**, 8, 303.

amount and type of surfactant and osmotic pressure agent, the uniformity and intensity of energy input used to create the dispersion, and the monomer polarity. Surfactants are usually needed during the process to decrease the interfacial tension between the two phases and to stabilize the resulting nanocapsules.^[160, 172, 173] In miniemulsion, the droplets are not densely covered with the surfactant molecules.^[174] Oil-soluble non-ionic surfactants^[311-313] and / or amphiphilic block copolymers are usually employed as stabilizers with low hydrophilic / lipophilic balance in water-in-oil emulsions.^[36, 174, 178] Most of these amphiphilic block copolymers possess a PEG-based hydrophilic block and are distinct in the hydrophobic block as well as the length of the different blocks.^[163, 238, 239, 314-318] The PEG-based amphiphilic block copolymers can be synthesized by anionic ring opening polymerization, a polymerization technique with a living character,^[319, 320] so that the surfactants have a narrow molecular weight distribution and a precise block length. Other amphiphilic block copolymers can be generated by controlled radical polymerization techniques. The reversible addition-fragmentation chain transfer polymerization technique used in this work was reported by Rizzardo and coworkers.^[321] The principle consists of introducing a thiocarbonyl thio compound acting as a chain-transfer agent (CTA). RAFT polymerization can be used for a wide range of monomers with a large variety of polymerization conditions and solvents.^[322-324]

For biomedical applications, nanocarriers loaded with hydrophilic cargo synthesized in inverse miniemulsions have to be transferred in water. Therefore, two surfactants are needed during the process. The first one is an oil-soluble surfactant with a hydrophilic-lipophilic balance value of 4-8 and stabilizes water droplets in the oil phase. The second surfactant is water-soluble, possesses a larger HLB value (8-18), and stabilizes the nanocapsules re-dispersed in water.^[178] During the transfer of the nanocapsules into water, the oil-soluble surfactant remains at the surface of the nanocapsule. This fact can have detrimental effects on the nanocapsule functionality.^[163, 325-327] To overcome this problem, surfactants that can switch their amphiphilicity on demand were developed. Such surfactants possess functionalities that can be triggered by different stimuli.^[12] Examples of pH-switchable surfactants include carboxylic,^[328] tertiary amine^[329, 330] or imidazole groups.^[331, 332] Müllen et al.^[14] reported the synthesis of a PEG-based surfactant for inverse emulsions with a photocleavable group in one block. Before deprotection, the block copolymer is

soluble in the oil phase and can stabilize the PLLA nanoparticles in the oil phase. During the transfer into water, the protection groups can be cleaved by light and stabilize the nanoparticles in water.

Herein, we simplify the procedure by using a protected homopolymer. Triisopropylsilyl protected poly(acrylic acid) was used as surfactant in inverse miniemulsions (Scheme 11). The surfactant properties of the polymer are first tested by stabilizing droplets of water and formamide in cyclohexane. The miniemulsion droplets were then used as nanoreactors^[163] to form polyurea (PU) nanocapsules. The triisopropylsilyl protection group was cleaved during the transfer step of the nanocapsules from an organic dispersion into an aqueous dispersion in order to form a hydrophilic polymer. Because the hydrophobic block of amphiphilic stabilizers shields the chemistry of the nanocapsule surface, they have a strong influence on further grafting of functional biomolecules and on the protein corona. This problem of generally used amphiphilic polymers can be overcome by using a cleavable homopolymer as surfactant in miniemulsions.



Scheme 11. Polyisopropylsilylacrylate as pH-sensitive oil-soluble surfactant to produce stable polyurea nanocapsules by inverse miniemulsion.

Results and Discussion

Synthesis and Characterization of poly(triisopropylsilyl acrylate)

A desirable polymer surfactant for inverse miniemulsions should stabilize water-in-oil miniemulsions and then stabilize the formed colloids when they are re-dispersed in water. Therefore, we introduced switchable groups in the side-chain of the polymers.

The soluble polymer backbone consisted in the water-soluble poly(acrylic acid) that was connected to hydrolysis-labile protecting groups. When the side-chains of the polymer are not cleaved, the polymer is oil-soluble. Acrylic acid with trialkylsilyl protecting groups was used as monomer, triisopropylsilyl acrylate (TIPSA), because the TIPS-group is easy to cleave under rather mild basic and/or acidic hydrolysis reactions.^[333-337] On the other hand, the hydrolysis kinetics of the TIPS groups are relatively slow in the presence of the aqueous dispersed phase of water-in-oil emulsions. Indeed, the isopropylsilyl protection group is 700,000 times more stable towards acid catalyzed hydrolysis than the trimethylsilyl protection group, because the three isopropyl substituents show a strong steric screening for the silicon and also to the atom to which silicon is connected.^[338-341]

RAFT polymerization was used to prepare polymers with adjustable molecular weights that are suitable for the stabilization of the inverse miniemulsion droplets, as demonstrated by interfacial tension measurements. The polymers (PTIPSA) were synthesized as shown in Figure 31 with different molecular weights by changing the monomer: initiator ratio. Two polymers with molecular weights of 4,600 g·mol⁻¹ and 10,100 g·mol⁻¹ and a molecular weight dispersity of $M_w/M_n = 1.19$ and 1.67, respectively, were generated and used as stabilizers in the inverse miniemulsion process. The prepared molecular weights are typical for inverse miniemulsions and correspond to short polymer chains.^[121] The polymers chains are sufficiently small to allow for reaching rapidly the adsorption equilibrium at the surface of the droplets, and are large enough to allow efficient steric stabilization of the droplets without imparting the viscosity of the suspending phase. A narrow polydispersity for polymers is important in colloid science for the preparation of micelles of precise and predictive sizes. However, in our study we use the surfactant to stabilize large nanodroplets. The difference between the molecular weight dispersity ($\mathcal{D}=M_w/M_n$) values of the two polymers will therefore not impact significantly impact the colloidal stabilization.

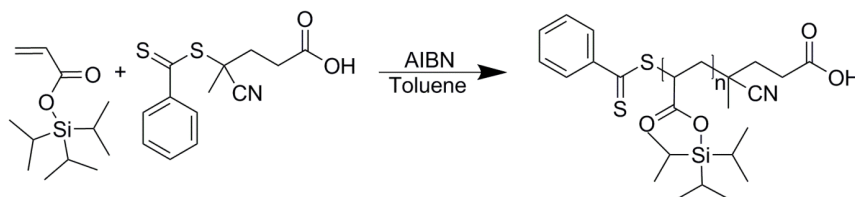


Figure 31. Synthesis of polymerized triisopropylsilyl acrylate (PTIPSA) by reversible addition-fragmentation chain transfer (RAFT) polymerization.

Stabilization of inverse miniemulsions by PTISA

The higher molecular weight polymer ($10,100 \text{ g}\cdot\text{mol}^{-1}$) was used to stabilize inverse (water-in-cyclohexane) miniemulsions, because it showed better stability than PTIPSA with $4,600 \text{ g}\cdot\text{mol}^{-1}$. Therefore, water-in-oil miniemulsions were prepared with a concentration of $9 \text{ mg}\cdot\text{mL}^{-1}$ PTIPSA in cyclohexane. However, no stable emulsion was achieved. Thus, we selected water-free formamide as polar solvent to replace water, because the interfacial tension between cyclohexane and formamide ($\gamma = 21.6 \text{ mN/m}$ at 22°C , Figure 32) is lower than the one of cyclohexane and water ($\gamma = 48.7 \text{ mN/m}$ at 22°C , Figure 32, literature $\gamma = 50.2 \text{ mN/m}$ at 20°C ^[271]). Water-free formamide was also chosen to eliminate the possible hydrolysis of the TIPS-group during the nanocapsules synthesis. After testing the surface active properties of PTIPSA in cyclohexane (PTIPSA concentration $9 \text{ mg}\cdot\text{mL}^{-1}$) by interfacial tension measurement against formamide ($\gamma = 10.3 \text{ mN}\cdot\text{M}^{-1}$ at 22°C , Figure 32), stable droplets of formamide in cyclohexane were formed using the inverse miniemulsion procedure due to the lower interfacial tension of formamide/cyclohexane compared to water/cyclohexane.

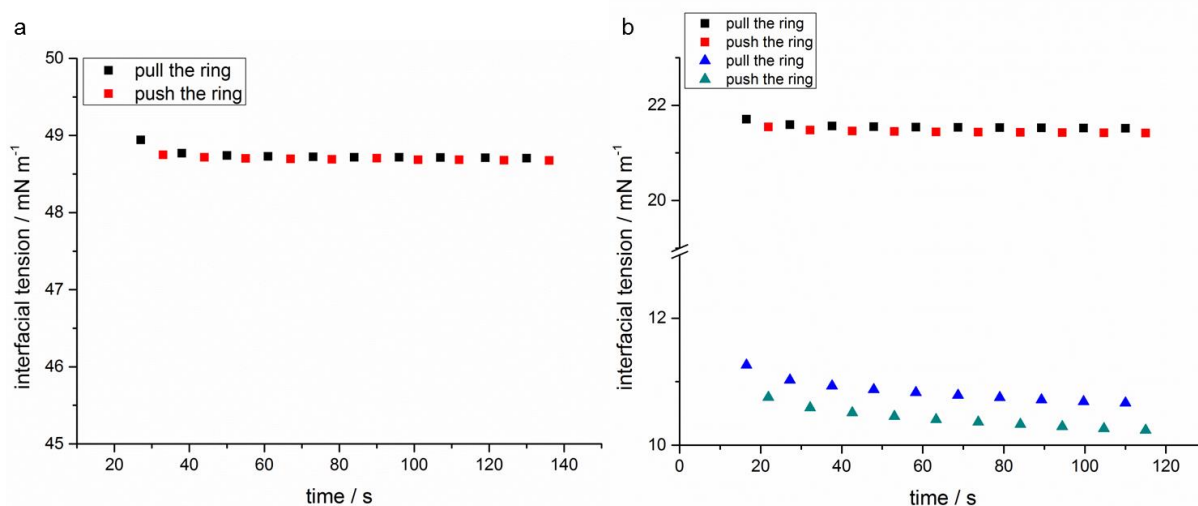
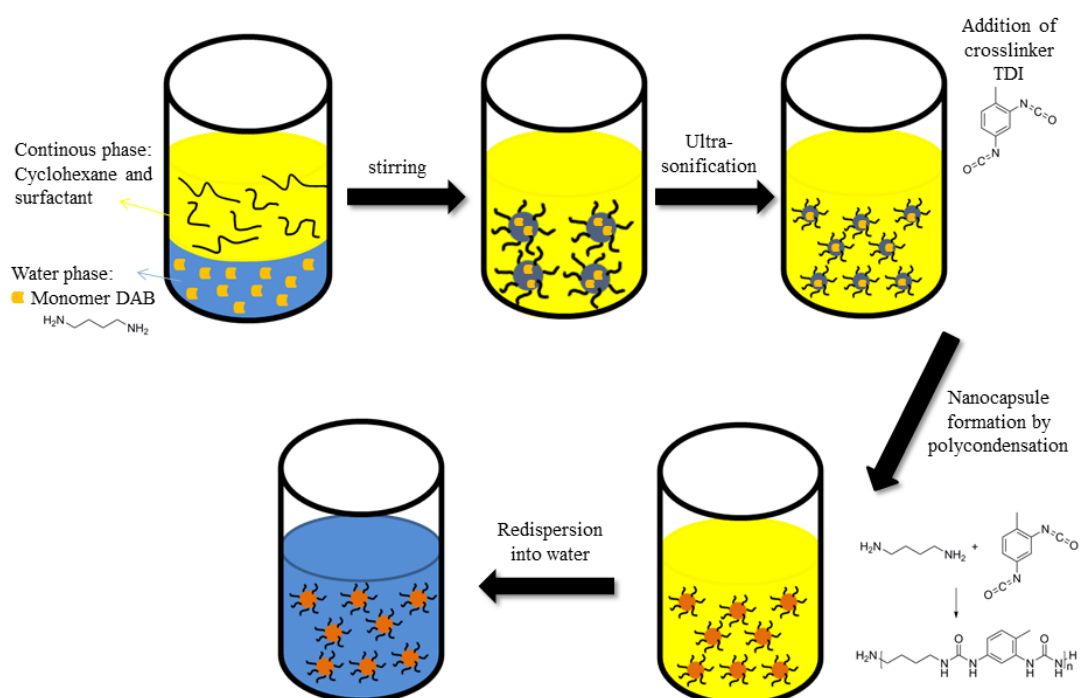


Figure 32. Interfacial tension measurement of cyclohexane and water ($\gamma = 48.7 \text{ mN m}^{-1}$ at 22°C) (a) and water-free formamide and cyclohexane ($\gamma = 21.6 \text{ mN m}^{-1}$ at 22°C) as well as water-free formamide and PTIPSA-cyclohexane solution ($\gamma = 10.3 \text{ mN m}^{-1}$ at 22°C) (b).

To check the utility of such a system for further synthesis of nanoparticles, the droplets of formamide-in-cyclohexane miniemulsions were then used as

nanoreactors for the fabrication of polyurea nanocapsules by an interfacial polyaddition reaction (Scheme 12). We first verified that the triisopropylsilyl protection groups were stable in the presence of the monomers used in the polyaddition reaction. For this, 1,4-diaminobutane (DAB) or TDI was added to a PTIPSA solution in cyclohexane- d_{12} and was analyzed by $^1\text{H-NMR}$ spectroscopy after stirring for 3 days. In both cases, no cleavage of the protecting group was observed. The monomer DAB and the lipophobe sodium chloride in anhydrous formamide were added to the surfactant solution. After the emulsion was formed, the second monomer TDI was added via the hydrophobic phase to form polyurea nanocapsules by interfacial polycondensation.



Scheme 12. Procedure of an inverse miniemulsion with 1,4-diaminobutane (DAB) and toluene-2,4-diisocyanate (TDI) as monomers to generate polyurea (PU) nanocapsules and their re-dispersion into water.

Whereas the miniemulsions with the lower molecular weight polymer ($4,600 \text{ g}\cdot\text{mol}^{-1}$) were not stable or formed agglomerated nanocapsules ($d > 1 \text{ }\mu\text{m}$), the miniemulsions with the higher molecular weight ($10,100 \text{ g}\cdot\text{mol}^{-1}$) and a surfactant concentration of $9 \text{ mg}\cdot\text{mL}^{-1}$ yielded capsules with z-average sizes of 306 nm (DLS). After the polyaddition reaction, the typical morphology of hollow nanocapsules was

detected by electron microscopy (see Figure 33). The nanocapsules determined in Figure 33 are collapsed and broken due to high vacuum chamber ($3.8 \cdot 10^{-6}$ mbar) during electron microscopy measurement and led to evaporation of the liquid core independent of the polymer shell material. [146, 185, 229]

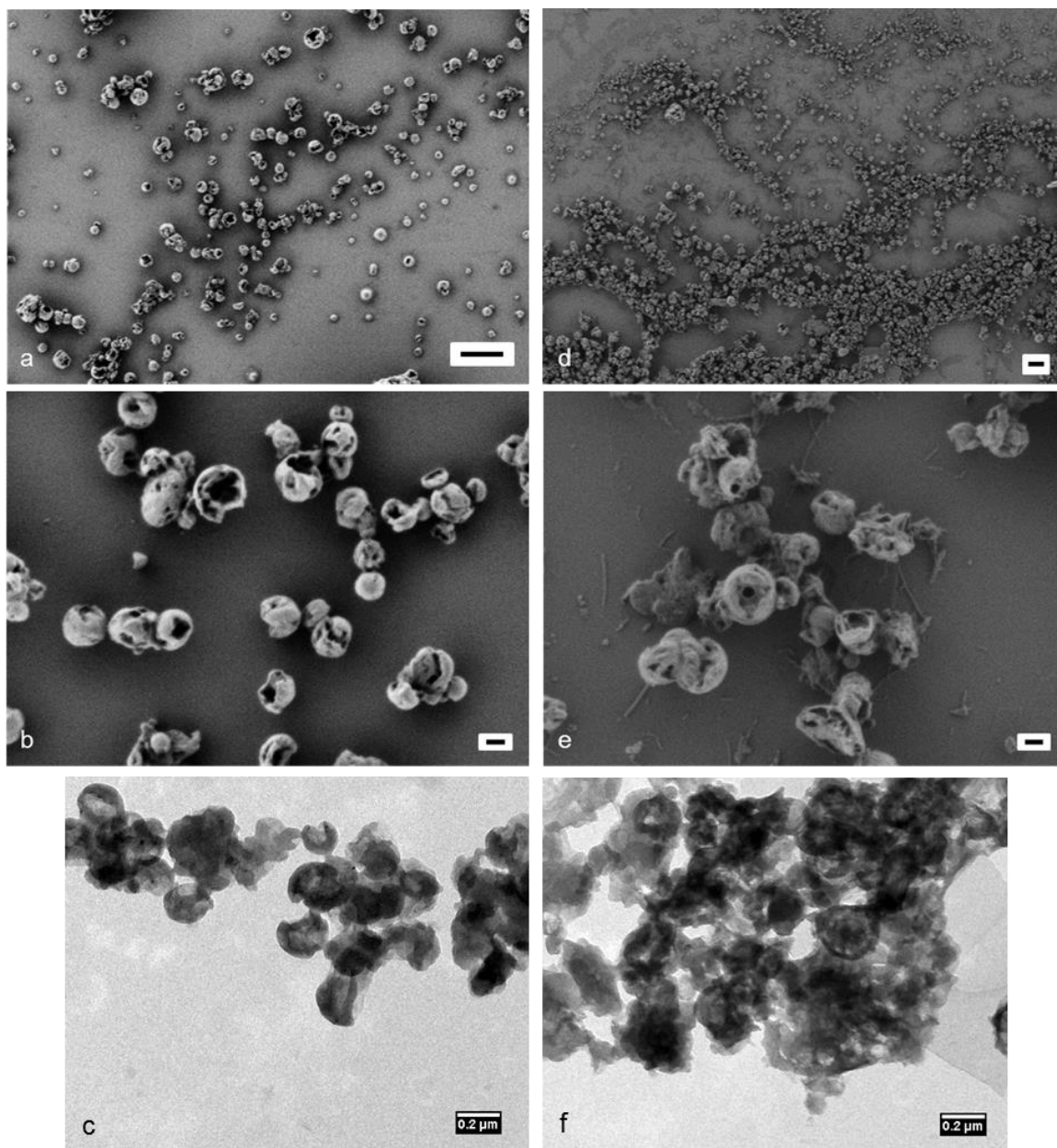


Figure 33. SEM images of PU nanocapsules before ((a) scale bar 1 μm ; (b) scale bar 100 nm) and after redispersion ((d) scale bar 1 μm ; (e) scale bar 100 nm) into 0.1 wt% SDS solution as well as TEM images of prepared PU nanocapsules before ((c) scale bar 200 nm) and after redispersion ((f) scale bar 200 nm) into 0.1 wt% SDS solutions.

Deprotection of the triisopropylsilyl groups

For the study of the deprotection of the triisopropylsilyl groups by ^1H -NMR spectroscopy, the monomer TIPSA was chosen as model molecule because we always observed a phase separation for the investigations of the deprotection of PTIPSA in solution. Indeed, there was no common solvent for the PTIPSA, the hydrolyzed PTIPSA, and the leaving protecting group. TFA was selected for the cleavage of the protecting group because it was used successfully for the *t*-butyldimethylsilyl protection groups.^[342, 343] Complete deprotection was detected after 1 h for TFA concentrations of 1 M and 0.1 M in the reaction solution (Figure 34a). Therefore, the cleavage of the TIPS group is fast although it is anticipated that the deprotection should take longer time for the polymer. Furthermore, partial hydrolysis of the TIPS group was observed in water after 2 days without adding a catalyst or cleavable agent into the solution (Figure 34b).

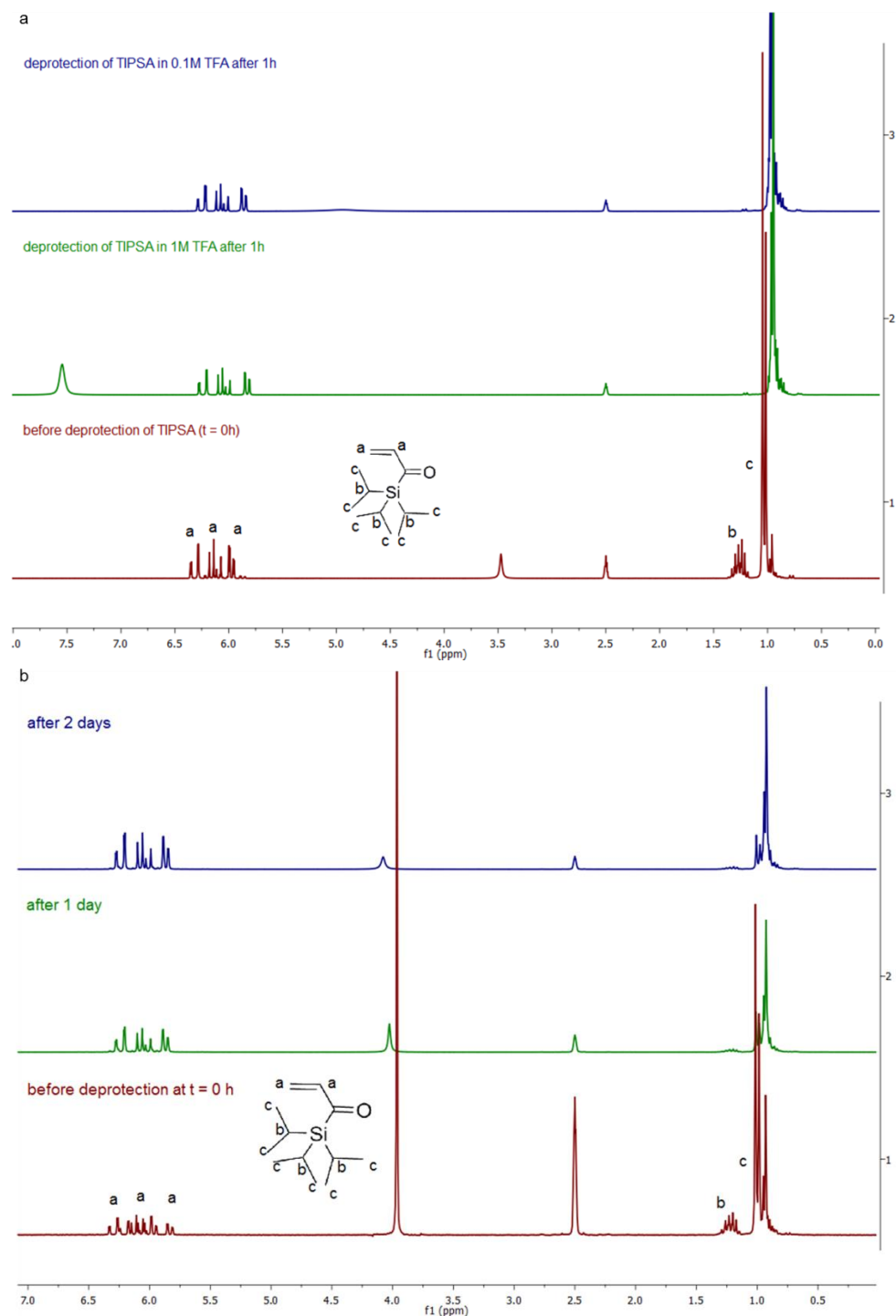


Figure 34. Kinetic measurements of deprotection of TIPSA with TFA solutions (a, red: $t = 0$ h, green: deprotection in 1M TFA at $t = 1$ h, blue: deprotection in 0.1M TFA at $t = 1$ h) or water (b, red: $t = 0$ h, green: $t = 1$ day, blue: $t = 2$ days) measured by ^1H -NMR spectroscopy in solvent mixtures of $\text{DMSO}-d_6$ and D_2O . The signal around 1.38–1.16 ppm completely disappeared and the signal at 1.03 shifted from the red to the blue and green spectra in 1.00–0.83 ppm region.

Transfer of the nanocapsules in water

The transfer of the nanocapsules from oil to water is crucial for their use in biomedical applications. Both TFA concentrations (1 M and 0.1 M) were prepared and tested in parallel. The TFA solutions were mixed with a defined amount of miniemulsion (1 g in 5 g TFA solution). During the re-dispersion process, the evaporation of cyclohexane in water was found to take around 3 h – as detected by $^1\text{H-NMR}$ analysis against DMF as an internal standard – meaning that the deprotection should be faster or in the same time frame as for the evaporation of cyclohexane. No stable dispersion was formed after evaporation of cyclohexane, meaning that the deprotected PTIPSA alone is not efficient enough to stabilize the nanocapsules in the aqueous solutions of TFA. Indeed, large agglomerates were generated with diameters larger than 500 nm. The agglomeration was attributed to the acidic environment as the formed polyacrylic acid remained protonated and could therefore not contribute to an electrostatic stabilization of the nanocapsules. Aggregates were still present after neutralization. To overcome this issue, a slight amount of water-soluble surfactant (SDS) was added in the suspending phase (reaching concentrations of 0.1 wt% or 0.01 wt% SDS in the water phase). Indeed, stabilization under acidic conditions with lower SDS concentration was not efficient, because large agglomerates were formed ($d > 3\ \mu\text{m}$).

Thus under acidic conditions (1 M TFA, low pH $\sim \text{pK}_a[\text{TFA}]$) the addition of only 0.1 wt% or 0.01 wt% SDS were sufficient for the stabilization of the nanocapsule dispersion in water. The nanocapsules stabilized with the lower SDS concentration (0.01 wt% in 1 M TFA) also showed large agglomerates ($d > 3\ \mu\text{m}$). The dispersion stabilized with the higher SDS concentration (0.1 wt% in 1M TFA) displayed particles with an average diameter of 203 nm, but also with a small amount of agglomerates ($d > 4\ \mu\text{m}$). Under acidic conditions the addition of SDS seems to be necessary to obtain stable nanocapsules. Therefore, we also used only SDS (0.1 wt%) as surfactant for the redispersion step without adding a chemical for deprotection of the silyl group. With 0.1 wt% SDS solution, we could generate stable nanocapsules with a diameter of 406 nm (Figure 33).

Conclusions

We demonstrated that poly(acrylic acid) protected with isopropyl silyl groups could stabilize polyurea nanocapsules produced by an inverse miniemulsion process. No amphiphilic block copolymer was needed for the stabilization in the cyclohexane phase. To prepare the stabilizer, isopropylsilyl acrylate was polymerized with 4-cyano-4-(phenylcarbonothioylthio)pentanoic acid as chain transfer agent by the RAFT polymerization process. The polymer was found to stabilize formamide-in-cyclohexane miniemulsions and polyurea nanocapsules were successfully formed. Afterwards the miniemulsion could be re-dispersed with a minimal amount of additional surfactant. This method therefore overcomes the major issue of the presence of the hydrophobic blocks of amphiphilic block copolymer surfactant that are present on the surface of nanoparticles after re-dispersion in water.

Experimental Section

Materials

2,2'-Azobis(2-methylpropionitrile) AIBN (Acros Organics, 98%) was recrystallized in MeOH before used. Triisopropylsilyl acrylate TIPSA (CHEMOS GmbH), 4-cyano-4-(phenylcarbonothioylthio)pentanoic acid (Sigma-Aldrich, 97%), sodium dodecyl sulfate SDS (Alfa Aesar, 99%), sodium chloride (Sigma-Aldrich, 99.5%), 1,4-diaminobutane DAB (Fluka, 98%), toluene-2,4-diisocyanate TDI (Fluka, 99.9%), and toluene (Sigma-Aldrich, anhydrous 99.8%) were used as received. The solvents tetrahydrofuran (THF), methanol (MeOH), and cyclohexane were of analytical grade. Formamide (Fluka, 99%) was dried over 4 Å molecular sieves before used. Dichloromethane- d_2 (Roth, 99.5% atom%D), dimethylsulfoxide- d_6 (Roth, 99.8% atom%D), deuterium oxide- d_2 (Sigma-Aldrich, 99.9% atom%D) and cyclohexane- d_{12} (Sigma-Aldrich, 99.6% atom%D) were used as received.

Methods

Size exclusion chromatography (SEC) carried out in THF was used to detect the molecular weights of the synthesized polymers and their molecular weight dispersity (\bar{D}) with an Agilent PSS SECcurity. The concentration of the samples were 5 mg·mL⁻¹. After filtered through a 0.45 µm teflon filter, the samples were injected. The elution rate through the three SDV columns (PSS) was 1 mL·min⁻¹. The SDV columns with

dimensions of 300 x 80 mm have a particle size of 10 μ m and pore sizes of 106, 104 and 500 Å. For detection a UV-(254 nm) S-3702 detector and a DRI shodex RI-101 detector (ECR) were utilized. The molecular weights were calculated by comparing with a polystyrene standard provided by the Polymer Standards Service GmbH.

^1H -NMR spectra were measured on a Bruker Avance 300 spectrometer operating at 300.23 MHz Larmor frequency. In 0.5 mL CD_2Cl_2 15 mg of the synthesized polymers was dissolved and the spectra were calibrated according to the chemical shift of 5.32 ppm. For the studies of deprotection of the TIPS group the reaction solution was measured every hour. The spectra were calibrated according to the chemical shift of 2.5 ppm (DMSO-d_6). ^{13}C -NMR spectra were measured using a 700 MHz Bruker Avance III spectrometer. In 0.6 mL deuterated dichloromethane (CD_2Cl_2) 30 mg of the synthesized polymers was dissolved and the spectra were calibrated according to the chemical shift of 1.38 ppm. Dynamic light scattering (DLS) with a Nicomp 380 Submicron particle Sizer (PSS-Nicomp) at a fixed scattering angle of 90° was used to detect the hydrodynamic diameter of the nanocapsules. 10 μL of the emulsion was diluted in 1000 μL cyclohexane or distilled water. For nanocapsule detection a JEOL 1400 transmission electron microscope (TEM) with a LaB_6 cathode (JEOL GmbH, Echting, Germany) was used. The copper grid had been modified with a carbon film (200 mesh, Science Services, Munich, Germany), before the TEM specimen was prepared. Therefore the nanocapsules were diluted in cyclohexane or water and drop-cast on a copper grid. After drying of the TEM grid at room temperature, it was inserted into a sample holder and transferred into the TEM. The TEM was operated at an acceleration voltage of 120 kV. Scanning electron microscopy (SEM) was carried out on a Zeiss 1530 LEO Gemini microscope. The working distance was ~ 3 mm and the accelerating voltage 0.2 kV. The nanocapsules were diluted in cyclohexane or water, drop-cast onto silica wafers, and dried under ambient conditions. 10 μL of the nanocapsule dispersion was diluted with 3 mL cyclohexane or distilled water and placed on silica platelets (SEM) or on a carbon-coated grid (TEM). Infrared (IR) spectroscopy was performed on a PerkinElmer Spectrum BX FT-IR spectrometer. The range of the wavelength was between 4000 cm^{-1} and 400 cm^{-1} . For solid samples, 3 mg of the nanocapsules were mixed with KBr, pressed and subsequently measured. The interfacial tensions were measured

with a ring tensiometer DCAT 21 from DataPhysics. The obtained value of cyclohexane in water ($\sigma = 48.7 \text{ mN}\cdot\text{m}^{-1}$ at 22°C) was comparable to the value reported in the literature ($\sigma = 50.2 \text{ mN}\cdot\text{m}^{-1}$ at 20°C).^[271]

Synthesis

Synthesis of PTIPSA

TIPSA (5.50 mL, 21 mmol) and AIBN (10.46 mg, 0.06 mmol) were added to 4-cyano-4-(phenylcarbonothioylthio)pentanoic acid (55.6 mg, 0.2 mmol) in a dry Schlenk flask and dissolved in 5 mL dry toluene. After three freeze-pump thaw cycles, the mixture was stirred at 70°C for three days under nitrogen. The polymer was precipitated into cold methanol and dried *in vacuo*. Yield = 77%.

^1H -NMR (300 MHz, CD_2Cl_2) $\delta(\text{ppm}) = 7.38$ (t, 5H, Ar H), 2.71-1.42 (m, 10H, CHCH_2 , CH_2CH_2 , CH_3), 1.29 (h, $J = 6.9, 4.9 \text{ Hz}$, 3H, 3^*CH), 1.15-0.92 (m, 18H, 6^*CHCH_3); ^{13}C NMR (700 MHz, CD_2Cl_2) $\delta(\text{ppm}) = 13.19$ (C1-C6), 19.79 (C7-C9), 44.39 (C10-C16), 128.8 (C17-C20), 130.27 (C21, C22), 175.99 (C23, C24); IR (KBr): $\nu = 3416$ (br), 2954 (s), 2872 (s), 2724 (w), 2375 (w), 1719 (s, C=O), 1467 (s), 1396 (m), 1371 (m), 1336 (w), 1266 (s, C-O), 1185 (s, C-O), 1115 (m), 1069 (m, Si-O-C), 1017 (m), 1001 (m), 923 (m), 885 (s, Si-C), 738 (s), 685 (s), 571 (m), 512 (m), 460 cm^{-1} (m); M_n (SEC) = 10,100 g mol^{-1} ; M_w/M_n (SEC) = 1.67.

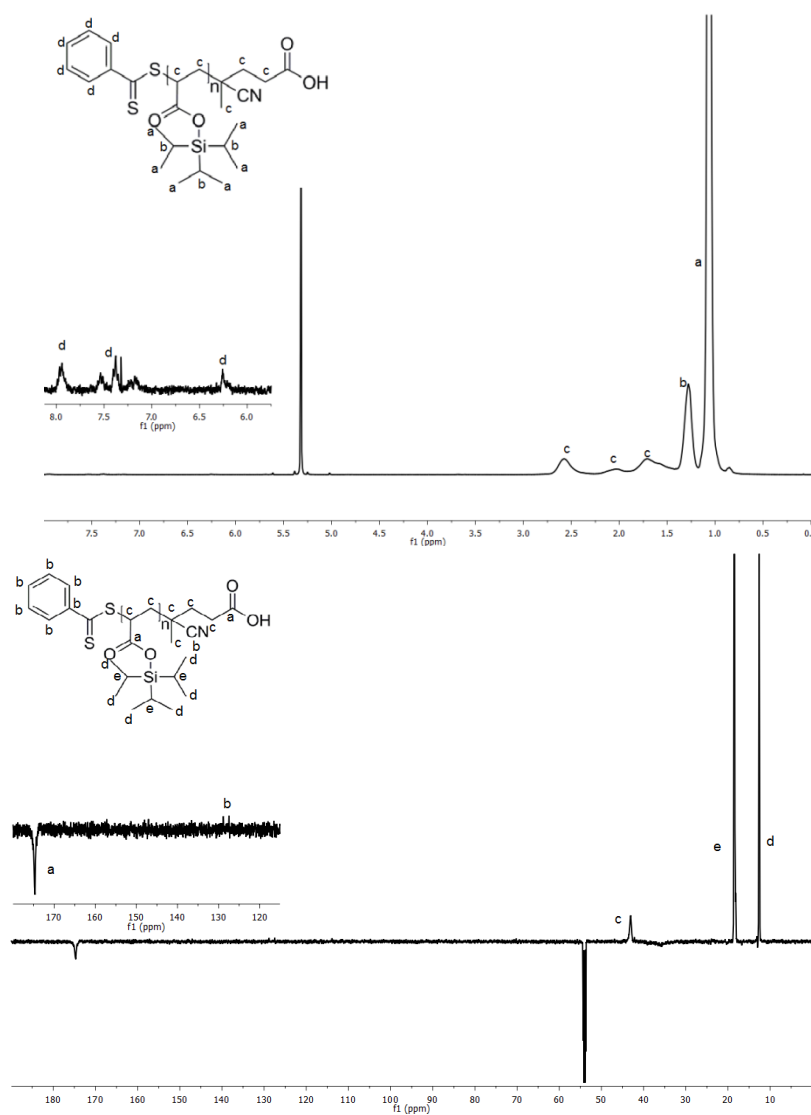


Figure S1. ^1H -NMR (a) and ^{13}C -NMR (b) spectra of PTIPSA in deuterated dichloromethane.

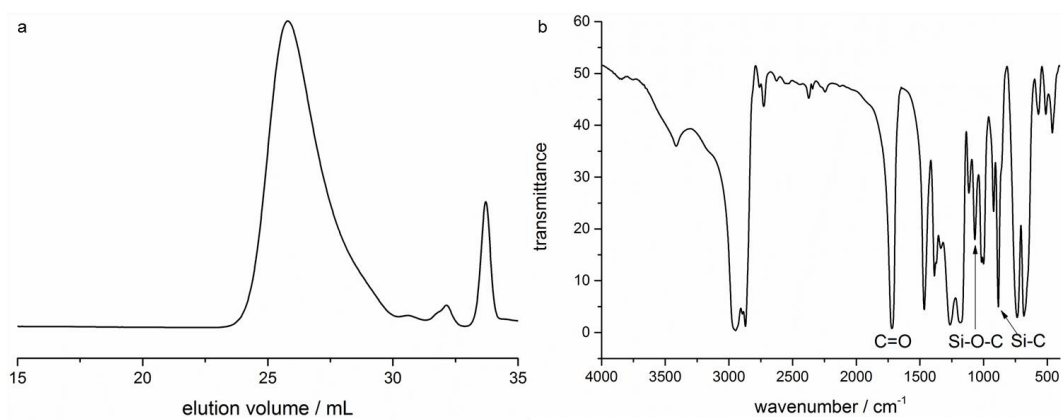


Figure S2. SEC trace (a, THF, 303 K, RI detection, 1 mL min^{-1}) and IR spectrum (b) of PTIPSA.

Preparation of inverse miniemulsions

The dispersed phase containing NaCl (7.56 mg) and DAB (25 μ L) in formamide (375 mg) was added dropwise to a solution of PTIPSA (45 mg) in cyclohexane (3.75 g) at room temperature. After stirring at 1000 rpm for 1 h, the emulsion was subjected to ultrasonication under ice-cooling with a Branson W450-D sonifier equipped with a ½ inch tip for 3 min in a pulse-pause regime of 30 s and 10 s. TDI (54 μ L) dissolved in cyclohexane (1.25 g) was added drop-wise to the emulsion and stirred for 24 h at room temperature. The size and morphology of the nanocapsules size and morphology were analyzed by DLS and SEM/TEM measurements. The capsules dispersion was washed three times by centrifugation at 3000 rpm for 15 min at 22 °C in 2 mL Eppendorf tubes to remove unreacted monomers. For redispersion of the nanocapsules into water, the washed miniemulsion (1 g) was added dropwise into a 0.1 wt% SDS solution (5 g) and stirred for 24 h without cap. Afterwards, the aqueous dispersion was dialyzed against distilled water for 36 h (average pore size of the membrane 14,000 g/mol) and analyzed by DLS and TEM/SEM.

Deprotection of TIPSA

TIPSA (100 μ L) was dissolved in DMSO- d_6 (1.45 mL) and D₂O (50 μ L). After the addition of TFA (116 μ L or 11.6 μ L), the mixture was stirred at 1000 rpm. Every hour a sample was measured by ¹H-NMR. After 1 h, the deprotection was completed. Furthermore, deprotection was studied without the addition of TFA. After 1h, 2h, 1 day, 2 days and 3 days a sample was measured by ¹H-NMR spectroscopy. Partial deprotection could be determined after 2 days.

2.4 Carbohydrate-functionalized HES nanocapsules – changes in protein bindings?⁵

As the nanocapsules generated in inverse miniemulsions have the potential to be applied in biomedical applications, not only surfactant studies for stabilization in different media are important. For biomedical applications, the interaction of proteins with the nanocapsule surface plays an important role, which have an influence on nanocapsule stability in protein mixtures, additionally affects the blood half-life time and could led to unspecific cell-uptake. Therefore, the surface of nanocapsule has to be modified to change protein composition on the nanocapsule surface resulted in enhanced blood half-life time and decreased unspecific cell-uptake. Thus, the surface of hydroxyethyl starch nanocapsules were functionalized with different azide-modified saccharides (glucose, HES and dextran) by the copper-free click reaction on the nanocapsule surface to produce biodegradable completely carbohydrate-based nanocapsules. Their protein adsorption properties in human blood plasma were studied and compared to each other and to PEGylated HES nanocapsules. Afterwards, the stability of the modified nanocapsules in citrate plasma was determined by DLS. Furthermore, the amount of adsorbed proteins and the protein composition on the sugar functionalized surfaces was studied by sodium dodecylsulfate polyacrylamide gel electrophoresis (SDS-PAGE) and mass spectrometry (MS). Comparing the results with each other and with the PEGylated HES nanocapsules similar binding patterns of such blood proteins were determined, whereas clusterin showed highest binding affinity followed by ApoE towards all modified nanocapsules as reported in previous studies from our group. However, also minor differences in the protein patterns were detected, e.g. the adsorption of serum albumin, which less adsorbed on dextrane modified surfaces and ApoA1 as well as ApoA4, which showed stronger adsorption on glycosylated and PEGylated nanocapsule surfaces. The stealth properties of the different functionalized

⁵ This work was done in collaboration with Johanna Simon. I synthesized the nanocapsules, different azide functionalized sugar derivatives, did the surface modification with different sugar derivatives and conducted all characterizations including DLS, SEM and anthracene azide assay. Protein quantification and characterization as well as cell uptake studies were conducted by Johanna Simon, which is acknowledged after each corresponding contribution.

nanocapsules were studied *in-vitro* using macrophages and immature dendritic cells (iDCs) in presence and absence of proteins showing only small changes in cell-uptake was detected between incubated and non-incubated nanocapsules. Future *in vivo* studies are still necessary to determine their behavior in blood and the fate of such nanocarriers for biomedical applications.

Motivation

Nanocapsules based on HES, ethoxylated starch, are promising candidates for nanometer-sized drug carriers for delivery of mainly water-soluble drugs. Encapsulation of the drugs is important to protect the drug against the environment as well as the healthy environment against the drugs and to release it selectively at the diseased place in the body.

However, if the nanocapsules are injected into blood, proteins will adsorb on the nanocapsule surface. Thus, the surface of the nanocapsules is shielded from the environment, which could change the properties of the nanocapsule in the body.^[344, 345] The nature and the amount of proteins adsorbing on the surface depend on the used protein source, which have differences in protein compositions, and the physicochemical properties of the nanocarrier like the surface modification and the surface charge.^[345, 346] Thus, different proteins can adsorb on the surface with strong or weak binding. Depending on the binding affinity, they are part of the so called hard or soft protein corona. Proteins with strong binding affinity to the surface are part of the hard protein corona.^[345] The soft protein corona includes proteins, which weakly adsorb at the nanocarrier surface and can reversibly be exchanged from the surface.^[345] Proteins adsorb on the nanocarrier surface due to hydrophobic interactions of the proteins and the nanocarrier surface, as well as hydrogen bonding, electrostatic and Van-der-Waals interactions.^[345, 347] In addition, the protein coverage on the surface depends on the roughness of the surface and the size of the nanocarrier.^[344, 347, 348]

To reduce unspecific protein adsorption, the surface of the nanocapsules is functionalized with materials that decrease protein adsorption. In addition to often used PEG,^[16, 17] polyphosphoesters^[18] are known to adsorb selective proteins especially Clusterin on nanocarrier surfaces. Furthermore, polyglycidol, polyoxazolines, poly(amino acids), polyamines, polybetaine and polysaccharides are

discussed as alternative surface modifiers to reduce protein adsorption and to guarantee a long circulation time in the blood stream.^[19] The advantages using polysaccharides as natural polymer instead of PEG^[19] are their biodegradability, low toxicity and immunogenicity as well as their multiple functional groups for further functionalization for example with cell specific linkers or drugs.^[349] First studies with hydroxyethyl starch as nanocapsule shell material exhibited protein repellent behavior and decreased unspecific uptake into HeLa cells.^[23] Moreover, dextran as another polysaccharide decreased protein adsorption after grafted onto a polystyrene surface.^[350] However, due to the multitude of saccharides, each chiral center might influence the interaction with proteins and needs to be carefully evaluated. That is the reason why in most cases to date, PEG is the standard protein repellent.

In general, functionalization of the nanocapsule surface shall be simple with high conversion. Thus, click reactions can be used, because they are easy to perform, with good yields, high rates and if necessary simple purification.^[351] A common click reaction is the copper-catalyzed 1,3-Huisgen reaction of an azide and an alkyne.^[352] In addition, copper-free alternatives were investigated using strained alkyne compounds like cyclooctynes,^[353] which was prior used for dynamic *in vivo* studies and drug discovery.^[354, 355]

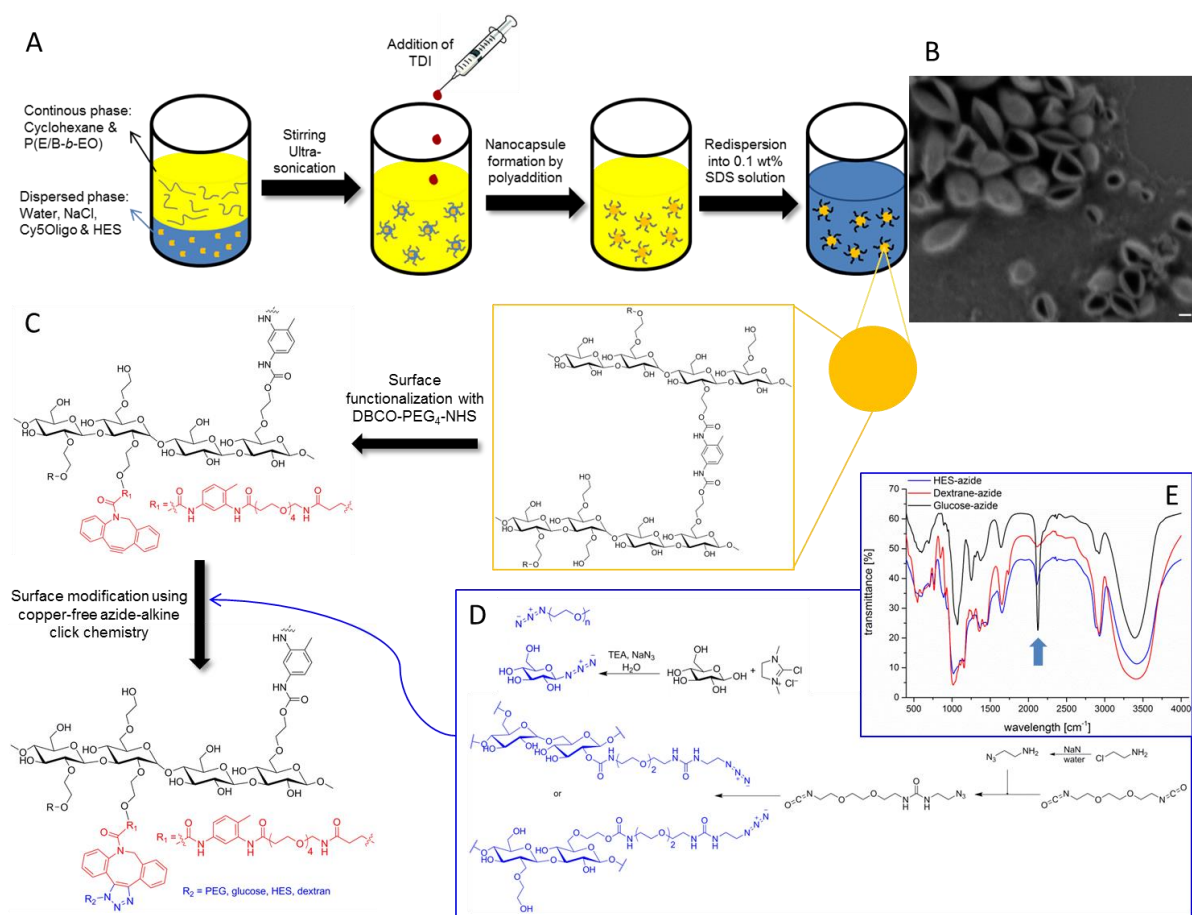
Herein, HES and dextran were functionalized with at least one azide group using an azido-isocyanate-urea as linker molecule. Additionally, glucose, which is part of both polysaccharides, was modified with an azide at β -position. The hydrophilic sugar derivatives were then coupled to the HES nanocapsule surfaces by copper-free azide-alkyne click reaction to produce completely carbohydrate-based biocompatible and biodegradable nanocapsules. To compare the results with known protein repellent surfaces PEG-N₃ was used as a control reagent. Afterwards, the post-functionalized nanocapsules were studied by DLS in plasma and the protein composition was analyzed by SDS-PAGE and MS.

Results and Discussion

Preparation of functionalized nanocapsules

The different sugar derivatives have to be functionalized with at least one azide group to introduce them on the nanocapsule surface by copper-free click reaction. Glucose was functionalized at the anomeric position by a one-step reaction with

sodium azide in combination with 2-chloro-1,3-dimethylimidazolinium chloride and triethylamine (Scheme 13E).^[356, 357] HES and dextran were modified in a three step synthesis starting with 2,2'-(ethylenedioxy)bis(ethylamine), as shown in Scheme 13E. After the two amine groups were converted to isocyanate groups using triphosgene and triethylamine, one isocyanate group was transferred with 2-azidoethan-1-amine to obtain the water-soluble 1-(2-azidoethyl)-3-(2-(2-(2-isocyanatoethoxy)ethoxy)ethyl)urea, the isocyanate-azide linker. This linker was subsequently added to HES or dextran to attach at least one azide group per molecule by reaction of the hydroxyls with the isocyanate of the linker by creating an urethane bond. All azide-modified saccharides were attached onto crosslinked hydroxyethyl starch nanocapsules in water to generate biodegradable completely carbohydrate nanocapsules. The nanocapsules were prior produced by polyaddition reaction at the droplet-oil interface in inverse miniemulsions using HES and toluene-2,4-diisocyanate according to previously published protocols (Scheme 13A).^[23, 206, 358, 359] The generated nanocapsules with encapsulated fluorescent dye (Cy5 Oligo) typically exhibit mean diameters of ca. 330 nm (Table 12 and Scheme 13B). After transfer of the nanocapsule dispersion into 0.1 wt% aqueous SDS solution (diameter around 280 – 346 nm), the surface based on free amine or hydroxyl groups was functionalized with the strained cyclooctyne-derivative DBCO-PEG₄-NHS by amidation of the activated *N*-hydroxysuccinimid (NHS) ester (Scheme 13C). Afterwards, the azide carbohydrates and mPEG-azide were linked on the nanocapsule surface by copper-free click reaction adding an excess of the azide component (3 eq per triple bond).^[360, 361]



Scheme 13. General scheme of HES nanocapsules synthesis by inverse miniemulsion polyaddition and their transfer into 0.1 wt% SDS solution (A) with mean diameter of around 300 nm determined by scanning electron microscopy (B, scale bar 100 nm in cyclohexane). Afterwards, the surface was functionalized with strained cyclooctyne derivatives using DBCO-PEG₄-NHS esters for further copper-free azide-alkyne click reaction (C). Before functionalization of the nanocapsule surface with the sugar derivatives, an azide group had to be introduced to the sugars as shown in D. Successful azide functionalization of the sugars was analyzed by infrared spectroscopy (E).

The degree of functionalization was determined by a fluorescent assay with 9-(azidomethyl)anthracene reacting with the remaining alkynes. Substraction yields the degree of functionalization after azide coupling between $2.3 \cdot 10^{-7}$ and $2.8 \cdot 10^{-7}$ mol mL⁻¹ (Table 12).^[362] Although, an excess of each azide compound was added to reach dense surface coverage, still some DBCO groups (between $9 \cdot 10^{-8}$ and $5 \cdot 10^{-8}$ mol mL⁻¹, Table 12) were detected after saccharide or PEG modification. The zeta potential of all nanocapsule dispersions was between -10 and -13 mV (Table 12)

after removal of SDS, independent of the surface modification. The slightly negative charge of the nanocapsule surface is probably attributed to residual SDS in the dispersion.

Table 12. Results of modified HES nanocapsule surfaces with glucose (Gluc), dextran (Dex), HES and mPEG.

	d / nm ^a	d / nm ^b	d / nm ^c	DBCO / mol mL ^{-1d}	DBCO / mol mL ^{-1e}	ζ-potential / mV ^f	ζ-potential / mV ^g
HES- Gluc	330	392	> 1000	$3.26 \cdot 10^{-7}$	$6.11 \cdot 10^{-8}$	-13.40 ± 0.60	n.d.
HES- Dex	330	445	946	$3.26 \cdot 10^{-7}$	$7.10 \cdot 10^{-8}$	-12.83 ± 0.13	-20.35 ± 0.05
HES- HES	330	448	970	$3.26 \cdot 10^{-7}$	$4.75 \cdot 10^{-8}$	-13.00 ± 0.60	-20.90 ± 0.50
HES- PEG	330	428	> 1000	$3.26 \cdot 10^{-7}$	$9.82 \cdot 10^{-8}$	-12.10 ± 0.90	-20.50 ± 0.80
a) in cyclohexane, b) in PBS, c) after incubation in citrate plasma, d) before azide-alkyne reaction, e) after azide-alkyne reaction, f) in $1 \cdot 10^{-3}$ M KCl solution, g) in $1 \cdot 10^{-3}$ M KCl solution after incubation with citrate plasma.							

Protein adsorption analysis

In order to investigate the stability of the different modified nanocapsules in protein mixtures dynamic light scattering was used. Independent of the functionalization, the nanocapsules formed aggregates in citrated human plasma in the range of 900 to larger than 1000 nm in diameter (Figure 35), which is double of the diameter detected in PBS solution before incubation. Certainly, DLS analysis only exhibited a trend of the nanocapsule stability in citrate plasma due to the size and polydispersity of the analyzed nanocapsules in PBS. Nanocapsules with diameters of 400 to 500 nm are at the limit of Rayleigh scattering. Thus, small changes of the parameters during evaluation led to huge changes of the detected aggregation size. However, the detected aggregates in human blood plasma were stable, because they did not precipitate out of the protein mixture or changed their size during DLS analysis over 2 h. However, the type of surface modification, nanocapsule size or dispersion stability

itself could have an influence on nanocapsule stability in human plasma and protein adsorption, because in prior studies no aggregates of PEGylated nanocapsules were determined in human plasma.^[17] At the end, the carbohydrate functionalized nanocapsules possessed similar behavior in protein mixtures as the PEGylated nanocapsules using azide-alkyne reaction for surface functionalization.

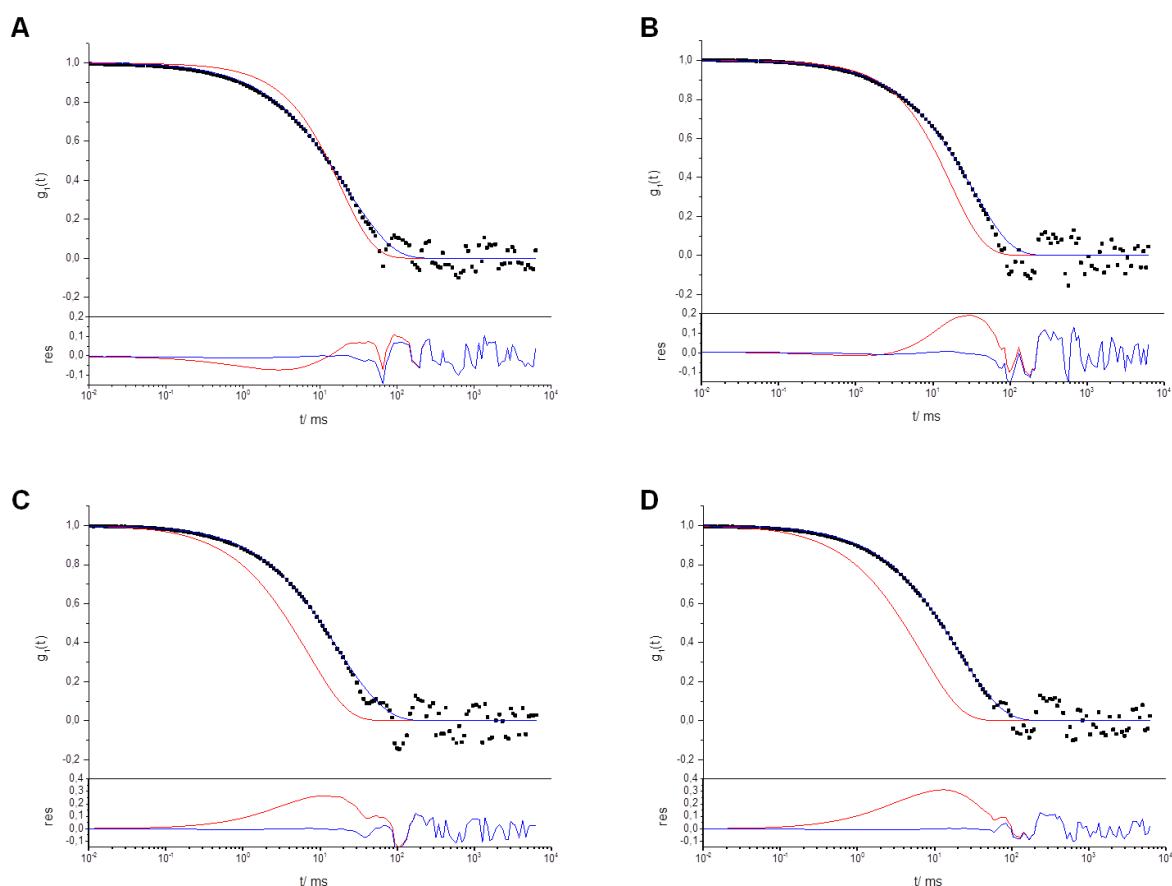


Figure 35. Dynamic light scattering analysis after incubation of the sugar-modified nanocapsules into 100% citrate plasma. Autocorrelation functions (ACFs) of the different nanocapsules in human plasma at $\Theta = 30^\circ$ including data points (\bullet), forced fit (red) as the sum of the individual components and fit with additional aggregate function (blue) with the corresponding residuals resulting from the difference between data and the two fits (**A** HES-PEG, **B** HES-Gluc, **C** HES-Dex, **D** HES-HES).

Although, HES nanocapsules themselves caused low protein adsorption rates,^[22] the amount and type of protein, which adsorb directly on the modified nanocapsules surface had to be studied to describe the stealth behavior. Therefore, the quantity and composition of the hard protein corona of all nanocapsules were analyzed. Surprisingly, HES modified with HES on the surface caused lower protein amounts (~

300 $\mu\text{g m}^{-2}$) compared to other modifications, while PEGylation showed protein adsorption of around 400 $\mu\text{g m}^{-2}$. In general, the amount of adsorbed proteins on all nanocapsules is low (300 - 500 $\mu\text{g m}^{-2}$ at 100% citrate plasma, Figure 36) and similar to previous reports using HES nanocapsules with a negatively charged surface.^[22] The zeta potential after incubation in citrate plasma for all nanocapsules is ca -20 ± 1 mV due to the adsorbed proteins.

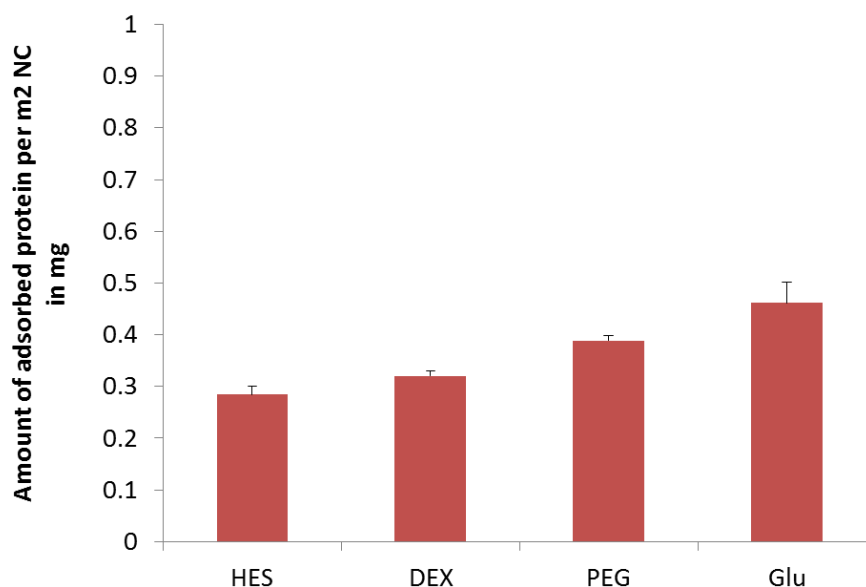


Figure 36. Protein quantification of purified hard protein corona. 0.05 m² capsule surface was incubated with 100% citrate plasma for 1 h at 37 °C. Released proteins were quantified by the Pierce 660 nm Protein Assay Reagent in combination with the Ionic Detergent Compatibility Reagent for Pierce 660 nm Protein Assay Reagent (experiments conducted by Johanna Simon).

Separation of proteins by SDS-PAGE and visualization by silver staining illustrated only minor differences between all surface modifications (Figure 37A), which was further shown in other publications.^[22, 363, 364] Differences were visible at 98 kDa and 62 kDa, which is less at PEGylated nanocarriers than at the carbohydrate modified surfaces. Although, prior studies demonstrate less clusterin binding onto PEG modified HES surface,^[22] the adsorbed amount of clusterin in this study was rather high (~ 30%, see Figure 37B). However, similar clusterin binding was found for all analyzed nanocarriers possibly due to low surface functionalization. Consequently, the surface is not densely covered and the surface of the nanocapsule itself is visible for the proteins, which led in similar protein adsorption. In addition, the amount of

ApoA1 looked similar at all nanocarriers surfaces by SDS-PAGE analysis. In mass spectrometry the amount of ApoA1 was different. Thus, the highest amount was identified on glucose modified surfaces followed by PEGylated nanocapsules. The ApoA1 quantity on dextran and HES functionalized nanocapsules was similar and lower compared to PEGylated and glycosylated nanocapsules. The same trend was detected with the protein ApoA4. Furthermore, ApoE adsorbed with an amount of around 25% to HES and dextrane modified surface and less on glucose or PEG modified surfaces (~ 20%). Serum albumin stronger adsorbed on HES and glucose functionalized nanocapsule surfaces than to PEGylated ones and even less to dextrane functionalized surfaces. Thus, sugar surfaces decreased the amount of adsorbed proteins similar to PEG. Depending on the sugar derivative on the nanocapsule surfaces, different protein compositions and amounts were identified in the hard protein corona, which could have an influence on cell-uptake and blood half-life time.

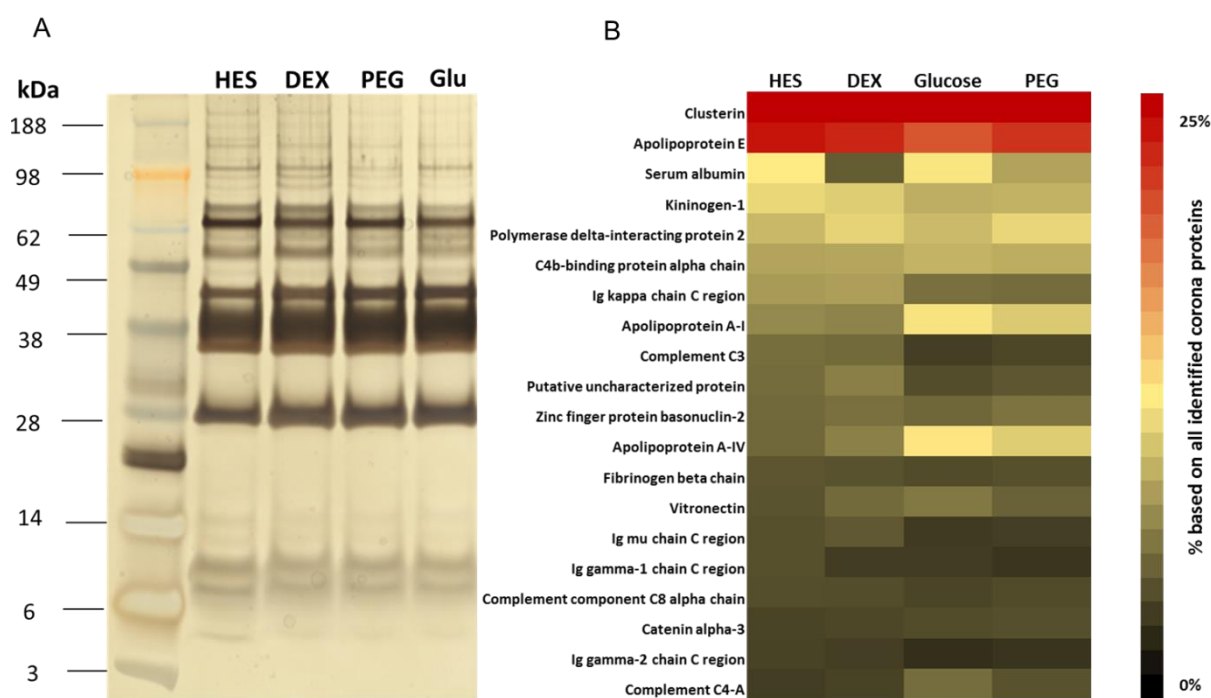


Figure 37. Hard protein corona of all nanocapsules. 0.05 m^2 capsule surface was incubated for 1 h at 37°C with 100% citrate plasma to allow protein corona formation. After purification of hard corona proteins 1 mg protein was visualized by silver staining (A) and hard corona proteins were identified by mass spectrometry (B) (experiments conducted by Johanna Simon).

Therefore, cell uptake of the differently modified nanocapsules in presence and absence of blood plasma was studied using macrophages and immature dendritic cells. As shown in Figure 38, cell uptake into macrophages and iDCs could be detected for all studied nanocapsules. Strongly reduced cell uptake was observed for the PEGylated and sugar-modified nanocapsules compared to non-functionalized HES nanocapsules, as expected. Cell uptake into macrophages was additionally decreased in the presence of proteins, especially for unmodified HES nanocapsules. Using iDCs, cell uptake was slightly increased with plasma for the different modified nanocapsules. However, no significant differences were detected between the different modified sugar-modified nanocapsules with or without plasma. Thus, little changes in the protein composition seemed not to have an influence on cell uptake. Nevertheless, further *in vitro* studies shall be done using nanocapsules with higher surface functionalization.

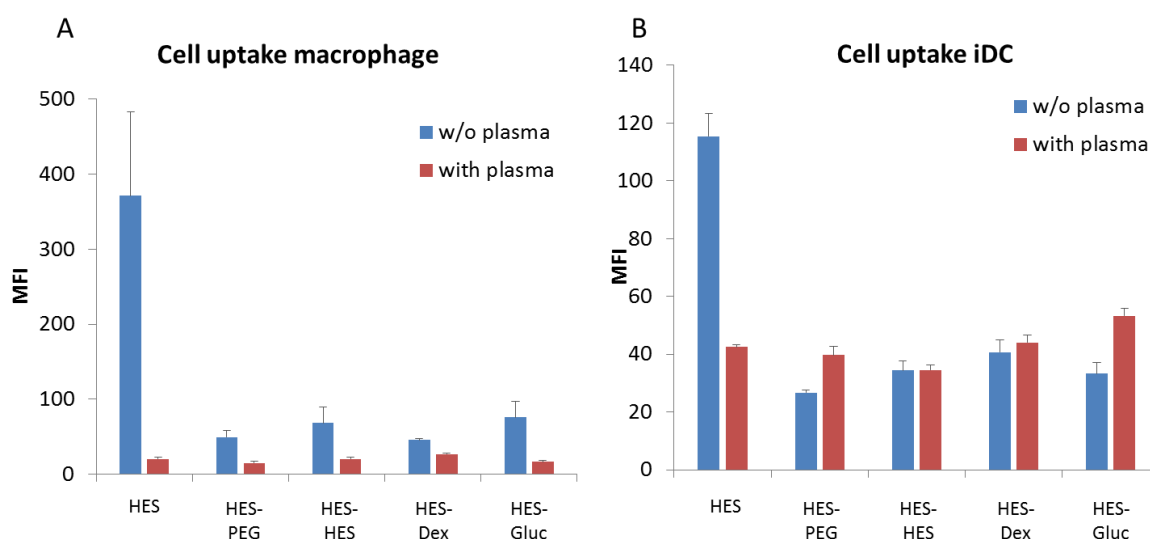


Figure 38. Cell uptake into macrophages (A) and immature dendritic cells (iDC, B) of the unmodified HES and modified HES nanocapsules (HES-PEG, HES-HES, HES-Dex and HES-Gluc) was determined by flow cytometry analysis with and without plasma. Therefore, the cells were incubated for 2 h with nanocapsules ($50 \mu\text{g mL}^{-1}$) before uptake was analyzed (experiments conducted by Johanna Simon).

Summary and Outlook

Crosslinked hydroxyethyl starch nanocapsules were functionalized by copper-free azide-alkyne click reaction with PEG, glucose, HES and dextran. Afterwards, their stability in citrated human plasma was determined by DLS, whereat in all disperions stable aggregates were identified. In addition, the hard protein corona on the nanocapsule surface was quantified and the protein composition was analyzed by SDS-PAGE and MS. The total amount of adsorbed proteins was in a range between 300 to 500 $\mu\text{g m}^{-2}$. Clusterin was identified as a major fraction in the corona with similar amounts, independent on the surface modification. However, the protein composition on the functionalized nanocapsule surface was different especially for serum albumin, ApoA1 and ApoA4, which might have an influence on their *in vivo* performance. Thus, after the first protein adsorption tests, it seems that glucose, dextrane and HES could be used as stealth materials like PEG, whereat the protein amount and composition of the hard protein corona depend on the used sugar derivative. However, the slight differences in protein composition after incubation with blood plasma had no significant influence on cell-uptake into macrophages or iDCs. In the future, cell uptake experiments have to be repeated and the amount of sugars as well as PEG on the nanocapsule surface shall be increased. Afterwards, *in vivo* studies are necessary to use the completely sugar nanocapsules for biomedical applications.

Experimental Part

Materials

D-Glucose (Sigma-Aldrich, $\geq 99.5\%$), sodium azide (NaN_3 , Sigma-Aldrich, *ReagentPlus*, $\geq 99.5\%$), 2-chloro-1,3-dimethylimidazolinium chloride (Sigma-Aldrich, DMC), Amberlite IR-120 (Sigma-Aldrich, hydrogen from), 2-chloroethylamine hydrochloride (Sigma-Aldrich, 99%), sodium hydroxide (NaOH , Fluka, ACS reagent, $\geq 97.0\%$), magnesium sulfate (MgSO_4 , Fluka, anhydrous, reagent grade, $\geq 99.5\%$), triphosgene (Sigma-Aldrich, reagent grade, 98%), methoxypolyethylene glycol azide (mPEG azide, 5 kDa, Sigma-Aldrich), sodium dodecylsulfate (SDS, Fluka, ACS reagent grade, $\geq 99.0\%$), Cy5Oligo (BioChemica) and DBCO-PEG₄-NHS ester (Jana Bioscience) were used as received. Triethylamine (TEA, Fluka, HPLC, $\geq 99.5\%$) and 2,2'-(ethylenedioxy)bis(ethylamine) (Sigma-Aldrich, 98%) were stored over molecular

sieve before use. Dextran (5.2 kDa, PSS Polymer Standard Service GmbH) and hydroxyethyl starch (HES, 8.2 kDa, Fresenius Kabi) were dried at 40 °C *in vacuo* overnight. HES (200kDa, 0.5 degree of substitution) was purchased from Fresenius Kabi and freeze-dried before used. Dichloromethane (DCM, Fisher Scientific), ethanol (VWR Chemicals, 96%), dimethylsulfoxide (DMSO, Sigma-Aldrich, anhydrous, ≥99.9%) and diethyl ether (Sigma-Aldrich, anhydrous, ≥99.7%) were used as received. The deuterated solvents chloroform-*d* (CDCl₃-*d*, Acros Organics, 99.8 atom% D), deuterium oxide (D₂O, Sigma-Aldrich, 99.9 atom% D) and dimethyl sulfoxide-*d*₆ (DMSO-*d*₆, Carl Roth, 99.8 atom% D) were used for NMR analysis as obtained.

The oil-soluble surfactant poly((ethylene-co-butylene)-*b*-(ethylene oxide)) was synthesized by anionic ring-opening polymerization of ethylene oxide using ω-hydroxypoly-(ethylene-co-butylene) as initiator in toluene with a poly(ethylene-co-butylene) block of 3700 g mol⁻¹ and a polyethylene oxide block of 3600 g mol⁻¹.^[365]

Methods

¹H-NMR spectra were measured on a Bruker Avance 250 spectrometer (Bruker, Billerica, MA, USA) operating at a Larmor frequency of 250 MHz or a Bruker Avance 300 spectrometer (Bruker, Billerica, MA, USA) with a Larmor frequency of 300.23 MHz. As deuterated solvents D₂O, CDCl₃ and DMSO-*d*₆ were used. In 0.5 mL deuterated solvent around 15 mg of the product was dissolved and the spectra was calibrated according to the chemical shift of the used deuterated solvent (4.79 ppm for D₂O, 7.26 ppm for CHCl₃ or 2.5 ppm for DMSO-*d*₆). ¹³C-NMR spectra were measured on a Bruker Avance 300 spectrometer (Bruker, Billerica, MA, USA) with a Larmor frequency of 300.23 MHz. 30 mg of the product was dissolved in 0.5 mL deuterated solvent (D₂O, CHCl₃ and DMSO-*d*₆) and the spectra were calibrated according to the chemical shift of the used deuterated solvent (77.16 ppm for CHCl₃ or 39.52 ppm for DMSO-*d*₆). Fourier transformed infrared spectroscopy (FT-IR) was performed using a PerkinElmer Spectrum BX FT-IR spectrometer (PerkinElmer, Shelton, CT, USA) between wavelength of 4000 cm⁻¹ and 400 cm⁻¹ to determine successful azidation of the linker and the sugar derivatives. Therefore, the samples were mixed with potassium bromide (KBr), pressed and subsequently measured. At the Zeiss 1530 LEO Gemini microscope (Carl Zeiss, Oberkochen, Germany) the

morphology and size of generated nanocapsules were analyzed. Therefore, 10 μL of the nanocapsule dispersion were diluted in 3 mL cyclohexane, dropped onto a silica wafer and dried under ambient conditions. Then, the wafer was placed under the microscope, working with an accelerating voltage of 0.2 kV and a distance of ~ 3 mm. The zeta potential of 10 μL nanocapsule dispersion was measured at 25 $^{\circ}\text{C}$ in $1 \cdot 10^{-3}$ mol L^{-1} in potassium chloride solution with a Zetasizer ZEN2600 from Malvern Instruments. An average of at least two measurements, each with at least ten runs is reported. In addition, the hydrodynamic radii of the nanocapsules was determined by DLS using a Nicomp 380 Submicron particle Sizer (PSS-Nicomp, Particle Sizing System, Port Richey, FL, USA) with a fixed angle of 90 $^{\circ}$. To measure the size, 10 μL of the emulsion was diluted in 1 mL cyclohexane. After incubation with 100 % citrate plasma the stability of the nanocapsules in the presence of protein was analyzed by DLS on a commercially available instrument from ALV GmbH (Langen, Germany). The DLS instrument is composed of a goniometer and an ALV-5000 multiple tau full-digital correlator with 320 channels. A helium-neon laser with an operating intensity of 25 mW and a wavelength of $\lambda = 632.8$ nm was used as a light source from JDS Uniphase (Milpitas, USA). All solutions were filled into dust-free quartz cuvettes with an inner diameter of 18 mm from Hellma (Müllheim, Germany), which were cleaned before use with distilled acetone. Before the nanocapsules were added to the plasma, 1 mL of citrate plasma was filtered through a Millex-GS filter (Merck Millipore, Darmstadt, Germany) with a pore size of 0.2 μm into the cuvette. Afterwards, 2 μL of the nanocapsule dispersion (~ 0.5 wt%) were added into the citrate plasma and incubated at 37 $^{\circ}\text{C}$ for 30 min followed by DLS analysis at the same temperature.

Purification of hard protein corona

Nanocapsules with a 0.05 m^2 surface area were incubated with 1 mL 100% citrate plasma for 1 h at 37 $^{\circ}\text{C}$ to allow protein corona formation. Purification of hard protein corona was executed according prior instructions.^{[366],[367]} Briefly, nanocapsules were centrifuged three times for 30 min at 4 $^{\circ}\text{C}$ and 420,000 g followed by resuspension with 1 mL PBS at 4 $^{\circ}\text{C}$. After the last washing step capsules were redispersed and incubated with 62.5 mM Tris-HCL supplemented with 2% SDS for 5 min at 95 $^{\circ}\text{C}$ and bound proteins were eluted from nanocapsules. To remove capsules in suspension

the samples were centrifuged again for 30 min at 420,000 g and 4 °C. The Pierce 660 nm Protein Assay Reagent was used for protein quantification in combination with the Ionic Detergent Compatibility Reagent for Pierce 660 nm Protein Assay Reagent (both Thermo Scientific, Dreieich, Germany) corresponding the manufacturer instructions.

Determination of the hard protein corona by SDS-PAGE

1 mg of the hard corona proteins was supplemented with sample buffer and reducing agent (Novex, Carlsbad, USA) for SDS polyacrylamide gel electrophoresis (SDS-PAGE) and afterwards incubated for 5 min at 95 °C. Then, SDS-PAGE was run for 1 h at 100 mV before protein bands were visualized by the SilverQuest Silver Staining Kit (Thermo Scientific) corresponding the manufacturer instructions.

Digestion of the protein corona for MS analysis

SDS was eliminated via Pierce detergent removal columns (Thermo Fisher) prior to protein digestion. Tryptic digestion was performed as described by Tenzer et al.^[348] with the following adjustments. Proteins were precipitated according to the manufactures instructions' using ProteoExtract protein precipitation kit (CalBioChem). The resulting protein pellet was resuspended in RapiGest SF (Waters Cooperation) dissolved in 50 mM ammonium bicarbonate (Sigma-Aldrich) and afterwards incubated at 80 °C for 15 min. The addition of dithithreitol (Sigma-Aldrich) reduced the proteins to gain a final concentration of 5 mM and incubated for 45 min at 56 °C. Iodoacetamide (final concentration 15 mM, Sigma-Aldrich) was added and the solution was incubated for 1h in the dark. Tryptic digestion with a protein:trypsin ratio of 50:1 was carried out over 16 h at 37 °C. The reaction was quenched by adding 2 µL hydrochloric acid (Sigma-Aldrich). Degradation products of RapiGest SF were removed via centrifugation (14.000 g, 15 min).

Determination of the hard protein corona by Liquid-chromatography mass-spectrometry (LC-MS) analysis

For absolute protein quantification, the peptide samples were spiked with 10 fmol/µl of Hi³ Ecoli Standard (Waters Cooperation). Digested peptides were applied to a C18 nanoACQUITY Trap Column (5 µm, 180 µm x 20 mm,) and separated on a C18 analytic reversed phase column (1.7 µm, 75 µm x 150 mm) using a nanoACQUITY UPLC systems. The column is further coupled to a Synapt G2-Si

mass spectrometer. A two phase mobile system consisting of phase (A) 0.1% (v v⁻¹) formic acid in water and phase (B) acetonitrile with 0.1% (v v⁻¹) formic acid was utilized at a sample flow rate of 300 µl min⁻¹ with a gradient of 2 – 37% mobile phase (A) to (B) over 70 min. As a reference component, Glu-Fibrinopeptide (150 fmol µL⁻¹, Sigma) was infused at a flow rate of 500 µl min⁻¹.

Electrospray ionization (ESI) was executed in positive ion mode with nanoLockSpray source and the mass spectrometer was operated in resolution mode performing data-independent acquisition (MS^E).

Data were recorded over 90 mins with a mass to charge range (m z⁻¹) over 50 – 2000 Da, scan time of 1 s and ramped trap collision energy from 20 to 40 V. Each sample was run in triplicates. Data was arranged with MassLynx 4.1. For protein identification Progenesis QI for Proteomics Version 2.0 with continuum data using a reviewed human data base (Uniprot) was chosen. Several parameters as noise reduction thresholds for low energy, high energy and peptide intensity were set to 120, 250, and 750 counts.

The peptide sequence of Hi³ Ecoli standard (Chaperone protein CLpB, Waters Cooperation) was added to the database for absolute quantification.^[368] The following search criteria were used for protein and peptide identification: one missed cleavage, maximum protein mass 600 kDa, fixed carbamidomethyl modification for cysteine, variable oxidation for methionine and protein false discovery rate of 4%.

At least two assigned peptides and five assigned fragments are required for protein identification and three assigned fragments for protein identification.

A score parameter for identified peptides was set to 4 and quantitative protein identification was generated based on the TOP³/Hi³ approach, providing the amount of each identified protein in fmol.^[369]

Cell uptake

The murine macrophage-like cells (RAW 264.7) were kept in Dulbecco's modified eagle medium (DMEM) supplement with 10% fetal bovine serum (FBS) and 1% penicillin/streptomycin. Cells were grown in humidified incubator at 37°C and 5% CO₂. Immature human dendritic cells were generated according to literature and kept in RPMI-1640 supplemented with 2 % human serum, 100 U mL⁻¹ penicillin and 100 mg mL⁻¹ streptomycin.

For flow cytometry analysis, cells were seeded out (100.000 cells) in 24 well plates (200 μ L). After 12 h cells were washed with PBS to remove remaining proteins from FBS and kept in DMEM *without* additional proteins.

Nanocapsules were incubated with human citrated plasma according to the ratio as described for the protein corona analysis (0.05 m^2 in 1 mL plasma).

Plasma coated or untreated nanocapsules were added to cell culture medium without FBS (75 $\mu\text{g mL}^{-1}$ or 50 $\mu\text{g mL}^{-1}$) for 2 h. Afterwards, cells were washed two times with PBS, detached with 2.5% trypsin, centrifuged (5 min, 500 g) and resuspended in PBS. Flow cytometry analysis was performed on a CyFlowML cytometer and cells were selected on a forward/sideward scatter plot, thereby excluding cell debris.

Fluorescent Cy5 labelled nanoparticles (ex: 650 nm, em: 670 nm) were analyzed in the FL6 channels. The median (FL6 channel, MFI) was determined from a 1D histogram. Data analysis was performed using FCS Express V4 software.^[231]

Synthesis

All reactions involving air or moisture sensitive reagents or intermediates were conducted under an inert atmosphere of argon in glassware, which were dried in an oven before use. Reaction temperatures referred to the temperature of the particular cooling/heating bath.

Synthesis of β -glucose azide

Glucose was selectively functionalized with one azide group at the OH- β -position using the synthesis published by Vinson et al..^[356] Glucose (1.00 g, 5.6 mmol, 1 eq) and sodium azide (3.63 g, 55.8 mmol, 10 eq) were dissolved in water (20 mL) and added to a solution of 2-chloro-1,3-dimethylimidazolinium chloride (2.80 g, 16.6 mmol, 3 eq) and TEA (7.80 mL, 55.9 mmol, 10 eq) under ice cooling. After stirring for 1 h at 0 $^{\circ}\text{C}$, the mixture was concentrated at reduced pressure and mixed with ethanol (20 mL). The generated solid was separated by filtration and ethanol was removed from the filtrate at reduced pressure. The obtained solid was dried and redissolved in water (15 mL). After the water phase was washed five times with dichloromethane (10 mL), the water phase was stirred for 4 h with acidic Amberlite IR-120 at room temperature (RT). The Amberlite was activated before with 1 M sodium hydroxide solution. Then, the ion exchanger was removed by filtration and

the filtrate was freeze-dried again to obtain the β -glucose azide as a white powder in 58% yield (0.58 g).

$^1\text{H-NMR}$ (D_2O , 300 MHz): $\delta(\text{ppm}) = 4.73$ (d, $J = 8.8$ Hz, 1H), 4.05 – 3.59 (m, 2H), 3.59 – 3.32 (m, 3H), 3.23 (h, $J = 7.6$ Hz, 1H). $^{13}\text{C-NMR}$ (D_2O , 300 MHz): $\delta(\text{ppm}) = 90.1$ (C_1), 77.9 (C_5), 75.7(C_3), 72.82(C_2), 69.17(C_4), 60.53 (C_6). FT-IR $\nu = 2120\text{ cm}^{-1}$ ($-\text{N}_3$).

Synthesis of 2-azido-1-ethylamine

2-Chloroethylamine hydrochloride (6 g, 0.052 mol, 1 eq) was dissolved with sodium azide (10.3 g, 0.158 mol, 3 eq) in MilliQ water (140 mL) and stirred for 20 h at 80 °C. After neutralization with sodium hydroxide (2.08 g, 0.052 mol, 1 eq), the product was extracted four times into diethyl ether (160 mL) and dried over magnesium sulfate. The solvent was partially removed under reduced pressure. At the end, 2-azido-1-ethylamine with a concentration of 81.6% (quantified by $^1\text{H-NMR}$ spectroscopy), containing 2.28 g (yield 51%) in diethyl ether was obtained as yellow solution.

$^1\text{H-NMR}$ (CDCl_3 , 300 MHz) $\delta(\text{ppm}) = 3.37$ (t, $J = 5.6$ Hz, 4H, $\text{NH}_2\text{-CH}_2$), 2.93-2.84 (m, 1H, $\text{N}_3\text{-CH}_2$), 1.44 (s, 1H, NH_2). $^{13}\text{C-NMR}$ (CDCl_3 , 300 MHz) $\delta(\text{ppm}) = 54.6$ ($\text{CH}_2\text{-N}_3$), 41.31 ($\text{CH}_2\text{-NH}_2$). FT-IR (ATR) $\nu = 3380$ ($-\text{NH}_2$), 3310 ($-\text{NH}_2$), 2101 ($-\text{N}_3$).

Synthesis of 2,2'-(ethylenedioxy)bis(ethylisocyanate)

2,2'-(ethylenedioxy)bis(ethylamine) (2.5 mL, 0.017 mol, 1 eq) and TEA (11.28 mL, 0.081 mol, 4.8 eq) was dissolved in anhydrous DCM (6 mL) and dropwise added to a stirred solution of triphosgene (4.458 g, 0.015 mol, 0.9 eq) in anhydrous DCM (40 mL) under ice-cooling in an argon atmosphere. After complete addition, the mixture was stirred for 40 min at 4 °C, then for 1 h at RT and additionally heated for 5 ½ h under reflux. DCM was removed *in vacuo* and the product was extracted from the solid using anhydrous diethyl ether (two times 50 mL). The product was identified by $^1\text{H NMR}$ and used without further purification for the next step.

$^1\text{H-NMR}$ (CDCl_3 , 300 MHz) $\delta(\text{ppm}) = 3.99$ (dq, $J = 14.2, 8.2, 7.4$ Hz, 4 H), 3.69-3.43 (m, 4 H), 3.41-3.22 (m, 4 H). $^{13}\text{C-NMR}$ (CDCl_3 , 300 MHz) $\delta(\text{ppm}) = 124.78$ ($\text{O}=\text{C}=\text{N}$), 69.93 ($\text{CH}_2\text{-O}$), 69.91 ($\text{CH}_2\text{-O}$), 69.8($\text{CH}_2\text{-O}$), 42.8 ($\text{CH}_2\text{-N}$).

Synthesis of 1-(2-azidoethyl)-3-(2-(2-(2-isocyanatoethoxy)ethoxy)ethyl)urea and sugar functionalization

2-azido-1-ethylamine (1.17 g, 0.014 mol, 0.8 eq) was dissolved in anhydrous diethyl ether (2 mL), and added at a speed of 6 mL h⁻¹ by a syringe pump into the diisocyanate solution at -56 °C. Afterwards, anhydrous DMSO (5 mL) was added at ambient temperature and diethylether was removed *in vacuo*. The product was checked by IR and used without further purification for the next step. 500 µL of the 1-(2-azidoethyl)-3-(2-(2-(2-isocyanatoethoxy)ethoxy)ethyl)urea solution in DMSO was added dropwise into a sugar solution (250 mg of HES of 5.5 kDa or dextran of 5 kDa) in anhydrous DMSO (5 mL). The reaction was continued for 32 h, and the product was purified by dialysis against MilliQ water in a dialyzing tube with MWCO of 1 kDa for 4 days. After dialysis, the solution was freeze-dried to obtain the product (185 mg HES and 150 mg dextran). FT-IR of 1-(2-azidoethyl)-3-(2-(2-(2-isocyanatoethoxy)ethoxy)ethyl)urea (ATR) ν = 2339 (N=C=O), 2101 (N₃), 1676 (urethane), 1438 (N=C=O). **HES-azide**. FT-IR (ATR) ν = 2111 (N₃). **Dextrane-azide**. FT-IR (ATR) ν = 2116 (N₃), 1740 (urethane).

Synthesis of HES nanocapsules by inverse miniemulsion

The nanocapsules were prepared as described in prior publications by polyaddition reactions at the cyclohexane-water droplet interfaces.^[23, 206, 358, 359]

The dispersed phase consisted of HES (140 kDa, 130 mg), NaCl (10 mg), Cy5 Oligo solution (100 µL) and PBS buffer (240 µL). The dispersed phase was added to cyclohexane (7.5 g) containing P(E/B-*b*-EO) (80 mg). After stirring at 500 rpm for 30 min, the emulsion was subjected to ultrasonication under ice-cooling with a Branson W450-D sonifier equipped with a ½ inch tip for 3 min in a pulse-phase regime of 20 s and 10 s. 5 g cyclohexane and 55 mg P(E/B-*b*-EO) were added and the dispersion was stirred for 30 min at 500 rpm. After a second ultrasonication using same conditions as before, TDI (175 mg) and P(E/B-*b*-EO) (25 mg) dissolved in cyclohexane (2 g) were added dropwise to the miniemulsion and stirred for 24 h at 25 °C. The size and morphology of the obtained nanocapsules were analyzed by DLS and SEM/TEM measurements as described above.

Nanocapsule transfer into water

Before the nanocapsules were transferred into water, they were washed to remove unreacted monomer and excess of surfactant. Therefore, 2 mL nanocapsule dispersion were filled into a 2 mL Eppendorf tube and centrifuged by 4000 rpm for 45 min. The supernatant was removed and the nanocapsules were redispersed with 400 μ L cyclohexane. The redispersed nanocapsules were slowly added into 5 mL of a 0.1 wt% prepared SDS solution while shaking in a sonication bath (Bandelin Sonorex, type RK 52H). The whole dispersion was stirred over night without cap at 1000 rpm at RT, to allow evaporation of cyclohexane. To remove the excess of SDS, the emulsion was dialyzed against water for 1 day by changing the water three times. To obtain the solid content of the nanocapsule dispersion, three times 50 μ L of the nanocapsule dispersion were freeze-dried overnight. The remained solid was used to detect the PEG on the nanocapsule surface by ^1H -NMR spectroscopy as published previously.^[17]

Functionalization of the HES nanocapsule surface with DBCO-PEG₄-NHS

After the solid content was adjusted to 1 wt%, the nanocapsules were functionalized with DBCO-PEG₄-NHS. Therefore, a DBCO-PEG₄-NHS (3.29 mg per mL nanocapsule dispersion, 5.06×10^{-6} mol) solution in anhydrous DMSO (167 μ L) was added into 1 wt% nanocapsules dispersion. After stirring over night at room temperature and 1000 rpm, the dispersion was washed two times by centrifugation at 4500 rpm for 30 min. The amount of DBCO groups on the nanocapsules surface was determined by a fluorescent assay with 9-(azidomethyl)anthracene.^[362]

Coupling of β -glucose azide, HES-azide, dextrane-azide or PEG-azide to the nanocapsule surface

To 1 mL nanocapsule dispersion with 1 wt% solid content, a solution of the azide-derivative (3 eq per detected DBCO group, 2.24×10^{-6} mol) in DMSO (200 μ L) was added and stirred for 4 days at 500 rpm at ca. 4°C. Afterwards, the dispersion was washed two times by centrifugation at 4500 rpm for 30 min. At the end, the solid content of the nanocapsule dispersion was analyzed by freeze-drying 50 μ L of the dispersion and the amount of functionalization was determined using a fluorescent assay with 9-(azidomethyl)anthracene.^[362]

2.5 Mannose vs Trimannose: Targeting for dendritic cells⁶

In addition to decrease protein binding on the nanocapsule surface for a longer circulation time in the body, the uptake of the nanocarriers into selective cells is important to release the incorporated drug at the right place in the body. Therefore, the nanocapsule surface has further to be functionalized with cell specific linkers. Herein, the effect on specific cellular uptake of mannose- and trimannose-modified nanocarriers was studied in monocyte-derived dendritic cells and monocytes. Thus, mannose as well as trimannose was modified with an azido group for further azide-alkyne click reactions. The carbohydrate moieties were attached through linkers to hydroxyethyl starch nanocapsules which were PEGylated on the surface to decrease the adsorption of proteins from human serum. Successful surface PEGylation and further functionalization with the sugar linkers by copper-free azide-alkyne click reaction was detected by NMR, fluorescence assay using 9-(azidomethyl)anthracene and *Galanthus nivalis* lectin binding. In addition to cell uptake and cytotoxicity test, the hard protein corona on the nanocapsule surfaces of naked HES, PEGylated HES, and sugar functionalized HES was studied by SDS-PAGE and mass spectrometry, whereat very similar patterns of bound proteins were found.

Motivation

Specific delivery of drugs to certain cell types is a highly desirable strategy in pharmacotherapy. Nanotechnology offers the opportunity to use nanocarriers, modified with specific targeting moieties designed to reach desired target sites. However, Salvati et al. showed that a complex serum environment can lead to the loss of specific binding properties of nanocarriers because serum proteins can hide the

⁶ The work in this chapter is based on the manuscript 'Mannose vs trimannose: targeting for dendritic cells' by Sarah Wald, Manuel Tonigold, Jens Langhanki, Matthias Krumb, Patricia Renz, Johanna Simon, Christin Sauer, Ingo Lieberwirth, Frederik R. Wurm, Volker Mailänder, Till Opatz and Katharina Landfester. I synthesized the mannose azide, the nanocapsules, developed the surface modification and conducted their characterization concerning DLS, SEM, NMR, FT-IR, anthracene azide assay and c-type lectin binding assay; the synthesis of trimannose, the in vitro and protein adsorption studies were conducted by the collaboration partners, which are acknowledged after each corresponding contribution.

targeting structures on the surface of the nanocarriers and generate a “biological identity” of the nanocarrier that determines its fate.^[370] This finding raised the question whether the concept of specific targeting can be used *in vivo* to target cells specifically. Proteins adsorb on the nanocarrier surface because of the high surface energy and hydrophobic interactions.^[370, 371] To reduce unspecific adsorption of proteins to nanocarrier surfaces and thereby unspecific uptake of immune cells - the so called “stealth effect” – poly(ethylene glycol) (PEG) can be attached to the surface of the nanocarrier.^[17, 372-374] However, new findings suggest that a limited protein adsorption of specific proteins is required for the stealth effect.^[18] We were able to prove recently that nanocarriers based on crosslinked hydroxyethyl starch shells with attached targeting moieties are still recognized by dendritic cells in presence of hard protein corona.^[22] In comparison to hydrophobic nanoparticles, the surface of hydrophilic HES nanocarriers exhibits significantly lower protein binding after addition into biological liquids. This is advantageous for cell-specific uptake after surface modification with a cell-specific linker,^[22] because less proteins can lower the risk that the target sites mask the surface modifications. Dendritic cells play a key role in immune system because they can activate the adaptive immune response^[375] and therefore are a suitable target for nanocarriers. The loading of nanomaterials with specific antigens to elicit immune responses directed e.g. against malignant cells or pathogenic microorganisms offers a broad spectrum of treatment opportunities when the nanomaterials are able to selectively enter dendritic cells in the human body. Immature dendritic cells can actively internalize glycoconjugates with terminal mannose units through the mannose receptor CD206^[376] while branched oligomannosidic structures, in particular trimannose (3,6-di-(α -D-mannopyranosyl)- α -D-mannopyranose), are internalized through DC-SIGN (CD209).^[377-379] As mannose-rich glycostructures are found on the surface of various microorganisms, this internalization plays an important role in the body's defense against microbial pathogens.

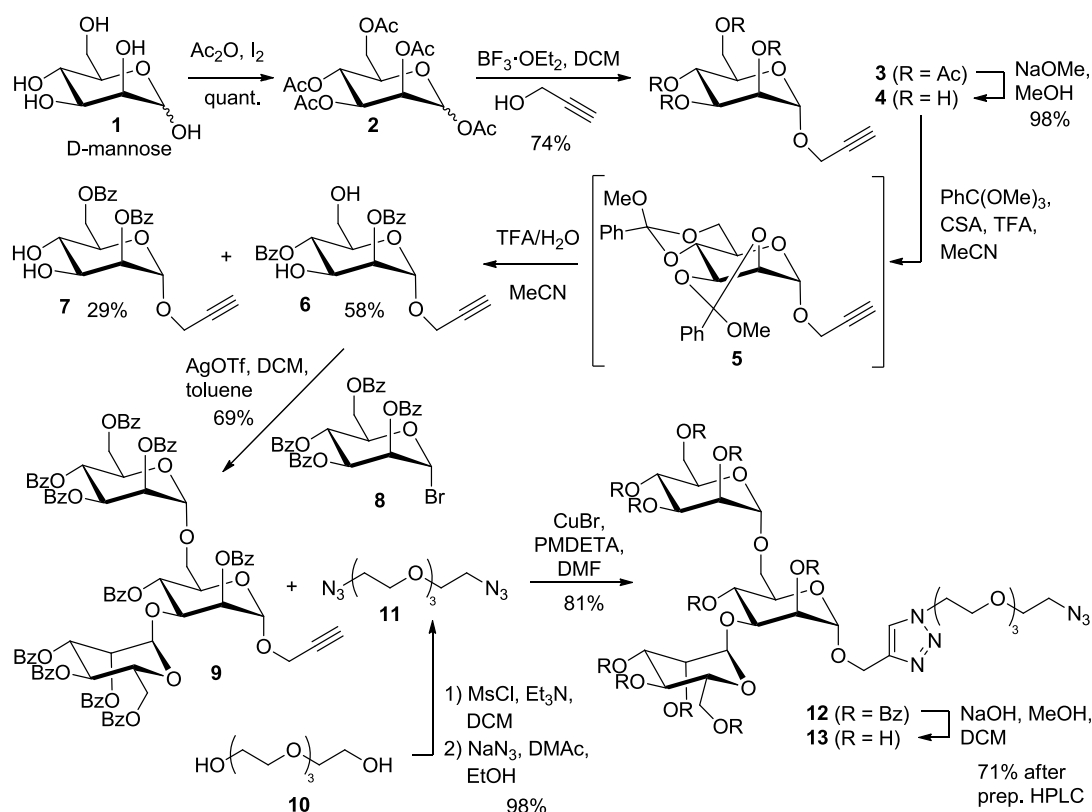
Herein, we compare the effect on specific cellular uptake of mannose- and trimannose-modified nanocarriers: The synthesis of novel azide-functionalized oligosaccharides for further azide-alkyne click reactions is the basis for further investigations. They can be covalently linked to the surface of PEGylated HES nanocarriers by copper free 1,3-dipolar cycloaddition (Scheme 14). Afterwards, their

Results and Discussion

Trimannosesynthesis

For the synthesis of the azide-substituted trimannose **13** (Scheme 15), D-mannose (**1**) was peracetylated and reacted with propargyl alcohol in the presence of boron trifluoride etherate.^{[380], [381]} Zemplén methanolysis furnished 1-propargyl- α -D-mannopyranoside (**4**) in 73% yield over three steps.^[381] Attempts to install protecting groups in 2- and 4-position via formation of a 2,4-di-O-benzoyl-3-O-*tert*-butyldimethylsilyl-6-O-trityl glycoside in a one-pot procedure met with little success.^[382] In contrast, method protocol by Oscarson through double orthobenzoate **5** gave after acidic ring opening the desired 2,4-protected mannoside **6** in 58% yield along with its regioisomer **7**^[383] which could be separated by flash chromatography.

While the double α -mannosylation of **6** through using Schmidt's trichloroacetimidate method produced a mixture of mono- and diglycosylated products, the Koenigs-Knorr procedure using 2,3,4,6-tetra-O-benzoyl- α -D-mannosylpyranosyl bromide (**8**)^{[384], [385]} in combination with silver triflate provided trimannoside **9** in high yield. Diazide linker **11** was readily prepared from tetraethylene glycol (**10**) by double O-mesylation and subsequent nucleophilic displacement with NaN_3 .^{[386], [387]} Attachment of linker **11** to trisaccharide **9** was accomplished by copper-catalyzed azide-alkyne-cycloaddition (CuAAC) using CuBr / pentamethyldiethylenetriamine (PMDETA) to furnish the clickable trimannose **13** after alkaline hydrolysis under forcing conditions required to remove the persistent 4-O-benzoyl group in the bisecting mannose unit.



Scheme 15: Synthesis of clickable trimannose **13** (synthesis conducted by Jens Langhanki).

Synthesis and surface functionalization of HES nanocapsules

Cross-linked hydroxyethyl starch nanocarriers were prepared according to the previously published synthesis by polyaddition of HES with TDI at the droplet interface of an inverse miniemulsion.^[23, 206, 358, 359] The generated nanocarriers had a mean diameter of 240 nm including the hydrophilic Cy5oligo as fluorescent dye (Figure 38).

To decrease protein adsorption onto the nanocapsule surface, the shell was modified with 5000 g mol⁻¹ diisocyanate-PEG (NCO-PEG₁₁₄-NCO, Table 13) as reported by Kang et al.^[17] After transfer of the nanocarrier dispersion into water containing 0.1 wt% SDS, the unreacted isocyanate end-groups of PEG on the surface hydrolyzed to primary amine groups. The PEGylation on the nanocarrier was measured by NMR spectroscopy and obtained to be 4.8·10⁻⁵ mmol PEG mL⁻¹ dispersion (Table 13). Linkage of azide-functionalized carbohydrates to the nanocarriers was performed by the reaction of free primary amino groups with DBCO-PEG₄-NHS, a reactive dibenzocyclooctyne-derivative. **13** or α-D-

mannopyranosyl azide (**14**) was connected by copper-free click reaction onto the nanocarrier surface.^[360, 361] The degree of functionalization was determined by a fluorescent assay with 9-(azidomethyl)anthracene revealing around $5.1 \cdot 10^{-8}$ mol DBCO groups per mL dispersion^[362] before coupling and complete functionalization (i.e. no detectable DBCO signal) to $5.1 \cdot 10^{-8}$ mol carbohydrate molecules per mL dispersion (Table 13). The mean diameter of the nanocapsules analyzed in PBS increased in all cases. The unmodified HES exhibited a mean diameter of 340 nm, after PEGylation a slight increase to 360 nm was detected (Figure 38).

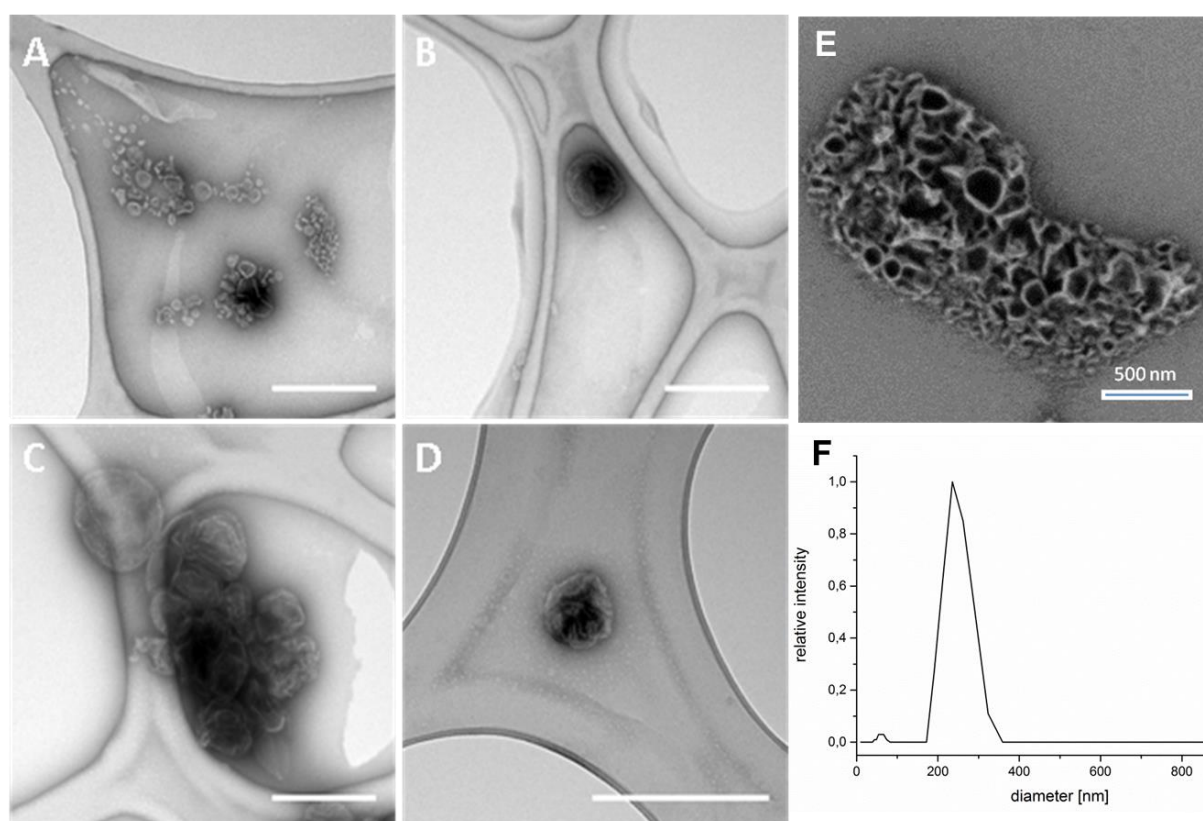


Figure 38: TEM micrograph of HES-capsules embedded in a thin film of trehalose with additional uranyl acetate negative staining (A: HES; B: HES-PEG; C: HES-PEG-Man; D: HES-PEG-Triman; Scale bar: 500 nm, experiments conducted by Patrizia Renz), SEM micrograph of HES nanocapsules (E) as well as dynamic light scattering results in cyclohexane with mean diameter at 240 nm.

Care has to be taken in all cases as the nanocarrier dispersions were dialyzed to a minimum amount of SDS (SDS concentration was analyzed via the Stains-All assay^[388]) that no aggregation occurs. All employed emulsions contained SDS concentration below 0.1 mmol L^{-1} after complete purification, detected at a

wavelength of 438 nm against Standard SDS solution with concentrations between 10 mmol L^{-1} to 0.05 mmol L^{-1} (Figure 39).

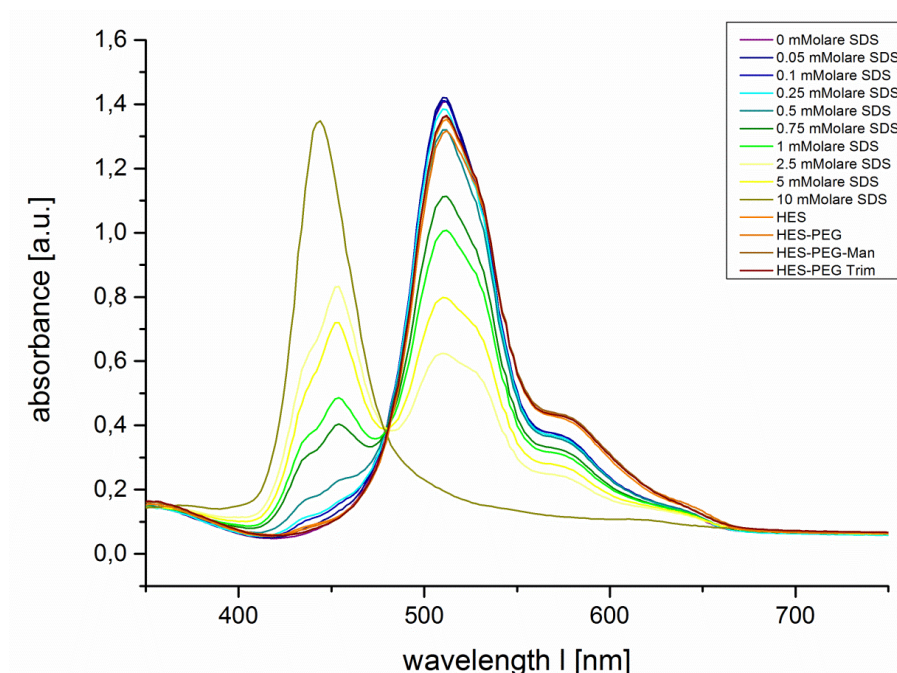


Figure 39. SDS concentrations of HES, HES-PEG and sugar-functionalized HES-PEG are all below 0.1 mM compared to standard SDS concentrations analyzed with AllStain dye at 438 nm.

This procedure ensured a similar zeta potential for all nanocarrier dispersions of ca. -10 mV before and after functionalization (Table 13).

Table 13. Characterization of hydroxyethyl starch nanocarriers.

code	PEG / $\text{mol mL}^{-1\text{a}}$	Sugar / $\text{mol mL}^{-1\text{b}}$	ζ -potential / mV^{c}	ζ -potential / mV^{d}	ζ -potential / mV^{e}
HES	0	0	-10.40 ± 3.87	-22.80 ± 8.51	-29.20 ± 6.80
HES-PEG	$4.8 \cdot 10^{-8}$	0	-10.30 ± 3.84	-18.40 ± 7.32	-32.90 ± 5.16
HES-PEG- Man	$4.8 \cdot 10^{-8}$	$5.1 \cdot 10^{-8}$	-9.88 ± 3.66	-26.80 ± 4.57	-29.85 ± 5.60
HES-PEG- Triman	$4.8 \cdot 10^{-8}$	$5.1 \cdot 10^{-8}$	-10.10 ± 3.82	-24.60 ± 6.77	-33.20 ± 6.70

a) Determined by NMR, b) Determined with anthrazene-azide, c) in $1 \cdot 10^{-3} \text{ M}$ KCl solution, d) in $1 \cdot 10^{-3} \text{ M}$ KCl solution after incubation with 10 % human serum, e) in $1 \cdot 10^{-3} \text{ M}$ KCl solution with 100% human serum.

C-type-lectin binding was studied to detect the available trimannose and mannose groups at the nanocarrier surface (Figure 40A); interestingly both carbohydrate-functionalized nanocarriers show a very similar binding to *Galanthus nivalis* lectin.

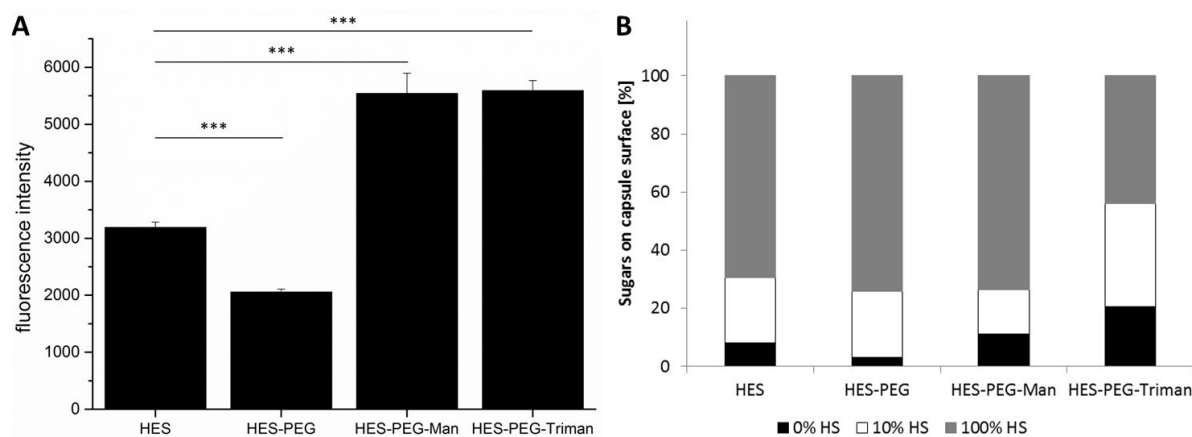


Figure 40. *Galanthus nivalis* lectin binding onto HES, HES-PEG and sugar-functionalized HES-PEG nanocapsules for mannose and trimannose detection before (A, *** $p < 0.001$) and after incubation (B, experiments conducted by Manuel Tonigold) in HS. Nanocapsules were treated for 2 h with HS (0%, 10% and 100%). Free proteins were discarded after centrifugation while capsules were incubated with C-type-lectin for 2 h at RT and then overnight at 4°C. After the next centrifugation step fluorescence intensity was determined by flow cytometry.

Protein corona analysis and cell uptake studies

For cell experiments, all dispersions were incubated in different concentrations of human serum (HS, 10% and 100%). The lectin binding increased with increasing HS concentration in all studied dispersions (Figure 40B). During incubation with HS, glycosylated and especially mannosylated^[389] proteins can adsorb on the surface of the carriers, thus undesirable and unspecific binding of lectin with the nanocarriers increased.

In order to investigate the stability of the different modified nanocapsules, dynamic light scattering was used after incubation with 10% HS. No variation in size was detected (Figure 41).

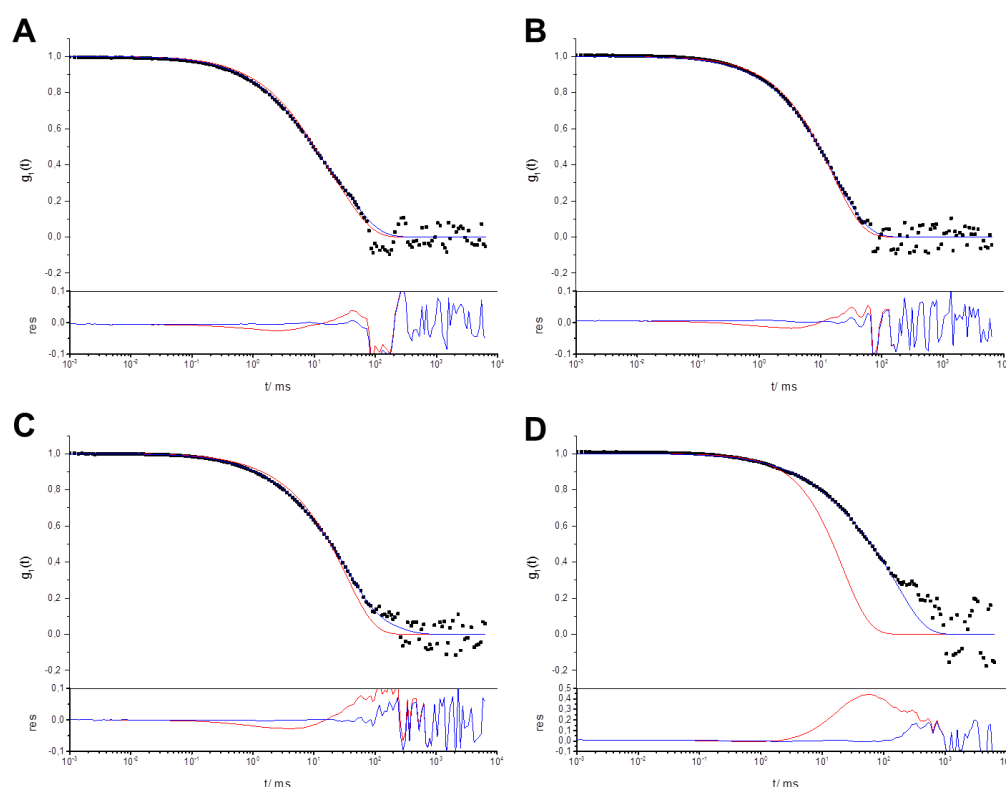


Figure 41. Autocorrelation functions (ACFs) of the different particles in human plasma at $\Theta = 30^\circ$ including data points (\bullet), forced fit (red) as the sum of the individual components and fit with additional aggregate function (blue) with the corresponding residuals resulting from the difference between data and the two fits (**A** HES, **B** HES-PEG, **C** HES-PEG-Man, **D** HES-PEG-Trim, experiments done by Christine Rosenauer).

In general, the detected zeta potential decreased after incubation with HS with increasing HS concentrations (10% and 100% HS). Comparison of the different dispersions at 10% HS concentration revealed differences at PEGylated surfaces. The surface charge of PEGylated nanocapsules was -18.4 mV, whereas all other incubated nanocapsule dispersions generated zeta potentials between -22.8 and -26.8 mV. Thus, unspecific adsorption of proteins at PEGylated surfaces was decreased. Incubation with 100% HS concentration did not show significant differences between the studied systems with values between -29.85 mV to -33.20 mV. Thus at high protein concentrations all surfaces were charged equally.

It is well known that primary cells respond more sensitively towards cytotoxic effects compared to cell lines. Therefore, moDCs were treated with different concentrations of nanocarriers to analyze their toxicity. Detection of dead cells was

performed by 7AAD staining, which revealed low cytotoxic effects (> 80% viable cells) even at the highest concentration of $150 \mu\text{g mL}^{-1}$ (Figure 42).

Notably, no significant differences were observed when concentration was raised from 18.8 to $150 \mu\text{g mL}^{-1}$.

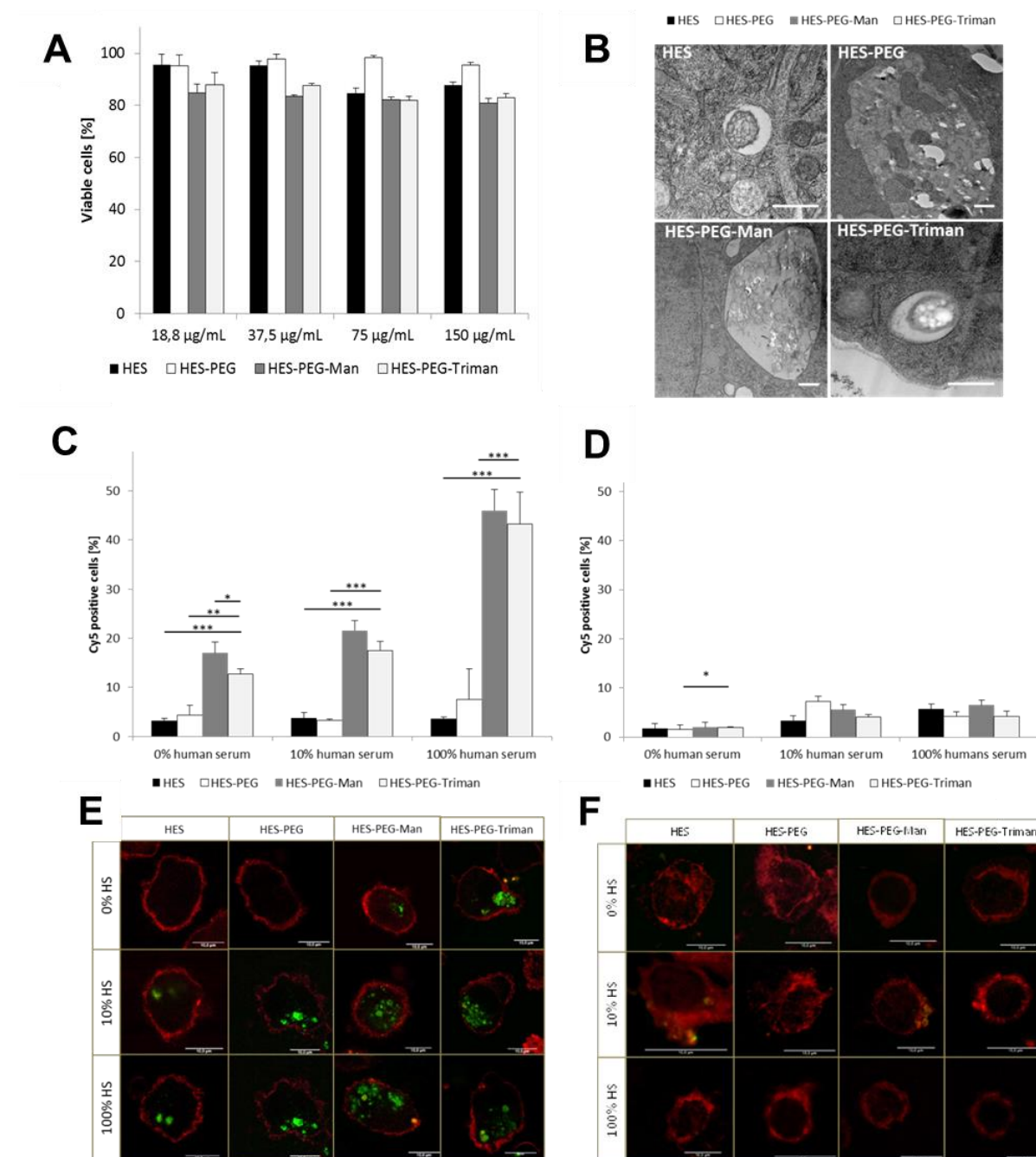


Figure 42. Nanocapsules reveal a very low amount of cytotoxic effects. To determine the percentage of death cells moDCs were incubated for 24 h at different nanocapsule concentrations (0, 18.8, 37.5, 75 and $150 \mu\text{g/mL}$, **A**). Cells were stained with 7-AAD to visualize dead cells. Cell uptake and intracellular trafficking of the

nanocapsules was determined by transmission electron microscopy (TEM, **B**, Scale bar: 500 nm, * $p < 0.05$, ** $p < 0.01$, *** $p < 0.001$, $n = 3$, conducted by Patrizia Renz) in moDCs. HS does not decrease specific uptake of mannose and trimannose modified particles in moDCs. MoDCs (**C**) or monocytes (**D**) were incubated for 2 h with capsules ($37.5 \mu\text{g mL}^{-1}$) before uptake was determined by flow cytometry analysis. **E** + **F** CLSM pictures of capsule uptake described at (C) in moDCs or in monocytes. Visualization of cell membrane was caused by cellmask green staining (red) while capsules are displayed in green (experiments conducted by Manuel Tonigold).

Dendritic cells play a key role in immune system function because of their ability to present foreign antigens to naive T cells very efficiently in order to initiate adaptive immune responses.^[375] Uptake of nanocapsules after 2 h in moDCs firstly was analyzed by flow cytometry. As serum proteins can have great impact on nanocapsule modification, different HS concentrations were used.^[390] Figure 42C demonstrates that trimannose modified capsules offer a significantly better uptake in moDCs compared to the unmodified or PEGylated analogues at all HS concentrations. No significant differences were however observed between mannose and trimannose functionalization at medium containing HS suggesting similar uptake of both modifications. Interestingly, 100% HS clearly increased the uptake of HES-PEG-mannose and HES-PEG-trimannose while the control capsules are not influenced maybe indicating uptake through the complement system.^[391] CLSM pictures of moDCs verify (Figure 42E) that most nanocarriers are detected in vesicles after 2 h. TEM pictures of engulfed HES-capsules support the observation from CLSM analysis (Figure 42B). Uptake in monocytes was analyzed to control unspecific uptake by mannose and trimannose modification compared to that in dendritic cells. As expected, the uptake of mannose and trimannose modified capsules is low and no difference to the controls are detected (Figure 42D and 42F). It is well known that mannosylation of nanocarriers can improve the uptake in dendritic cells.^[22, 231, 392-394]

Going more into detail, the results are more contradictory when mannose modifications are directly compared. In contrast to our results, White and colleagues showed that only trimannose but not mannose functionalization of liposomes increased uptake in moDCs.^[395] These results suggest that besides the chemical structure of the carbohydrate, i.e. mannose or trimannose, further factors influence

the binding to cells (e.g. binding chemistry and nanocarrier properties such as size, material etc.). Of course, impact from different donors cannot be excluded since the expression of the mannose receptor family members, which have diverse binding affinities to mannose and trimannose,^[396] can be different. As expected, incubation of monocytes with all capsules resulted in similar uptake because they have no specific uptake mechanisms for mannose^[397] and do not express DC-SIGN,^[398] which is also shown in Figure 43.

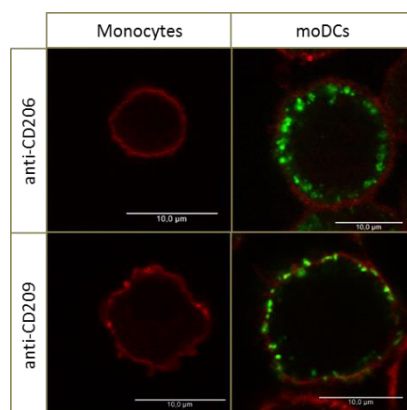


Figure 43. Surface expression of CD206 and CD209 by monocytes and moDCs. Cells were stained with anti-CD206 and anti-CD209 for 30 min at 4 °C. Visualization of antibody binding was offered by secondary antibody staining (green). By incubation with CellMask Green (red) cell membrane was displayed in CLSM (experiments conducted by Manuel Tonigold).

These results are further hints for the specific uptake behavior of mannose and trimannose modifications. However, the impact of serum proteins towards immature moDCs uptake of mannose- and trimannose modified nanocarriers has not yet been reported in the literature although serum proteins are known to shield specific functionalizations of nanomaterials.^[390] PEG can decrease protein adsorption to nanomaterials and unspecific uptake of immune cells.^[399, 400] However, PEGylation alone is no guarantee for successful specific cell targeting in complex protein environments,^[390] possibly because protein adsorption is still required to induce a stealth effect^[18] and therefore proteins can still influence surface modifications. Dai and colleagues postulated that material of the nanomaterial and sufficient size of the modifying molecules are important factors for an efficient targeting in complex protein environments.^[401] While smaller modifying molecules like single-domain antibodies

and transferrin (15 kDa and 80 kDa) led to great loss of their uptake properties in serum^[390, 402] larger molecules like antibodies (150 kDa) were able to maintain specific targeting properties.^[401] However, our results are in part contradictory to this hypothesis because small molecules like mannose (180 Da) and trimannose (540 Da) caused specific targeting of our nanocapsules. Maybe this disadvantage is compensated by the fact that we used HES capsules which caused low protein adsorption^[22] rates so that there is a smaller hiding effect by the protein corona at these capsules.

To analyze the effect of protein adsorption the hard protein corona of all nanocarriers was analyzed. Surprisingly, HES-PEG-trimannose caused lower protein concentrations compared to other modifications while PEGylation alone did not show a dramatic decrease in protein adsorption. In general, the amount of adsorbed protein on all nanocarriers is low (100 - 300 $\mu\text{g m}^{-2}$ at 100% HS, Figure 44) and a bit lesser pronounced compared to previous reports.^[22]

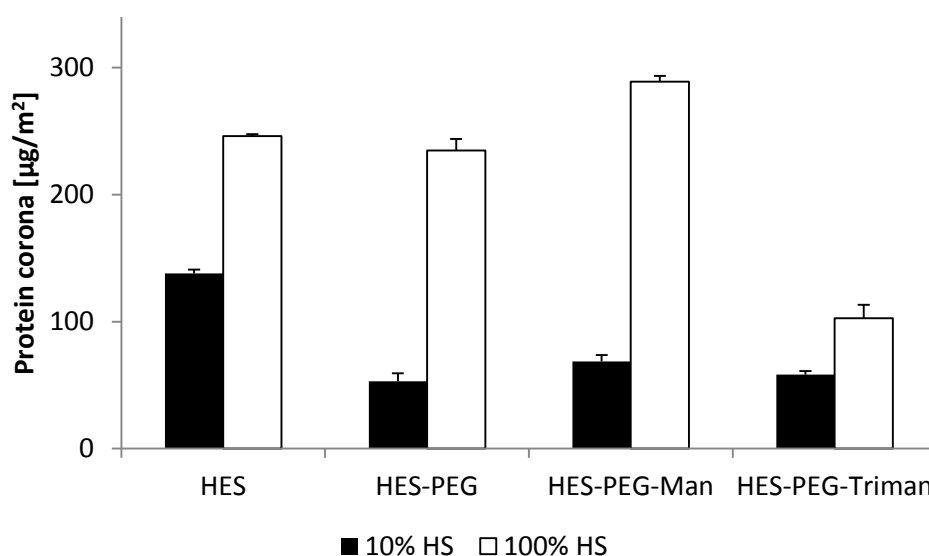


Figure 44. Protein quantification of purified hard protein corona. 0.05 m^2 capsule surface were either incubated with 10% or 100% HS and incubated for 2 h at 37 °C. Released proteins were quantified by the Pierce 660 nm Protein Assay Reagent in combination with the Ionic Detergent Compatibility Reagent for Pierce 660 nm Protein Assay Reagent (experiments conducted by Manuel Tonigold).

Separation of proteins by SDS-PAGE and visualization by silver staining demonstrates little differences between all modifications (Figure 45). Proteomic mass spectrometry analysis revealed very similar protein compositions in all cases (Figure 45).^[403] However, other groups also observed no dramatic changes in protein corona upon different surface modifications.^[22, 363, 364] Visible differences were detected at the IgG light (25 kDa) and heavy chain (50 kDa) which is more abundant at mannose and trimannose modified capsules supporting the theory about uptake via the complement system in moDCs. Adsorption of IgG, which is highly abundant in serum,^[404] to nanomaterials is known to enhance uptake in phagocytic cells.^[405] Clusterin, which reduces unspecific uptake at polystyrene particles,^[18] was detected in all cases, with a slight decrease on the carbohydrate-functionalized nanocarriers. However, former studies underline that modification of HES nanocarriers caused a minor adsorption of clusterin.^[22]

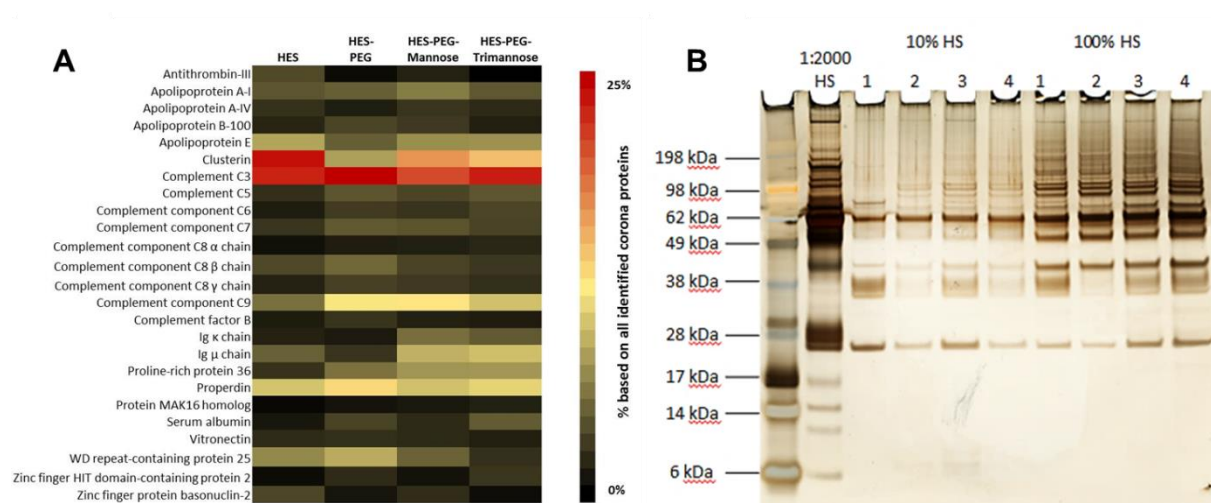


Figure 45. Hard protein corona of all nanocapsules. **A** Heatmap of top 20 most abundant hard corona proteins identified by liquid chromatography mass spectrometry. Nanocapsules with 0.05 m^2 capsule surface were incubated for 2 h, 37°C with 100% HS (and 10% HS in B) under constant agitation and the hard protein corona was isolated via repetitive centrifugation to remove unbound proteins. All measurements were performed in triplicate (experiments conducted by Johanna Simon). After purification of hard protein corona proteins 0.5 mg proteins were visualized by silver staining (**B**). As control HS (1:2,000) was used for SDS-PAGE. **1** HES, **2** HES-PEG, **3** HES-PEG-Man, **4** HES-PEG-Trimannose (experiments conducted by Manuel Tonigold).

Conclusion

In summary, functionalized trimannose as well as α -D-mannosylazide could be coupled onto PEG modified HES crosslinked nanocapsules by copper free click reaction detected by NMR, fluorescence assay using 9-(azidomethyl)anthracene and *Galanthus nivalis* lectin binding. mannose and trimannose modified capsules caused similar uptakes in moDCs and were significantly more efficiently compared to naked and PEGylated ones even in presence of 100% HS. In contrast, we did not observe a significantly higher uptake in monocytes which do not express CD206 and DC-SIGN. Analysis of the hard protein corona demonstrates a very similar pattern of bound proteins.

Experimental section

Materials

All reagents were reagent grade and used without further purification unless otherwise noted. Dimethylformamide (DMF, Extra dry, AcroSeal[®]) and pyridine was purchased from Acros and used without further purification. Acetonitrile and dichloromethane was distilled from calcium hydride. The eluents for column chromatography (cyclohexane and ethyl acetate) were distilled prior to use. Deuteriochloroform was stored over alumina (Brockmann activity I). HES (200 kDa, degree of substitution 0.5) was purchased from Fresenius Kabi, the fluorescence dye Cy5-oligo was bought from BioChemica, isocyanate-PEG and diisocyanate-PEG with a molecular weight of 5000 g mol⁻¹ was used from Nanocs Inc., USA. Sodium dodecyl sulfate (SDS) was purchased from Fluka. DBCO-PEG4-NHS was bought from Jana Bioscience. The C-type-lectine (*Galanthus nivalis* snowdrop lectin fluorescein labeled 2 mg) was bought from BIOZOL Diagnostica Vertrieb GmbH. All other chemicals were purchased from Sigma Aldrich and used as received.

The oil-soluble surfactant poly((ethylene-co-butylene)-*b*-(ethylene odixe)) (P(E/B-*b*-EO)) was synthesized starting from ω -hydroxypoly-(ethylene-co-butylene) dissolved in toluene after addition of ethylene oxide via anionic polymerization to generate a poly(ethylene-co-butylene) block of 3700 g mol⁻¹ and a polyethylene oxide block of 3600 g mol⁻¹.^[365] 1M borate buffer was produced by adjusting pH of boric

acid (B6768 Sigma) water solution to desired value of 9.5 by sodium hydroxide solution.

Methods

Thin-layer chromatography (TLC) was carried out on silica gel 60 F254 plates (*Merck*) or RP silica gel RP-18 F_{254s} plates (*Merck*). Compounds were visualized using UV light and/or by immersion in a solution of cerium(IV) sulfate (1 g) and phosphomolybdic acid (2.5 g) in water (95 mL) and concentrated sulfuric acid (4 mL) followed by heating. Alternatively the TLC plates were immersed in a solution of *m*-methoxyphenol (0.1 mL) in ethanol (95 mL) and sulfuric acid (2 mL) followed by heating. Chromatography was performed using flash chromatography of the indicated solvent system on 35-70 μ m silica gel (*Acros Organics*) unless otherwise noted. Alternatively the purifications were performed on an Isolera™ Flash Purification System (*Biotage*®) with an integrated diode array detector. Preparative reverse phase separation was carried out on a *Smartline* HPLC system (*Knauer*) with mixtures of acetonitrile or methanol and water as eluents on a ACE 5 C18-PFP, 150mm \times 30 mm column (*Macherey & Nagel*), at a flow rate of 37.5 mL min⁻¹. The eluents were degassed prior to use by means of ultrasonication for 30 min. Two *Smartline K-1800* pumps (pump head size: 100 mL each, high pressure gradient mode; *Knauer*) and a *S-2600 diode array detector* (*Knauer*) were used. NMR spectra were recorded on an *Avance III HD 300* (300 MHz ¹H NMR, 75 MHz ¹³C NMR, COSY, HSQC, HMBC; *Bruker*), an *Avance II 400* (400 MHz ¹H NMR, 101 MHz ¹³C NMR, COSY, HSQC, HMBC; *Bruker*), an *Avance III HD 400* (400 MHz ¹H NMR, 101 MHz ¹³C NMR, COSY, HSQC, HMBC, NOESY; *Bruker*) or an *Avance III 600* (600 MHz ¹H NMR, 151 MHz ¹³C NMR, COSY, HSQC, HMBC, NOESY; *Bruker, with TCI cryoprobe*) using 5 mm probe heads at a temperature of 23 °C. The ¹³C-NMR spectra are ¹H broadband decoupled. The HSQC spectra are phase-sensitive (opposite signs for CH/CH₃ and CH₂). The ¹H and ¹³C chemical shifts (δ) were referenced to the residual solvent signal as internal standard (CDCl₃: δ = 7.26 ppm and 77.16 ppm, DMSO-*d*₆: δ = 2.50 ppm and 39.52 ppm, CD₃OD: δ = 3.31 ppm and 49.00 ppm, D₂O: δ = 4.79 ppm, for ¹H and ¹³C NMR, respectively).^[406] Coupling constants (*J*) are reported in Hz (splitting abbreviations: s, singlet; d, doublet; t, triplet; q, quartet; m, multiplet; br, broad; and combinations thereof). ¹H NMR spectra for PEG detection on the nanocapsule surface were measured at 250 MHz on a Bruker Avance 250

spectrometer (Burker, Billerica, MA, USA) as described by Kang et al.^[17] using deuterated water as solvent and CD_2Cl_2 as internal standard. HPLC-ESI-MSⁿ was performed on a 1200 series HPLC system with a UV diode array detector coupled with a LC/MSD trap XCT mass spectrometer (Agilent Technologies). Mixtures of water (with 0.1% formic acid) and acetonitrile were used as eluents at a total flow rate of 0.5 to 1.0 mL min⁻¹. An Ascentis Express C18 column (pore size: 2.7 μm , length: 3 cm, diameter: 2.1 mm; Supelco) was used at a temperature of 40 °C. High-resolution masses (ESI) were recorded on a Q-ToF-Ultima 3 instrument (Waters) with LockSpray[®] interface and a suitable external calibrant. FT-IR spectra were recorded on a Tensor 27 spectrometer (Bruker) equipped with a diamond ATR unit. For detection of azide functionality on Mannose, fourier transform infrared spectroscopy (FT-IR) was performed. KBr and Mannose-azide was mixed together, pressed and measured directly on a PerkinElmer Spectrum BX FT-IR spectrometer (PerkinElmer, Shelton, CT, USA) between wavelength of 4000 cm⁻¹ and 400 cm⁻¹. Detection of nanocapsules using transmission electron microscopy was done at a Joel 1400 transmission electron microscope (TEM) including a LaB₆ cathode (JOEL GmbH, Echting, Germany). Before the TEM copper grid was transferred into the TEM, it was layered with a carbon film (200 mesh, Science Service, Munich, Germany), afterwards a diluted nanocapsule dispersion in cyclohexane was dropped onto the grid surface and dried at RT. The TEM images were operated at an acceleration voltage of 120 kV. For embedding capsules with trehalose a solution with 1 % wt/wt aqueous trehalose and 4 % wt/wt uranyl acetate for the negative staining is prepared. For the preparation a droplet of the capsule dispersion is applied to a lacey carbon grid. Subsequently, a drop of the trehalose uranyl acetate solution is added to the grid. Finally, the surplus removed by a filter paper and the specimen is allowed to dry at ambient conditions.^[407] For the purpose of visualize the cellular uptake of nanocapsules at high resolution we investigated moDCs using TEM. Prior treatment, cells were seeded for 24 h onto 3 mm Ø sapphire discs at a density of 100 000 cells mL⁻¹ in a 24-well plate. After 2 h of incubation with capsules (300 $\mu\text{g mL}^{-1}$), cells were fixed by high pressure freezing (HPF) using a Compact 01 HPF machine (Wohlwend GmbH, Switzerland) followed by freeze-substitution using a Leica EM AFS 2 device (Leica Microsystems, Germany). The substitution solution, containing acetone p. a., 0.2 wt% osmium tetroxide, 0.1 wt% uranyl acetate and 5 wt% water, was pre-cooled

to -90 °C before addition of the samples. After freeze-substitution for 12 h and warm-up to 0 °C the samples were washed with acetone p. a. and embedded into EPON 812 resin at RT. Ultrathin slices were produced using a Leica Ultracut UTC (Leica Microsystems, Germany) and a diamond knife. After collecting slices on 300-mesh copper grids images were recorded on a FEI Tecnai F20 transmission electron microscope working at 200 kV. Bright field images were acquired using a Gatan US1000 slow scan CCD camera (Gatan Inc., USA). SEM images of the formed nanocapsules were determined at the Zeiss 1530 LEO Gemini microscope (Carl Zeiss, Oberkochen, Germany) with an accelerating voltage of 0.2 kV and a working distance of ~3 mm. Before, the nanocapsule dispersions (10 µL) were diluted in cyclohexane (3 mL), dropped onto a silica wafer and dried under ambient conditions. The generated nanocapsules were also analyzed by dynamic light scattering to detect the hydrodynamic radii. Therefore, 10 µL of the emulsion was diluted in 1 mL cyclohexane and measured in a Nicomp 380 Submircon particle Sizer (PSS-Nicomp, Particle Sizing System, Port Richey, FL, USA) at a fixed scattering angle of 90 °. DLS measurements after incubation with 10 % HS were performed on a commercially available instrument from ALV GmbH (Langen, Germany). The DLS instrument consists of a goniometer and an ALV-5000 multiple tau full-digital correlator with 320 channels. A helium-neon laser from JDS Uniphase (Milpitas, USA) with an operating intensity of 25 mW and a wavelength of $\lambda = 632.8$ nm was used as a light source. All solutions were filled into dust-free quartz cuvettes from Hellma (Müllheim, Germany) with an inner diameter of 18 mm, which were cleaned before with distilled acetone. To measure the nanocapsule-plasma mixture, 2 mL of 1:10 diluted HS in PBS solution was filtered through a Millex-GS filter (Merck Millipore, Darmstadt, Germany) with a pore size of 0.2 µm into the cuvette. 10 µL of a 1.2 g L⁻¹ or 5 µL of a 3.5 g L⁻¹ nanocapsule dispersion were added into the diluted HS solution and incubated at 37 °C for 30 min followed by DLS analysis at the same temperature.

Synthesis

Reactions Conditions

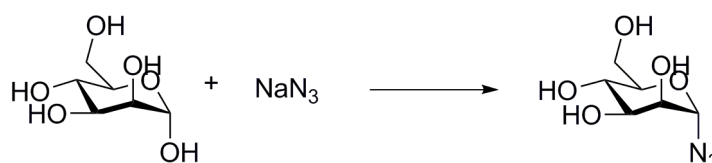
All reactions involving air or moisture sensitive reagents or intermediates were performed under an inert atmosphere of argon in glassware that was oven dried

using standard Schlenk techniques. Reaction temperatures referred to the temperature of the particular cooling/heating bath.

Synthesis of trisaccharide 13 is described in detail in the appendix, because the whole synthesis was done by Jens Langhanki.

Synthesis of α -D-mannopyranosyl azide 14

Mannose was selectively functionalized with one azide group at the OH- α -position using the synthesis published by Vinson et al..^[356]



To 1.00 g mannose and 3.63 g sodium azide dissolved in 20 mL water was added a solution of 2.80 g 2-chloro-1,3-dimethylimidazolinium chloride and 7.80 mL trimethylamine under ice cooling and stirred for 1 h at 0 °C. Subsequently, the mixture was concentrated under reduced pressure and mixed with 20 mL ethanol. The generated solid was removed by filtration and ethanol was removed from the filtrate under reduced pressure. The obtained solid was freeze-dried overnight and dissolved in 15 mL water again. After the water phase was washed with 10 mL dichloromethane five times, the water phase was stirred with acidic Amberlite IR-120 for 4 h at room temperature (RT). The Amberlite was activated with 1 M sodium hydroxide solution. Then, the ion exchanger was removed by filtration and the filtrate was freeze-dried again to obtain the α -D-mannopyranosyl azide as a white powder in 51% yield (0.58 g).

¹H-NMR (D₂O, 350 MHz): δ (ppm) = 5.43 (d, 1H, J = 1.9 Hz), 3.94 – 3.56 (m, 6H).

¹³C-NMR (D₂O, 350 MHz): δ (ppm) = 89.69 (C₁), 74.59, 69.78, 69.71, 66.34, 60.77 (C₆).

IR n: 2120 cm⁻¹ (-N₃).

Synthesis of HES nanocapsules by inverse miniemulsion

The nanocapsules were prepared by polyaddition reactions at the miniemulsion droplet interfaces as described in previously published publications.^[23, 206, 358, 359]

The dispersed phase containing 1.4 g HES solution (10 wt%), 20 mg NaCl and 100 mL Cy5Oligo solution was added to 7.5 g cyclohexane containing 100 mg of

P(E/B-*b*-EO). After stirring at 1000 rpm for 1 h, the emulsion was subjected to ultrasonication under ice-cooling with a Branson W450-D sonifier equipped with a ½ inch tip for 3 min in a pulse-pase regime of 20 s and 10 s. 100 mg TDI and 30 mg P(E/B-*b*-EO) dissolved in 5 g cyclohexane were added dropwise to the miniemulsion and stirred for 24 h at RT. The size and morphology of the obtained nanocapsules were analyzed by DLS and SEM/TEM measurements as described above.

The following synthesis for surface modification of the HES crosslinked nanocapsules with isocyanate-PEG and afterwards with the sugar azide were performed as reported by Kang et al.^[22] All reactions involving air or moisture sensitive reagents or intermediates were conducted under an inert atmosphere of argon in glassware, which were dried in an oven before use. Reaction temperatures referred to the temperature of the particular cooling/heating bath.

Functionalization of the HES nanocapsule surface with monoisocyanate-PEG or diisocyanate-PEG

To remove the excess of surfactant before surface functionalization, 2 mL of the nanocapsule dispersion is centrifuged at 4000 rpm for 30 min, for a typical coupling reaction. The upper phase was neglected, while the precipitate was redispersed in 3.2 mL anhydrous cyclohexane. In 800 mL anhydrous acetone either 16 mg monoisocyanate-PEG or diisocyanate-PEG both with a molecular weight of 5000 g mol⁻¹ was dissolved and added dropwise to the nanocapsule dispersion by stirring at 500 rpm. After stirring for 5h, the nanocapsules were centrifuged at 4000 rpm to remove the non-coupled PEG and the precipitate was redispersed in 400 µL cyclohexane for using in further steps.

Nanocapsule transfer into water

Before transferring the nanocapsules into water, a 0.1 wt% SDS solution was prepared and filtered through a 0.2 mm pore size filter. Then, 5 mL of the prepared SDS solution were shaken in a sonication bath (Bandelin Sonorex, type RK 52H) during slow addition of 400 µL redispersed nanocapsule dispersion in cyclohexane. The whole dispersion was stirred over night at 1000 rpm at RT without cap, to allow evaporation of cyclohexane and hydrolyzation of the remained isocyanate groups to primary amines. To remove the excess of SDS, the emulsion was ultrafiltrated using Amicon Centrifugal Filters (Ultra-0.5, Ultracel-100 Membrane, 100 kDa) and used for

further steps. To obtain the solid content of the nanocapsule dispersion, three times 50 mL of the nanocapsule dispersion was freeze-dried overnight. The remained solid was used to detect the PEG on the nanocapsule surface by ^1H NMR spectroscopy as published previously.

Coupling of mannosyl azide (14) or trisaccharide 13 to diisocyanate-PEG functionalized HES nanocapsules

500 μL of 0.8 M borate buffer were added to 5 mL nanocapsule dispersion in water and adjusted to pH 8.29. A stock solution of 6.77 mg DBCO-PEG4-NHS in 1 mL dry DMSO was prepared and 100 μL of the stock solution were added to the nanocapsule dispersion, which was stirred for 4 h at RT. Afterwards, the excess of DBCO-PEG4-NHS was removed by ultrafiltration (four times). To quantify the mol of DBCO per mL nanocapsule dispersion the fluorescence assay with 9-(azidomethyl)anthracene was performed.^[362] Thus, the amount of DBCO per mL emulsion was found to be approximately $5.1 \cdot 10^{-5}$ mmol per mL. Finally, metal free click reaction with the azide functionalized sugars were prepared. Therefore, a stock solution of 1.88 mg α -mannosyl azide (**14**) or 7.25 mg of trisaccharide **13** in 1 mL water was generated. 10 μL of **14** or **13** stock solution was added to the nanocapsule dispersion and shaken overnight at 300 min^{-1} at RT on a combined shaker KL2 (Edmund Bühler GmbH). After centrifugation of the dispersion at 5500 rpm for 20 min for purification and redispersion in 500 μL water, the remaining DBCO groups were quantified as well with 9-(azidomethyl)anthracene. After azide-alkyne reaction no DBCO groups could be detected, thus quantitative coupling was expected.

Quantification of SDS concentration

To use functionalized nanocapsules for biomedical application, the SDS concentration should only be as high as necessary for stabilization of the nanocapsules in emulsion. For SDS quantification a solution of light sensitive Stains-All dye was used, because depending on the amount of SDS a colour change from intense fuchsia to yellow could be occurred as a result of the generated complex between the dye and SDS.^[388] Therefore, a stock solution containing 1 mg of Stains-All in 500 μL isopropanol and 500 μL water was prepared and mixed with formamide and water in a ratio of 1 : 1 : 18 to generate the reactive dye solution. In addition, also a background solution without Stains-All with the same ratio of isopropanol,

formamide and water (1 : 1 : 18) was prepared. 2 μL of every nanocapsule dispersion (HES, HES-PEG, HES-PEG-Man and HES-PEG-Triman nanocapsule dispersion) was mixed with 200 μL of reactive dye solution (or background solution) without visible colour change of the solution. Thus, the SDS concentration seemed to be very low. To quantify the exact SDS concentration of the nanocapsule dispersions, the absorbance measured at 438 nm was compared with the absorbance of dye solutions including 2 μL of SDS standard solutions. To make sure, that no molecule in the sample interfere with the dye, also the absorbance spectra from 350 to 750 nm for all solutions were recorded (Figure S3, in Supporting information) without showing any difference. After comparison of the detected absorbance at 438 nm of the samples with the standard SDS concentrations, the concentration of SDS in all miniemulsions was lower than 0.1 mmol L⁻¹.

Interaction of the functionalized nanocapsules with *Galanthus nivalis* lectin

A fluorescein labeled Mannose specific c-type lectin, *Galanthus nivalis* snowdrop lectin, was used to study the availability of mannose **14** or trimannose **15** on the surface of 0.1 wt% HES nanocapsules after incubation in 0 %, 10 % and 100 % HS for 2 h at 37 °C. Supernatant was discarded after nanocapsules were centrifuged for 1 h at 4000 rpm and 4 °C. 10 μg of c-type lectin in water was added to 500 μL 0.1 M HEPES buffer solution at pH 7.5 and then used for resuspension of HES, HES-PEG, HES-PEG-Man or HES-PEG-Triman. After shaking the lectine-nanocapsule dispersion for 2 h at RT, it was stored at 4 °C overnight and centrifuged at 4000 rpm for 10 min at the next day. The precipitate was isolated, redispersed in 500 μL 0.1 M HEPES buffer at pH 7.5 and measured the fluorescence intensity at 25 °C by detecting excitation at 495 nm and emission at 519 nm at the Tecan plate reader. All fluorescence measurements were repeated three times. In the case capsules were incubated with HS then fluorescence was determined at the flow cytometer.

In-vitro tests

Isolation of monocytes from healthy donors

Monocytes were isolated from healthy human donor buffy coats which were obtained according to the votum of local ethics committee and the Declaration of Helsinki. Peripheral blood mononuclear cells (PBMCs) were isolated by standard Ficoll separation. PBMCs were allowed to attach by seeding $1.5 \cdot 10^7$ cells in 3 mL

DC-medium containing RPMI-1640 (Sigma-Aldrich Chemie GmbH, Steinheim, Germany), 2% HS, 100 IU/mL penicillin and 100 $\mu\text{g mL}^{-1}$ streptomycin (Life Technologies GmbH, Darmstadt, Germany) in 6-well plates. After 1 h incubation under standard conditions (37 °C, 5% CO₂) cells in the supernatant were removed and adherent monocytes were detached by incubation with cold 2.5 mM ethylenediaminetetraacetic acid (EDTA, AppliChem GmbH, Darmstadt, Germany) in PBS for 30 min at 4 °C. Before usage monocytes were transferred in freezing medium and stored in liquid nitrogen.

Generation of moDCs from healthy donors

For the generation of moDCs monocytes which were isolated as described before were not detached but incubated with 3 mL DC-medium supplemented with 800 IU/mL granulocyte-macrophage colony-stimulating factor (GMCSF, Sanofi-Aventis, Bridgewater, NJ, USA) and 500 IU mL⁻¹ interleukin (IL)4 (PromoCell GmbH, Heidelberg, Germany) for 2 d under standard conditions. Then, 800 μL of supernatant was centrifuged and replaced by 1 mL DC-medium containing 1,600 IU mL⁻¹ GMCSF and 500 IU mL⁻¹ IL4. After further 3 d of incubation this procedure was repeated. Finally after 24 h, cells were detached with 0.5 mM EDTA in PBS, transferred in freezing medium and frozen in liquid nitrogen. To control moDC cell generation cells were stained against the surface markers CD11c (Miltenyi Biotec, Bergisch Gladbach, Germany), CD14 (Invitrogen, Eugene, OR, USA), CD45 (Beckman Coulter, Marseille, France), CD80, CD83, CD86 and HLA-DR (all Biolegend, Fell, Germany) for 30 min at 4 °C. Surface expression was determined by flow cytometry in Cyflow ML (Partec GmbH, Germany, Münster). Like as usual all following flow cytometry experiments data were analysed by the program FCS express.

Cell culture

MoDCs and monocytes were seeded 1 d before experimental usage in DC-medium with or rather without 1,600 IU mL⁻¹ GMCSF and 500 IU mL⁻¹ IL4 and incubated for 24 h under standard conditions for recovering.

Cytotoxicity assay

Approximately 200,000 moDCs were incubated for 24 h at different nanocapsule concentrations (0, 18.8, 37.5, 75 and 150 $\mu\text{g mL}^{-1}$) under standard conditions. Cells

were detached and washed twice with PBS supplemented with 0.5% BSA (Sigma-Aldrich) and 2 mM EDTA before resuspension with 100 μ L PBS. Staining of death cells was performed by pipetting 5 μ L 7-AAD Viability Staining Solution (Biolegend) to the samples followed by an incubation for 15 min at room temperature (RT). Then, volume was filled up to 800 μ L with PBS and fluorescence of 7-AAD was determined by flow cytometry. The viability of the sample without nanocapsules was defined as 100% viable to calculate the living cells in all other samples.

Uptake of nanocapsules in moDCs and monocytes

37.5 μ g mL⁻¹ nanocapsules were incubated for 2 h at different HS concentrations (0, 10 and 100%) with moDCs or monocytes. Cells without nanocapsule incubation were used as negative control. Cells were detached with 0.5 mM or rather 2.5 mM EDTA in PBS. For flow cytometry analysis cells were centrifuged and resuspended with 100 μ L PBS supplemented with 1 μ L Zombie Aqua (Biolegend) to stain death cells. After 20 min of incubation at RT cells were centrifuged again and resuspended in 800 μ L PBS (4 °C). Finally, uptake was determined by flow cytometry by defining 1% of cells of negative control as false positive for uptake. For confocal laser scanning microscopy (CLSM) cells were seeded into 8-well chamber slides which were coated with poly L-lysine after detachment and resuspension with DC-medium. After that cells were allowed to adhere for 30 min at 4 °C before they were fixed with PBS containing 4% formaldehyde for 10 min at RT. Visualization of cell membranes by CLSM at Leica TCS SP5 II (Leica, Wetzlar, Germany) was allowed by staining with cellmask green (Invitrogen) just before measurement.

Purification of hard protein corona

0.05 m² surface area of nanocapsules were used for incubation with 1 mL 10% or 100% HS for 2 h at 37 °C to allow protein corona formation. Purification of hard protein corona was executed according former instructions ^{[366], [367]} at which g-force was reduced to preserve capsules. Briefly, nanocapsules were centrifuged three times for 1 h at 4,000 g and 4°C followed by resuspension with 1 mL PBS (4 °C). After the last washing step capsules were resuspended and incubated for 5 min at 95 °C with 64.5 mM Tris-HCL supplemented with 2% SDS to remove serum proteins from capsules. Again, samples were centrifuged for 1 h at 4,000 g and 4 °C to remove capsules in suspension. For protein quantification the Pierce 660 nm Protein

Assay Reagent was used in combination with the Ionic Detergent Compatibility Reagent for Pierce 660 nm Protein Assay Reagent (both Thermo Scientific, Dreieich, Germany) according the manufacturer instructions.

Determination of the hard protein corona by SDS-Page

For SDS polyacrylamide gel electrophoresis (SDS-PAGE) 0.5 mg of the proteins of the hard corona were supplemented with sample buffer and reducing agent (Novex, Carlsbad, USA) and subsequently incubated for 5 min at 95 °C. HS (1:2,000) was used as positive control and therefore it was prepared like the other protein samples. Then, SDS-PAGE was run at 100 mV for 1.5 h before protein bands were visualized by the SilverQuest Silver Staining Kit (Thermo Scientific) according the manufacturer instructions.

In solution digestion

SDS was removed via Pierce detergent removal columns (Thermo Fisher) prior to protein digestion. Tryptic digestion was performed after the protocol of Tenzer et al.^[348] with the following adjustments. Proteins were precipitated using ProteoExtract protein precipitation kit (CalBioChem) according to the manufactures instructions'. The resulting protein pellet was re-suspended in RapiGest SF (Waters Cooperation) dissolved in 50 mM ammonium bicarbonate (Sigma-Aldrich) and incubated at 80 °C for 15 mins. Proteins were reduced by adding dithithreitol (Sigma-Aldrich) to gain a final concentration of 5 mM and incubated for 45 mins at 56 °C. Iodoacetamide (final concentration 15 mM, Sigma-Aldrich) was added and the solution was incubated in the dark for 1 h. Tryptic digestion with a protein:trypsin ratio of 50:1 was carried out over 16h at 37 °C. The reaction was quenched by adding 2 µL hydrochloric acid (Sigma-Aldrich). Degradation products of RapiGest SF were removed via centrifugation (14.000 g, 15 mins).

Determination of the hard protein corona by Liquid-chromatography mass-spectrometry (LC-MS) analysis

Peptide samples were spiked with 10 fmol/µl of Hi³ EColi Standard (Waters Cooperation) for absolute protein quantification. Digested peptides were applied to a C18 nanoACQUITY Trap Column (5 µm, 180 µm x 20 mm,) and separated on a C18 analytic reversed phase column (1.7 µm, 75 µm x 150 mm) using a nanoACQUITY UPLC systems which is further coupled to a Synapt G2-Si mass spectrometer. A two

phase mobile system consisting of phase (A) 0.1% (v v⁻¹) formic acid in water and phase (B) acetonitrile with 0.1% (v v⁻¹) formic acid was used at a sample flow rate of 300 µl min⁻¹ with a gradient of 2 – 37% mobile phase (A) to (B) over 70 min. Glu-Fibrinopeptide (150 fmol µL⁻¹, Sigma) was infused at a flow rate of 500 µl min⁻¹ and served as a reference component.

Electrospray ionization (ESI) was performed in positive ion mode with nanoLockSpray source and the mass spectrometer was operated in resolution mode performing data-independent acquisition (MS^E).

Data was acquired over 90 mins with a mass to charge range (m/z) over 50 – 2000 Da, scan time of 1 s and ramped trap collision energy from 20 to 40 V. Each sample was run in triplicates. Data was processed with MassLynx 4.1. Protein identification was carried out with Progenesis QI for Proteomics Version 2.0 with continuum data using a reviewed human data base (Uniprot). Several parameters as noise reduction thresholds for low energy, high energy and peptide intensity were set to 120, 25, and 750 counts.

The peptide sequence of Hi3 Ecoli standard (Chaperone protein CLpB, Waters Cooperation) was added to the database for absolute quantification.^[368] The following search criteria were used for protein and peptide identification: one missed cleavage, maximum protein mass 600 kDa, fixed carbamidomethyl modification for cysteine, variable oxidation for methionine and protein false discovery rate of 4%.

For protein identification at least two assigned peptides and five assigned fragments are required and for peptide identification three assigned fragments are necessary.

A score parameter for identified peptides was set to 4 and quantitative protein identification was generated based on the TOP³/Hi³ approach, providing the amount of each identified protein in fmol.^[369]

A list of all identified proteins [fmol] is found in a separate excel document.

Staining of CD206 and CD206 on cell surface

100,000 cells were dissolved in 200 µl PBS (4 °C) and then treated with anti-CD206 and anti-CD209 (both Biolegend) for 30 min at 4 °C. After washing and centrifugation for 5 min at 500 g cells were resuspended again with 200 µl PBS (4 °C) and incubated again for 30 min at 4 °C with anti-mouse Alexa Fluor 633 (Life Technologies GmbH). Cells were subsequently washed and centrifuged again and

then seeded on 8-well chamber slides coated with poly L-Lysine. Visualization of the cell membrane was performed by CellMask Green staining before fluorescence intensity was determined by CLSM.

Statistical analysis

Statistical analysis was performed with the Student's t-test. In detail, the two-tailed and unpaired t-test was used.

3. Summary and Outlook

In this thesis, functional surfactants were synthesized using different polymerizations techniques for direct and / or inverse miniemulsion polymerization to produce various nanocarriers. Furthermore, nanocapsules based on biocompatible hydroxyethyl starch were functionalized with different sugar derivatives to study the stealth properties or cell specific uptake, which is important for drug delivery applications. Polymer and nanocarrier characterization was done with different kinds of techniques ranging from SEC to surface tension measurements to spectroscopy and spectrometry analysis as well as dynamic light scattering measurements. In addition, different methods were utilized to study protein-nanocarrier interactions.

In chapter 2.1, orthogonal protected block copolymers based on polyglycerol were synthesized by anionic ring-opening polymerization using EGE and AGE or *t*BuGE as monomers with defined block length ratios. After deprotection of the acetal groups, they reached an amphiphilic structure with surface active properties. Thus, dependent on their solubility they were used as surfactant or surfmer due to the existing allyl and hydroxyl groups for direct and / or inverse miniemulsions to generate stable PS nanoparticles, polyurethane nanocapsules or PHEMA and PAA nanoparticles. Furthermore, the stability in protein solutions of the PS nanoparticles stabilized with the water-soluble surfmer or surfactant were studied. Besides, some aggregates single nanoparticles could be detected. Thus, the amphiphilic PGs seems to be promising stealth surfmers. However, stability tests in protein mixtures have to be optimized and protein adsorption as well as cell uptake studies have to be investigated in the future. In addition, further surface functionalization of the existing hydroxyl groups shall be researched to introduce for example cell specific linkers. The oil-soluble PG surfmers were used after successful nanocapsule synthesis for further surface functionalization by thiol-ene reactions. In the future, the surface shall be functionalized with other thiol compounds to increase cell uptake or introduce fluorescence compounds. Furthermore, the water-soluble PGs showed similar properties as SDS and LutensolAT50 to keep the nanocapsule stable after transfer into water.

Redox-responsive non-ionic and non-cytotoxic amphiphilic block copolymers, carrying a hydrophilic PEG block and a hydrophobic polyferrocenyl glycidyl ether

block with ferrocene units in the side chain, were produced by anionic ring-opening polymerization with defined block length ratios and different ferrocene amounts. Due to surface active properties, the amphiphilic block copolymers were used as building blocks for redox-responsive micelle to release hydrophobic dyes. More importantly, they were studied as first non-ionic redox-responsive polymeric surfactant to stabilize polystyrene nanoparticles in water and in saline solutions for several months. After oxidation using acids or oxidation agents, the dispersion destabilized due to the formation of hydrophilic ferrocinium ions, which was afterwards mainly found in the supernatant determined by ICP. Recovery of the surfactant in the supernatant by reduction has to be tested in the future to reduce surfactant waste.

Instead of amphiphilic block copolymers, also homopolymers based on poly(acrylic acid) with pH sensitive triisopropylsilyl protection groups synthesized by RAFT polymerization were tested as stabilizer for polyurea nanocapsules in inverse miniemulsions (Chapter 2.3). Surface active properties were proved by stabilization of formamide droplets in cyclohexane. Consequently, stable polyurea nanocapsules were synthesized with formamide core and transferred into water adding a low amount of a water-soluble surfactant. The use of amphiphilic homopolymers including pH sensitive groups instead of block copolymers could solve the problem of difficult surface functionalization due to the existing hydrophobic block of the surfactants, which is still present after transfer and shielded the surface.

For biomedical application, besides the type of surfactants also the modification of the nanocarrier surface is important to decrease protein adsorption. Therefore, the surface of HES nanocapsules, which even showed decreased protein adsorption properties, was functionalized with glucose, dextran, HES and for comparison with PEG by copper-free click reactions (chapter 2.4). All completely biodegradable carbohydrate nanocapsules as well as the PEGylated nanocapsules aggregated after incubation in citrate plasma due to low amount of protein adsorption on the surface. The protein composition on the different functionalized surfaces was tested by SDS-PAGE and MS and showed similar results for clusterin adsorption, whereat minor differences were discovered for ApoE, ApoA1, ApoA4 and serum albumin. In the future, cell uptake studies of the different nanocapsules have to be investigated and the protein studies shall be compared with densely covered carbohydrate HES nanocapsule surfaces.

For efficient drug release in the body the surface of HES nanocapsules was additionally functionalized with trimannose and mannose, which are known as cell specific linker (chapter 2.5). After surface PEGylation to reduce protein binding and introduction of the strained DBCO groups, the cell specific linkers were introduced by copper-free azide-alkyne reaction. The trimannose and mannose modified nanocapsules can be improved uptake by moDCs, which express the specific receptors, but not by monocytes, which do not express the specific receptors (CD206 and DC-SIGN). However, there is no significant difference of trimannose and mannose modified surfaces. Further studies could be done using less amount of trimannose (one-third) compared to mannose on the nanocapsule surface to exhibit the same amount of mannose-sugars on the surface.

4. Zusammenfassung

In dieser Arbeit wurden unterschiedliche funktionelle Tenside für die Herstellung verschiedener Nanokontainer durch direkte und / oder inverse Miniemulsion hergestellt. Zur Herstellung der amphiphilen Polymere, welche als Tenside verwendet wurden, wurde neben der anionischen Ringöffnungspolymerisation auch die kontrollierte radikalische Polymerisation verwendet. Desweiteren wurden auch die Nanokontainer über ausgewählte Polymerisationsarten wie der freien radikalischen Polymerisation oder Polyaddition hergestellt. Die Charakterisierung der Polymere und Nanokontainer geschah über verschiedene Techniken wie SEC, unterschiedliche Grenzflächenspannungsmessungen, Spektroskopiemessungen sowie Dynamische Lichtstreuung. Zusätzlich wurden bestimmte Nanokontainer in menschlichem Plasma inkubiert und deren Stabilität in der Proteinmischung sowie deren Zellaufnahme untersucht.

Die eingeführten orthogonal geschützten Polyglycerin Blockcopolymere in Kapitel 2.1 wurden über anionische Ringöffnungspolymerisation synthetisiert, wobei EEGE und AGE oder *t*BuGE als Monomere eingesetzt wurden. Dadurch konnten Polymere mit definiertem Blocklängenverhältnis, definiertem Molekulargewicht und enger Molekulargewichtsverteilung hergestellt werden. Nach Abspaltung der Acetalschutzgruppen, wurden die amphiphilen Blockcopolymere mit grenzflächenaktiven Eigenschaften als Tenside oder Surfmere, durch Einbau der Allyl- oder Hydroxylgruppen, in direkter oder inverser Miniemulsion verwendet. Somit wurden mit Hilfe der Tenside stabile PS Nanopartikeln, Polyurethan Nanokapseln oder PHEMA und PAA Nanopartikeln hergestellt. Da Polyglycerin proteinabweisende Eigenschaften aufweist, wurde die Stabilität der synthetisierten Polystyrol Nanopartikel in menschlichem Plasma untersucht. Allerdings, konnte sowohl bei den Polystyrol Nanopartikel stabilisiert mit den adsorbierten als auch mit den kovalent gebundenen Tensiden neben einzelnen stabilen Nanopartikeln auch leichte Aggregation festgestellt werden. Dennoch scheinen die hergestellten Tenside als Stealth Tenside oder Surfmere geeignet zu sein. In der Zukunft, sollen daher noch weitere Stabilitätsuntersuchungen in Plasma gemacht sowie die Menge und Art der adsorbierten Proteinen untersucht werden. Außerdem, sollen Zellaufnahmen gemacht werden. Die durch Polyaddition hergestellten HES Nanokapseln in inverser

Miniemulsion wurden nach dem Transfer in Wasser, durch ein wasserlösliches hergestelltes Polyglycerin Tensid, mittels Thiol-Ene Reaktion an der Oberfläche modifiziert. Dies war möglich durch den Einbau des Surfmers während der Nanokapselsynthese, wobei ein großer Teil der Allylgruppen dann auf der Oberfläche zu finden sein sollte. Auch hier wird in Zukunft die Synthese optimiert und weitere Thiolkomponenten eingeführt.

Neben den multifunktionellen Polyglycerin Blockcopolymeren wurden in dieser Arbeit nichtionische redox-schaltbare ferrocenhaltige Blockcopolymere zur Stabilisierung von Polystyrol Nanopartikeln in Wasser und Salzlösungen untersucht (Kapitel 2.2). Die diversen Ferrocenegruppen in den Seitenketten des hydrophoben Blocks wurden durch Oxidation mit Säuren oder Oxidationsmitteln zu Ferroceniumionen oxidiert, wodurch ein komplett wasserlösliches Polymer entstand. Dies führte zur Destabilisierung der Nanopartikel. Zukünftig soll die Reduktion der Ferrocengruppen untersucht werden um die Tenside erneut einzusetzen. Dadurch soll die Herstellung von Abfall verringert werden und ein nach Bedarf komplett schaltbares Tensid erhalten werden. Neben dem Einsatz als redox-labile Tensid, konnten diese über anionische Ringöffnung hergestellten ungiftigen Blockcopolymere auch als redox-sensitive Mizellen verwendet werden. Ein hydrophober eingekapselter Farbstoff wurde nach Oxidation der Ferrocengruppen freigesetzt.

Statt dem Einsatz von amphiphilen Blockcopolymeren als Tenside in inversen Miniemulsionen wurde in dieser Arbeit die Verwendung eines Homopolymers als Tensid untersucht (Kapitel 2.3). Über RAFT Polymerization von Triisopropylsilylacrylat wurde ein pH-sensitives Homopolymer synthetisiert. Nach Ermittlung der grenzflächenaktiven Eigenschaften, wurde diese als Tensid in der inversen Miniemulsion zur Herstellung von stabilen Polyharnstoffnanokapseln in Cyclohexan eingesetzt. Der Transfer in Wasser war möglich durch eine geringe Menge SDS, um die Nanokapseln in Wasser stabil zu halten. Durch die Verwendung eines pH-labilen Homopolymers könnte die Oberfläche der Nanokapsel weniger stark abgeschirmt sein, da es nach Abspaltung der Schutzgruppe zu weniger hydrophoben Wechselwirkungen zwischen dem Tensid und der hydrophoben Kapseloberfläche kommen kann. Daher ist die Oberfläche für weitere Funktionalisierung besser zugänglich, was in Zukunft untersucht werden soll.

Für biomedizinische Anwendungen der Nanokontainer ist neben deren Herstellung mit möglichst ungiftigen Tensiden auch die Art der Oberflächenfunktionalisierung von Bedeutung. Durch Inkubation in proteinhaltige Lösungen werden oft unterschiedliche Proteine auf den hydrophoben Oberflächen adsorbiert. Deshalb werden häufig proteinabweisende Hüllen auf Oberflächen angebracht. In dieser Arbeit wurde die HES Nanokapseloberfläche mit Glucose, Dextran, HES und zum Vergleich mit PEG, welches oft zur Verringerung der Proteinadsorption verwendet wird, über kupferfreie Klickchemie funktionalisiert (Kapitel 2.4). Anschließend wurde die Adsorption von Proteinen an der Oberfläche mittels SDS-PAGE und MS untersucht und untereinander verglichen. Geringe Unterschiede wurden in der adsorbierten Menge und der Proteinzusammensetzung in Bezug auf ApoE, ApoA1, ApoA4 und Serumalbumin festgestellt. Somit weisen auch komplett biokompatible und kohlenhydrathaltige Nanokapseln ähnliche Eigenschaften wie PEGylierte Nanokapseln in Bezug auf Proteinadsorption auf und sind in Zukunft vielleicht in biomedizinische Anwendungen einsetzbar. In weiteren Untersuchungen soll daher die adsorbierte Zuckermenge erhöht werden, die Analysen wiederholt werden und außerdem Zellaufnahmeuntersuchungen gemacht werden.

Um den eingekapselten Wirkstoff in Nanokapseln in gezielten Organen freizusetzen, ist es weiterhin notwendig neben einer proteinabweisenden Oberfläche auch eine zellspezifische Adressierung anzubringen. Dafür wurde die PEGylierte HES Nanokapseloberfläche mit einem Trimannose oder Mannose Linker über kupferfreie Klickchemie modifiziert (Kapitel 2.5). Nach Inkubation in Plasma, konnte eine bessere Zellaufnahme beider Nanokapseln in moDCs, welche den spezifischen Rezeptor besitzen, festgestellt werden. Die Aufnahme in Monozyten, welche den spezifischen Rezeptor nicht aufweisen, fand wie erwartend nicht statt. Somit scheint es keinen Unterschied zu machen, ob die Nanokapseln mit Trimannose oder Mannose als zellspezifische Erkennung modifiziert sind. In zukünftigen Untersuchungen soll die Oberfläche der HES Nanokapseln nur mit einem Drittel Trimannose im Vergleich zu Mannose funktionalisiert und die Zellaufnahmen erneut untersucht werden, um die Annahme zu bestätigen.

5. Literature

- [1] B. Fabry, *Fett Wiss Technol* **1990**, 92, 287-291.
- [2] B. Fabry, *Chem Unserer Zeit* **1991**, 25, 214-222.
- [3] K. Hill, O. Rhode, *Lipid/ Fett* **1999**, 101, 25-33.
- [4] L. L. Schramm, E. N. Stasiuk, D. G. Marangoni, *Annu Rep Prog Chem, Sect C:Phys Chem* **2003**, 99, 3-48.
- [5] S. Warwel, F. Bruse, C. Demes, M. Kunz, M. R. G. Klaas, *Chemosphere* **2001**, 43, 39-48.
- [6] S. Warwel, M. R. G. Klaas, H. Schier, F. Burse, B. Wiege, *Eur J Lipid Sci Tech* **2001**, 103, 645-654.
- [7] F. Goursaud, M. Berchel, J. Guilbot, N. Legros, L. Lemiegre, J. Marcilloux, D. Plusquellec, T. Benvegnu, *Green Chem* **2008**, 10, 310-320.
- [8] H. Maag, *J Am Oil Chem Soc* **1984**, 61, 259-267.
- [9] K. Holmberg, *Curr Opin Colloid In* **2001**, 6, 148-159.
- [10] I. Johansson, M. Svensson, *Curr Opin Colloid In* **2001**, 6, 178-188.
- [11] Y. X. Liu, P. G. Jessop, M. Cunningham, C. A. Eckert, C. L. Liotta, *Science* **2006**, 313, 958-960.
- [12] P. Brown, C. P. Butts, J. Eastoe, *Soft Matter* **2013**, 9, 2365-2374.
- [13] X. Liu, N. L. Abbott, *J Colloid Interface Sci* **2009**, 339, 1-18.
- [14] R. Dorresteyn, N. Billecke, S. H. Parekh, M. Klapper, K. Mullen, *J. Polym. Sci. Pol. Chem.* **2015**, 53, 200-205.
- [15] W. Meier, *Chem Soc Rev* **2000**, 29, 295-303.
- [16] S. Schöttler, K. Landfester, V. Mailander, *Angew Chem Int Ed Engl* **2016**, 55, 8806-8815.
- [17] B. Kang, P. Okwieka, S. Schöttler, O. Seifert, R. E. Kontermann, K. Pfizenmaier, A. Musyanovych, R. Meyer, M. Diken, U. Sahin, V. Mailander, F. R. Wurm, K. Landfester, *Biomaterials* **2015**, 49, 125-134.
- [18] S. Schöttler, G. Becker, S. Winzen, T. Steinbach, K. Mohr, K. Landfester, V. Mailänder, F. R. Wurm, *Nat Nano* **2016**, 11, 372-377.
- [19] Z. Amoozgar, Y. Yeo, *Wiley Interdiscip Rev Nanomed Nanobiotechnol* **2012**, 4, 219-233.
- [20] T. Basinska, S. Slomkowski, A. Dworak, I. Panchev, M. M. Chehimi, *Colloid Polym Sci* **2001**, 279, 916-924.
- [21] T. Basinska, S. Slomkowski, S. Kazmierski, A. Dworak, M. M. Chehimi, *J Polym Sci Pol Chem* **2004**, 42, 615-623.
- [22] B. Kang, P. Okwieka, S. Schöttler, S. Winzen, J. Langhanki, K. Mohr, T. Opatz, V. Mailander, K. Landfester, F. R. Wurm, *Angew Chem Int Edit* **2015**, 54, 7436-7440.
- [23] G. Baier, D. Baumann, J. M. Siebert, A. Musyanovych, V. Mailander, K. Landfester, *Biomacromolecules* **2012**, 13, 2704-2715.
- [24] K. L. White, T. Rades, R. H. Furneaux, P. C. Tyler, S. Hook, *J Pharm Pharmacol* **2006**, 58, 729-737.
- [25] A.-C. Bijlard, S. Wald, D. Crespy, A. Taden, F. R. Wurm, K. Landfester, *Adv Mater Interfaces* **2016**, 1600443.
- [26] E. R. Smulders, W.; Sung, E.; Rähse, W.; Steber, J.; Wiebel, F.; Nordskog, A., *Ullmann's Encyclopedia of Industrial Chemistry* **2007**, 1-184.

-
- [27] L. A. T. W. Asri, M. Crismaru, S. Roest, Y. Chen, O. Ivashenko, P. Rudolf, J. C. Tiller, H. C. van der Mei, T. J. A. Loontjens, H. J. Busscher, *Adv Funct Mater* **2014**, *24*, 346-355.
- [28] F. Siedenbiedel, J. C. Tiller, *Polymers-Basel* **2012**, *4*, 46-71.
- [29] J. C. Tiller, *Adv Polym Sci* **2011**, *240*, 193-217.
- [30] R. P. Moraes, R. A. Hutchinson, T. F. L. McKenna, *J Polym Sci Pol Chem* **2010**, *48*, 48-54.
- [31] A. Dundua, K. Landfester, A. Taden, *Polymer* **2014**, *55*, 3543-3550.
- [32] K. Hill, O. Rhode, *Fett-Lipid* **1999**, *101*, 25-33.
- [33] A. Guyot, *Adv Colloid Interfac* **2004**, *108*, 3-22.
- [34] K. Holmberg, *Prog Org Coat* **1992**, *20*, 325-337.
- [35] A. Guyot, *Curr Opin Colloid In* **1996**, *1*, 580-586.
- [36] W. C. Griffin, *J Cosmet Sci* **1949**, *1*, 311-326.
- [37] C. Dingels, M. Schomer, H. Frey, *Chem Unserer Zeit* **2011**, *45*, 338-349.
- [38] E. J. Routledge, J. P. Sumpter, *Environ Toxicol Chem* **1996**, *15*, 241-248.
- [39] C. Sonnenschein, A. M. Soto, *J Steroid Biochem* **1998**, *65*, 143-150.
- [40] G. H. Yao, Y. Y. Hou, *Environ Toxicol Phar* **2004**, *17*, 19-27.
- [41] S. Hocine, M. H. Li, *Soft Matter* **2013**, *9*, 5839-5861.
- [42] J. K. Weil, R. G. Bistline, A. J. Stirton, *J Phys Chem-Us* **1958**, *62*, 1083-1085.
- [43] R. G. Bistline, A. J. Stirton, J. K. Weil, E. W. Maurer, *J Am Oil Chem Soc* **1957**, *34*, 516-518.
- [44] L. Breucker, K. Landfester, A. Taden, *Acs Appl Mater Inter* **2015**, *7*, 24641-24648.
- [45] D. Crespy, A. Musyanovych, K. Landfester, *Colloid Polym Sci* **2006**, *284*, 780-787.
- [46] B. Müller, W. Rath, *Formulierung von Kleb- und Dichtstoffen: das kompetente Lehrbuch für Studium und Praxis*, Vol. 2, Vincentz network, **2009**.
- [47] H. Thiele, H. S. von Lavern, *J Colloid Interf Sci* **1965**, *20*, 679-694.
- [48] C. A. Oksanen, G. Zografi, *Pharmaceut Res* **1990**, *7*, 654-657.
- [49] C. Sawaryn, K. Landfester, A. Taden, *Macromolecules* **2011**, *44*, 5650-5658.
- [50] K. Chiou, P. Froimowicz, K. Landfester, A. Taden, H. Ishida, *Macromolecules* **2014**, *47*, 3297-3305.
- [51] E. Bouyer, G. Mekhloufi, V. Rosilio, J. L. Grossiord, F. Agnely, *Int J Pharmaceut* **2012**, *436*, 359-378.
- [52] P. Raffa, D. A. Z. Wever, F. Picchioni, A. A. Broekhuis, *Chem Rev* **2015**, *115*, 8504-8563.
- [53] M. Manguian, M. Save, C. Chassenieux, B. Charleux, *Colloid Polym Sci* **2005**, *284*, 142-150.
- [54] S. George, R. Champagne-Hartley, G. Deeter, D. Campbell, B. Reck, D. Urban, M. Cunningham, *Macromolecules* **2015**, *48*, 8913-8920.
- [55] A. Guyot, K. Tauer, in *Polymer Synthesis*, Springer Berlin Heidelberg, **1994**, pp. 43-65.
- [56] A. Guyot, *Macromol Symp* **2002**, *179*, 105-132.
- [57] J. M. Asua, H. A. S. Schoonbrood, *Acta Polym* **1998**, *49*, 671-686.
- [58] H. A. S. Schoonbrood, M. J. Unzué, O.-J. Beck, J. M. Asua, A. M. Goñi, D. C. Sherrington, *Macromolecules* **1997**, *30*, 6024-6033.
- [59] M. J. Unzué, H. A. S. Schoonbrood, J. M. Asua, A. M. Goñi, D. C. Sherrington, K. Stähler, K.-H. Goebel, K. Tauer, M. Sjöberg, K. Holmberg, *J Appl Polym Sci* **1997**, *66*, 1803-1820.

-
- [60] F. Stoffelbach, B. Belardi, J. M. Santos, L. Tessier, K. Matyjaszewski, B. Charleux, *Macromolecules* **2007**, *40*, 8813-8816.
- [61] B. T. Pham, D. Nguyen, C. J. Ferguson, B. S. Hawkett, A. K. Serelis, C. H. Such, *Macromolecules* **2003**, *36*, 8907-8909.
- [62] Y. Luo, H. Gu, *Macromol Rapid Comm* **2006**, *27*, 21-25.
- [63] P. Ni, M. Zhang, L. Ma, S. Fu, *Langmuir* **2006**, *22*, 6016-6023.
- [64] M. Herold, H. Brunner, G. E. Tovar, *Macromol Chem Physic* **2003**, *204*, 770-778.
- [65] K. L. Thompson, S. Armes, J. Howse, S. Ebbens, I. Ahmad, J. Zaidi, D. York, J. Burdis, *Macromolecules* **2010**, *43*, 10466-10474.
- [66] W. Li, J. A. Yoon, K. Matyjaszewski, *J Am Chem Soc* **2010**, *132*, 7823-7825.
- [67] G. Baier, K. Friedemann, E.-M. Leuschner, A. Musyanovych, K. Landfester, *Macromol Symp* **2013**, *331-332*, 71-80.
- [68] E.-M. Rosenbauer, K. Landfester, A. Musyanovych, *Langmuir* **2009**, *25*, 12084-12091.
- [69] P. Chambon, E. Cloutet, H. Cramail, *Macromolecules* **2004**, *37*, 5856-5859.
- [70] A.-C. Bijlard, S. Winzen, K. Itoh, K. Landfester, A. Taden, *ACS Macro Letters* **2014**, *3*, 1165-1168.
- [71] Y. Dong, Y. Jin, D. Wei, *Polym Int* **2007**, *56*, 14-21.
- [72] H. Naghash, R. Akhtarian, M. Iravani, *Korean J Chem Eng* **2014**, *31*, 1281-1287.
- [73] T. Liu, Z. Li, Q. Wu, X. Ma, *Polym Bull* **2010**, *64*, 511-521.
- [74] S. E. Shim, H. Jung, K. Lee, J. M. Lee, S. Choe, *J Colloid Interf Sci* **2004**, *279*, 464-470.
- [75] S. Klein, V. Manoharan, D. Pine, F. Lange, *Colloid Polym Sci* **2003**, *282*, 7-13.
- [76] C. Racles, M. Cazacu, G. Hitruc, T. Hamaide, *Colloid Polym Sci* **2009**, *287*, 461-470.
- [77] H. Wang, J. Zou, Y. Shen, G. Fei, J. Mou, *J Appl Polym Sci* **2013**, *130*, 1855-1862.
- [78] Z. Jiang, X. Li, G. Yang, L. Cheng, B. Cai, Y. Yang, J. Dong, *Langmuir* **2012**, *28*, 7174-7181.
- [79] J. Zataray, A. Aguirre, J. de la Cal, J. Leiza, *Macromol Symp* **2013**, *333*, 80-92.
- [80] B. Brugger, W. Richtering, *Langmuir* **2008**, *24*, 7769-7777.
- [81] A. Darabi, A. R. Shirin-Abadi, J. Pinaud, P. G. Jessop, M. F. Cunningham, *Polym Chem* **2014**, *5*, 6163-6170.
- [82] A. Darabi, P. G. Jessop, M. F. Cunningham, *Macromolecules* **2015**, *48*, 1952-1958.
- [83] J. Huang, J. Xu, K. Chen, T. Wang, C. Cui, X. Wei, R. Zhang, L. Li, X. Guo, *Ind Eng Chem Res* **2015**, *54*, 1564-1575.
- [84] F. Wang, Y. Luo, B.-G. Li, S. Zhu, *Macromolecules* **2015**, *48*, 1313-1319.
- [85] P. Perrin, I. Porcar, C. Tribet, *Polym Int* **2003**, *52*, 465-470.
- [86] Q. J. Chen, X. T. Cao, H. Liu, W. Zhou, L. J. Qin, Z. S. An, *Polym Chem* **2013**, *4*, 4092-4102.
- [87] D. Dupin, J. R. Howse, S. P. Armes, D. P. Randall, *J Mater Chem* **2008**, *18*, 545-552.
- [88] A. J. Morse, D. Dupin, K. L. Thompson, S. P. Armes, K. Ouzineb, P. Mills, R. Swart, *Langmuir* **2012**, *28*, 11742-11753.

-
- [89] A. Morse, S. Armes, K. Thompson, D. Dupin, L. Fielding, P. Mills, R. Swart, *Langmuir* **2013**, 29, 5466-5475.
- [90] C. Yi, N. Liu, J. Zheng, J. Jiang, X. Liu, *J Colloid Interf Sci* **2012**, 380, 90-98.
- [91] S. Fujii, D. P. Randall, S. P. Armes, *Langmuir* **2004**, 20, 11329-11335.
- [92] C. Zhao, J. Tan, W. Li, K. Tong, J. Xu, D. Sun, *Langmuir* **2013**, 29, 14421-14428.
- [93] Y. Wei, J. Chen, Y. Zhang, Z. Lu, *RSC Advances* **2015**, 5, 71824-71829.
- [94] Z. Wei, C. Wang, S. Zou, H. Liu, Z. Tong, *Colloid Surface A* **2011**, 392, 116-123.
- [95] Z. Wei, C. Wang, S. Zou, H. Liu, Z. Tong, *Polymer* **2012**, 53, 1229-1235.
- [96] C. Yi, J. Sun, D. Zhao, Q. Hu, X. Liu, M. Jiang, *Langmuir* **2014**, 30, 6669-6677.
- [97] K. Fuhrmann, A. Polomska, C. Aeberli, B. Castagner, M. A. Gauthier, J.-C. Leroux, *ACS Nano* **2013**, 7, 8243-8250.
- [98] J. Yin, S. Shi, J. Hu, S. Liu, *Langmuir* **2014**, 30, 9551-9559.
- [99] S. Lee, J. H. Nam, Y. J. Kim, Y. J. Cho, N. H. Kwon, J. Y. Lee, H.-J. Kang, H. T. Kim, H. M. Park, S. Kim, *Macromol Res* **2011**, 19, 827-834.
- [100] K. Kim, T. H. Kim, J. H. Choi, J. Y. Lee, S. S. Hah, H. O. Yoo, S. S. Hwang, K. N. Ryu, H. J. Kim, J. Kim, *Macromol Chem Physic* **2010**, 211, 1127-1136.
- [101] J. Amalvy, G.-F. Unali, Y. Li, S. Granger-Bevan, S. Armes, B. P. Binks, J. Rodrigues, C. P. Whitby, *Langmuir* **2004**, 20, 4345-4354.
- [102] J. V. M. Weaver, S. P. Rannard, A. I. Cooper, *Angew Chem* **2009**, 121, 2165-2168.
- [103] E. Marie, K. Landfester, M. Antonietti, *Biomacromolecules* **2002**, 3, 475-481.
- [104] Y. Wang, X. Zhang, Y. Han, C. Cheng, C. Li, *Carbohydr Polym* **2012**, 89, 124-131.
- [105] D. Dupin, S. P. Armes, C. Connan, P. Reeve, S. M. Baxter, *Langmuir* **2007**, 23, 6903-6910.
- [106] G. R. Deen, L. Gan, Y. Gan, *Polymer* **2004**, 45, 5483-5490.
- [107] G. R. Deen, L. Gan, *J Polym Sci Pol Chem* **2009**, 47, 2059-2072.
- [108] S. Fujii, M. Mochizuki, K. Aono, S. Hamasaki, R. Murakami, Y. Nakamura, *Langmuir* **2011**, 27, 12902-12909.
- [109] S. Fujii, K. Aono, M. Suzuki, S. Hamasaki, S.-i. Yusa, Y. Nakamura, *Macromolecules* **2012**, 45, 2863-2873.
- [110] S. Fujii, K. Akiyama, S. Nakayama, S. Hamasaki, S.-i. Yusa, Y. Nakamura, *Soft Matter* **2015**, 11, 572-579.
- [111] L.-H. Lin, K.-M. Chen, *Colloid Surface A* **2006**, 275, 99-106.
- [112] K. Dan, R. Pan, S. Ghosh, *Langmuir* **2011**, 27, 612-617.
- [113] C.-K. Chen, Q. Wang, C. H. Jones, Y. Yu, H. Zhang, W.-C. Law, C. K. Lai, Q. Zeng, P. N. Prasad, B. A. Pfeifer, C. Cheng, *Langmuir* **2014**, 30, 4111-4119.
- [114] X. Liu, N. L. Abbott, *J Colloid Interf Sci* **2009**, 339, 1-18.
- [115] A. Alkan, C. Steinmetz, K. Landfester, F. R. Wurm, *ACS Applied Materials & Interfaces* **2015**, 7, 26137-26144.
- [116] M. Zhang, P. A. Rugar, C. Feng, K. Lin, D. J. Lunn, A. Oliver, A. Nunns, G. R. Whittell, I. Manners, M. A. Winnik, *Macromolecules* **2013**, 46, 1296-1304.
- [117] A. Natalello, A. Alkan, A. Friedel, I. Lieberwirth, H. Frey, F. R. Wurm, *ACS Macro Letters* **2013**, 2, 313-316.
- [118] M. Susan, K. Tani, M. Watanabe, *Colloid Polym Sci* **1999**, 277, 1125-1133.

-
- [119] E. A. Zaragoza-Contreras, M. Stockton-Leal, C. A. Hernández-Escobar, Y. Hoshina, J. F. Guzmán-Lozano, T. Kobayashi, *J Colloid Interf Sci* **2012**, *377*, 231-236.
- [120] L.-P. Lv, Y. Zhao, K. Landfester, D. Crespy, *Polym Chem* **2015**, *6*, 5596-5601.
- [121] A. Durand, E. Marie, *Adv Colloid Interfac* **2009**, *150*, 90-105.
- [122] W. von Rybinski, K. Hill, *Angew Chem Int Ed* **1998**, *37*, 1328-1345.
- [123] S. Warwel, F. Brüse, C. Demes, M. Kunz, M. R. g. Klaas, *Chemosphere* **2001**, *43*, 39-48.
- [124] A. Szűts, P. Szabó-Révész, *Int J Pharmaceut* **2012**, *433*, 1-9.
- [125] H. Laroui, L. Grossin, M. Léonard, J.-F. Stoltz, P. Gillet, P. Netter, E. Dellacherie, *Biomacromolecules* **2007**, *8*, 3879-3885.
- [126] G. Morral-Ruiz, P. Melgar-Lesmes, M. L. García, C. Solans, M. J. García-Celma, *Int J Pharmaceut* **2014**, *461*, 1-13.
- [127] M. T. Calejo, A. M. S. Cardoso, E. F. Marques, M. J. Araújo, A.-L. Kjøniksen, S. A. Sande, M. C. P. de Lima, A. S. Jurado, B. Nyström, *Colloid Surface B* **2013**, *102*, 682-686.
- [128] L. Pérez, A. Pinazo, M. Teresa García, M. Lozano, A. Manresa, M. Angelet, M. Pilar Vinardell, M. Mitjans, R. Pons, M. Rosa Infante, *Eur J Med Chem* **2009**, *44*, 1884-1892.
- [129] A. Colomer, A. Pinazo, M. A. Manresa, M. P. Vinardell, M. Mitjans, M. R. Infante, L. Pérez, *J Med Chem* **2011**, *54*, 989-1002.
- [130] D. R. Nogueira, M. Mitjans, M. A. Busquets, L. Pérez, M. P. Vinardell, *Langmuir* **2012**, *28*, 11687-11698.
- [131] X.-L. Wang, S. Ramusovic, T. Nguyen, Z.-R. Lu, *Bioconjugate Chem* **2007**, *18*, 2169-2177.
- [132] N. Alemdar, A. T. Erciyes, N. Bicak, *Polymer* **2010**, *51*, 5044-5050.
- [133] Y. Liu, K. Deng, S. Wang, M. Xiao, D. Han, Y. Meng, *Polym Chem* **2015**, *6*, 2076-2083.
- [134] X. Cui, C. Qiao, S. Wang, Y. Ding, C. Hao, J. Li, *Colloid Polym Sci* **2015**, *293*, 1971-1981.
- [135] M. Yan, J. J. Du, Z. Gu, M. Liang, Y. F. Hu, W. J. Zhang, S. Priceman, L. L. Wu, Z. H. Zhou, Z. Liu, T. Segura, Y. Tang, Y. F. Lu, *Nat. Nanotechnol.* **2010**, *5*, 48-53.
- [136] T. Y. Liu, K. H. Liu, D. M. Liu, S. Y. Chen, I. W. Chen, *Adv Funct Mater* **2009**, *19*, 616-623.
- [137] C. E. Mora-Huertas, H. Fessi, A. Elaissari, *Int J Pharm* **2010**, *385*, 113-142.
- [138] A. Musyanovych, K. Landfester, *Macromol Biosci* **2014**, *14*, 458-477.
- [139] B. Carletto, J. Berton, T. N. Ferreira, L. F. Dalmolin, K. S. Paludo, R. M. Mainardes, P. V. Farago, G. M. Favero, *Colloid Surface B* **2016**, *144*, 65-72.
- [140] N. Jagielski, S. Sharma, V. Hombach, V. Mailander, V. Rasche, K. Landfester, *Macromol Chem Phys* **2007**, *208*, 2229-2241.
- [141] E. Pisani, N. Tsapis, B. Galaz, M. Santin, R. Berti, N. Taulier, E. Kurtisovski, O. Lucidarme, M. Ourevitch, B. T. Doan, J. C. Beloeil, B. Gillet, W. Urbach, S. L. Bridal, E. Fattal, *Adv Funct Mater* **2008**, *18*, 2963-2971.
- [142] F. Maia, A. P. Silva, S. Fernandes, A. Cunha, A. Almeida, J. Tedim, M. L. Zheludkevich, M. G. S. Ferreira, *Chem Eng J* **2015**, *270*, 150-157.
- [143] J. Fickert, M. Makowski, M. Kappl, K. Landfester, D. Crespy, *Macromolecules* **2012**, *45*, 6324-6332.
- [144] Y. Zhao, J. Fickert, K. Landfester, D. Crespy, *Small* **2012**, *8*, 2954-2958.

-
- [145] J. Fickert, P. Rupper, R. Graf, K. Landfester, D. Crespy, *J Mater Chem* **2012**, 22, 2286-2291.
- [146] J. Fickert, C. Wohnhaas, A. Turshatov, K. Landfester, D. Crespy, *Macromolecules* **2013**, 46, 573-579.
- [147] L.-P. Lv, Y. Zhao, N. Vilbrandt, M. Gallei, A. Vimalanandan, M. Rohwerder, K. Landfester, D. Crespy, *J Am Chem Soc* **2013**, 135, 14198-14205.
- [148] H. Y. Huang, E. E. Remsen, T. Kowalewski, K. L. Wooley, *J Am Chem Soc* **1999**, 121, 3805-3806.
- [149] H. T. Sun, C. K. Chen, H. G. Cui, C. Cheng, *Polym Int* **2016**, 65, 351-361.
- [150] F. Caruso, M. Spasova, V. Saigueirino-Maceira, L. M. Liz-Marzan, *Adv Mater* **2001**, 13, 1090-1094.
- [151] F. Caruso, *Adv Mater* **2001**, 13, 11-22.
- [152] M. K. Park, C. J. Xia, R. C. Advincula, P. Schutz, F. Caruso, *Langmuir* **2001**, 17, 7670-7674.
- [153] R. Xinyu, X. Yinghua, H. Xiaomei, C. Tao, W. Yingming, L. Yuanyuan, *Curr Drug Discov Technol* **2011**, 8, 173-187.
- [154] S. S. Huang, Y. Y. Chen, B. Liu, F. He, P. A. Ma, X. R. Deng, Z. Y. Cheng, J. Lin, *J Solid State Chem* **2015**, 229, 322-329.
- [155] U. Paiphansiri, P. Tangboriboonrat, K. Landfester, *Macromol Biosci* **2006**, 6, 33-40.
- [156] C. E. Mora-Huertas, O. Garrigues, H. Fessi, A. Elaissari, *Eur J Pharm Biopharm* **2012**, 80, 235-239.
- [157] R. H. Staff, K. Landfester, D. Crespy, *Adv Polym Sci* **2013**, 262, 329-344.
- [158] R. Alvarez-Roman, G. Barre, R. H. Guy, H. Fessi, *Eur J Pharm Biopharm* **2001**, 52, 191-195.
- [159] D. Crespy, K. Landfester, *Macromol Chem Physic* **2007**, 208, 457-466.
- [160] F. Tiarks, K. Landfester, M. Antonietti, *Langmuir* **2001**, 17, 908-918.
- [161] Y. W. Luo, X. D. Zhou, *J. Polym. Sci. Poly. Chem.* **2004**, 42, 2145-2154.
- [162] M. Bathfield, C. Graillat, T. Hamaide, *Macromol. Chem. Physic.* **2005**, 206, 2284-2291.
- [163] D. Crespy, M. Stark, C. Hoffmann-Richter, U. Ziener, K. Landfester, *Macromolecules* **2007**, 40, 3122-3135.
- [164] H. D. Koh, J. S. Lee, *Macromol. Rapid Comm.* **2007**, 28, 315-321.
- [165] D. Crespy, A. Musyanovych, K. Landfester, *Colloid Polym. Sci.* **2006**, 284, 780-787.
- [166] J. M. Asua, *Prog Polym Sci* **2002**, 27, 1283-1346.
- [167] K. Landfester, V. Mailänder, *Expert Opin Drug Del* **2013**, 10, 593-609.
- [168] K. Landfester, *Angew Chem Int Edit* **2009**, 48, 4488-4507.
- [169] F. Gaudin, N. Sintès-Zydowicz, *Colloids and Surfaces A: Physicochemical and Engineering Aspects* **2011**, Volume 384, 698-712.
- [170] F. Ganachaud, J. L. Katz, *Chemphyschem* **2005**, 6, 209-216.
- [171] F. J. Schork, G. W. Poehlein, S. Wang, J. Reimers, J. Rodrigues, C. Samer, *Colloid Surface A* **1999**, 153, 39-45.
- [172] K. Landfester, *Annu. Rev. Mater. Res.* **2006**, 36, 231-279.
- [173] W. W. Li, J. A. Yoon, K. Matyjaszewski, *J. Am. Chem. Soc.* **2010**, 132, 7823-7825.
- [174] M. Antonietti, K. Landfester, *Prog. Polym. Sci.* **2002**, 27, 689-757.
- [175] M. Antonietti, R. Basten, S. Lohmann, *Macromol Chem Physic* **1995**, 196, 441-466.

-
- [176] K. Landfester, *Macromol Symp* **2000**, 150, 171-178.
- [177] K. Landfester, N. Bechthold, F. Tiarks, M. Antonietti, *Macromolecules* **1999**, 32, 2679-2683.
- [178] W. C. Griffin, *J Cosmet Sci* **1954**, 5, 249-256.
- [179] J. Delgado, M. S. Elaasser, C. A. Silebi, J. W. Vanderhoff, *Abstr Pap Am Chem S* **1986**, 191, 107-Pmse.
- [180] Y. T. Choi, M. S. Elaasser, E. D. Sudol, J. W. Vanderhoff, *J Polym Sci Pol Chem* **1985**, 23, 2973-2987.
- [181] J. Ugelstad, M. S. Elaasser, Vanderho.Jw, *J Polym Sci Pol Lett* **1973**, 11, 503-513.
- [182] D. Mouran, J. Reimers, F. J. Schork, *J Polym Sci Pol Chem* **1996**, 34, 1073-1081.
- [183] C. S. Chern, T. J. Chen, *Colloid Polym Sci* **1997**, 275, 546-554.
- [184] A. P. Romio, C. Sayer, P. H. H. Araujo, M. Al-Haydari, L. B. Wu, S. R. P. da Rocha, *Macromol Chem Physic* **2009**, 210, 747-751.
- [185] S. Behzadi, C. Rosenauer, M. Kappl, K. Mohr, K. Landfester, D. Crespy, *Nanoscale* **2016**, 8, 12998-13005.
- [186] K. Landfester, N. Bechthold, S. Forster, M. Antonietti, *Macromol Rapid Comm* **1999**, 20, 81-84.
- [187] A. Musyanovych, K. Landfester, in *Surface and Interfacial Forces - From Fundamentals to Applications* (Eds.: G. K. Auernhammer, H.-J. Butt, D. Vollmer), Springer, Berlin, **2008**, pp. 120 - 127.
- [188] K. Katta, D. Busko, Y. Avlasevich, R. Munoz-Espi, S. Balushev, K. Landfester, *Macromol Rapid Comm* **2015**, 36, 1084-1088.
- [189] F. Chouinard, F. W. K. Kan, J. C. Leroux, C. Foucher, V. Lenaerts, *Int J Pharm* **1991**, 72, 211-217.
- [190] I. Hofmeister, K. Landfester, A. Taden, *Macromolecules* **2014**, 47, 5768-5773.
- [191] Z. H. Cao, G. R. Shan, N. Sheibat-Othman, J. L. Putaux, E. Bourgeat-Lami, *J Polym Sci A1* **2010**, 48, 593-603.
- [192] C. Scott, D. Wu, C.-C. Ho, C. C. Co, *J Am Chem Soc* **2005**, 127, 4160-4161.
- [193] L. Wu, T. Pang, Y. B. Guan, *Chinese J Polym Sci* **2016**, 34, 523-531.
- [194] B. Huang, S. X. Zhou, M. Chen, L. M. Wu, *Macromolecules* **2014**, 47, 1914-1921.
- [195] K. F. Ni, G. R. Shan, Z. X. Weng, *Macromolecules* **2006**, 39, 2529-2535.
- [196] D. Sarkar, J. El-Khoury, S. T. Lopina, J. Hu, *Macromolecules* **2005**, 38, 8603-8605.
- [197] D. Wu, C. Scott, C.-C. Ho, C. C. Co, *Macromolecules* **2006**, 39, 5848-5853.
- [198] R. H. Utama, M. Drechsler, S. Forster, P. B. Zetterlund, M. H. Stenzel, *Acs Macro Letters* **2014**, 3, 935-939.
- [199] K. Landfester, M. Willert, M. Antonietti, *Macromolecules* **2000**, 33, 2370-2376.
- [200] N. Anton, J. P. Benoit, P. Saulnier, *J Control Release* **2008**, 128, 185-199.
- [201] I. Montasser, H. Fessi, S. Briancon, J. Lieto, *Polym Bull* **2003**, 50, 169-174.
- [202] K. Bouchemal, S. Briancon, E. Perrier, H. Fessi, I. Bonnet, N. Zydowicz, *Int J Pharm* **2004**, 269, 89-100.
- [203] R. Vecchione, G. Luciani, V. Calcagno, A. Jakhmola, B. Silvestri, D. Guarnieri, V. Belli, A. Costantini, P. A. Netti, *Nanoscale* **2016**, 8, 8798-8809.
- [204] A. Jakhmola, R. Vecchione, D. Guarnieri, V. Belli, D. Calabria, P. A. Netti, *Adv Healthc Mater* **2015**, 4, 2688-2698.
- [205] L. Spornath, S. Magdassi, *Polym Advan Technol* **2011**, 22, 2469-2473.

-
- [206] G. Baier, A. Musyanovych, M. Dass, S. Theisinger, K. Landfester, *Biomacromolecules* **2010**, *11*, 960-968.
- [207] L. Torini, J. F. Argillier, N. Zydowicz, *Macromolecules* **2005**, *38*, 3225-3236.
- [208] H. Johnsen, R. B. Schmid, *J Microencapsul* **2007**, *24*, 731-742.
- [209] F. Gaudin, N. Sintès-Zydowicz, *Colloid Surface A* **2008**, *331*, 133-142.
- [210] E. M. Rosenbauer, M. Wagner, A. Musyanovych, K. Landfester, *Macromolecules* **2010**, *43*, 5083-5093.
- [211] M. A. Hood, U. Paiphansiri, D. Schaeffel, K. Koynov, M. Kappl, K. Landfester, R. Munoz-Espi, *Chem Mater* **2015**, *27*, 4311-4318.
- [212] D. Yiamsawas, G. Baier, E. Thines, K. Landfester, F. R. Wurm, *Rsc Adv* **2014**, *4*, 11661-11663.
- [213] K. Piradashvili, M. Fichter, K. Mohr, S. Gehring, F. R. Wurm, K. Landfester, *Biomacromolecules* **2015**, *16*, 815-821.
- [214] S. Taheri, G. Baier, P. Majewski, M. Barton, R. Forch, K. Landfester, K. Vasilev, *J Mater Chem B* **2014**, *2*, 1838-1845.
- [215] G. Baier, S. Winzen, C. Messerschmidt, D. Frank, M. Fichter, S. Gehring, V. Mailänder, K. Landfester, *Macromol Biosci* **2015**, *15*, 765-776.
- [216] U. Paiphansiri, G. Baier, A. Kreyes, D. Yiamsawas, K. Koynov, A. Musyanovych, K. Landfester, *Macromol Chem Phys* **2014**, *215*, 2457-2462.
- [217] J. Zou, C. C. Hew, E. Themistou, Y. K. Li, C. K. Chen, P. Alexandridis, C. Cheng, *Adv Mater* **2011**, *23*, 4274-4277.
- [218] C. K. Chen, W. C. Law, R. Aalink, Y. Yu, B. Nair, J. C. Wu, S. Mahajan, J. L. Reynolds, Y. K. Li, C. K. Lai, E. S. Tzanakakis, S. A. Schwartz, P. N. Prasad, C. Cheng, *Nanoscale* **2014**, *6*, 1567-1572.
- [219] D. Yiamsawas, M. Wagner, G. Baier, K. Landfester, F. R. Wurm, *Rsc Adv* **2016**, *6*, 51327-51331.
- [220] E. M. Alexandrino, P. Buchold, M. Wagner, A. Fuchs, A. Kreyes, C. K. Weiss, K. Landfester, F. R. Wurm, *Chem Commun* **2014**, *50*, 10495-10498.
- [221] R. Roux, L. Sallet, P. Alcouffe, S. Chambert, N. Sintès-Zydowicz, E. Fleury, J. Bernard, *Acs Macro Letters* **2012**, *1*, 1074-1078.
- [222] G. Baier, M. Fichter, A. Kreyes, K. Klein, V. Mailänder, S. Gehring, K. Landfester, *Biomacromolecules* **2016**, *17*, 148-153.
- [223] J. M. Siebert, G. Baier, A. Musyanovych, K. Landfester, *Chem Commun* **2012**, *48*, 5470-5472.
- [224] K. Malzahn, F. Marsico, K. Koynov, K. Landfester, C. K. Weiss, F. R. Wurm, *Acs Macro Letters* **2014**, *3*, 40-43.
- [225] L. P. Lv, K. Landfester, D. Crespy, *Chem Mater* **2014**, *26*, 3351-3353.
- [226] C. Wohnhaas, K. Friedemann, D. Busko, K. Landfester, S. Balushev, D. Crespy, A. Turshatov, *Acs Macro Letters* **2013**, *2*, 446-450.
- [227] L. Thomi, P. Schaefer, K. Landfester, F. R. Wurm, *Macromolecules* **2016**, *49*, 105-109.
- [228] R. H. Staff, M. Gallei, M. Mazurowski, M. Rehahn, R. Berger, K. Landfester, D. Crespy, *Acs Nano* **2012**, *6*, 9042-9049.
- [229] R. H. Staff, M. Gallei, K. Landfester, D. Crespy, *Macromolecules* **2014**, *47*, 4876-4883.
- [230] S. Behzadi, M. Gallei, J. Elbert, M. Appold, G. Glasser, K. Landfester, D. Crespy, *Polym Chem-Uk* **2016**, *7*, 3434-3443.
- [231] H. Freichels, M. Wagner, P. Okwieka, R. G. Meyer, V. Mailänder, K. Landfester, A. Musyanovych, *J Mater Chem B* **2013**, *1*, 4338-4348.

-
- [232] K. Malzahn, S. Ebert, I. Schlegel, O. Neudert, M. Wagner, G. Schutz, A. Ide, F. Roohi, K. Munnemann, D. Crespy, K. Landfester, *Adv Healthc Mater* **2016**, *5*, 567-574.
- [233] F. Tiarks, K. Landfester, M. Antonietti, *Langmuir* **2001**, *17*, 908.
- [234] V. Holzapfel, A. Musyanovych, K. Landfester, M. R. Lorenz, V. Mailander, *Macromol Chem Physic* **2005**, *206*, 2440-2449.
- [235] K. Mohr, S. Maria, B. Grit, S. Susanne, P. Okwieka, S. Tenzer, K. Landfester, V. Mailaender, M. Schmidt, R. G. Meyer, *J Nanomed Nanotechnol* **2014**, *05*, 193
- [236] H. Matahwa, J. B. McLeary, R. D. Sanderson, *J Polym Sci Pol Chem* **2006**, *44*, 427-442.
- [237] R. Sauer, P. Froimowicz, K. Scholler, J. M. Cramer, S. Ritz, V. Mailander, K. Landfester, *Chem-Eur J* **2012**, *18*, 5201-5212.
- [238] H. Y. Liu, S. Prevost, M. Gradzielski, *Z. Phys. Chem.* **2012**, *226*, 675-694.
- [239] B. A. Kerwin, *J. Pharm. Sci.* **2008**, *97*, 2924-2935.
- [240] S. Sharma, R. W. Johnson, T. A. Desai, *Langmuir* **2004**, *20*, 348-356.
- [241] T. V. Kryuk, V. M. Mikhal'chuk, L. V. Petrenko, O. A. Nelepova, A. N. Nikolaevskii, *Pharm Chem J* **2002**, *36*, 31-34.
- [242] Q. Wei, T. Becherer, S. Angioletti-Uberti, J. Dzubiella, C. Wischke, A. T. Neffe, A. Lendlein, M. Ballauff, R. Haag, *Angew. Chem. Ger. Edit* **2014**, *126*, 8138-8169.
- [243] M. Lange, S. Braune, K. Luetzow, K. Richau, N. Scharnagl, M. Weinhart, A. T. Neffe, F. Jung, R. Haag, A. Lendlein, *Macromol Rapid Comm* **2012**, *33*, 1487-1492.
- [244] M. Weinhart, I. Grunwald, M. Wyszogrodzka, L. Gaetjen, A. Hartwig, R. Haag, *Chem-Asian J* **2010**, *5*, 1992-2000.
- [245] A. Thomas, S. S. Muller, H. Frey, *Biomacromolecules* **2014**, *15*, 1935-1954.
- [246] A. Dworak, I. Panchev, B. Trzebicka, W. Walach, *Macromol Symp* **2000**, *153*, 233-242.
- [247] R. K. Kainthan, S. R. Hester, E. Levin, D. V. Devine, D. E. Brooks, *Biomaterials* **2007**, *28*, 4581-4590.
- [248] A. Sunder, R. Mulhaupt, R. Haag, H. Frey, *Adv Mater* **2000**, *12*, 235-239.
- [249] A. Sunder, H. Frey, R. Mulhaupt, *Macromol Symp* **2000**, *153*, 187-196.
- [250] C. Siegers, M. Biesalski, R. Haag, *Chem-Eur J* **2004**, *10*, 2831-2838.
- [251] M. Wyszogrodzka, R. Haag, *Langmuir* **2009**, *25*, 5703-5712.
- [252] P. Dimitrov, S. Rangelov, A. Dworak, C. B. Tsvetanov, *Macromolecules* **2004**, *37*, 1000-1008.
- [253] S. Halacheva, S. Rangelov, C. Tsvetanov, *Macromolecules* **2006**, *39*, 6845-6852.
- [254] S. Halacheva, S. Rangelov, C. Tsvetanov, V. M. Garamus, *Macromolecules* **2010**, *43*, 772-781.
- [255] S. Rangelov, M. Almgren, S. Halacheva, C. Tsvetanov, *J Phys Chem C* **2007**, *111*, 13185-13191.
- [256] S. Halacheva, S. Rangelov, V. M. Garamus, *Macromolecules* **2007**, *40*, 8015-8021.
- [257] T. Basinska, S. Krolik, S. Slomkowski, *Macromol Symp* **2009**, *281*, 96-105.
- [258] S. Slomkowski, T. Basinska, *Macromol Sy* **2010**, *295*, 13-22.
- [259] S. Pargen, C. Willems, H. Keul, A. Pich, M. Moller, *Macromolecules* **2012**, *45*, 1230-1240.

- [260] A. Dworak, G. Baran, B. Trzebicka, W. Walach, *React Funct Polym* **1999**, *42*, 31-36.
- [261] M. Hans, H. Keul, M. Moeller, *Polymer* **2009**, *50*, 1103-1108.
- [262] A. O. Fitton, J. Hill, D. E. Jane, R. Millar, *Synthesis-Stuttgart* **1987**, 1140-1142.
- [263] M. Erberich, H. Keul, M. Moller, *Macromolecules* **2007**, *40*, 3070-3079.
- [264] M. Backes, L. Messenger, A. Mourran, H. Keul, M. Moeller, *Macromolecules* **2010**, *43*, 3238-3248.
- [265] B. Obermeier, H. Frey, *Bioconjugate Chem* **2011**, *22*, 436-444.
- [266] E. J. V. C. C. Price, in *Polymer science and Technology*, Vol. 19, Plenum Press, New York, **1983**.
- [267] F. Wurm, J. Nieberle, H. Frey, *Macromolecules* **2008**, *41*, 1184-1188.
- [268] J. L. Atkinson, S. Vyazovkin, *Macromolecular Chemistry and Physics* **2011**, *212*, 2103-2113.
- [269] L. L. Hecht, A. Schoth, R. Munoz-Espi, A. Javadi, K. Kohler, R. Miller, K. Landfester, H. P. Schuchmann, *Macromol Chem Phys* **2013**, *214*, 812-823.
- [270] B. Vonnegut, *Rev Sci Instrum* **1942**, *13*, 6-9.
- [271] L. A. Girifalco, R. J. Good, *J Phys Chem* **1957**, *61*, 904-909.
- [272] N. B. Vargaftik, B. N. Volkov, L. D. Voljak, *J Phys Chem Ref Data* **1983**, *12*, 817-820.
- [273] A. Alkan, S. Wald, B. Louage, B. G. De Geest, K. Landfester, F. R. Wurm, *Langmuir* **2016**.
- [274] L. L. Schramm, E. N. Stasiuk, D. G. Marangoni, *Annual Reports Section "C" (Physical Chemistry)* **2003**, *99*, 3-48.
- [275] C. Rosslee, N. L. Abbott, *Curr Opin Colloid In* **2000**, *5*, 81-87.
- [276] A. L. Fameau, A. Carl, A. Saint-Jalmes, R. von Klitzing, *Chemphyschem* **2015**, *16*, 66-75.
- [277] P. H. Anton, J.; Laschwesky, A., *Langmuir* **1993**, *9*, 77-85.
- [278] T. Saji, K. Hoshino, S. Aoyagui, *J Am Chem Soc* **1985**, *107*, 6865-6868.
- [279] C. Jacob, H. T. Yang, H. A. O. Hill, *J Electroanal Chem* **1996**, *416*, 83-88.
- [280] N. Aydogan, C. A. Rosslee, N. L. Abbott, *Colloid Surface A* **2002**, *201*, 101-109.
- [281] S. S. Datwani, V. Truskett, C. A. Rosslee, N. L. Abbott, K. J. Stebe, *Langmuir* **2003**, *19*, 8292-8301.
- [282] K. Tajima, T. Huxur, Y. Imai, I. Motoyama, A. Nakamura, M. Koshinuma, *Colloid Surface A* **1995**, *94*, 243-251.
- [283] B. S. Gallardo, N. L. Abbott, *Langmuir* **1997**, *13*, 203-208.
- [284] C. M. Jewell, M. E. Hays, Y. Kondo, N. L. Abbott, D. M. Lynn, *J Control Release* **2006**, *112*, 129-138.
- [285] Y. Kakizawa, H. Sakai, K. Nishiyama, M. Abe, H. Shoji, Y. Kondo, N. Yoshino, *Langmuir* **1996**, *12*, 921-924.
- [286] C. L. Pizzey, C. M. Jewell, M. E. Hays, D. M. Lynn, N. L. Abbott, Y. Kondo, S. Golan, Y. Tahnon, *J Phys Chem B* **2008**, *112*, 5849-5857.
- [287] K. S. Wang, G. W. Gokel, *J Phys Org Chem* **1997**, *10*, 323-334.
- [288] T. Saji, *Chem Lett* **1988**, 693-696.
- [289] T. Saji, *B Chem Soc Jpn* **1989**, *62*, 2992-2994.
- [290] T. Saji, Y. Ishii, *J Electrochem Soc* **1989**, *136*, 2953-2956.
- [291] T. Takei, H. Sakai, Y. Kondo, N. Yoshino, M. Abe, *Colloid Surface A* **2001**, *183*, 757-765.

- [292] Y. Takeoka, T. Aoki, K. Sanui, N. Ogata, M. Yokoyama, T. Okano, Y. Sakurai, M. Watanabe, *J Control Release* **1995**, *33*, 79-87.
- [293] Z. Y. Cheng, B. Y. Ren, M. Gao, X. X. Liu, Z. Tong, *Macromolecules* **2007**, *40*, 7638-7643.
- [294] B. S. Gallardo, M. J. Hwa, N. L. Abbott, *Langmuir* **1995**, *11*, 4209-4212.
- [295] B. S. Gallardo, K. L. Metcalfe, N. L. Abbott, *Langmuir* **1996**, *12*, 4116-4124.
- [296] T. Saji, K. Hoshino, S. Aoyagui, *J Chem Soc Chem Comm* **1985**, 865-866.
- [297] N. Aydogan, N. L. Abbott, *Langmuir* **2001**, *17*, 5703-5706.
- [298] R. D. A. Hudson, *J. Organomet. Chem.* **2001**, 637-639, 47-69.
- [299] A. Alkan, F. R. Wurm, *Macromol. Rapid Commun.* **2016**, *37*, 1482-1493.
- [300] R. Pietschnig, *Chem. Soc. Rev.* **2016**, *45*, 5216-5231.
- [301] A. Natalello, A. Alkan, A. Friedel, I. Lieberwirth, H. Frey, F. R. Wurm, *ACS Macro Lett.* **2013**, *2*, 313-316.
- [302] J.-F. Gohy, B. G. G. Lohmeijer, A. Alexeev, X.-S. Wang, I. Manners, M. A. Winnik, U. S. Schubert, *Chemistry – A European Journal* **2004**, *10*, 4315-4323.
- [303] Z. M. Hudson, C. E. Boott, M. E. Robinson, P. A. Rupar, M. A. Winnik, I. Manners, *Nat. Chem.* **2014**, *6*, 893-898.
- [304] K. N. Power-Billard, J. Massey, R. Resendes, M. A. Winnik, I. Manners, in *Synthetic Macromolecules with Higher Structural Order, Vol. 812*, American Chemical Society, **2002**, pp. 149-162.
- [305] C. Tonhauser, A. Alkan, M. Schoemer, C. Dingels, S. Ritz, V. Mailaender, H. Frey, F. R. Wurm, *Macromolecules* **2013**, *46*, 647-655.
- [306] A. Alkan, L. Thomi, T. Gleede, F. R. Wurm, *Polym Chem-Uk* **2015**, *6*, 3617-3624.
- [307] A. Alkan, R. Klein, S. I. Shylin, U. Kemmer-Jonas, H. Frey, F. R. Wurm, *Polym Chem-Uk* **2015**, *6*, 7112-7118.
- [308] F. Wurm, U. Kemmer-Jonas, H. Frey, *Polym. Int.* **2009**, *58*, 989-995.
- [309] J. Elbert, M. Gallei, C. Rüttiger, A. Brunsen, H. Didzoleit, B. Stühn, M. Rehahn, *Organometallics* **2013**, *32*, 5873-5878.
- [310] S. Wald, F. Wurm, K. Landfester, D. Crespy, *Polymers* **2016**, *8*, 303.
- [311] S. F. Medeiros, A. M. Santos, H. Fessi, A. Elaissari, *J. Polym. Sci. Poly. Chem.* **2010**, *48*, 3932-3941.
- [312] C. L. Lin, W. Y. Chiu, T. M. Don, *J. Appl. Polym. Sci.* **2006**, *100*, 3987-3996.
- [313] J. K. Oh, F. Perineau, K. Matyjaszewski, *Macromolecules* **2006**, *39*, 8003-8010.
- [314] M. J. Kositza, C. Bohne, P. Alexandridis, T. A. Hatton, J. F. Holzwarth, *Macromolecules* **1999**, *32*, 5539-5551.
- [315] J. Rieger, C. Passirani, J. P. Benoit, K. Van Butsele, R. Jerome, C. Jerome, *Adv. Funct. Mater.* **2006**, *16*, 1506-1514.
- [316] S. Cajot, P. Lecomte, C. Jerome, R. Riva, *Polym. Chem.* **2013**, *4*, 1025-1037.
- [317] J. K. Oh, *Soft. Matter.* **2011**, *7*, 5096-5108.
- [318] Z. X. Zhu, *Biomaterials* **2013**, *34*, 10238-10248.
- [319] A. Thomas, H. Schlaad, B. Smarsly, M. Antonietti, *Langmuir* **2003**, *19*, 4455-4459.
- [320] R. Klein, F. R. Wurm, *Macromol Rapid Comm* **2015**, *36*, 1147-1165.
- [321] J. Chiefari, Y. K. Chong, F. Ercole, J. Krstina, J. Jeffery, T. P. T. Le, R. T. A. Mayadunne, G. F. Meijs, C. L. Moad, G. Moad, E. Rizzardo, S. H. Thang, *Macromolecules* **1998**, *31*, 5559-5562.

- [322] E. Rizzardo, J. Chiefari, B. Y. K. Chong, F. Ercole, J. Krstina, J. Jeffery, T. P. T. Le, R. T. A. Mayadunne, G. F. Meijs, C. L. Moad, G. Moad, S. H. Thang, *Macromol. Symp.* **1999**, *143*, 291-307.
- [323] G. Moad, E. Rizzardo, S. H. Thang, *Aust. J. Chem.* **2005**, *58*, 379-410.
- [324] E. Rizzardo, J. Chiefari, R. T. A. Mayadunne, G. Moad, S. H. Thang, in *ACS Symposium Series, Vol. 768*, **2000**, pp. 278-296.
- [325] J. Andrieu, N. Kotman, M. Maier, V. Mailander, W. S. L. Strauss, C. K. Weiss, K. Landfester, *Macromol. Rapid Comm.* **2012**, *33*, 248-253.
- [326] R. Dorresteiijn, R. Ragg, G. Rago, N. Billecke, M. Bonn, S. H. Parekh, G. Battagliarin, K. Peneva, M. Wagner, M. Klapper, K. Müllen, *Biomacromolecules* **2013**, *14*, 1572-1577.
- [327] C. Geidel, S. Schmachtel, A. Riedinger, C. Pfeiffer, K. Müllen, M. Klapper, W. J. Parak, *Small* **2011**, *7*, 2929-2934.
- [328] J. V. Weaver, S. P. Rannard, A. I. Cooper, *Angew Chem Int Ed Engl* **2009**, *48*, 2131-2134.
- [329] J. I. Amalvy, G. F. Unali, Y. Li, S. Granger-Bevan, S. P. Armes, B. P. Binks, J. A. Rodrigues, C. P. Whitby, *Langmuir* **2004**, *20*, 4345-4354.
- [330] D. Dupin, S. P. Armes, *Abstr Pap Am Chem S* **2007**, 233.
- [331] K. Kim, T. H. Kim, J. H. Choi, J. Y. Lee, S. S. Hah, H. O. Yoo, S. S. Hwang, K. N. Ryu, H. J. Kim, J. Kim, *Macromol Chem Physic* **2010**, *211*, 1127-1136.
- [332] S. Lee, J. H. Nam, Y. J. Kim, Y. J. Cho, N. H. Kwon, J. Y. Lee, H. J. Kang, H. T. Kim, H. M. Park, S. Kim, J. Kim, *Macromol Res* **2011**, *19*, 827-834.
- [333] K. I. Oyama, T. D. Kondo, *Org. Lett.* **2003**, *5*, 209-212.
- [334] A. S. Y. Lee, F. Y. Su, *Tetrahedron Lett.* **2005**, *46*, 6305-6309.
- [335] M. Schelhaas, H. Waldmann, *Angew Chem Int Edit* **1996**, *35*, 2056-2083.
- [336] T. W. Greene, P. G. M. Wuts, *Protective Groups in Organic Synthesis, Vol. 3rd ed*, Wiley and Sons, New York, **1999**.
- [337] P. J. Kocienski, *Protecting Groups*, George Thieme Verlag, New York, **1999**.
- [338] D. K. Heldmann, J. Stohrer, R. Zauner, *Synlett.* **2002**, 1919-1921.
- [339] G. van Look, G. Simchen, J. Heberle, in *Fluka Chemie AG: Buchs, Vol. 2nd*, Buchs, Switzerland, **1995**, pp. 1-45.
- [340] E. J. Corey, C. Rucker, *Tetrahedron Lett.* **1982**, *23*, 719-722.
- [341] E. J. Corey, H. Cho, C. Rucker, D. H. Hua, *Tetrahedron Lett.* **1981**, *22*, 3455-3458.
- [342] K. C. Nicolaou, S. Ninkovic, F. Sarabia, D. Vourloumis, Y. He, H. Vallberg, M. R. V. Finlay, Z. Yang, *J. Am. Chem. Soc.* **1997**, *119*, 7974-7991.
- [343] M. Lalonde, T. H. Chan, *Synthesis-Stuttgart* **1985**, 817-845.
- [344] M. Mahmoudi, V. Serpooshan, *J Phys Chem C* **2011**, *115*, 18275-18283.
- [345] S. T. Yang, Y. Liu, Y. W. Wang, A. Cao, *Small* **2013**, *9*, 1635-1653.
- [346] M. Lundqvist, J. Stigler, G. Elia, I. Lynch, T. Cedervall, K. A. Dawson, *Proc Natl Acad Sci U S A* **2008**, *105*, 14265-14270.
- [347] A. Schrade, V. Mailander, S. Ritz, K. Landfester, U. Ziener, *Macromol Biosci* **2012**, *12*, 1459-1471.
- [348] S. Tenzer, D. Docter, S. Rosfa, A. Wlodarski, J. Kuharev, A. Rekik, S. K. Knauer, C. Bantz, T. Nawroth, C. Bier, J. Sirirattanapan, W. Mann, L. Treuel, R. Zellner, M. Maskos, H. Schild, R. H. Stauber, *Acs Nano* **2011**, *5*, 7155-7167.
- [349] J. Pushpamalar, A. K. Veeramachineni, C. Owh, X. J. Loh, *ChemPlusChem* **2016**, *81*, 504-514.

-
- [350] W. T. E. Bosker, K. Patzsch, M. A. C. Stuart, W. Norde, *Soft Matter* **2007**, *3*, 754-762.
- [351] H. C. Kolb, M. G. Finn, K. B. Sharpless, *Angew Chem Int Ed Engl* **2001**, *40*, 2004-2021.
- [352] R. Huisgen, *Proc. Chem. Soc* **1961**, 357-369.
- [353] J. F. Lutz, *Angew Chem Int Ed Engl* **2008**, *47*, 2182-2184.
- [354] J. M. Baskin, J. A. Prescher, S. T. Laughlin, N. J. Agard, P. V. Chang, I. A. Miller, A. Lo, J. A. Codelli, C. R. Bertozzi, *Proc Natl Acad Sci U S A* **2007**, *104*, 16793-16797.
- [355] H. C. Kolb, K. B. Sharpless, *Drug Discov Today* **2003**, *8*, 1128-1137.
- [356] N. Vinson, Y. Z. Gou, C. R. Becer, D. M. Haddleton, M. I. Gibson, *Polym Chem-Uk* **2011**, *2*, 107-113.
- [357] T. Tanaka, H. Nagai, M. Noguchi, A. Kobayashi, S. Shoda, *Chem Commun* **2009**, 3378-3379.
- [358] H. Freichels, M. Wagner, P. Okwieka, R. G. Meyer, V. Mailander, K. Landfester, A. Musyanovych, *J Mater Chem B* **2013**, *1*, 4338-4348.
- [359] K. Landfester, A. Musyanovych, V. Mailander, *J Polym Sci Pol Chem* **2010**, *48*, 493-515.
- [360] C. R. Becer, R. Hoogenboom, U. S. Schubert, *Angew Chem Int Edit* **2009**, *48*, 4900-4908.
- [361] X. Ning, J. Guo, M. A. Wolfert, G.-J. Boons, *Angew Chem Int Ed* **2008**, *47*, 2253-2255.
- [362] G. Baier, J. M. Siebert, K. Landfester, A. Musyanovych, *Macromolecules* **2012**, *45*, 3419-3427.
- [363] S. Winzen, S. Schoettler, G. Baier, C. Rosenauer, V. Mailaender, K. Landfester, K. Mohr, *Nanoscale* **2015**, *7*, 2992-3001.
- [364] S. Tenzer, D. Docter, J. Kuharev, A. Musyanovych, V. Fetz, R. Hecht, F. Schlenk, D. Fischer, K. Kiouptsi, C. Reinhardt, *Nat Nanotechnol* **2013**, *8*, 772-781.
- [365] H. Schlaad, H. Kukula, J. Rudloff, I. Below, *Macromolecules* **2001**, *34*, 4302-4304.
- [366] S. Schöttler, K. Klein, K. Landfester, V. Mailänder, *Nanoscale* **2016**, *8*, 5526-5536.
- [367] S. Ritz, S. Schöttler, N. Kotman, G. Baier, A. Musyanovych, J. r. Kuharev, K. Landfester, H. r. Schild, O. Jahn, S. Tenzer, *Biomacromolecules* **2015**, *16*, 1311-1321.
- [368] R. A. Bradshaw, A. L. Burlingame, S. Carr, R. Aebersold, *Mol Cell Proteomics* **2006**, *5*, 787-788.
- [369] J. C. Silva, M. V. Gorenstein, G.-Z. Li, J. P. C. Vissers, S. J. Geromanos, *Mol Cell Proteomics* **2006**, *5*, 144-156.
- [370] A. Salvati, A. S. Pitek, M. P. Monopoli, K. Prapainop, F. B. Bombelli, D. R. Hristov, P. M. Kelly, C. Aberg, E. Mahon, K. A. Dawson, *Nat Nanotechnol* **2013**, *8*, 137-143.
- [371] P. Del Pino, B. Pelaz, Q. Zhang, P. Maffre, G. U. Nienhaus, W. J. Parak, *Mater Horizons* **2014**, *1*, 301-313.
- [372] Q. Dai, C. Walkey, W. C. W. Chan, *Angew Chem Int Edit* **2014**, *53*, 5093-5096.
- [373] C. D. Walkey, J. B. Olsen, H. B. Guo, A. Emili, W. C. W. Chan, *J Am Chem Soc* **2012**, *134*, 2139-2147.

-
- [374] X. Shan, C. Liu, Y. Yuan, F. Xu, X. Tao, Y. Sheng, H. Zhou, *Colloid Surfaces B* **2009**, 72, 303-311.
- [375] A. Savina, S. Amigorena, *Immunol Rev* **2007**, 219, 143-156.
- [376] L. Martinez-Pomares, *Journal of leukocyte biology* **2012**, 92, 1177-1186.
- [377] H. Feinberg, D. A. Mitchell, K. Drickamer, W. I. Weis, *Science* **2001**, 294, 2163-2166.
- [378] Y. Guo, H. Feinberg, E. Conroy, D. A. Mitchell, R. Alvarez, O. Blixt, M. E. Taylor, W. I. Weis, K. Drickamer, *Nat Struct Mol Biol* **2004**, 11, 591-598.
- [379] A. Holla, A. Skerra, *Protein Eng Des Sel* **2011**, 24, 659-669.
- [380] V. Percec, P. Leowanawat, H.-J. Sun, O. Kulikov, C. D. Nusbaum, T. M. Tran, A. Bertin, D. A. Wilson, M. Peterca, S. Zhang, N. P. Kamat, K. Vargo, D. Moock, E. D. Johnston, D. A. Hammer, D. J. Pochan, Y. Chen, Y. M. Chabre, T. C. Shiao, M. Bergeron-Brele, S. André, R. Roy, H.-J. Gabius, P. A. Heiney, *J Am Chem Soc* **2013**, 135, 9055-9077.
- [381] R. Daly, G. Vaz, A. M. Davies, M. O. Senge, E. M. Scanlan, *Chem Eur J* **2012**, 18, 14671-14679.
- [382] Y. Du, M. Zhang, F. Kong, *Org Lett* **2000**, 2, 3797-3800.
- [383] S. Oscarson, A.-K. Tidén, *Carbohydr Res* **1993**, 247, 323-328.
- [384] D. Sail, P. Kováč, *Carbohydr Res* **2012**, 357, 47-52.
- [385] H. Franzyk, M. Meldal, H. Paulsen, K. Bock, *J Chem Soc Perk T 1* **1995**, 2883-2898.
- [386] A. Lill, K. Scholich, H. Stark, *Tetrahedron Lett* **2013**, 54, 6682-6686.
- [387] M. E. Bakleh, V. Sol, K. Estieu-Gionnet, R. Granet, G. Délérís, P. Krausz, *Tetrahedron* **2009**, 65, 7385-7392.
- [388] F. Rusconi, E. Valton, R. Nguyen, E. Dufourc, *Anal Biochem* **2001**, 295, 31-37.
- [389] J. L. Praissman, L. Wells, *Biochemistry* **2014**, 53, 3066-3078.
- [390] A. Salvati, A. S. Pitek, M. P. Monopoli, K. Prapainop, F. B. Bombelli, D. R. Hristov, P. M. Kelly, C. Åberg, E. Mahon, K. A. Dawson, *Nat Nanotechnol* **2013**, 8, 137-143.
- [391] J. Li, R. Peters, S. Lapatra, M. Vazzana, J. O. Sunyer, *Dev Comp Immunol* **2004**, 28, 1005-1021.
- [392] F. Al-Barwani, S. L. Young, M. A. Baird, D. S. Larsen, V. K. Ward, *PloS one* **2014**, 9, 104523.
- [393] Y. Phanse, B. R. Carrillo-Conde, A. E. Ramer-Tait, R. Roychoudhury, N. L. Pohl, B. Narasimhan, M. J. Wannemuehler, B. H. Bellaire, *Acta Biomater* **2013**, 9, 8902-8909.
- [394] L. Cui, J. A. Cohen, K. E. Broaders, T. T. Beaudette, J. M. Fréchet, *Bioconjug Chem* **2011**, 22, 949-957.
- [395] K. L. White, T. Rades, R. H. Furneaux, P. C. Tyler, S. Hook, *J Pharm Pharmacol* **2006**, 58, 729-737.
- [396] L. East, C. M. Isacke, *BBA-Gen Subjects* **2002**, 1572, 364-386.
- [397] V. Shepherd, E. Campbell, R. Senior, P. Stahl, *J Reticuloendoth Soc* **1982**, 32, 423-431.
- [398] T. B. Geijtenbeek, R. Torensma, S. J. van Vliet, G. C. van Duijnhoven, G. J. Adema, Y. van Kooyk, C. G. Figdor, *Cell* **2000**, 100, 575-585.
- [399] X. Shan, C. Liu, Y. Yuan, F. Xu, X. Tao, Y. Sheng, H. Zhou, *Colloid Surfaces B* **2009**, 72, 303-311.
- [400] S. Essa, J. M. Rabanel, P. Hildgen, *Int J Pharm* **2011**, 411, 178-187.

-
- [401] Q. Dai, Y. Yan, C.-S. Ang, K. Kempe, M. M. Kamphuis, S. J. Dodds, F. Caruso, *Acs Nano* **2015**, *9*, 2876-2885.
- [402] K. Zarschler, K. Prapainop, E. Mahon, L. Rocks, M. Bramini, P. Kelly, H. Stephan, K. Dawson, *Nanoscale* **2014**, *6*, 6046-6056.
- [403] M. Lundqvist, J. Stigler, G. Elia, I. Lynch, T. Cedervall, K. A. Dawson, *P Natl Acad Sci* **2008**, *105*, 14265-14270.
- [404] A. Gonzalez-Quintela, R. Alende, F. Gude, J. Campos, J. Rey, L. Meijide, C. Fernandez-Merino, C. Vidal, *Clin Exp Immunol* **2008**, *151*, 42-50.
- [405] Q. Peng, S. Zhang, Q. Yang, T. Zhang, X.-Q. Wei, L. Jiang, C.-L. Zhang, Q.-M. Chen, Z.-R. Zhang, Y.-F. Lin, *Biomaterials* **2013**, *34*, 8521-8530.
- [406] G. R. Fulmer, A. J. M. Miller, N. H. Sherden, H. E. Gottlieb, A. Nudelman, B. M. Stoltz, J. E. Bercaw, K. I. Goldberg, *Organometallics* **2010**, *29*, 2176-2179.
- [407] P. Renz, M. Kokkinopoulou, K. Landfester, I. Lieberwirth, *Macromol Chem Phys* **2016**, *217*, 1879-1885.
- [408] C. P. r. Morales, J. Catalán, V. Domingo, J. A. González Delgado, J. A. Dobado, M. M. Herrador, J. F. Quílez del Moral, A. F. Barrero, *J. Org. Chem.* **2011**, *76*, 2494-2501.
- [409] J. Zhao, S. Wei, X. Ma, H. Shao, *Green Chem.* **2009**, *11*, 1124-1127.

a) to chapter 2.5 - Part of the experimental section



192

title compound as a colorless powder (36.6 g, 52.3 mmol, 94%, mixture of both anomers α/β 4.3:1).

α -anomer: $R_f = 0.48$ (silica gel, toluene/ethyl acetate, 19:1).

β -anomer: $R_f = 0.36$ (silica gel, toluene/ethyl acetate, 19:1).

Signals assignable to α -anomer **8a-alpha**: ^1H NMR, COSY (400 MHz, CDCl_3) δ (ppm) = 8.23–7.84 (m, 10H, H–Ar), 7.71–7.27 (m, 15H, H–Ar), 6.64 (d, $^3J = 2.0$ Hz, 1H, H-1), 6.29 (pseudo-t, 1H, $^3J = 10.2$ Hz H-4), 6.08 (dd, $^3J = 10.3$ Hz, $^3J = 3.3$ Hz, 1H, H-3), 5.92 (dd, $^3J = 3.3$ Hz, $^3J = 2.0$ Hz, 1H, H-2), 4.70 (dd, $^3J = 12.2$ Hz, $^3J = 3.7$ Hz, 1H, H-6_a), 4.51 (pseudo-dt, $^3J = 10.0$ Hz, $^3J = 2.9$ Hz, 1H, H-5), 4.51 (dd, $^3J = 12.2$ Hz, $^3J = 3.7$ Hz, 1H, H-6_b); ^{13}C NMR, HSQC, HMBC (100 MHz, CDCl_3) δ (ppm) = 166.2, 165.8, 165.4, 165.3, 163.7 (5 \times CO–Ar), 134.2, 133.8, 133.7, 133.5, 133.2 (5 \times C_q), 130.3, 130.1, 130.0, 129.9, 129.1, 129.0, 128.9, 128.8, 128.6, 128.6, 128.5 (C–Ar), 91.5 ($^1J_{\text{CH}} = 180$ Hz, C–1), 71.3 (C-5), 70.1 (C-3), 69.6 (C-2), 66.3 (C-4), 62.5 (C-6).

Signals assignable to β -anomer **8a-beta**: ^1H NMR, COSY (400 MHz, CDCl_3) δ (ppm) = 8.18–7.84 (m, 10H, H–Ar), 7.67–7.27 (m, 15H, H–Ar), 6.44 (d, $^3J = 1.2$ Hz, 1H, H-1), 6.18 (pseudo-t, 1H, $^3J = 9.8$ Hz H-4), 6.11 (dd, $^3J = 3.2$ Hz, $^3J = 1.1$ Hz, 1H, H-2), 5.81 (dd, $^3J = 10.0$ Hz, $^3J = 3.2$ Hz, 1H, H-3), 4.76 (dd, $^3J = 12.4$ Hz, $^3J = 2.8$ Hz, 1H, H-6_a), 4.56 (dd, $^3J = 12.3$ Hz, $^3J = 4.4$ Hz, 1H, H-6_b), 4.38 (ddd, $^3J = 9.7$ Hz, $^3J = 4.3$ Hz, $^3J = 2.8$ Hz, 1H, H-5); ^{13}C NMR, HSQC, HMBC (100 MHz, CDCl_3) δ (ppm) = 166.2, 165.7, 165.6, 165.4, 164.3 (5 \times CO–Ar), 133.9, 133.7, 133.7, 133.6, 133.2 (5 \times C_q), 130.3, 130.2, 130.0, 130.0, 129.5, 128.9, 128.8, 128.8, 128.6, 128.6, 128.6, 128.5 (C–Ar), 91.4 ($^1J_{\text{CH}} = 163$ Hz, C–1), 73.5 (C-5), 71.7 (C-3), 69.5 (C-2), 66.5 (C-4), 62.8 (C-6).

The spectral data are in accordance with literature.^[408]

2,3,4,6-Tetra-O-benzoyl- α -D-mannopyranosyl bromide **8**

1,2,3,4,6-Penta-O-benzoyl- α,β -D-mannopyranose (**8a**, 5.0 g, 7.14 mmol, 1.0 eq.) was dissolved in dichloromethane (25 ml) and treated with HBr (33% in acetic acid, 12.3 ml, 71.4 mmol, 10 eq.) at 0 °C. After 2 h, another portion of HBr (1.0 mL, 33% in acetic acid) was added, TLC (cyclohexane/ethylacetate 2:1) showed complete conversion after 4 h. Then the reaction mixture was diluted with dichloromethane (25 ml), washed with water (25 ml), saturated aqueous NaHCO_3 solution (4 \times 25 ml) and brine (25 ml). The separated organic layer was dried over anhydrous MgSO_4 and

the solvent was removed *in vacuo* to give the title compound (4.51 g, 6.85 mmol, 94%,) as a yellowish viscous oil.

R_f = 0.60 (silica gel, cyclohexane/ethyl acetate, 2:1).

^1H NMR, COSY (400 MHz, CDCl_3) δ (ppm) = 8.13–7.82 (m, 8H, H–Ar), 7.64–7.27 (m, 12H, H–Ar), 6.59 (d, 3J = 1.1 Hz, 1H, H-1), 6.32–6.22 (m, 2H, H-3, H-4), 5.91 (dd, 3J = 2.9 Hz, 3J = 1.7 Hz, 1H, H-2), 4.75 (dd, 2J = 12.5 Hz, 3J = 2.4 Hz, 1H, H-6_a), 4.66 (pseudo-dt, 3J = 9.4 Hz, 3J = 3.1 Hz, 1H, H-5), 4.51 (dd, 2J = 12.5 Hz, 3J = 3.7 Hz, 1H, H-6_b); ^{13}C NMR, HSQC, HMBC (100 MHz, CDCl_3) δ (ppm) = 166.1, 165.5, 165.4, 165.1 (4 x CO–Ar), 133.9, 133.8, 133.5, 133.3 (4 x C_q), 130.0, 129.9, 129.9, 129.8, 128.9, 128.8, 128.8, 128.7, 128.6, 128.5 (C–Ar), 83.4 (C–1), 73.3 (C-5), 73.1 (C-2), 69.2 (C-3), 66.1 (C-4), 61.9 (C-6).

The spectral data are in accordance with literature.^[409]

1,2,3,4,6-Penta-O-acetyl- α,β -D-mannopyranose 2

Iodine (560 mg, 2.2 mmol, 0.04 eq.) and acetic anhydride (50 ml) were mixed under Ar-atmosphere. D-Mannose (**1**, 10.0 g, 55.5 mmol, 1.0 eq.) was added portion by portion at 0 °C. After stirring for 30 min at 0 °C and additionally for 18 hours at room temperature TLC (cyclohexane/toluene/ethylacetate 3:3:1) showed complete consumption of the starting material. The reaction mixture was diluted with dichloromethane (50 ml) and was washed twice with cold saturated aqueous Na_2SO_3 solution (2 x 80 ml), then with a saturated aqueous solution of NaHCO_3 (4 x 50 ml). The separated organic layer was dried over anhydrous MgSO_4 . The solvent was remove *in vacuo* to afford the desired peracetylated D-mannose (21.5 g, 55.1 mmol, 99%, mixture of both anomers α/β 1:4.75) as a yellowish high viscous oil.

R_f = 0.30 (silica gel, cyclohexane/toluene/ethyl acetate, 3:3:1).

Signals assignable to β -anomer: ^1H NMR, COSY (600 MHz, CDCl_3) δ (ppm) = 6.09 (d, 3J = 1.9 Hz, 1H, H-1), 5.34–5.36 (m, 2H, H-3, H-4), 5.25–5.27 (m, 1H, H-2), 4.28 (dd, 2J = 12.4 Hz, 3J = 4.9 Hz, 1H, H-6_a), 4.10 (dd, 2J = 12.4 Hz, 3J = 2.5 Hz, 1H, H-6_b), 4.03–4.07 (m, 1H, H-5), 2.18, 2.17, 2.10, 2.05, 2.01 (5 x s, 15H, COCH_3); ^{13}C NMR, HSQC, HMBC (151 MHz, CDCl_3) δ (ppm) = 170.8, 170.2, 169.9, 169.7, 168.2 (5x COCH_3), 90.7 (C-1), 70.7 (C-5), 68.8 (C-3), 68.4 (C-2), 65.6 (C-4), 62.2 (C-6), 21.0, 20.9, 20.9, 20.8, 20.8 (5 x COCH_3).

The spectral data are in accordance with literature.^[380]

Propargyl 2,3,4,6-tetra-O-acetyl- α -D-mannopyranoside **3**

1,2,3,4,6-Penta-O-acetyl- α,β -D-mannopyranose (**2**, 10.0 g, 25.6 mmol, 1.0 eq.) and propargyl alcohol (7.18 g, 7.48 ml, 128 mmol, 5.0 eq.) was dissolved in dichloromethane (100 ml). After stirring for 20 minutes at room temperature, the reaction mixture was cooled to 0 °C and $\text{BF}_3 \cdot \text{OEt}_2$ (16.22 ml, 128 mmol, 5.0 eq.) was added dropwise. The mixture was stirred for 15 min at this temperature then at room temperature for 24 h. The solution was treated with saturated NaHCO_3 solution (25 ml) the aqueous layer was extracted with dichloromethane (2 \times 50 ml) and the combined organic layers were dried over anhydrous MgSO_4 . The solvent was removed *in vacuo* and the residue was purified by flash column chromatography (cyclohexane/ethyl acetate, 1:1) to give the title compound (7.23 g, 18.7 mmol, 73%) as a colorless viscous oil.

R_f = 0.43 (silica gel, cyclohexane/ethyl acetate, 1:1).

^1H NMR, COSY (400 MHz, CDCl_3) δ (ppm) = 5.36 (m, 3H, H-2, H-3, H-4), 5.02 (d, 1H, 3J = 1.7 Hz, H-1), 4.31–4.25 (m, 3H, H-6_a, $\text{CH}_2\text{--C}\equiv\text{C}$), 4.10 (dd, 2J = 12.2 Hz, 3J = 2.5 Hz, 1H, H-6_b), 4.01 (ddd, 3J = 9.3 Hz, 3J = 5.2 Hz, 3J = 2.5 Hz, 1H, H-5), 2.47 (t, 4J = 2.4 Hz, 1H, CH), 2.15, 2.09, 2.03, 1.98 (4 \times s, 12H, COCH_3); ^{13}C NMR, HSQC, HMBC (100.6 MHz, CDCl_3) δ (ppm) = 170.8, 170.1, 170.0, 169.8 (4 \times COCH_3), 96.4 (C-1), 86.0 ($\text{C}\equiv\text{CH}$), 75.7 ($\text{C}\equiv\text{CH}$), 69.5 (C-2), 69.1 (C-5), 69.1 (C-3), 66.1 (C-4), 62.4 (C-6), 55.1 (CH_2), 21.0, 20.9, 20.8, 20.8 (4 \times COCH_3).

IR (ATR) $\lambda_{\text{max}}/\text{cm}^{-1}$ 1756, 1738, 1431, 1256, 1232, 1186, 1056, 1013, 979, 795, 691.

$[\alpha]_D^{22} + 53.4^\circ$ (c = 1.00, CHCl_3).

HRMS (ESI): calculated for $[\text{C}_{17}\text{H}_{22}\text{O}_{10} + \text{Na}]^+$: 409.1111, found: 409.1116.

The spectral data are in accordance with literature.^[381]

Propargyl α -D-mannopyranoside **4**

Propargyl 2,3,4,6-Tetra-O-acetyl- α -D-mannopyranoside (**3**, 7.00 g, 18.1 mmol) was dissolved in methanol (70 ml) and sodium methoxide was added until pH 9–10 (approx. 60 mg). The reaction mixture was stirred at room temperature for 16 h. Subsequently, the solution was neutralized by Amberlite 120 H^+ resin until pH 7. The

mixture was filtered over Celite which was washed thoroughly with methanol. The solvent was removed *in vacuo* to afford the desired 1-propargyl- α -D-mannopyranoside (3.50 g, 16.1 mmol, 89%) as a highly viscous syrup which solidified soon to an amorphous solid.

$R_f = 0.85$ (RP-silica gel, acetonitrile/water, 1:9).

^1H NMR, COSY (400 MHz, MeOD) δ (ppm) = 4.96 (d, $^3J = 1.7$ Hz, 1H, H-1), 4.27 (d, 1H, $^4J = 2.4$ Hz, CH_2), 3.84 (dd, $^2J = 11.8$ Hz, $^3J = 2.3$ Hz, 1H, H-6_a), 3.79 (dd, 1H, $^3J = 3.1$ Hz, $^3J = 1.7$ Hz, H-2), 3.74–3.58 (m, 3H, H-3, H-4, H-6_b), 3.54–3.47 (m, 1H, H-5), 2.86 (t, $^4J = 2.4$ Hz, CH); ^{13}C NMR, HSQC, HMBC (100.6 MHz, MeOD) δ (ppm) = 99.8 (C-1), 80.0 ($\text{C}\equiv\text{CH}$), 76.0 ($\text{C}\equiv\text{CH}$), 75.1 (C-5), 72.5 (C-3), 72.0 (C-2), 68.5 (C-4), 62.8 (C-6), 54.8 ($\text{CH}_2\text{-C}\equiv\text{CH}$).

IR (ATR) $\lambda_{\text{max}}/\text{cm}^{-1}$ 3403, 3276, 2934, 2909, 1586, 1343, 1252, 1134, 1061, 963, 916, 814, 663.

$[\alpha]_D^{22} + 116.7^\circ$ ($c = 1.00$, MeOH).

HRMS (ESI): calculated for $[\text{C}_9\text{H}_{14}\text{O}_6 + \text{Na}]^+$: 241.0688, found: 214.0692.

The spectral data are in accordance with literature.^[381]

Propargyl 2,4-O-di-benzoyl- α -D-mannopyranoside 6 and Propargyl 2,6-O-di-benzoyl- α -D-mannopyranoside 7

Trimethyl orthobenzoate (3.1 ml, 18.1 mmol, 2.6 eq.) was added to a mixture of 1-propargyl- α -D-mannopyranoside (**4**, 1.5 g, 6.87 mmol, 1.0 eq.), trifluoroacetic acid (45 μl) and camphorsulfonic acid (75 mg) in acetonitrile (60 ml) at room temperature. The suspension was stirred for 2 h, it was obtained a clear colorless solution. The solvent was removed *in vacuo* and the residue was taken up in acetonitrile (45 ml). The solution was treated with 10% aqueous trifluoroacetic acid (2.6 ml) at room temperature. After stirring for 1 h, the solvent was removed *in vacuo* and the residue was co-evaporated with toluene (4 \times 50 ml). The crude product was purified by flash column chromatography (cyclohexane/ethyl acetate, gradient 0% to 60% ethyl acetate, Isolera Flash Purification System) to afford the two title compounds (1.61 g, 3.78 mmol, 55%, 1-propargyl 2,4-O-di-benzoyl- α -D-mannopyranoside; 1.11 g, 2.60 mmol, 38%, 1-propargyl 2,6-O-di-benzoyl- α -D-mannopyranoside) as colorless foams.

Propargyl 2,4-di-benzoyl- α -D-mannopyranoside 6

$R_f = 0.48$ (silica gel, cyclohexane/ethyl acetate, 2:1).

^1H NMR, COSY (400 MHz, CDCl_3) δ (ppm) = 8.12 – 8.05 (m, 4H, H-2-Ar), 7.64 – 7.58 (m, 2H, H-4-Ar), 7.51 – 7.44 (m, 4H, H-3-Ar), 5.52 (pseudo-t, $^3J = 10.0$ Hz, 1H, H-4), 5.45 (dd, $^3J = 3.5$, $^3J = 1.7$ Hz, 1H, H-2), 5.25 (d, $^3J = 1.7$ Hz, 1H, H-1), 4.45 (dd, $^3J = 9.8$, $^3J = 3.5$ Hz, 1H, H-3), 4.33 (d, $^4J = 2.4$ Hz, 2H, CH_2), 4.00 (ddd, $^3J = 10.0$, $^3J = 4.1$, $^3J = 2.3$ Hz, 1H, H-5), 3.82 (dd, $^2J = 12.6$, $^3J_{\text{H,H}} = 2.4$ Hz, 1H, H-6_a), 3.74 (dd, $^2J = 12.6$, $^3J = 4.1$ Hz, 1H, H-6_b), 2.51 (t, $^4J = 2.4$ Hz, 1H, CH); ^{13}C NMR, HSQC, HMBC (100.6 MHz, CDCl_3) δ (ppm) = 167.4, 166.1 (2 \times CO-Ar), 133.9, 133.8 (2 \times C-4-Ar), 130.1 (2 \times C-2-Ar, 2 \times C-2'-Ar), 129.3, 129.1 (2 \times C_q), 128.8, 128.7 (C-3-Ar), 96.7 (C-1, $^1J_{\text{C,H}} = 173$ Hz), 78.4 ($\text{C}\equiv\text{CH}$), 75.6 ($\text{C}\equiv\text{CH}$), 72.8 (C-2), 71.2 (C-5), 70.3 (C-4), 68.7 (C-3), 61.5 (C-6), 55.4 ($\text{CH}_2\text{-C}\equiv\text{CH}$).

IR (ATR) $\lambda_{\text{max}}/\text{cm}^{-1}$ 3465, 3292, 2927, 1715, 1601, 1451, 1317, 1261, 1111, 1059, 1011, 884, 708.

$[\alpha]_D^{22} - 11.9^\circ$ ($c = 1.00$, CHCl_3).

HRMS (ESI): calculated for $[\text{C}_{23}\text{H}_{22}\text{O}_8 + \text{Na}]^+$: 449.1212, found: 449.1225.

Propargyl 2,6-di-O-benzoyl- α -D-mannopyranoside 7

$R_f = 0.23$ (silica gel, cyclohexane/ethyl acetate, 2:1).

^1H NMR, COSY (400 MHz, CDCl_3) δ (ppm) = 8.14 – 8.09 (m, 2H, H-2-Ar⁶), 7.93 – 7.88 (m, 2H, H-2-Ar²), 7.65 – 7.59 (m, 1H, H-4-Ar²), 7.53 – 7.48 (m, 1H, H-4-Ar⁶), 7.48 – 7.42 (m, 2H, H-3-Ar⁶), 7.26 – 7.21 (m, 2H, H-3-Ar²), 5.41 (dd, $^3J = 3.4$ Hz, $^3J = 1.7$ Hz, 1H, H-2), 5.15 (d, $^3J = 1.7$, 1H, H-1), 4.93–4.87 (m, 1H, H-6_a), 4.51 (dd, $^2J = 12.2$, $^3J = 1.8$ Hz, 1H, H-6_b), 4.31 (d, $^4J = 2.4$ Hz, 2H, CH_2), 4.20 (dd, $^3J = 8.7$, $^3J = 3.3$, 1H, H-3), 4.22–3.89 (m, 2H, H-4, H-5), 2.47 (t, $^4J = 2.4$ Hz, 1H, CH); ^{13}C NMR, HSQC, HMBC (100.6 MHz, CDCl_3) δ (ppm) = 167.5 (CO-Ar⁶), 166.1 (CO-Ar²), 133.5, 133.5 (2 \times C-4-Ar), 130.0, 129.9 (2 \times C-2-Ar), 129.7, 129.4 (2 \times C_q), 128.7, 128.8 (2 \times C-3-Ar), 96.9 (C-1, $^1J_{\text{C,H}} = 173$ Hz), 78.5 ($\text{C}\equiv\text{CH}$), 75.5 ($\text{C}\equiv\text{CH}$), 72.1 (C-2), 72.1 (C-4), 71.5 (C-5), 70.0 (C-3), 67.8 (C-4), 63.5 (C-6), 55.1 ($\text{CH}_2\text{-C}\equiv\text{CH}$).

IR (ATR) $\lambda_{\text{max}}/\text{cm}^{-1}$ 3458, 3345, 3236, 2957, 1717, 1703, 1451, 1317, 1262, 1109, 1053, 977, 706, 648.

$[\alpha]_D^{22} - 17.7^\circ$ ($c = 1.00$, CHCl_3).

HRMS (ESI): calculated for $[\text{C}_{23}\text{H}_{22}\text{O}_8 + \text{H}]^+$: 427.1393, found: 427.1404.

2,4-Di-O-benzoyl-3,6-di-O-(2,3,4,6-tetra-O-benzoyl- α -D-mannopyranosyl)-1-propargyl- α -D-mannopyranoside **9**

1-Propargyl 2,4-O-di-benzoyl- α -D-mannopyranoside (**6**, 415 mg, 0.97 mmol, 1.0 eq.) and 2,3,4,6-tetra-O-benzoyl- α -D-mannosylpyranosyl bromide (**8**, 1.27 g, 1.94 mmol, 2.0 eq.) was dissolved in dichloromethane (11 ml) in a thoroughly flame dried flask under argon. The solution was stirred for 20 min at 0 °C. AgOTf (543 mg, 2.11 mmol, 2.4 eq.) was dissolved in toluene (3 ml) and added dropwise to the solution. Immediately a yellowish precipitate is formed and after 1.5 h the greenish reaction mixture was treated with NEt₃ (500 μ l). It was filtered over Celite which was washed thoroughly with dichloromethane. The solvent was removed *in vacuo* and the residue was purified by flash column chromatography (cyclohexane/ethyl acetate, gradient 0% to 50% ethyl acetate, Isolera Flash Purification System) to afford the title compound (1.06 g, 0.67 mmol, 69%) as a colorless foam.

R_f = 0.40 (silica gel, cyclohexane/ethyl acetate, 2:1).

¹H NMR, COSY, TOCSY (600 MHz, CDCl₃) δ (ppm) = 8.33–8.30 (m, 2H, H–Ar), 8.14–8.10 (m, 4H, H–Ar), 8.09–8.01 (m, 6H, H–Ar), 7.88–7.80 (m, 6H, H–Ar), 7.74–7.70 (m, 2H, H–Ar), 7.64–7.47 (m, 8H, H–Ar), 7.46–7.27 (m, 20H, H–Ar), 7.22–7.19 (m, 2H, H–Ar), 6.14 (t, ³ J = 10.1 Hz, 1H, H–4''), 6.02–5.96 (m, 2H, H–3'', H–4'), 5.93 (t, ³ J = 10.0 Hz, 1H, H–4), 5.79–5.76 (m, 2H, H–2'', H–2), 5.71 (dd, ³ J = 10.1 Hz, ³ J = 2.8 Hz, 1H, H–3'), 5.37–5.35 (m, 3H, H–1, H–1', H–2'), 5.15 (d, ³ J = 1.8 Hz, 1H, H–1''), 4.68 (dd, ³ J = 9.8 Hz, ³ J = 3.5 Hz, 1H, H–3), 4.65–4.52 (m, 4H, H–6_a'', H–5'', H–5', H–6_a'), 4.47 (dd, ² J = 16.0 Hz, ⁴ J = 2.4 Hz, 1H, O–CH_{2,a}–C \equiv C), 4.43–4.36 (m, 3H, H–6_b'', H–6_b', O–CH_{2,b}–C \equiv C), 4.33 (ddd, ³ J = 10.3 Hz, ³ J = 6.1 Hz, ⁴ J = 2.1 Hz, 1H, H–5), 4.17 (dd, ² J = 10.8 Hz, ³ J = 6.2 Hz, 1H, H–6_a), 3.81 (dd, ² J = 10.9 Hz, ³ J = 2.1 Hz, 1H, H–6_b), 2.60 (t, ⁴ J = 2.4 Hz, 1H, –C \equiv C–H); ¹³C NMR, HSQC, HMBC (151 MHz, CDCl₃) δ (ppm) = 166.7, 166.3, 166.2, 165.7, 165.6, 165.4, 165.4, 165.4, 164.8, 164.7 (10 \times CO), 133.8, 133.6, 133.6, 133.5, 133.4, 133.4, 133.2, 133.1, 133.1, 133.0 (10 \times C–4–Ar), 130.4, 130.1, 130.1, 130.0, 130.0, 129.8, 129.8, 129.8, 129.7 (C–Ar), 129.4, 129.3, 129.3, 129.3, 129.3, 129.1, 129.1, 129.1, 129.0, 129.0 (10 \times C_q–Ar), 128.7, 128.6, 128.5, 128.4, 128.4, 128.3 (C–Ar), 99.6 (C–1'), 97.6 (C–1''), 96.4 (C–1), 78.3 (–C \equiv C–H), 76.1 (–C \equiv C–H), 76.0 (C–3), 71.7 (C–2''), 70.4 (C–3''), 70.4 (C–2), 70.3 (C–5), 70.3 (C–2'), 69.7 (C–3'), 69.4 (C–5'), 69.0 (C–5''), 68.6 (C–4), 67.1 (C–6), 66.7 (C–4'), 66.7 (C–4''), 62.8 (C–6''), 55.2 (–CH₂–C \equiv C).

IR (ATR, cm^{-1}): $\tilde{\nu}$ = 3064, 2955, 2926, 1778, 1722, 1642, 1451, 1257, 1066, 1026, 1001, 705, 686, 648.

$[\alpha]_D^{22}$ – 50.7° (c = 1.00, CHCl_3).

HRMS (ESI): calculated for $[\text{C}_{91}\text{H}_{74}\text{O}_{26} + \text{Na}]^+$: 1605.4366, found: 1605.4390.

1-Methanesulfonyl-2-(2-(2-(2-methanesulfonylethoxy)ethoxy)ethoxy)ethane

11a

Methanesulfonyl chloride (4.48 ml, 56.6 mmol, 2.2 eq.) and tetraethylene glycol (**10**, 5.00 g, 25.7 mmol, 1.0 eq.) were dissolved in dichloromethane (125 ml) at 0 °C. The reaction mixture was treated with NEt_3 (10.7 ml, 77.2 mmol, 3.0 eq.) and stirred for 45 min. Subsequently water (125 ml) was added and the separated organic layer was washed with ice cold 2 *N* HCl (125 ml), saturated aqueous NaHCO_3 solution (125 ml) and brine (125 ml). The organic layer was dried over anhydrous Na_2SO_4 and the solvent was removed *in vacuo* to give the title compound (8.78 g, 25.1 mmol, 98%) as a yellowish oil.

R_f = 0.20 (silica gel, cyclohexane/ethyl acetate, 1:2).

^1H NMR, COSY (300 MHz, CDCl_3) δ (ppm) = 4.40–3.35 (m, 4H, $2 \times \text{MsO}-\text{CH}_2$), 3.79–3.74 (m, 4H, $\text{MsO}-\text{CH}_2-\text{CH}_2$), 3.70–3.61 (m, 8H, $\text{MsO}-\text{Et}-\text{O}[(\text{CH}_2)_2-\text{O}]_2-\text{Et}-\text{OMs}$), 3.07 (m, 6H, $2 \times -\text{CH}_3$); ^{13}C NMR, HSQC, HMBC (75 MHz, CDCl_3) δ (ppm) = 70.8 ($2 \times \text{CH}_2-\text{CH}_2-\text{O}$), 70.7 ($2 \times \text{CH}_2-\text{CH}_2-\text{O}$), 69.3 ($2 \times \text{MsO}-\text{CH}_2$), 69.2 ($2 \times \text{MsO}-\text{CH}_2-\text{CH}_2$), 37.8 ($2 \times -\text{CH}_3$).

The spectral data are in accordance with literature.^[386]

1-Azido-2-(2-(2-(2-azidoethoxy)ethoxy)ethoxy)ethane **11**

1-Methanesulfonyl-2-(2-(2-(2-methanesulfonylethoxy)ethoxy)ethoxy)ethane (**11a**, 2.00 g, 5.71 mmol, 1.0 eq.) was dissolved in a mixture of EtOH (12 ml) and dimethylacetamide (3 ml) and NaN_3 (1.15 g, 17.7 mmol, 3.1 eq.) was added. The reaction mixture was refluxed for 6 h and subsequently poured slowly into water (20 ml) and dichloromethane (20 ml). The separated organic layer was washed with water (50 ml) and brine (50 ml). The organic layer was dried over anhydrous Na_2SO_4 and the solvent was removed *in vacuo*. The residue was co-evaporated with toluene (4×50 ml) to give the title compound (1.36 g, 5.57 mmol, 98%) as a colorless oil.

R_f = 0.60 (silica gel, cyclohexane/ethyl acetate, 4:2).

^1H NMR, COSY (300 MHz, CDCl_3) δ (ppm) = 3.72–3.62 (m, 12H, $2 \times \text{N}_3\text{—CH}_2\text{—CH}_2$, $2 \times \text{CH}_2\text{—CH}_2\text{—O}$), 3.39 (t, $^3J = 5.1$ Hz 4H, $\text{N}_3\text{—CH}_2$); ^{13}C NMR, HSQC, HMBC (75 MHz, CDCl_3) δ (ppm) = 70.9 ($2 \times \text{CH}_2\text{—CH}_2\text{—O}$), 70.2 ($2 \times \text{N}_3\text{—CH}_2\text{—CH}_2$), 50.8 ($2 \times \text{N}_3\text{—CH}_2$).

The spectral data are in accordance with literature.^[387]

(1-(2-(2-(2-(2-Azidoethoxy)ethoxy)ethoxy)ethyl)-1*H*-1,2,3-triazole-4-yl)methoxy)-2,4-di-*O*-benzoyl-3,6-di-*O*-(2,3,4,6-tetra-*O*-benzoyl- α -D-mannopyranosyl)- α -D-mannopyranoside 12

Dimethylformamide (50 ml) was degassed by freeze-pump-thaw-cycle three times then 2,4-di-*O*-benzoyl-3,6-di-*O*-(2,3,4,6-tetra-*O*-benzoyl- α -D-mannopyranoside)-1-propargyl- α -D-mannopyranoside (**9**, 325 mg, 0.21 mmol, 1.0 eq.) and 1-azido-2-(2-(2-(2-azidoethoxy)ethoxy)ethoxy)ethane (**11**, 725 mg, 3.08 mmol, 15 eq.) was dissolved under argon atmosphere. Subsequently the freeze-pump-thaw-cycle was repeated again for three times. CuBr (15 mg, 0.10 mmol, 50 mol%) and *N,N,N',N',N'*-pentamethyldiethylenetriamine (50 μl , 0.24 mmol, 85 mol%) was added and the teal reaction mixture was stirred at 45 °C for 1.5 h. Subsequently it was diluted with ethyl acetate (40 ml) and washed with aqueous saturated NH_4Cl solution (2×40 ml). The aqueous layer was diluted with water so that all salts were dissolved and washed with ethyl acetate (30 ml). The combined organic layers were washed with brine and dried over anhydrous MgSO_4 . The solvent was removed *in vacuo* and the residue was purified by flash column chromatography (cyclohexane/ethyl acetate, gradient 0% to 90% ethyl acetate, Isolera Flash Purification System) to afford the title compound (302 mg, 0.40 mmol, 81%) as a colorless oil.

$R_f = 0.28$ (silica gel, cyclohexane/ethyl acetate, 2:4).

^1H NMR, COSY, TOCSY (600 MHz, CDCl_3) δ (ppm) = 8.33–8.29 (m, 2H, H–Ar), 8.14–8.00 (m, 10H, H–Ar), 7.89 (s, 1H, H_{triazole}), 7.86–7.82 (m, 4H, H–Ar), 7.78–7.75 (m, 2H, H–Ar), 7.72–7.69 (m, 2H, H–Ar), 7.61–7.35 (m, 20H, H–Ar), 7.31–7.27 (m, 8H, H–Ar), 7.22–7.18 (m, 2H, H–Ar), 6.14 (t, $^3J = 10.1$ Hz, 1H, H–4 $''$), 6.06–5.99 (m, 3H, H–3 $''$, H–4 $'$, H–4), 5.82–5.81 (m, 1H, H–2 $''$), 5.76–5.74 (m, 1H, H–2), 5.70 (dd, $^3J = 10.0$ Hz, $^3J = 2.8$ Hz, 1H, H–3 $'$), 5.34–5.32 (m, 2H, H–1 $'$, H–2 $'$), 5.27 (s, 1H, H–1), 5.19 (s, 1H, H–1 $''$), 5.00 (d, $^2J = 12.2$ Hz, 1H, $\text{O—CH}_{2a}\text{—C=C}$), 4.84 (d, $^2J = 12.2$ Hz, 1H, $\text{O—CH}_{2b}\text{—C=C}$), 4.64 (dd, $^3J = 9.8$ Hz, $^3J = 3.4$ Hz, 1H, H–3), 4.61 (dd, $^2J = 12.4$ Hz, $^3J = 2.5$ Hz, 1H, H–6 a'), 4.58–4.53 (m, 4H, triazole- CH_2 , H–6 a'' , H–5 $''$), 4.47

(dt, $^3J = 10.1$ Hz, $^3J = 2.9$ Hz, 1H, H-5'), 4.42–4.39 (m, 1H, H-5), 4.34 (dd, $^2J = 12.2$ Hz, $^3J = 4.4$ Hz, 1H, H-6_b'), 4.29 (dd, $^2J = 12.4$ Hz, $^3J = 3.1$ Hz, 1H, H-6_b'), 4.18 (dd, $^2J = 10.9$ Hz, $^3J = 5.2$ Hz, 1H, H-6_a), 3.89 (t, $^3J = 5.0$ Hz, 2H, triazole-CH₂-CH₂), 3.80 (dd, $^2J = 11.0$ Hz, $^3J = 2.2$ Hz, 1H, H-6_b), 3.64 (m, 10H, alkyl CH₂), 3.33 (t, $^3J = 5.0$ Hz, 2H, N₃-CH₂); ¹³C NMR, HSQC, HMBC (151 MHz, CDCl₃) δ (ppm) = 166.3, 166.2, 166.2, 165.7, 165.6, 165.3, 165.3, 165.3, 164.8, 164.7 (10 \times CO), 143.3 (C_q-in triazole), 133.7, 133.5, 133.5, 133.5, 133.4, 133.4, 133.2, 133.1, 133.1, 133.0 (10 \times C-4-Ar), 130.3, 130.1, 130.1, 130.0, 130.0, 129.9, 129.9, 129.9, 129.8, 129.7, 129.7 (C-Ar), 129.4, 129.4, 129.3, 129.3, 129.3, 129.1, 129.1, 129.1, 129.0, 129.0 (10 \times C_q-Ar), 128.6, 128.6, 128.6, 128.5, 128.5, 128.5, 128.5, 128.4, 128.4, 128.2 (C-Ar), 124.6 (triazole-CH), 99.7 (C-1'), 97.8 (C-1''), 97.0 (C-1), 76.9 (C-3), 71.8 (C-2), 70.7 (3 signals, respectively alkyl CH₂), 70.4 (C-2'), 70.3 (C-3'), 70.3 (C-2''), 70.1 (alkyl CH₂), 69.9 (C-5), 69.6 (C-5'), 69.5 (triazole-CH₂-CH₂), 69.5 (C-3'), 69.0 (C-5''), 68.4 (C-4), 66.9 (C-6), 66.6 (C-4'), 66.5 (C-4''), 62.8 (C-6''), 62.5 (C-6'), 61.0 (O-CH₂-C=C), 50.7 (N₃-CH₂), 50.3 (triazole-CH₂).

IR (ATR) $\tilde{\nu}_{\max}/\text{cm}^{-1}$ 2954, 2927, 2876, 2106, 1727, 1602, 1452, 1264, 1108, 1097, 1028, 710.

$[\alpha]_D^{22} - 33.7^\circ$ ($c = 1$, CHCl₃).

HRMS (ESI): calculated for [C₉₉H₉₀N₆O₂₉ + Na]⁺: 1849.5650, found: 1849.5684.

(1-(2-(2-(2-(2-Azidoethoxy)ethoxy)ethoxy)ethyl)-1H-1,2,3-triazole-4-yl)methoxy)-3,6-di-O- α -D-mannopyranosyl- α -D-mannopyranoside 13

(1-(2-(2-(2-(2-Azidoethoxy)ethoxy)ethoxy)ethyl)-1H-1,2,3-triazole-4-yl)methoxy)-2,4-di-O-benzoyl-3,6-di-O-(2,3,4,6-tetra-O-benzoyl- α -D-mannopyranosyl)- α -D-mannopyranoside (**12**, 500 mg, 0.27 mmol) was dissolved in a mixture of MeOH (4 ml) and dichloromethane (4 ml) and treated with NaOMe (15 mg, 0.27 mmol, 1 eq.). After stirring for 24 hours at room temperature RP-TLC (acetonitrile/water 2:8) showed complete conversion. The reaction mixture was neutralized with conc. HCl (two drops were required). Subsequently the solvents were removed *in vacuo* and the residue was coevaporated with toluene (3 \times 50 ml). The residue was purified by preparative HPLC (MeOH/H₂O, 80:20 for 10 min, then 50:50 for 10 min, flow rate: 37.5 ml/min, R_t 14.7 min) to give the desired unprotected product (150 mg, 0.19 mmol, 71%) as a colorless lyophilisat.

R_f = 0.57 (RP-silica gel, acetonitrile/water, 2:8).

^1H NMR, COSY (600 MHz, D_2O) δ (ppm) = 8.07 (s, 1H, H-Ar), 5.03 (d, $^3J = 1.7$ Hz, 1H, H-1'), 4.89 (d, $^3J = 1.7$ Hz, 1H, H-1), 4.85 (d, $^3J = 1.7$ Hz, 1H, H-1''), 4.79–4.78 (m, 1H, O-CH_{2a}-C=C), 4.69 (d, $^2J = 12.6$ Hz, 1H, O-CH_{2b}-C=C), 4.60 (t, $^3J = 5.0$ Hz, 2H, triazole-CH₂), 4.05 (dd, $^3J = 3.0$ Hz, $^3J = 1.7$ Hz, 1H, H-2), 4.01 (dd, $^3J = 3.3$ Hz, $^3J = 1.7$ Hz, 1H, H-2'), 3.99–3.93 (m, 4H, H-2', H-6_a'', triazole-CH₂-CH₂), 3.90–3.56 (m, 24H, H-3, H-4, H-5, H-6_b'', H-3', H-4', H-5', 2x H-6', H-3'', H-4'', H-5'', 2x H-6'', 10x alkyl CH₂), 3.45–3.42 (m, 2H, N₃-CH₂); ^{13}C NMR, HSQC, HMBC (151 MHz, D_2O) δ (ppm) = 143.4 (C_q-triazole), 125.4 (CH in triazole), 102.3 (C-1'), 99.6 (C-1), 99.3 (C-1''), 78.5 (C-3), 73.2, 72.6, 71.2, 70.5, 70.3, 69.9 (C-2'), 69.8 (C-2''), 69.6 (C-2), 69.5, 69.4, 69.1, 68.7 (triazole-CH₂-CH₂), 66.6, 65.4, 64.9 (C-6), 60.9 (2C, C-6', C-6''), 59.9 (O-CH₂-C=C), 50.0 (2C, N₃-CH₂, triazole-CH₂).

IR (ATR) $\lambda_{\text{max}}/\text{cm}^{-1}$ 3355, 2929, 2114, 1642, 1454, 1350, 1302, 1256, 1130, 1048, 1026, 980.

$[\alpha]_D^{22} - 63.2^\circ$ ($c = 0.75$, MeOH).

HRMS (ESI): calculated for $[\text{C}_{29}\text{H}_{50}\text{N}_6\text{O}_{19} + \text{Na}]^+$: 809.3028, found: 809.3030.

a. List of abbreviation

ACPEG	α -anthraquinonyloxyhexyl- ω -hydroxy- <i>oligo</i> (ethylene oxide)
ACFs	autocorrelation functions
AGE	allyl glycidyl ether
AIBA	α,α' -azodiisobutyramidine dihydrochloride
AIBN	α,α' -azobisisobutyronitrile
ALPU	acetic acid lignin containing polyurethane
APEG	α -anthraquinonyl- ω -hydroxy- <i>oligo</i> (ethylene oxide)
AROP	anionic ring-opening polymerization
ATRP	atom transfer radical polymerization
BMA	<i>n</i> -butyl methacrylate
<i>t</i> BuGE	<i>tert</i> -butyl glycidyl ether
CLSM	confocal laser scanning microscopy
CMC	critical micelle concentration
CS	chondroitin sulfate
CTMA-Cl/Br	cetyltrimethylammonium chloride or bromide
CTA	chain-transfer agent
CuAAC	copper-catalyzed azide-alkyne-cycloaddition
DAB	1,4-diaminobutane
DBCO	dibenzylcyclooctyne
Dex	dextran
DLS	dynamic light scattering
DMA	2-(diethylamino)ethyl methacrylate
DMAEP	di(methacryloyloxy-1-ethoxy)isopropane
DMF	dimethyl formamide
DOSY	diffusion-ordered spectroscopy
DSC	differential scanning calorimetry
DSDMA	bis(2-methacryloyloxyethyl)disulfide
DVB	divinylbenzene
EEGE	ethoxyethyl glycidyl ether
EHEC	ethyl (hydroxyethyl) cellulose

EO	ethylene oxide
fcGE	ferrocenyl glycidyl ether
FT-IR	fourier transformed infrared spectroscopy
G	glycerol
Gluc	glucose
HA	hyaluronic acid
HDDA	1,6-hexanediol diacrylate
HES	hydroxyl ethyl starch
HIPEs	high internal phase emulsions
HLB	hydrophilic-lipophilic balance
HMDI	hexamethylene diisocyanate
HS	human serum
HUVEC	human umbilical vein endothelial
ICP	inductive coupled plasma
IPDI	isophorone diisocyanate
IR	infra red
ITC	isothermal titration calorimetry
LC-MS	liquid-chromatography mass-spectrometry
LCST	lower critical solution temperature
MAA	methacrylic acid
MBTMA	2-benzothiazolyl-2'-methacryloyloxyethyl disulfide
MMA	methyl methacrylate
MRI	magnetic resonance imaging
MS	mass spectrometry
N ₃ -POEOMA- <i>b</i> -PBMA-Cl	α -azido- ω -2-chloroisobutyrate-poly(oligo(ethylene oxide) monomethyl ether methacrylate)- <i>b</i> -poly(<i>n</i> -butyl methacrylate)
NC	nanocapsule
NMP	nitroxide mediated polymerization
NMR	nuclear magnetic resonance
NP	nanoparticle
P2VP, P4VP	poly(vinyl pyridine)
P2VPH ⁺	protonated poly(2-vinylpyridine)

PAA	poly(acrylic acid)
PAA	poly(acrylamide)
((PAA-co-PAAPBA)- <i>b</i> -) ₂ PAEG	poly(acrylic acid-co-acrylamidophenylboronic acid)- <i>block</i> -poly(2-acryloxyethyl galactose)- <i>block</i> -poly(acrylic acid-co-acrylamidophenylboronic acid)
PAA- <i>b</i> -PS	poly(acrylic acid- <i>block</i> - styrene)
PBS	phosphate-buffered saline
PDEA	poly[2-(diethylamino) ethylmethacrylate]
PDI	polydispersity index
PDMA- <i>b</i> -PPMA- <i>b</i> -PLMA	poly[<i>N,N</i> -(dimethylamino) ethyl methacrylate- <i>b</i> -poly(ethylene glycol) methyl ether methacrylate- <i>b</i> -lauryl methacrylate]
P(DEAEMA-co-S)-SG1	poly(2-(diethylamino)ethyl methacrylate-co-styrene)- <i>N-tert</i> -butyl- <i>N</i> -(1-diethylphosphono-2,2-dimethylpropyl)nitroxide
PDMAEMA	poly[(<i>N,N</i> -dimethylamino)ethyl methacrylate]
P(DMAEMA-co-S)-SG1	poly(2-(dimethylamino)ethyl methacrylate-co-styrene)- <i>N-tert</i> -butyl- <i>N</i> -(1-diethylphosphono-2,2-dimethylpropyl)nitroxide
PDMS	poly(dimethylsiloxane)
PEG	polyethylene glycol
PEG-PBMA-Cl	poly(ethylene glycol)- <i>b</i> -poly(<i>n</i> -butyl methacrylate)
PEG/PPG	poly(ethylene glycol)-poly(propylene glycol) copolymers
PEG- <i>b</i> -PS-Br	poly(ethylene glycol)- <i>b</i> -poly(styrene)-Br
PEG- <i>b</i> -PS- <i>b</i> -PBMA	poly(ethylene glycol)- <i>b</i> -polystyrene- <i>b</i> -poly(<i>n</i> -butyl methacrylate)
PEG- <i>b</i> -PS- <i>b</i> -P(BMA-co-S)	poly(ethylene glycol)- <i>b</i> -polystyrene- <i>b</i> -poly(<i>n</i> -butyl methacrylate-co-styrene)
PEG- <i>b</i> -PVIIm	poly(ethylene glycol)- <i>b</i> -poly(<i>N</i> -vinylimidazole)
mPEG- <i>b</i> -[PδVL]	methoxy polyethylene glycol- <i>b</i> -[α-propagyl-δ-valerolactone]
mPEG- <i>b</i> -[PδVL-co-εCL]	methoxy polyethylene glycol- <i>b</i> -[α-propagyl-δ-valerolactone-co-ε-caprolactone]
PEI	poly(ethylene imine)
PEGMA	poly(ethylene glycol) methacrylate
PEGMA-PDEA	poly(ethylene glycol) methacrylate-poly(2-(diethylamino)ethyl

	methacrylate)
PFS	poly(ferrocenyl silane)
PG	polyglycerol
PGMA ₅₀ -PS	poly(glycerol monomethacrylate)- <i>b</i> -polystyrene
PGPR	polyglycerol-polyricinoleate
PHEMA	poly(hydroxyethyl methacrylate)
PLLA	poly(L-lactide)
PLGA	poly(lactic-co-glycolic acid)
PMAA	poly(methacrylic acid)
PMDETA	pentamethyldiethylenetriamine
PMMA	poly(methyl methacrylate)
PNIPAm-co-PMAA	poly(<i>N</i> -isopropylacrylamide-co-methacrylic acid)
PPG-TDI	toluene 2,4-diisocyanate-terminated poly(propylene glycol)
PPO	poly(propylene oxide)
PS	polystyrene
PSMA- <i>g</i> -PNIPAm	poly(styrene- <i>alt</i> -maleic acid)- <i>graft</i> -poly(<i>N</i> -isopropyl acrylamide)
PS/P(DMA- <i>stat</i> -EGDMA	polystyrene/poly(2-(dimethylamino)ethyl methacrylate- <i>stat</i> -ethylene glycol dimethacrylate)
PSSMA	poly(4-styrenesulfonic acid-co-maleic acid) sodium salt
PTBAEMA	2-(tert-butylamino)ethyl methacrylate
PU	polyurea
PUR	polyurethane
PUR-PDMS	polyurethane-polysiloxane
PVA	polyvinyl alcohols
PVAm	polyvinylamine
PVfc	poly(vinyl ferrocene)
PVFc- <i>b</i> -P2VP	poly(vinylferrocene- <i>b</i> -2-vinylpyrrolidone)
PVMAA	poly(7-(4-vinylbenzoyloxy)-4-methylcoumarin-co-acrylic acid)
PVP	polyvinylpyrrolidone
o/w	oil in water

RAFT	reversible addition fragmentation transfer
Rho-C18	rhodamine octadecyl ester
RI	refractive index
RT	room temperature
SANS	small-angle neutron scattering
SDA	siloxane dialdehyde
SDBS	sodium dodecylbenzenesulfonate surfactants
SDS	sodium dodecyl sulfate
SDS-PAGE	sodium dodecylsulfate polyacrylamide gel electrophoresis
SEC	size exclusion chromatography
SEM	scanning electron microscopy
SG1	<i>N-tert</i> -butyl- <i>N</i> -(1-diethylphosphono-2,2-dimethylpropyl)nitroxide
TBHP	<i>tert</i> -butyl hydroperoxide
TDI	toluene-2,4-diisocyanate
TEM	transmission electron microscopy
TEOS	tetraethoxysilane
TFA	trifluoroacetic acid
THF	tetrahydrofuran
TIPSA	triisopropylsilyl acrylate
TLC	Thin-layer chromatography
VA-044	2,2'-azobis[2-(2-imidazoline-2-yl)propane] dihydrochloride
VA-061	2,2'-azobis[2-(2-imidazoline-2-yl)propane]
VP	1-vinyl-2-pyrrolidone
w/o	water in oil

b. List of Symbols

c	concentration
d	diameter
\bar{D}	polydispersity index
$\delta(\text{ppm})$	chemical shift in parts per million
DP_n	degree of polymerization
γ	surface / interfacial tension
L	length
λ	wavelength
M	molar mass
M_n	number-averaged molecular weight
M_w	weight-averaged molecular weight
N_{agg}	aggregation number
n / m	molar ratio in block copolymer
r	radius
$\Delta\rho$	density difference
T	temperature
t	time
T_g	glass temperatures
ω	angular speed
g_1	correlation function
Θ	angle
ζ -potential	zeta potential

c. Curriculum Vitae

d. Scientific Contributions

Publications

- S. Wald, F. R. Wurm, K. Landfester, Orthogonal protected polyglycidol surfmers, *in preparation*.
- S. Wald, M. Tonigold, J. Langhanki, M. Krumb, P. Renz, J. Simon, C. Sauer, I. Lieberwirth, F. R. Wurm, V. Mailänder, T. Opatz, K. Landfester, Mannose vs. Trimannose : Specific Targeting of nanocarriers towards dendritic cells, *in preparation*.
- S. Wald, A. Alkan, B. Louage, B.G. De Geest, K. Landfester, F. R. Wurm, Amphiphilic ferrocene-containing PEG block copolymers as micellar nanocarriers and smart surfactants, *Langmuir*, **2017**, 33 (1), 272-279.
- S. Wald, A. C. Bijlard, D. Crespy, A. Taden, F. R. Wurm, K. Landfester, Functional Colloidal Stabilization, *Adv. Mater. Interfaces*, **2017**, 4, 1600443.
- S. Wald, F. R. Wurm, K. Landfester, D. Crespy, Stabilization of inverse miniemulsions by silyl-protected homopolymers, *Polymers*, **2016**, 8, 303.